MESOSCALE WATER BALANCE OF THE BOREAL FOREST USING OPERATIONAL EVAPOTRANSPIRATION APPROACHES IN A DISTRIBUTED HYDROLOGIC MODEL

BY

TODD A.M. NEFF

UNIVERSITY OF WATERLOO

Mesoscale Water Balance of the Boreal Forest Using Operational Evapotranspiration Approaches in a Distributed Hydrologic Model

by

Todd A.M. Neff

A thesis
presented to the University of Waterloo
in fulfilment of the
thesis requirement for the degree of
Master of Applied Science
in
Civil Engineering

Waterloo, Ontario, Canada, 1996

I hereby declare that I am the sole author of this thesis.

I authorize the University of Waterloo to lend this thesis to other institutions or individuals for the purpose of scholarly research.

I further authorize the University of Waterloo to reproduce this thesis by photocopying or by other means, in total or in part, at the request of other institutions or individuals for the purpose of scholarly research.

The University of Waterloo requires the signatures of all persons using or photocopying this thesis. Please sign below, and give address and date.

ABSTRACT

Evapotranspiration is a very complex process that must be modelled rigorously in hydrologic simulations since it accounts for 60% of the mean losses in the global continental water budgets. Currently, the hydrologic simulation model, WATFLOOD, uses the published monthly mean evaporation losses to estimate evapotranspiration rates. For an operational model, such as WATFLOOD, there is a desire to maintain simplicity in the methods of modelling evapotranspiration, but to maintain a scientific approach a justifiable method must be used.

The objectives of this research are to improve the rigour with which evapotranspiration is modelled in WATFLOOD by using the hydrometric and meteorological data collected during the Boreal Ecosystem Atmosphere Study (BOREAS). A second objective is to provide an initial analysis of the hydrometric data collected during this study for use in comparison with independent measures of evapotranspiration.

This research has been carried out in three parts. First, three potential evapotranspiration models (the Hargreaves, Priestley-Taylor, and Turc equations) have been tested for spatial variation. It has been shown that the variation in meteorological inputs and the final estimates of potential evapotranspiration provided by these models are insignificant with respect to the total water budget, for the types of land cover and sizes of watersheds analyzed. Using a combined function of the cumulative degree-days and the soil moisture with the potential evapotranspiration estimates provides a satisfactory means of estimating evapotranspiration.

The second part of this research shows that the long-term estimates of evapotranspiration losses provided by the water balance are in agreement with the independent estimates made at the flux tower sites (10% difference); short-term estimates show more variation. The data sets are preliminary and require further refinement and analysis, but these first results are reassuring. The latest revisions to the flux tower data show an improvement in the correlation.

The final portion of the research calibrates the new evapotranspiration model using hydrologic simulations. Further refinement of the simulations are required in the Northern Study Area, but the simulations of the calibration and validation periods in the Southern Study Area are quite accurate. A comparison of the simulated and measured evapotranspiration shows good agreement with the long term flux tower estimates and good agreement with the shorter term water balance estimates.

In summary, a method has been incorporated into WATFLOOD for indexing actual evapotranspiration to potential evapotranspiration. Further research will improve the estimates of the parameters used in these indices. The estimates of the evapotranspiration produced using the water balance agree well with independent estimates made at the flux tower sites, although some differences do exist. The new evapotranspiration method produces estimates which agree well with the flux tower estimates. This new, more rigorous method of estimating evapotranspiration as a function of the meteorological inputs improves the spatial transferability of WATFLOOD.

ACKNOWLEDGMENTS

I would like to express my sincere gratitude to my supervisors, Dr. N. Kouwen and Dr. E.D. Soulis, who provided guidance and support throughout my research, as well as an expeditious review of my work.

I would also like to thank the technical support group for their assistance with various components of my research: Terry Ridgeway, for his field expertise; and a list of co-op students, Jonathan Van Dyken, Lisa Vleuten, Jayson Innes, and Allyson Graham for their efforts in organizing a vast amount of the hydrometric data.

A special thanks goes to my office mates, Larry Hamlin, Frank Seglenieks and, Ken Snelgrove who shared in my frustration with my research and with the seemingly endless renovations to our work place. Their fresh perspective on problems was always appreciated along with their general support and camaraderie.

As well I would like to thank Anna for accepting my complete immersion during the final months of my work and for enduring hours of travel to enable short but much needed diversions. A thank-you goes to my family for their eternal support and to Mr. Ken Betts for inspiration.

The author also gratefully acknowledges the assistance provided through the NSERC CSPP grant in support of the BOREAS university participation.

The provision of data by the following BOREAS investigators is sincerely appreciated: Dr. F. Hall, Dr. P. Sellers, and the TE-18 group for the LANDSAT-5 TM classifications; Dr. R. Cuenca and Mr. D. Stangel for the soil moisture data; Dr. S. Shewchuk, the Saskatchewan Research Council, and the AFM-7 group for meteorological data; and the preliminary data sets which were still being revised at the time of publishing from the following flux tower groups: Dr. P. Jarvis and the TF-9 group; Dr. S. Verma, Mr. R. Clemont, and the TF-11 group; Dr. D. Baldocchi, Mr. C. Vogel, and the TF-5 group; Dr. S. Wofsy and the TF-3 group; Dr. K. Moore, Dr. D. Fitzjarrald, and the TF-8 group; and Dr. H. McCaughey, Dr. D. Jelinski, and the TF-10 group.

TABLE OF CONTENTS

LIST OF FIGURES

LIST OF TABLES

Chapter 1
Introduction

1.1 Hydrologic Modelling

The relationship between the natural science of hydrology and the applied science of civil engineering is often not recognized. Hydrology has become a significant part of engineering science from the requirements to solve more classical engineering problems. The desire to understand flow through ancient canal works evolved in the current century to the goal of explaining flow in natural channels. The need for short-term flood prediction and control has inspired the development of the first generation of models that primarily simulate flows produced by short duration hydrologic events. The current development of models strives to simulate flows over a longer period of time (seasonal and annual), which are required for surface water planning and management (Morton, 1983).

1.2 Operational Hydrology

Science and mathematics are the basic tools used by engineers. Scientists are primarily theoreticians in their practice because they attempt to develop new knowledge or perform experiments to explain unknown phenomena. In contrast, the primary goal of the engineer is to apply these theories to assist society (Andrew and Kemper, 1992). Thus, hydrologic models may be broadly classified into two groups:

1. Research models used primarily for the advancement of science, and
2. Operational models utilized for the benefit of society.

Current hydrologic models have become vital components in atmospheric research. When combined with global climate models these hydrologic models are used to improve the understanding of the global climate system. The improvement of the reliability and accuracy of long-term precipitation and runoff modelling will produce large economic benefits (Mailhot *et al.*, 1992), thereby providing benefit to operational hydrology. Currently, long-duration large-scale hydrologic modelling is being applied to large watersheds, such as the Columbia River, for planning and management (Kouwen *et al.*, 1995; Kite and Welsh, 1995; Mailhot *et al.*, 1992).

Precise and accurate simulation of the physical hydrologic processes in scientific models requires vast amounts of input data. It is desirable to maintain a certain simplicity in models that are developed for technological applications. Simplicity enables them to be used in regions where meteorological instrumentation is scarce or where data acquisition costs need to be minimized. Thus, there exists a trade-off between simplicity and accuracy.

1.3 Objectives

The WATFLOOD/SIMPLE (WATFLOOD) model (Kouwen, 1973) is an example of a fully distributed hydrologic model. The basis of WATFLOOD has been to provide an operational-oriented hydrologic simulation model. Initially, the model was developed to assist in the management and development of rural watersheds. Similar to other models at the time of its conception, WATFLOOD was of the generation of hydrologic models that focused on the simulation of events lasting only a few hours. Modelling short-term hydrologic responses with a minimum number of calculations and few data inputs was the main concern.

The model has been under continuous development concurrent with improvements in the available computer resources and increases in the collection of meteorological data. The objective of each modification has been to increase the precision of the simulation of a specific hydrologic sub-process for the improvement in the overall accuracy of the flow simulation. With each modification, importance was placed on minimizing the increase in complexity of the overall model. Constant revision of the model has improved accuracy of simulating longer term flows. Current research involves the use of WATFLOOD for watershed management and global climate research where simulation periods are much longer, from a few months to many years.

One of the greatest difficulties in event modelling is defining the initial state variables, such as soil moisture (Kouwen and Soulis, 1994). The amount of water from a precipitation event that contributes to groundwater and surface water flow is a function of the antecedent moisture conditions (Kouwen and Soulis, 1994). These conditions are directly related to the evapotranspiration that has occurred prior to the event (Shuttleworth, 1994). Originally, it was postulated that evapotranspiration was not an important component in modelling short-term events (Donald, 1992). Based on the philosophy behind the model, and in response to the need for simulating flows between rainfall events, a simplistic approach to estimate evapotranspiration was introduced into the model. The current objective of modelling an increasingly longer duration has created the requirement for a more rigorous method of simulating the evapotranspiration process.

As with any complex model all of the parameters are not necessarily independent. During calibration, the response, which is a function of changes made to one parameter, may be confounded with the effects of changes made to another parameter. For example, during a long-duration hydrologic simulation, an overestimate of the initial snow water equivalent could be compensated for by an overestimation of the evapotranspiration (Kouwen *et al.*, 1995).

The validity of the model and the calibration is proven by the accuracy of simulating separate events, be they temporally separate (on the same watershed during a different period) or spatially separate (on a watershed with similar physiography). Parametric responses that are confounded and improperly calibrated will become apparent in a good validation. In WATFLOOD, a more rigorous evapotranspiration model is required for the accurate calibration and simulation of periods of longer duration (Kouwen et al,. 1995).

Future research will utilize WATFLOOD to study changes in flow with respect to time as a result of changes in climate and land cover. A scientific basis for this research is essential. The method that WATFLOOD uses for estimating evapotranspiration losses must be refined in order to improve the soundness of the model.

The objective of this thesis is to incorporate a method into WATFLOOD that better estimates evapotranspiration in order to improve the accuracy of simulated long-term river flows. At the time of writing, this work was being paralleled by research being conducted with a coupled WATFLOOD/CLASS (Canadian Land Surface Scheme) model (Verseghy, 1991). The resulting model is to be imbedded in the Canadian Climate Centre's (CCC) Global Circulation Model (GCM). This simultaneous modification of WATFLOOD uses CLASS to model the vertical water budget, including the evapotranspiration and other hydrologic sub-processes. The research with CLASS involves the utilization of an extensive meteorological data set, simulated with the Mesoscale Compressible Community (MC^2) model (Tanguay, 1990).

CLASS, while being maximal in its scientific accuracy, is very complex in nature and hence, is better suited to a research environment. An objective in this thesis is to follow the original philosophy of WATFLOOD, which was developed for operational hydrology modelling applications. The new evapotranspiration model must model the natural processes while remaining useful to practitioners as a flood forecasting model. The data requirements of the evapotranspiration model must be readily met so that the model can be easily applied.

In order to determine the largest increase in the accuracy with a minimal increase in complexity, a number of models have been be reviewed, from which a few have been be selected for further study. The selected evapotranspiration models must be calibrated and validated to ensure the accuracy of the hydrologic and evapotranspiration simulations in the current research and in future work with WATFLOOD.

A second objective of this thesis is to provide a preliminary analysis of the results of the hydrometric data collected as part of the Boreal Ecosystem Atmosphere Study (BOREAS). The use of a water balance is an effective means of validating measurements of other components of the hydrologic cycle, particularly, the evapotranspiration losses. Evapotranspiration losses, measured as part of BOREAS, will be compared to the losses calculated from the hydrometric data that are used to calibrate the new modifications to WATFLOOD.

1.4 The Boreal Ecosystem Atmosphere Study

The data utilized for the evapotranspiration model calibration and validation have been collected as part of the BOREAS. The project was designed to study the interaction between the boreal forest biome and the atmosphere (Sellers *et al.*, 1994) by acquiring and analyzing data from a variety of ecosystemic and atmospheric processes. The acquisition of data focused on two study areas. Located on the southern fringe of the Boreal Forest region is the Southern Study Area (SSA), situated approximately 50km north of Prince Albert, Saskatchewan (Figure 1.1). A second segment of the boreal forest region, the northern study area (NSA), is located closer to the northern limits of the forest (approximately 40km west of Thompson, Manitoba).

Within each of these study areas a watershed and a number of sub-watersheds have been selected for a more detailed hydrologic study. In the NSA, a portion of the headwaters of the Sapochi River watershed (NSA watershed), with an area of approximately 470 km^2, was identified for study, as shown in Figure 1.2. The entire watershed is located within the Canadian Shield Physiographic Province. Surficial geology consists mainly of clays, with overlying soil depths varying from 0-17m. The basin is relatively flat, with local relief typically being less than 15m. As a result, large tracts of land are covered with bogs and fens. The exception to this is the existence of two kame deposits with local relief of up to 60m. Many small lakes and ponds exist within the basin (with average areas of approximately 40ha). Permafrost is also present within a few feet of the surface in some areas. Forested regions consist mainly of Black Spruce, with some stands of Jack Pine and small amounts of mixed deciduous in drier parts. Forest fires have occurred over the southern parts of the basin within the last one and a half decades. Logging operations have been non-existent in both the past and present.

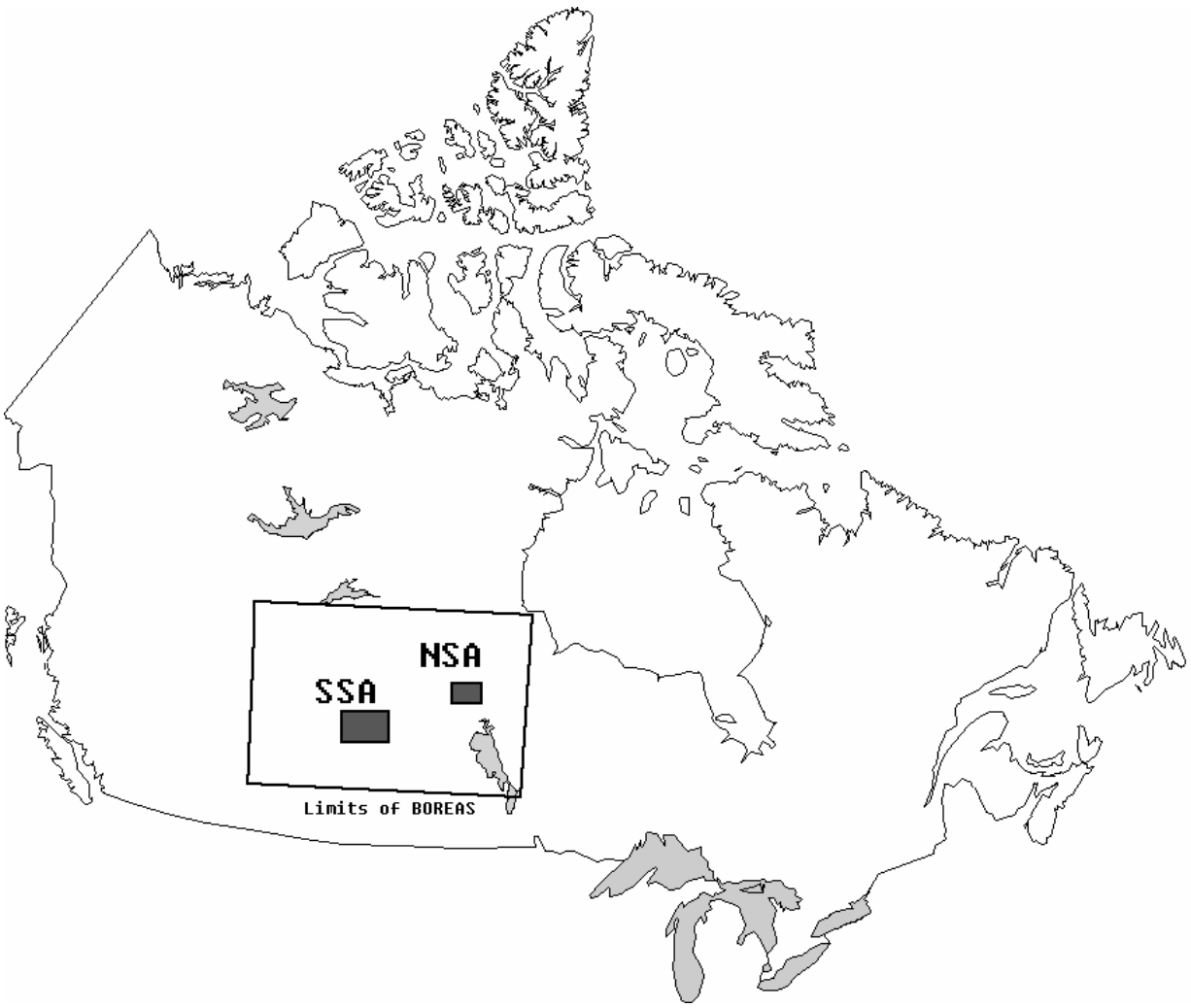

Figure 1.1: Location of BOREAS

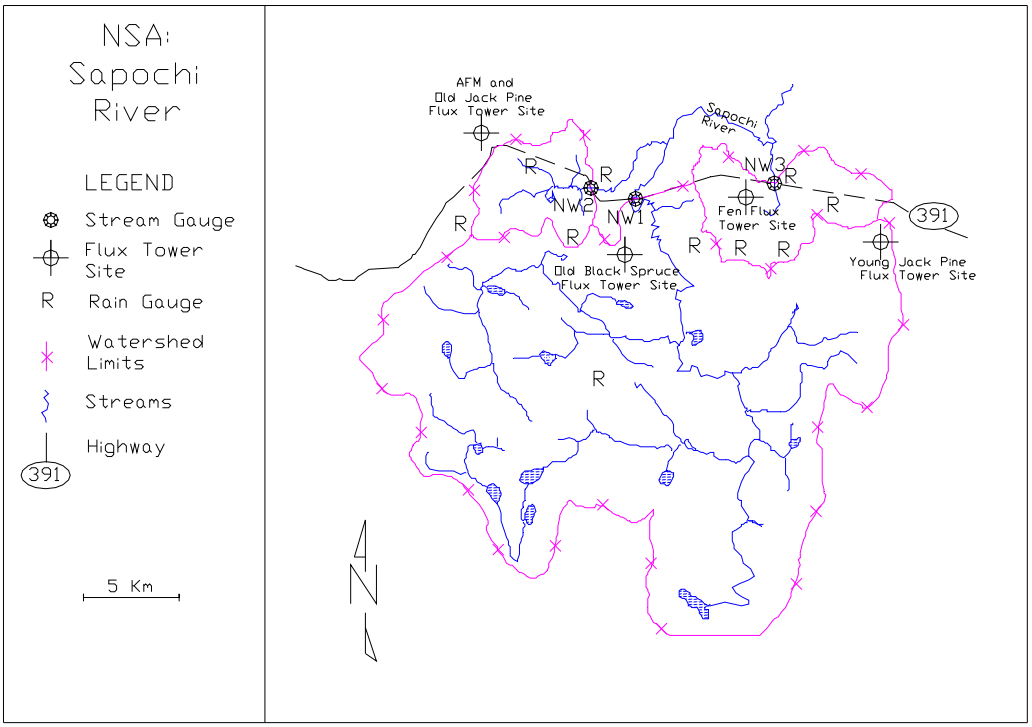

Figure 1.2: Sapochi River - NSA Watershed

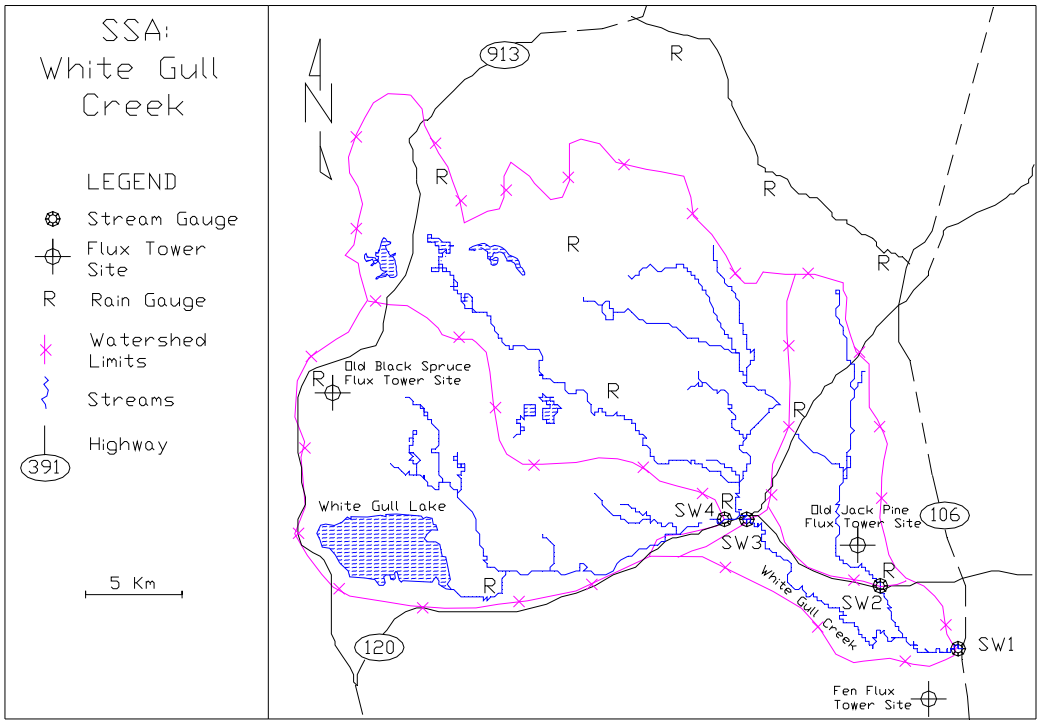

Figure 1.3: White Gull Creek - SSA Watershed

The sub-watersheds of the Sapochi River have gauging stations located at their outlets, labelled NW1, NW2, and NW3. Stations NW2 and NW3 are located at the intersections of two tributaries and Provincial Highway 391. The gauge at NW1 is located at the intersection of the Sapochi River's main channel and Highway 391. The NW1 gauge was operated by the Water Survey of Canada (WSC).

In the SSA, a section of the White Gull Creek watershed (SSA watershed) was chosen for a detailed study, having an approximate area of 610km^2, as shown in Figure 1.3. The entire SSA is located within the Saskatchewan Plains Region of the Great Plains Physiographic Province. Surficial geology consists of glacial tills and outwash materials ranging from 100m to 400m in thickness. The topography is a moderately rolling terrain of moraines and glacial till plains with local relief rising up to 300m, although within the watershed the relief differential is approximately 150m at its maximum. Treed regions consist of Aspen and Spruce in drier parts, Black Spruce and some Tamarack in poorly drained areas, and Jack Pine in well-drained sandy-soiled locations. Logging operations are currently taking place within some parts of the watershed. Forest fires have occurred in some of the northern sections within the last two decades. White Gull Lake (with an area of approximately 6.5km^2) lies in the south west corner of the basin, with many smaller lakes and ponds (with average areas of approximately 40ha) interspersed throughout the northern, western, and central portions of the watershed.

The basin upstream of White Gull Creek's intersection with Provincial Highway 106 has been divided into sub-basins. The outlet at highway 106 (labelled SW1) was gauged by the WSC. Upstream of the highway, a tributary to the main creek runs north and intersects a logging road. Two corrugated steel culverts provide a control to the flow for gauging station SW2 at this location. Gauging station SW3 is located at the intersection of the main channel with Provincial Highway 120. Approximately 2km upstream of this position is gauging station SW4. Between SW3 and SW4 is the confluence of a major tributary and White Gull Creek.

Both the NSA and the SSA watersheds have similar physiographic features. The areas were chosen for their location within BOREAS and the boreal forest biome. As a result, much of the vegetative cover is similar between the two basins with certain species being more dominant in each of the areas. Soils in the NSA tend to stay frozen longer as a result of colder average temperatures. In addition, some local areas of permafrost exist in the NSA. Even with warmer average temperatures in the SSA, some areas with thick insulating moss layers were found to be frozen during the month of June, in 1994 (personal field notes). The effects of logging in the SSA and past forest fires in the NSA are physiological factors differentiating the

two regions. Corresponding to the above description, shallow test pits indicated that the SSA is underlain by somewhat coarser soils than the NSA (personal field notes).

1.5 Preliminary Results from BOREAS (Sellers *et al.*, 1995)

Preliminary findings show that the boreal forest behaves like an arid landscape, particularly during the early growing season. The thick layer of moss covering the cool or frozen soils does not hold the precipitation, but allows the water to run off quickly. Incoming radiation is trapped by the thick vegetative canopies with very low albedo thereby transforming the energy into vast amounts of sensible heat. As a result, the plant physiology tends to have more control over the evapotranspiration process than the soil moisture. The factors most affecting evapotranspiration are the soil temperature in the spring, and the relative humidity and air temperature during the summer and fall.

Chapter 2
Literature Review

An improvement in the modelling of the evapotranspiration process in WATFLOOD is required to increase the accuracy of continuous long duration hydrologic simulations. Possible revisions include the modification of the existing process or the use of a different model. Various evapotranspiration models exist with different input data requirements. During the modification of the evapotranspiration sub-process in WATFLOOD, the relationship of evapotranspiration with the other hydrologic sub-processes must also be considered. The following literature review is relevant to the proposed modifications.

2.1 Processes of the Hydrologic Cycle

The general hydrologic processes that occur after precipitation reaches the earth's surface are interception, surface storage, evaporation, runoff, infiltration, transpiration, interflow, groundwater flow and groundwater discharge. Depending on the required accuracy of the simulation, all or some of these processes must be modelled. A simplified watershed model could consist of only the following three processes: precipitation, evapotranspiration and runoff. All other processes are simply a sub-process of either runoff or evapotranspiration that affect the timing of the runoff. The accuracy of the watershed simulation will increase with the accuracy and precision of the depiction of each process. If the evapotranspiration process is an important element in the local cycle, then the addition of an accurate depiction of this sub-process will increase the accuracy of the simulations, but at a cost to the simplicity of the model.

2.1.1 Precipitation

Precipitation is the primary input to the hydrologic system. The accuracy of the simulation will therefore be highly dependent of the accuracy of this input. Precipitation is typically measured at point locations. These measurements, which are sampled from minute areas, must be extrapolated to much larger areas in order to estimate the precipitation over a watershed. As with any extrapolation, the potential for introducing errors is present.

2.1.2 Evapotranspiration

Evapotranspiration, the combination of free-water evaporation and plant transpiration, is usually the largest loss component in rainfall-runoff modelling (Chiew and McMahon, 1991). It has been estimated that 60% of the mean global precipitation falling on the continents is lost from the surface through evapotranspiration (Brutsaert, 1986). To obtain a good understanding

of the hydrologic cycle it is necessary to recognize this component and obtain a reliable estimate of it (Morton, 1978, 1983). Increases in densely populated urban centres, the scarcity of water, and/or arid climate conditions will intensify the need for water. The consensus among researchers is that a comprehensive knowledge of the evapotranspiration process is required for effective management of water resources (Jones, 1991; Brutsaert, 1986), e.g. the operation of reservoirs for hydroelectricity, the development of canal works for irrigation purposes, and the accuracy of flood routing models for watershed planning and development.

As with precipitation, areal evapotranspiration is often estimated based on meteorological point observations. Depending on the homogeneity of the surrounding land cover, errors similar to those encountered in rainfall estimation may result from the extrapolation from point observations to produce areal estimates. Evapotranspiration is the combination of evaporation and transpiration losses.

2.1.2.1 Evaporation

Evaporation will occur from any body of water. It is the portion of water that is lost from surface storage. The scope of evaporation from surface storage includes those amounts of water lost from small puddles, ponds, lakes and flow channels, such as creeks and rivers, as well as from vegetated and bare soil surfaces.

2.1.2.2 Transpiration

Losses through transpiration are conducted by vegetation into the atmosphere. For modelling purposes, water is considered available for transpiration from the upper soil layer only.

2.1.3 Runoff

2.1.3.1 Surface Flow

Surface runoff is the only component of the hydrologic cycle that can be measured with a degree of certainty. The scope of overland flow includes "sheet flow" across open areas, to the routing of water in ditches, streams, and rivers. An accurate measure of basin outflow can be made by measuring the flow in any stable channel cross-section, provided that there is no significant groundwater flow, interflow or overland flow bypassing the measured section.

2.1.3.2 Interflow

Interflow is water that flows in the unsaturated zone, between the ground surface and the water table through macro-pores. Interflow is the portion of infiltrated water that is not taken up by

transpiration and emerges back to the surface water regime before it is able to percolate deeper into the groundwater regime.

2.1.3.3 Groundwater Flow

Water that is not removed from the surface through overland flow or evaporation and that is not eliminated from the top soil layer through transpiration or interflow drains into the groundwater regime. Water below the surface water regime has a very long residence time; this results in the damping of short-duration high-volume pulses before the water eventually emerges into the surface water system (Dingman, 1994). Groundwater flow is the source of surface water baseflow between precipitation events and during the winter months.

2.2 Physics of Evapotranspiration

2.2.1 Definitions

In the context of this thesis, the following terms are defined:

Evaporation is the transformation of liquid water, originating on the surface of water bodies, bare soil, or vegetation, into a vapour in the atmosphere.

Transpiration is the evaporation of liquid water from stomatal cavities in plants to the vegetal surface and then into the atmosphere.

Vapour Pressure is the partial pressure of water vapour in the atmosphere as defined by the Ideal Gas Law.

Saturated Vapour Pressure is the maximum vapour pressure for a specific temperature.

Latent Heat is the energy transferred during condensation (evaporation) to (from) the evaporating body out of (into) the atmosphere. In an evaporating body, the heat lost at the surface will be replaced by radiation from the atmosphere or advection from the lower layers of the water body.

Sensible Heat is the internal energy that is directly measurable in terms of temperature. The quantity of sensible heat per unit volume of air is linearly proportional to the difference between the measured temperature and some temperature reference datum (typically 0°C).

2.2.2 The Energy Balance

An analytical approach to determining the rate of evaporation is to measure the components of the energy budget. In order for the *Law of Conservation of Energy* to hold, in any closed system, the sum of the sources and sinks must be equal to the change in stored energy. By measuring all of the other sources and sinks and the change in stored energy, it is possible to deduce the energy used for evaporation (Latent Heat). Thus,

$$LE = K_n + L_n - H + G + A - P_s - \Delta Q, \qquad [1]$$

where all of the terms have the units of energy flux per unit area (W m^{-2}); LE is the Latent Heat flux, K_n is the net short-wave radiation, L_n is the net long-wave radiation, H is the sensible heat flux, G is the ground heat flux, A is the advection energy, P_s is the energy consumed by photosynthesis, and ΔQ is the change in the stored energy. A complete list of variables is shown in Appendix A.

2.2.2.1 Latent Heat (LE)

Latent heat is the energy that is utilized in the evaporative process in order to free the water molecules of their intramolecular bonds. The quantity of energy required to evaporate a unit mass of water is known as the latent heat of vaporization and is a function of the water temperature. The amount of water evaporated is calculated as the quotient of latent heat, and the product of the mass density of water and the latent heat of vaporization of water, where

$$E = \frac{LE}{\rho_w \cdot \lambda_v}, \qquad [2]$$

and E is the evaporation (mm s^{-1}), ρ_w is the mass density of water (kg m^3), and λ_v is the latent heat of vaporization (kJ kg^{-1}).

2.2.2.2 Net Short-Wave Radiation (K_n)

The net short-wave radiation is the incoming visible light that is trapped and can be converted into other forms of energy. The amount of light trapped is a function of the reflectivity of the material it is illuminating. That is

$$K_n = K_{in}(1 - a), \qquad [3]$$

where, K_{in} is the incoming short-wave radiation (W m^{-2}), which can be measured by a pyranometer or estimated empirically. Albedo, a, is a function of the angle of incidence of the incoming radiation to the reflecting material and the colour of the reflecting surface.

2.2.2.3 Net Long-Wave Radiation (L_n)

Similar to net short-wave radiation, net long-wave radiation is the amount of incoming long-wave electromagnetic energy that is trapped and can be converted to other forms of energy. All mass emits long-wave radiation. The sum of the incoming less the emitted and reflected equals the net long-wave radiation. This is given by

$$L_n = L_{at} - L_{aw}, \qquad [4]$$

where L_{at} is the incoming radiation, and L_w is the sum of the reflected and emitted radiation. Difficulties arise in the application of this equation since very few measurements of L_w and L_{at} are made. The Stefan-Boltzmann equation can be used to estimate $L_{n,}$:

$$L_n = \varepsilon_s \cdot \varepsilon_{at} \cdot \sigma\left(T_a + 273.15\right)^4 - \varepsilon_s \cdot \sigma\left(T_s + 273.15\right)^4, \qquad [5]$$

since the long-wave reflectivity of a surface is equal to 1.0 less the long-wave emissivity, where ε_s is the emissivity of the surface, ε_{at} is the atmospheric emissivity which (a function of cloud cover, humidity, and the concentration of pollutants), σ is the Stefan-Boltzmann constant (5.67×10^{-8} W m^{-2} day^{-1} K^{-4}), T_a is the air temperature (ºC), and T_s is the surface temperature (ºC).

2.2.2.4 Sensible Heat (H)

The sensible heat is the energy that affects the measurable temperature of the atmosphere. Energy is removed from the lower layers of the atmosphere by mixing it with the upper layers. Estimation of the sensible heat term (section 2.2.3.4) requires wind data, which are not always available. The use of the Bowen ratio (B) (section 2.2.3.6) to conveniently combine the sensible and latent heat terms into a single term eliminates the need for wind data and yields the following expression:

$$LE = \frac{\left(K_n + L_n + G + A - \Delta Q\right)}{\left(1 + B\right)}, \qquad [6]$$

where

$$B = H / LE \cdot \qquad [7]$$

2.2.2.5 Ground Heat Flux(G)

In many uses of the energy balance method, conduction to or from the underlying ground can be assumed to be negligible. Relative to the other terms in the balance, the energy conducted from the ground is small. Analyses have found the average ground heat flux to be about 5% of the daily energy budget (Munro, 1979). This term is higher in terrestrial energy budgets where vegetation is scarce. The magnitude of the ground heat flux is diurnally and annually sinusoidal. The affected depth is proportional to the length of the cycle. Ground heat flux can be estimated by the following mass balance equation:

$$G = \frac{c_s \cdot d_s \left(T_2 - T_1\right)}{\Delta t}, \qquad [8]$$

in which c_s is the specific heat capacity of the soil (for typical soils it is approximately 2.1×10^6 J m^{-3} $^oC^{-1}$), and T_1 and T_2 are the average temperature (^oC) of the depth of soil (d_s) in metres at the start and end of the time period (Δt) in seconds, respectively.

2.2.2.6 Advection (A)

Water

Advection energy may be considerable in the determination of evaporation from large bodies of water. A second energy balance of the body of water can be produced to evaluate the energy sources and sinks from rain, and groundwater and surface water flows.

Air

Energy may be added to or removed from a finite system by the movement of air horizontally across the systems boundaries. A sensible heat value that is higher or lower than that of the equilibrium value entering through the sides of a system would affect the latent heat flux rate and would constitute a source or sink to the above balance. Tests have shown that, in a region with homogeneous land cover, the horizontal energy flux has a negligible effect on the latent flux (Morton, 1975). As the size of the region decreases or the heterogeneity increases, the transportation of energy in the air mass through the sides of the system has increasing effects on the latent heat flux (Morton, 1975).

2.2.2.7 Photosynthetic Consumption (P_s)

The loss of energy strictly as a result of photosynthesis and plant respiration is usually considered to be negligible. Research suggests that an approximation of the loss can be made equal to 2% of the net radiation (Stewart and Thom, 1973).

2.2.2.8 Stored Energy (ΔQ)

The change in stored energy for a body of water can be determined using a mass balance approach. Problems exist with the requirements for large amounts of input data and accuracy of the balance. For typical land-based energy balances, the amount of energy stored in the biomass is negligible.

2.2.3 The Mechanics of Evaporation

The transfer of water from the layer of air just above the surface of a body into the atmosphere is governed by the laws of diffusion (Fick's Law). Fick's Law states that the rate of diffusion of a substance is proportional to the concentration gradient of that substance. Fick's Law in a differential form is shown as follows:

$$F_z(X) = -D_X \cdot {dC(X)}/{dz} \qquad [9]$$

The flux (F) of constituent X in the direction z is proportional to the change in concentration (C) of X per unit displacement in the direction z. The negative sign indicates that the flux occurs from high to low concentrations. The diffusivity (D_X) is the constant of proportionality.

The generalization of diffusion in Fick's Law is described more specifically for the evaporation of water by Dalton's theory, which states that the evaporation of a body of water is proportional to the vapour pressure differential between the surface and overlying air. The vapour pressure of the surface layer of air above a body of water is assumed to be at the saturated vapour pressure and is calculated as a function of the surface temperature by

$$E \propto \left(e_a - e_S(T_S)\right), \qquad [10]$$

where T_s is the surface temperature (°C), and e_a and e_s are the vapour pressures (kPa) in the air and at the surface, respectively.

2.2.3.1 Mechanical Diffusion

The resulting turbulence from the movement of air across a rough surface is an important mechanism for transporting moisture aloft (Shuttleworth, 1993). As a fluid travels along a solid surface, friction with the surface will cause the velocity of the fluid close to the boundary to be reduced. Because momentum is the product of mass and velocity, the momentum of air parcels is reduced as the distance to the surface decreases. Momentum must be continually transferred to the lower layers in order for the conservation of momentum to hold. The air currents which transfer this momentum are similarly responsible for the transportation of latent and sensible heat energy (Dingman, 1994).

The velocity profile of turbulent flows, known as the *Prandtl-von Karman Universal Velocity Distribution* for turbulent flows, is an empirical relationship between the flow velocity and the height above the surface boundary. The land surface-atmosphere boundary can be considered hydrodynamically rough (Jones, 1992), thereby inducing turbulent flow at the surface. The resulting velocity profile has been fitted to the Prandtl-von Karman logarithmic distribution. A finite difference form of the relation enables the velocity of the air (v_a) at a point above the surface (z_m) to be estimated based on a roughness height (z_0), the estimated height of zero velocity (referred to as the height of zero displacement (z_d), and an empirical constant (k_1)). Both the roughness height and the height of zero displacement have been found to be proportional to the vegetation height (Dingman, 1994) and must have consistent units. Therefore,

$$v_a = \frac{1}{k_1} \cdot u_* \cdot \ln\left(\frac{z_m - z_d}{z_0}\right), \qquad [11]$$

where v_a and the shear velocity (u_*) have the same units of length per time. An increase in vegetation height results in more turbulence at the ground level, and a velocity profile with a steeper gradient. The increased velocity gradient at the surface results in an increase in the momentum exchange and a corresponding increase in the latent and sensible heat exchanges. Thus, the atmospheric conductance of latent heat (the inverse of the atmospheric resistance) is directly proportional to the vegetation height.

2.2.3.2 Momentum Transfer

To describe momentum with respect to turbulent exchanges, a unit parcel of air can be considered to contain a certain amount of momentum (where the concentration of momentum is the product of the mass density of air and velocity):

$$F_z(M) = -D_M \cdot d(\rho_a \cdot v_a) / dz, \quad [12]$$

where $F_Z(M)$ is the flux of momentum in the z direction and represents the shear stress between adjacent horizontal layers of air (Dingman, 1994), D_M is the constant of diffusivity of momentum and ρ_a is the mass density of air (kg m^{-3}).

The shear stress (τ_0) exerted on the boundary by a turbulent flowing fluid can be estimated as a function of the velocity distribution (Keulegan, 1938). Keulegan notes that Prandtl termed the root of the ratio of boundary shear stress to the mass density of the fluid (ρ_f) as the shear velocity (u_*) which is also a function of the velocity distribution.

$$\left(\frac{\tau_0}{\rho_f}\right)^{1/2} = l \cdot dv_a / dz \left(\frac{\tau_0}{\tau}\right)^{1/2} = u_*, \quad [13]$$

where l is a characteristic length to which the distribution is related, dv/dz is the change in horizontal velocity with a change in height and τ is the stress at a point. The flux of momentum from the surface is related to the shear stress between the surface and the overlying layer (τ_0). That is,

$$F_z(M) = -\tau_0, \quad [14]$$

where the negative sign indicates a flux in the upward direction. By rearranging Prandtl-von Karman's shear velocity equation (as shown by Keulegan in equation 13), a definition of the momentum flux in the air is obtained as follows:

$$F_z(M) = -\tau_0 = -\rho_a \cdot u_*^2. \quad [15]$$

The ratio of equation [12] to equation [15] is equal to one. By assuming that the mass density of air is constant (a reasonable assumption across a short vertical distances), the following relationship is defined:

$$1 = \frac{u_*^2}{D_M \cdot dv_a / dz}. \quad [16]$$

This relationship is used for developing the aerodynamic coefficients for the latent and sensible heat transfers.

2.2.3.3 Latent Heat Transfer

The transfer of latent heat is the flux of water vapour, where ρ_v is the concentration of water vapour (mass of water per unit volume of air). According to Fick's Law, the flux of water vapour is found by the following equation:

$$F_z(WV) = -D_{WV} \cdot {}^{d\rho_v}\!/_{dz} = \rho_w \cdot E = {}^{LE}\!/_{\lambda_v}, \quad [17]$$

where D_{WV} is the diffusivity of water vapour ($m^2\ s^{-1}$) and $d\rho_v/dz$ is the rate of change in the mass density of water vapour in the air with respect to the distance above the ground surface ($kg\ m^{-3}\ m^{-1}$). There are 0.622 moles of water vapour per unit volume of air at the same partial pressure (the ratio of partial pressure to total pressure is e/P) according to the following relationship:

$$\rho_v = 0.622 \cdot \rho_a \cdot {}^{e}\!/_{P}, \quad [18]$$

where e is the vapour pressure (kPa), and P is the atmospheric pressure (kPa). Combining equations [17] and [18] and understanding that latent heat is equivalent to

$$LE = \lambda_v \cdot \rho_w \cdot E, \quad [19]$$

yields the following expression for latent heat flux:

$$LE = -D_{WV} \cdot \lambda_v \cdot 0.622 \cdot {}^{\rho_a}\!/_{P} \cdot {}^{de}\!/_{dz}. \quad [20]$$

Since the latent heat energy is diffused by the same turbulent air exchanges as momentum, the Prandtl-von Karman velocity profile is applicable. If the latent heat equation is multiplied by 1 (equation 16) a relation for the flux of latent heat results. The following gives it in a finite difference form:

$$LE = K_{LE} \cdot v_a \cdot (e_s - e_a), \quad [21]$$

where, K_{LE} is the mass transfer coefficient of latent heat which represents the efficiency of turbulent eddies in transporting water vapour vertically as shown below:

$$K_{LE} = {D_{WV}}/{D_M}\ \lambda_v \cdot 0.622 \cdot {\rho_a}/{P} \cdot \left\{ \frac{k_1}{\ln\left[\frac{(z_m - z_d)}{z_0}\right]} \right\}^2 . \qquad [22]$$

Evaporation

A similar relationship exists to describe evaporation, as

$$E = K_E \cdot v_a (e_s - e_a), \qquad [23]$$

where K_E is the mass transfer coefficient of evaporated water defined as

$$K_E = {D_{WV}}/{D_M} \cdot \frac{0.622 \cdot \rho_a}{\rho_w \cdot P} \cdot \left\{ \frac{k_1}{\ln\left[\frac{(z_m - z_d)}{z_0}\right]} \right\}^2 , \qquad [24]$$

since the latent heat flux can be described in the following way:

$$LE = E \cdot \lambda_v \cdot \rho_w . \qquad [25]$$

2.2.3.4 Sensible Heat Transfer

A finite difference relationship for the transfer of sensible heat also exists, since it is transported similarly to latent heat energy, so

$$H = K_H \cdot v_a (T_s - T_a), \qquad [26]$$

where T_s and T_a are the air temperatures (ºC) at the surface and the measurement height, respectively, and K_H is the mass transfer coefficient of sensible heat and is defined as follows:

$$K_H = D_H / D_M \; c_a \cdot \rho_a \left\{ \frac{k_1}{\ln\left[\frac{(z_m - z_d)}{z_0}\right]} \right\}^2 , \qquad [27]$$

where D_H is the diffusivity of sensible heat and c_a is the specific heat capacity of air (J $m^{-3o}C^{-1}$).

2.2.3.5 Atmospheric Stability

Adiabatic heating results from the compression of a parcel of air without any external inputs of heat energy (according to the Ideal Gas Law). The adiabatic lapse rate is the natural rate of decrease in air temperature with an increase in height above the earth's surface (due to the reduction in air pressure). The actual lapse rate is the actual decrease in air temperature with altitude. The adiabatic lapse rate may be greater than (stable), less than (unstable) or equal to (neutral) the actual lapse rate. Under stable conditions, air transported aloft by turbulent eddies undergoes adiabatic cooling; being cooler than the ambient air, it tends to sink back to the ground. Stable conditions are simulated by setting the ratio of D_H (D_{WV}) to D_M to a value greater than one. In unstable conditions, air transported aloft by turbulent eddies is warmer than the surrounding air and continues to rise, which is simulated by setting the ratio of D_H (D_{WV}) to D_M to a value less than one. Neutral conditions exist when the adiabatic and the actual lapse rates are simulated by setting the ratio of D_H (D_{WV}) to D_M equal to one.

2.2.3.6 The Bowen Ratio (B)

The Bowen ratio is the ratio of sensible (H) to latent heat flux (LE). Based on the mechanics of the latent heat and sensible heat transfer, the Bowen ratio in its expanded form is shown as follows:

$$B = \frac{D_H}{D_M} \cdot \frac{c_a \cdot P(T_s - T_a)}{\left[0.622 \cdot \lambda_v (e_s - e_a)\right]} . \qquad [28]$$

The assumption that D_H equals D_{WV} assumes that neutral atmospheric stability exists, and is usually valid (Dingman, 1994). The following expression is yielded for the Bowen Ratio:

$$B = \frac{c_a \cdot P(T_s - T_a)}{\left[0.622 \cdot \lambda_v (e_s - e_a)\right]} \qquad [29]$$

Using the Bowen ratio has the advantage of eliminating the need for wind speed data in the calculation of the velocity profile in the estimation of the sensible heat flux. The Bowen ratio can be described as the product of the ratio of the surface-air temperature difference to surface-air vapour pressure difference, and some value, namely

$$B = \frac{(T_s - T_a)}{(e_s - e_a)} \times \gamma \qquad [30]$$

This value is termed the psychrometric constant (γ) in kPa $^{o}C^{-1}$, where

$$\gamma = \frac{c_a \cdot P}{0.622 \cdot \lambda_v}, \qquad [31]$$

is approximately constant over short periods of time, varying only with pressure (a function of time and elevation) and with the value of the latent heat of vaporization (a function of temperature).

2.2.4 Mechanics of Interception Evaporation

Interception is the precipitation that is detained by the canopy. Interception loss, the water evaporated from intercepting surfaces, is a significant hydrologic process disposing of 25-55% of the annual rainfall (Johnson, 1990; Rowe, 1975,1979, 1983; Aldridge and Jackson, 1973; Pearce *et al.*, 1980). These interception losses were measured in mixed hardwood and evergreen forests where the lower percentages have been measured consistently in upland forests in the United Kingdom (Johnson, 1990).

The evaporation of intercepted water is driven by advection, and not radiant, energy (Pearce *et al.*, 1980; Iritz and Lindroth, 1994). A study of interception evaporation from an evergreen canopy showed that there was no significant difference between night-time and daytime interception evaporation rates. Night-time interception evaporation was measured as 40-50% of the total interception evaporation and 50-60% of the net interception evaporation (that which is in excess the amount that would have normally been transpired) (Pearce *et al.*, 1980).

From the perspective of moving air masses, tall vegetation is a rougher surface than short vegetation, resulting in more turbulent diffusion and consequently, a higher atmospheric conductance. However, forest vegetation tends to have a higher stomatal resistance, thereby making evapotranspiration rates similar to those of shorter field-type vegetation (Stewart and

Thom, 1973; Stewart, 1977). By eliminating the stomatal resistance, intercepted water is evaporated preferentially over water in the stomatal cavities. Wet vegetation will slow, if not completely preclude, transpiration. The net evapotranspiration from a stand of wet tall vegetation has been shown to be in excess of that from a dry canopy (Dingman, 1994). Consequently, the evaporation of intercepted water must be calculated separately from the transpiration (Munro, 1986). The rate of evaporation from interception storage in some environments may be up to three (Stewart, 1977) or five times (Stewart and Thom, 1973) the amount that would be evaporated normally through transpiration.

The aerodynamic roughness of short vegetation is much lower than that of forests. The atmospheric conductance of low vegetation is relatively unaffected by intercepted water (Stewart, 1977). The net addition of the interception losses to the total evapotranspiration loss from short vegetation is minimal (Dingman, 1994).

Interception loss is a function of the type of vegetation and the precipitation event. No throughfall was measured for storms with less than 1.0mm of precipitation in a hard beech forest (Aldridge and Jackson, 1973), and for 95 storms with gross rainfall of up to 2.7mm (Rowe, 1983). Of the storms studied by Rowe (1983), twelve events with gross rainfall measuring less than 1.0mm did have measurable rainfall, but were events of greater intensity and shorter duration. During the longer events, the interception storage was not filled because of concurrent evaporation.

Interception storage has been estimated with a number of different regressions between throughfall and gross rainfall. Studies have shown coniferous forests to have values of interception storage typically ranging from 1.5-2.0mm (Rowe, 1983). Linsley (1949) suggested a method for estimating interception to reproduce the vertical water budget in the canopy. The model describes the interception storage as a single reservoir that fills at an exponentially decaying rate (*i.e.* the first millimetre of storage is filled more quickly than the final millimetre for a given rainfall intensity). The exponent is a function of the amount of rain that has fallen since the beginning of the event. The maximum amount of intercepted precipitation is the sum of the maximum storage (h) and the total interception loss throughout the storm, so that

$$V = \left(h + C_P \cdot E_a \cdot t_R\right) \cdot \left(1 - e^{-k_2 \cdot P_i}\right), \qquad [32]$$

where V is the total volume of intercepted water per unit of projected area (mm m^2 m^{-2}), h is the storage capacity per unit projected area (a function of the leaf area index measured in mm m^2 m^{-2}), C_P is the ratio of the vegetal surface area to its projected area (the leaf area index), E_a is the evaporation rate per unit of surface area (mm m^2 m^{-2} hr^{-1}), t_R is the storm duration (hr), P_i is the sum of the precipitation per unit of projected area since the beginning of the storm (mm m^2 m^{-2}), and k_2 is the decay coefficient (mm^{-1} m^{-2} m^2). The decay coefficient is defined as follows:

$$k_2 = \left(h + C_P \cdot E_a \cdot t_R\right)^{-1} \qquad [33]$$

This relation evaluates interception in two distinct parts. First, the interception is the sum of the rain stored in the canopy and the amount of rain evaporated from interception storage during the storm. The second part of the relation establishes the rate of exponential decay as a function of the precipitation from the beginning of the storm and a constant which is equal to the inverse of the first bracket in the equation.

Rutter *et al.* (1971) proposed an accounting method for tracking the interception storage and interception loss for each time step in a hydrologic simulation. The model calculates the throughfall as the gross precipitation less the intercepted precipitation (calculated as some fraction of the gross precipitation from a regressed relationship). When the water on the canopy is greater than the maximum storage, it is reduced through drainage (according to an exponential decay function defined with regressed parameters), and evaporated at the Penman rate multiplied by the ratio of the canopy storage to maximum storage. When the canopy storage is less than the maximum storage, drainage is assumed to be zero and the evaporation rate is a fraction of the Penman rate, where the fraction is the ratio of the canopy storage to the maximum storage.

2.2.5 Mechanics of Transpiration

Plants obtain essential nutrients by absorbing them from solutions (ASCE, 1990). Soil water absorbed by roots contains dissolved minerals. Atmospheric gases, such as CO_2, are in solution in water open to the atmosphere, including the water molecules in stomatal cavities.

Transpiration is a physical not a metabolic process. Stomatal openings on the undersides of leaves release water vapour to the atmosphere. The translation of a molecule of water out of the stomatal cavity induces a vapour pressure gradient. This gradient drives the evaporation of a water molecule into the stomatal cavity from the leaf structure. The molecule in the leaf

structure is replaced by a molecule arriving from the plant's vascular system through capillary action (as a result of the induced moisture gradient). Movement of water molecules throughout the vascular structure of the plant is driven by the strong interactive hydrogen bonds between water molecules. Water removed from the roots is replaced by the absorption of water from the surrounding soil. The reduced water content of the soil in the root zone induces a driving gradient to replace that water through a Darcian-type of flow mechanism.

The number and size of stomatal openings directly affects water vapour conductance of a leaf. The size of the stomatal openings on a leaf can be varied by the plant, and is affected by environmental conditions. Different species react to differing amounts of stimulus. Most of these stomatal controls are the same or similar to the factors affecting free water evaporation, such as the following:

1. Light intensity (solar radiation),
2. Ambient CO_2 concentrations,
3. The leaf-air vapour pressure gradient,
4. The leaf temperature, and
5. The leaf water content.

The majority of the transpiration occurs during the daylight hours, when incoming radiation is at its maximum. As shown in some studies (Iritz and Lindroth, 1994), evaporation is not strictly a daytime phenomenon. In the Willow stand that Iritz and Lindroth studied, 4.1% of the average daily evapotranspiration occurred during the night. In their comparison with other researchers, values of up to 20% were reported. These values were observed under windy and dry conditions, when the mass transfer portion of the total evapotranspiration would be most significant.

2.3 Estimating Evapotranspiration

Estimates of the total evapotranspiration can be made separately for each of the two components (evaporation and transpiration) or as a combination of the components. Many hydrologic models require only a calculation of the combined total losses through evaporation and transpiration.

The methods for estimating evapotranspiration differ considerably, depending on their application. Estimates made for research purposes may involve complex theoretical formulae based on physical processes. Most practical models differ in the use of simpler formulae which require much less input data. These less complex relations usually have a theoretical

basis with empirical simplifications. Practical estimates of evapotranspiration often use a combination of two factors, a typical evapotranspiration rate multiplied by some coefficient.

Many different types of evapotranspiration models have been developed for use in specific conditions. Different models estimate the evapotranspiration based on characteristics such as the type of surface, availability of water, existence of stored energy, and the occurrence of water or air advection energy. Depending on the environment being modelled, certain terms in the energy budgets can be neglected. The discussion here will be limited to models that estimate evaporation and transpiration from water bodies and vegetated land masses, and models that estimate evaporation by indexing it to an estimate of the potential evapotranspiration.

The three different approaches taken for estimating evapotranspiration are as follows:

1. Analytical - measurements are made of the physical quantities in the energy or water budgets in order to deduce the evapotranspiration portion of the balance,
2. Theoretical - estimates are based on physical processes, and
3. Empirical - estimates are made by applying coefficients to some measure of water loss.

2.3.1 Analytical Methods

Direct measurements of evapotranspiration are difficult to make without affecting the factors that affect the process. Most analytical methods tend to evaluate the evaporation by measuring all of the other components of the budget. Typically, measures are made of flux rates in a closed system or measurements are integrated across an open system to obtain an estimate. The heat advection and storage terms in the energy and water budgets are difficult to evaluate, but the effects of these terms are minimized with the provision of estimates for longer averaging periods.

2.3.1.1 Water Budget

In this method a mass balance is completed for a control volume of water. The sum of the sources, less the sinks, less the change in storage is equated to the evapotranspiration as follows:

$$E = W + SW_{in} - SW_{out} + GW_{in} - GW_{out} - \Delta Q, \qquad [34]$$

where W is the incoming precipitation (mm m^2 m^{-2}), SW and GW are the surface water and groundwater flows, respectively, into and out of the control volume (mm m^2 m^{-2}), and ΔQ is the change in storage during the time integral of the balance (mm m^2 m^{-2}). It is a rare instance in which the above calculations can be carried out with accuracy because it is not feasible to measure all of the components. Estimates of areal precipitation are usually extrapolated from point observations. Although measurements of overland flows in defined channels can be made quite accurately, inaccuracies in the surface water term may arise from the estimation of non-channeled inputs. Net groundwater movements must be estimated from point observations of the phreatic surface, and estimates of the hydraulic conductivity and the saturated thickness. Inaccuracies in these estimates will directly affect the validity of the evaporation estimate. Errors in any of the sources and sink terms of the same magnitude as the evaporation will significantly affect the final accuracy of the estimate. Accuracy will increase with longer time integrals and larger areas by the averaging of errors.

This type of balance is more aptly produced for a watershed than a lake. Channeled overland flows are easily measured at a well positioned outlet. The outlet should be established in order to eliminate the problems associated with non-channeled overland flows and to minimize the possibilities of groundwater escaping the balance. To minimize the effects of groundwater storage, the time averaged year should begin during periods with similar levels of soil moisture. The result of the water balance is an average estimate of combined evapotranspiration for the watershed. This analytical method can be useful for the validation of other models.

Researchers have also shown that it is possible to use a confined acquifer to reproduce the water balance (Bardsley and Campbell, 1994). Generally, problems with groundwater seepage tend to create inaccuracies in evapotranspiration estimates when small basins are used for this type of balance.

2.3.1.2 Energy Budget

Similar to the water budget, the energy budget (equation 1) sums all of the energy sources and sinks and equates them to the change in storage. In large bodies of water, evaporation is influenced by changes in heat storage and advection within the water body which are functions of the physical characteristics of the lake. These terms are difficult to evaluate. Sinks due to photosynthesis are assumed to be negligible. The Bowen ratio is usually included to eliminate the requirement for sensible heat estimates. Dividing the energy terms (W m^{-2}) in the budget

(equation 6) by the mass density of water and the latent heat of vaporization provides the evaporation term (mm) explicitly as follows:

$$E = \frac{K_n + L_n + G + A - \Delta Q}{\rho_w \cdot \lambda_v (1 + B)} \qquad [35]$$

An underlying assumption of the energy budget in this form is that the air above the evaporating region exists in a local equilibrium; advection between neighbouring air masses is negligible at the regional scale. Depending on the environment being modelled, this approach can usually be simplified by assuming that both A and ΔQ are small. These assumptions become more applicable as the length of the time integral decreases, and are well suited for land energy balance applications. For land-based balances, the transpiration term again becomes relevant. Surface temperature data are scarce, making estimates of the Bowen ratio difficult.

As with the water balance method, the accuracy of the energy budget approach is improved with its application to longer periods of time. Periods in excess of seven days provide results with reasonable accuracy to a maximum of ±5% (Shuttleworth 1993). On average, the energy budget is in error by approximately 10 and 20% in the summer and winter months, respectively (Viessman *et al.*, 1989). Errors in the winter estimates can be attributed to difficulties in measuring ice reflected radiation, ice coverage, and ice surface temperature.

2.3.2 Theoretical Methods

2.3.2.1 Mass Transfer Techniques

Mass transfer techniques are based on the concept of the transfer of water vapour from the evaporating surface through turbulent air movement. There are many theoretical and empirical formulae which generally take the from of Dalton's Theory. The general form of the equation is shown below:

$$E = \left(b_0 + b_1 \cdot v_a\right)\left(e_s - e_a\right). \qquad [36]$$

The coefficients b_0 and b_1 are empirical and related to the height at which v_a is measured. In theory, b_0 approaches zero and b_1 approaches the value defined previously as K_E; many variations of the formula exist. A reasonable relationship has been developed from the momentum flux/Fick's Law mechanics of transfer equation by making the four following assumptions for a typical water body:

1. $D_{WV} = D_M$,
2. $k_1 = 0.4$,
3. $z_0 = 0.023$cm, and
4. $z_d = 0$ cm,

where z_0 and z_d are functions of wind velocity affecting wave heights, and using standard properties of mass density and pressure for air and water. Substitution into the equation for the evaporation constant yields a theoretical value for K_E of 1.26 x 10^{-4} (kPa^{-1}). The resulting estimate of evaporation is shown below:

$$E = 1.26 \times 10^{-4} v_a \left(e_s - e_a\right), \qquad [37]$$

where the measurement of e_a should be made in an area where equilibrium exists (far from the boundaries of land cover). Time averages of the surface temperatures should not be applied to obtain an estimate of vapour pressure, because vapour pressure is a non-linear function of temperature. It has been shown that the error is small for averages of less than one day. This approach is limited in its utility to a small number of water bodies where water surface temperature data are available.

Transpiration

Transpiration is similar to evaporation from a free-water surface, and is controlled by the same environmental variables. Evaporation is the product of an atmospheric constant, the atmospheric conductance, and some driving gradient. A mass transfer relationship describing evapotranspiration takes the same form as the mass transfer of water vapour.

$$ET = K_{ET} \cdot v_a \left(e_s - e_a\right), \qquad [38]$$

where K_{ET} is the mass transfer coefficient of evapotranspiration defined as

$$K_{ET} = {D_{WV}}/{D_M} \cdot \frac{0.622 \cdot \rho_a}{\rho_w \cdot P} \cdot \left\{ \frac{k_1}{\ln\left[\frac{\left(z_m - z_d\right)}{z_0}\right]} \right\}^2 . \qquad [39]$$

In analyzing the velocity distribution for vegetation, the following four assumptions are typical:

1. $z_d = 0.7\ z_{veg.}$,
2. $z_0 = 0.1\ z_{veg.}$,
3. $z_m = 2.0\text{m} + z_{veg.}$, and
4. $k_1 = 0.4$,

where $z_{veg.}$ is the vegetation height (m). For short vegetation, it can be assumed that D_{WV} is approximately equal to D_M. This assumption is not always valid for taller vegetation, which has an increased effective roughness resulting in increased turbulence.

2.3.2.2 Penman's Combination Energy-Mass Transfer Method

Penman combined the mass transfer method with the energy balance method to eliminate the need for surface temperature data required to analyze the sensible heat term. In the development of the equation, a finite difference estimate of sensible heat is used. The estimate is made by calculating the difference between the air and surface temperatures. The slope of the saturation-vapour pressure versus temperature curve, $s(T_a)$, is approximated by a finite difference relation (the difference in saturated vapour pressure between the surface and air over the difference in surface and air temperatures in kPa $^oC^{-1}$), and substituted into the estimate of sensible heat. The mass transfer relation for evaporation is a function of the differences in vapour pressure between the surface and the air. Penman substituted this relation into the energy balance equation (equation 6) to yield the following result:

$$E = \frac{\left[s\left(T_a\right)\right]\left(K_n + L_n\right) + \gamma \cdot K_E \cdot \rho_w \cdot \lambda_v \cdot v_a\left[e_s \cdot s\left(T_a\right)\right]\left(1 - w_a\right)}{\rho_w \cdot \lambda_v\left[s\left(T_a\right) + \gamma\right]}, \qquad [40]$$

where w_a is the relative humidity. It is assumed that the sensible heat, ground conducted heat and heat storage terms are negligible. In essence, the Penman combination equation defines evaporation as a weighted average of the net rates of radiation and the mass transfer of vapour. The mass transfer of vapour is a function of the difference between the actual and saturated vapour pressure of the air. The net radiation term is weighted with the slope of the saturation-vapour pressure versus temperature curve and the mass transfer term is weighted with the psychrometric constant:

$$E \propto \frac{\left\{s\left(T_a\right) \times \text{net radiation} + \gamma \times \text{mass transfer}\right\}}{\left\{s\left(T_a\right) + \gamma\right\}}. \qquad [41]$$

It should be noted that unless direct measurements of net long-wave radiation are available, surface temperature data are still required to estimate the net long-wave radiation. Kholer and Parmele (1967) developed a relationship in order to circumvent the need for surface temperature data. In the Penman-combination equation (equation 40), net long-wave radiation can be approximated by

$$L = \varepsilon_w \cdot L_{at} - \varepsilon_w \cdot \sigma\left(T_a + 273.15\right)^4, \quad [42]$$

with the substitution for γ of

$$\gamma + 4 \cdot \varepsilon_w \cdot \sigma \frac{\left(T_a + 273.15\right)^4}{K_E \cdot \rho_w \cdot \lambda_v \cdot v_a}. \quad [43]$$

Many other simplifications of the Penman combination equation have been developed by researchers. Linacre (1977) developed an empirical version of the model requiring only the average temperature, elevation, and latitude as input variables.

Analyses have shown that the equation provides a good approximation of actual evaporation for applications of at least one day. For this reason, and because of its underlying theoretical basis, the equation is widely used as a standard estimate of evaporation to which comparisons are made. The equation produces very reliable estimates for short crops, but is not strictly applicable to taller crops where the stomatal resistance is of increased importance (Calder, 1977).

Transpiration

In order to apply Penman's combination equation for free water evaporation to the transpiration process, Monteith (1965) modified it to include the canopy conductance. The mass transfer portion of the Penman combination equation can be considered as the product of a constant, a conductance, and the driving gradient, where

$$E = \text{atmospheric constant} \times \text{atmospheric conductance} \times \text{driving gradient}, \quad [44]$$

where the atmospheric constant is given by

$$\frac{0.622 \cdot \rho_a}{P \cdot \rho_w}, \quad [45]$$

the atmospheric conductance, C_{at}, is given by

$$v_a \left\{ \frac{k_1}{\ln\left[\frac{(z_m - z_d)}{z_0} \right]} \right\}^2 , \qquad [46]$$

and the driving gradient is

$$(e_s - e_a). \qquad [47]$$

The constant of proportionality and the atmospheric conductance are dependent on the wind velocity, atmospheric pressure, and other environmental factors.

Transpiration is a two stage process: evaporation from the stomatal cavity to the leaf surface, and evaporation from the leaf (canopy) surface into the atmosphere. The total resistance of resistors in series is the sum of the resistors (*Law of the Sum of Resistors*). Knowing that the conductance is the reciprocal of resistance, Monteith substituted the sum of the two reciprocal serial conductors (C_{at} atmospheric conductance and C_{can} canopy conductance) into the reciprocal of the atmospheric conductance to modify the Penman combination equation from

$$E = \left\{ \frac{\left[s(T_a) \right](K_n + L_n) + \gamma \cdot \rho_a \cdot c_a \cdot C_{at} \cdot \left[e_{sat}(T_a) \right](1 - w_a)}{\rho_w \cdot \lambda_v \left[s(T_a) + \gamma \right]} \right\} \qquad [48]$$

to

$$E = \left\{ \frac{\left[s(T_a) \right](K_n + L_n) + \gamma \cdot \rho_a \cdot c_a \cdot C_{at} \cdot \left[e_{sat}(T_a) \right](1 - w_a)}{\rho_w \cdot \lambda_v \left\{ s(T_a) + \gamma \left[1 + C_{at} / C_{can} \right] \right\}} \right\}, \qquad [49]$$

where $e_{sat}(T_a)$ is the saturation-vapour pressure at the air temperature. The conductance for transpiration provided by each leaf is in parallel to the conductance of every other leaf. The total of conductors in parallel is equal to the sum of the conductors. The conductance from an entire uniform canopy structure can be analogized to that of a single large leaf. The canopy conductance per unit ground area is calculated by multiplying the conductance per unit area of leaf (C_{leaf}) by the total leaf area per unit of area of ground, the Leaf Area Index (LAI):

$$C_{can} = LAI \cdot C_{leaf} . \qquad [50]$$

The leaf conductance is difficult to measure because it is constrained physiologically by the stomatal openings of the vegetation. Techniques have been postulated for computing the leaf resistance as a function of the factors that affect the plant physiology. These physiological parameters are significant in modelling forest transpiration (Sellers *et al.*, 1989). In recognizing this importance, physiological parameters play an important role in the evapotranspiration sub-processes of some complex models, such as the SiB (Simple Biosphere) model (Sellers *et al.*, 1986) and the CLASS model (Verseghy *et al.*, 1991). The correlation between observed and simulated conditions was improved with the inclusion of vegetal stomatal resistance factors in the latest version of CLASS (Verseghy *et al.*, 1991).

Some researchers have used calibrated values of leaf conductance to model the evapotranspiration process (Amiro, 1988), but the values were not transferable. Amiro (1988) found that the validation runs with subsequent years did not produce satisfactory results. It was postulated that the between year differences in soil moisture produced the erroneous simulations. It was concluded that the stomatal resistance was some function of the surface moisture, the canopy cover, and the physiological response to soil moisture (Amiro, 1988).

In a wet canopy, the C_{can} term approaches infinity, so that only C_{at} is effective. This is due to the increased evaporative potential of water on the surface of the leaves above that of water in the stomatal cavities. In this case, the Penman-Monteith equation reverts to the original form of the Penman combination equation for open water.

For land-based balances the change in heat storage of the biomass can be neglected. This is a reasonable assumption for a thickly vegetated canopy. Although, it is possible to include the ground heat conductance (G) with the short and long wave radiation terms as

$$K_n + L_n - G . \qquad [51]$$

2.3.3 Empirical Methods

Most empirical models apply some constant or coefficient to some measure of water loss. The most commonly used measure of water loss is the rate of potential evapotranspiration (PET) (Granger, 1989; Brutsaert, 1986). Two parts now exist in the estimation of actual

evapotranspiration (AET): a calculation of the potential evapotranspiration is required and some reduction of that potential must be made.

Two cases exist in which potential evapotranspiration can be used as a forcing function. The first definition of potential evapotranspiration (similar to Penman's definition) is the rate of evapotranspiration from an area that is saturated and so large that the effects of the evapotranspiration on the temperature and humidity are fully developed to the point of equilibrium. Conversely, the potential evapotranspiration can be used to describe the rate of evapotranspiration from saturated areas that are so small that the effects of evapotranspiration on the temperature and humidity of the atmosphere are negligible (Morton, 1978). As discussed by Granger (1989), a problem exists with the incongruities in the precise definition of potential evapotranspiration. Potential evapotranspiration, as defined by Penman, is the rate at which evapotranspiration would occur from a uniformly covered area of growing vegetation without advection or the storage of energy, if an unlimited supply of soil water was available. This is the definition of potential evapotranspiration used in this thesis. However, in the case where saturation does not exist, the precise Penman definition no longer holds, and theoretically, potential evapotranspiration should be increased.

As indicated by Granger (1989), Penman's definition and model is still helpful because it calculates a type of potential evapotranspiration which is based on the existing conditions. With the use of a separately defined value of potential evapotranspiration to estimate the potential under “wet” conditions, Granger (1989) postulated that actual evapotranspiration could be defined in terms of the two potential evapotranspiration values. Defining a relationship between the two potential evapotranspiration values and the actual evapotranspiration eliminates the need to represent the local soil-vegetation system with adjustment factors, or the use of some direct calibration index (Morton, 1975; Granger, 1989).

The potential evapotranspiration over an unsaturated region would be greater than the potential evapotranspiration if the region was saturated and under the same atmospheric conditions. This statement exposes the seemingly backward approach to obtaining the actual evapotranspiration as a function of potential evapotranspiration, when in actuality the potential evapotranspiration is the dependent variable (Morton, 1969). Morton's definition of potential evapotranspiration is identical to Penman's, except that Morton rejects the notion that when water supply is limiting, actual evapotranspiration is proportional to the potential evapotranspiration and some function of water supply (Nash, 1989). As would be expected,

both models provide similar estimates of the upper limit of evapotranspiration when water supply is not limiting (Chiew and McMahon, 1991).

2.3.3.1 The Complementary Relationship Between Actual Evapotranspiration and Potential Evapotranspiration

Bouchet (1963) defined potential evapotranspiration as the rate at which evaporation would occur with an abundant supply of water (identical to Penman's definition). Bouchet's definition differs from Penman's under conditions of limited supply. Under these conditions, Bouchet suggests that potential evapotranspiration is a negative index of actual evapotranspiration (Granger, 1989), known as the complementary relationship, whereas under these conditions the Penman potential evapotranspiration remains the same and the actual evapotranspiration is merely calculated as a fraction of the potential evapotranspiration. Bouchet (1963) suggested that feedback effects should be considered when estimating the actual evapotranspiration. It has been shown that the "oasis effect", the effect of an air current crossing a boundary between wet and dry surface conditions, reaches equilibrium very quickly. Researchers have shown that evapotranspiration reaches a steady state within 5 to 10 metres after crossing such a boundary (Shuttleworth, 1993). Tests conducted by Davenport and Hudson (1967) showed steady state conditions were achieved within 300 metres of the boundary. Both of these cases substantiate Bouchet's hypothesis by showing that there is a feedback in the evapotranspiration process that must be considered.

According to Bouchet's hypothesis, under steady atmospheric conditions and an abundant supply of water (soil moisture (θ) is greater than the field capacity (θ_{fc})), evapotranspiration occurs at the Penman rate. Eventually, the supply of water becomes partially depleted (θ is less than θ_{fc}), the rate of evapotranspiration is constrained by the soil moisture deficit, and excess energy is available beyond that required for evapotranspiration. This energy is transformed into sensible heat. The additional sensible heat changes the environmental conditions, thereby increasing the potential for evapotranspiration.

Algebraically, at a point when soil moisture is greater than the field capacity, the difference between the energy available for potential evapotranspiration (PET) and the energy used for the actual evapotranspiration (AET) is

$$PET - AET = Q. \qquad [52]$$

With the left over energy, Q, a new potential evapotranspiration rate, PET_{new}, would be that much larger than the original PET:

$$PET_{new} - PET = Q. \quad [53]$$

By equating these two relations (equations 52 and 53), the complementary relationship is defined as

$$AET = 2 \cdot PET - PET_{new}. \quad [54]$$

Morton (1978) developed Bouchet's hypothesis into a model that estimates the potential evapotranspiration (the wet environment areal evapotranspiration) using an empirical equation. The method of estimating potential evapotranspiration has since been modified by Morton to use a form based on the Priestley-Taylor equation (Morton, 1985). PET_{new} is the actual potential evapotranspiration under current equilibrium conditions, estimated by solving the energy balance and mass transfer equations simultaneously for the equilibrium potential evapotranspiration temperature. Morton (1985) also indicated that Penman's equation adequately estimates the PET_{new} since it is a function of the net radiation temperature, humidity and wind speed.

In the most empirical version of Morton's complementary relationship model only data inputs of temperature, humidity, and sunshine hours are required. Morton (1983) indicated that the values estimated for evapotranspiration by the complementary relationship are limited to a minimum averaging period of three to five days. This is a result of the inaccuracies produced by short-term subsurface heat storage changes and lag times associated with the heat and vapour storage in the atmosphere associated with the passage of frontal systems.

2.3.3.2 Temperature-Based Estimates of Potential Evapotranspiration

Temperature-based models represent the radiation and energy terms of the more theoretical relations simply with a measure of temperature. This may be a very rough approximation, but some of the relations have been shown to provide good estimates.

Hamon (1961)

Hamon developed the following equation for calculating potential evapotranspiration:

$$PET_H = 0.00138 \cdot D_{hr}^2 \left[\rho_{sat} \left(T_{avg} \right) \right], \quad [55]$$

where PET_H is the potential evapotranspiration (cm d^{-1}), D_{hr} is number of daylight hours in the day, $\rho_{sat}(T_a)$ is the saturation absolute humidity at the mean daily temperature (g m^{-3}), and $T_{avg.}$ is the average daytime temperature (ºC) since evapotranspiration is assumed to occur only during the daylight period. The equation produced excellent estimates of seasonal and annual averages for irrigated areas, (Hamon, 1961) and has been recommended where lack of radiation and other data prevents the use of more complex equations (Winter *et al.*, 1995). Hamon noted that the equation was developed for humid areas where the soil moisture was not limiting. In the case where soil moisture is limiting (or in an arid region), Hamon noted that the potential evapotranspiration would be higher. It was suggested that if the soil moisture was limiting then the actual evapotranspiration would be proportional to the soil moisture.

Malmstrom (1969)

Malmstrom developed a similar equation:

$$PET_M = 0.409\left[e_{sat}\left(T_{avg.m}\right)\right], \qquad [56]$$

where PET_M is the potential evapotranspiration (cm $month^{-1}$), e_{sat} is the saturated vapour pressure (mb), and $T_{avg.m}$ are the mean monthly temperatures (ºC). Estimates made by these models are much improved by averaging rates over longer periods of time.

Hargreaves Equation

The Hargreaves model is empirical in nature and with some recent modifications (Hargreaves and Samani, 1982) takes the form:

$$PET = 0.0075 \cdot R_a \cdot C_t \cdot \delta_t^{1/2} \cdot T_{avg.d}, \qquad [57]$$

where PET is the potential evapotranspiration rate (mm d^{-1}), R_a is the total incoming extraterrestrial solar radiation (in the same units as evaporation), C_t is a temperature reduction coefficient which is a function of relative humidity, δ_t is the difference between the mean monthly maximum and mean monthly minimum temperatures (°C), and $T_{avg.d}$ is the mean daily temperature (°C). A relationship between the temperature reduction coefficient and the relative humidity has been regressed from measurements made at 18 locations in the United States to account for the reduction in potential evapotranspiration with increased relative humidity.

$$C_t = 0.035(1.00 - w_a)^{1/3} \quad w_a \geq 0.54$$
$$C_t = 0.125 \quad w_a < 0.54 \qquad [58]$$

The following empirical simplifications permit the use the formula with the sole input of temperature data, latitude (ϕ in degrees), and the Julian day (J), by using the following relationships to estimate incoming solar energy (Shuttleworth, 1993):

$$R_a = 15.392 \cdot d_r \left(w_s \cdot \sin\phi \cdot \sin\delta + \cos\phi \cdot \cos\delta \cdot \sin w_s \right), \qquad [59]$$

where d_r is the relative distance between the earth and the sun given by

$$d_r = 1 + 0.033 \cdot \cos\left(\frac{2\pi \cdot J}{365} \right), \qquad [60]$$

δ is the solar declination (radians) defined by

$$\delta = 0.4093 \cdot \sin\left(\frac{2\pi \cdot J}{365} \right) - 1.405, \qquad [61]$$

and w_s is the sunset hour angle (radians) given by

$$w_s = \arccos\left(-\tan\phi \cdot \tan\delta \right). \qquad [62]$$

With these modifications, the equation is more universally applicable, as it does not require the observed solar input.

A number of independent investigations have compared the estimates of evapotranspiration from different models. The Hargreaves equation consistently produces accurate estimates of potential evapotranspiration (as measured using energy balance techniques, the Penman combination equation, or lysimetric observations), and in some cases, much better than estimates made using other methods (Hargreaves and Samani, 1982; Mohan, 1991; Saeed, 1986). Mohan found the Hargreaves equation to have a high correlation with the Penman combination equation for estimates of average weekly evapotranspiration in humid regions.

The reason for the success with such an empirical model is because of the theory which it reflects. In a comparison with the Penman combination equation, the model considers the following: the incoming solar energy (R_a), the average amount of energy removed in the form

of sensible heat from the amount available for evaporation (δ_t), an approximation of the ratio of $s(T_a)$ to the sum of $s(T_a)$ and γ by using the temperature (T), and a reduction in the driving gradient when the vapour pressure deficit is small (C_t).

Linacre Model

The Linacre model, a vast simplification of the Penman equation, requires inputs of temperature, latitude, and elevation. Empirical relationships are used to estimate net radiation (as a function of temperature) and other variables in the Penman formula (ground heat conduction is neglected). It has been shown that once the model with these simplifications has been calibrated, it provides a viable method for estimating daily evapotranspiration (Hope and Evans, 1992). It was concluded that further studies should be employed to compare the simplified model with other temperature-based models

Turc Model

A number of different forms of the Turc equation (Turc, 1961) have been utilized in a variety of different experiments (Saeed, 1986; Silvestri *et al.*, 1990; Turc, 1972). The data requirements of each of the forms are temperature, and solar radiation; as well, the relative humidity is used as a reduction factor. Turc provides the following estimates of potential evapotranspiration (mm 10days^{-1}):

$$\begin{aligned} PET &= 0.13\left[\frac{T}{T+15}\right]\left(R_a + 50\right) && w_a < 0.50 \\ PET &= 0.13\left[\frac{T}{T+15}\right]\left(R_a + 50\right)\left[\frac{1.20 - w_a}{0.70}\right] && w_a \geq 0.50 \end{aligned} \quad . \qquad [63]$$

For a 10 day period, T is the average temperature, R_a is the total incoming extraterrestrial radiation (as the equivalent depth of evaporated water in mm/10days), and w_a is the average relative humidity. The incoming solar radiation can be estimated using equations [59] to [62] any from any number of empirical techniques. This simplification makes the equation temperature-dependent only. In a comparison of evapotranspiration models, the Turc equation was shown to provide good estimates of potential evapotranspiration (Saeed, 1986).

2.3.3.3 Radiation Based Estimates of Potential Evapotranspiration

The Priestley-Taylor model (Priestley and Taylor, 1972) is a modification of Penman's more theoretical equation. Used in areas of low moisture stress, the two equations have produced estimates within ± 5% of each other (Shuttleworth and Calder, 1979). An empirical

approximation of the Penman combination equation (equation 40) is made by the Priestley-Taylor to eliminate the need for input data other than radiation. The adequacy of the assumptions made in the Priestley-Taylor equation has been validated by a review of 30 water balance studies in which it was commonly found that, in vegetated areas with no water deficit or very small deficits, approximately 95% of the annual evaporative demand was supplied by radiation (Stagnitti *et al.*, 1989).

It is reasoned that under ideal conditions evapotranspiration would eventually attain a rate of equilibrium for an air mass moving across a vegetation layer with an abundant supply of water; the air mass would become saturated and the actual rate of evapotranspiration would be equal to the Penman rate of potential evapotranspiration. Under these conditions evapotranspiration is referred to as equilibrium potential evapotranspiration (PET_{eq}). The mass transfer term in the Penman combination equation (the second half of equation 40) approaches zero and the radiation terms dominate. Priestley and Taylor (1972) found that the actual evapotranspiration from well watered vegetation was generally higher than the equilibrium potential rate and could be estimated by multiplying the PET_{eq} by a factor (α) equal to 1.26:

$$PET = \alpha \frac{s(T_a)}{s(T_a) + \gamma} (K_n + L_n) \cdot \frac{1}{\rho_w \lambda_v}, \qquad [64]$$

Although the value of α may vary throughout the day (Munro, 1979), there is general agreement that a daily average value of 1.26 is applicable in humid climates (DeBruin and Keuijman, 1979; Stewart and Rouse, 1976; Shuttleworth and Calder, 1979), and temperate hardwood swamps (Munro, 1979). Morton (1983) notes that the value of 1.26, estimated by Priestley and Taylor, was developed using data from both moist vegetated and water surfaces. It has been recommended that the value be increased slightly to 1.32 for estimates from vegetated areas as a result of the increase in surface roughness (Morton, 1983; Brutsaert and Stricker, 1979). Generally, the coefficient α for an expansive saturated surface is usually greater than 1.0. This means that true equilibrium potential evapotranspiration rarely occurs; there is always some component of advection energy that increases the actual evapotranspiration. Higher values of α, ranging up to 1.74, have been recommended for estimating potential evapotranspiration in more arid regions (ASCE, 1990).

The α coefficient may also have a seasonal variation (DeBruin and Keuijman, 1979), depending on the climate being modelled. The study by DeBruin and Keuijman indicated a variation in α with minimum values occurring during the mid-summer when radiation inputs

were at their peaks, and maximums during the spring and autumn (winter values were not determined), when in relation to advective effects, radiation inputs were large. The equation has performed very well, not only for open water bodies, but also for vegetated regions. The satisfactory performance of the equation is probably because the incoming solar radiation has some influence on both the physiological and the meteorological controls of evapotranspiration.

Priestley and Taylor (1972) indicated that use of the model should be constrained to relatively advection-free conditions. Reasonable estimates using the Priestley-Taylor equation have been provided for homogeneous areas of vegetation (3-4km^2). DeBruin and Keuijman (1979) concluded that the model was valid for all shallow lakes regardless of their size.

The equation developed for estimating average daily evapotranspiration can produce estimates with an error of ± 5%, but has also provided reasonably good estimates of half-hourly evapotranspiration (Stewart and Rouse, 1976). Monthly average estimates produced by the equation have compared well to values calculated using the energy budget (Winter *et al.*, 1995).

2.3.3.4 The Penman Combination Method Estimates of Potential Evapotranspiration

The Penman combination equation provides very accurate estimates of potential evapotranspiration in saturated conditions, particularly with short vegetation, and is frequently used as the standard to which other models are compared. With the use of the Monteith modification, the inclusion of a value for canopy resistance, the combination model is useful for estimating the actual evapotranspiration in arid regions (Lemeur and Zhang, 1990).

2.3.3.5 Indexing actual evapotranspiration to potential evapotranspiration

In the case where surface conditions are not saturated, the actual rate of evapotranspiration will not be the same as the potential rate. The potential evapotranspiration must be reduced by some amount to estimate the actual evapotranspiration. Different factors have be used as an index.

Soil Moisture

Actual evapotranspiration can be estimated as a function of the potential evapotranspiration and the soil moisture. Priestley and Taylor (1972) stated that a measure of soil moisture must be made in order to understand the relationship between actual and potential evapotranspiration, as shown by

$$AET = f(\theta) \cdot PET\,, \qquad [65]$$

where θ is the soil moisture (%). The soil moisture deficit has been used as an index to limit the actual evapotranspiration in many hydrologic models: HBV/Pulse (Bergstrom *et al.*, 1985) models, Broughton Model (Broughton, 1966,1968), and HYDROLOG (Porter and McMahon, 1971, 1976; Arp and Yin, 1992). The most common form of the soil moisture function constraining actual transpiration rates is based on the soil moisture deficit or relative water content (θ_{rel}), given by

$$f(\theta_{rel}) = \frac{\theta - \theta_{pwp}}{\theta_{fc} - \theta_{pwp}}\,, \qquad [66]$$

where θ_{pwp} and θ_{fc} are the permanent wilting point and field capacity soil water contents, respectively.

As a generalization, Spittlehouse (1989) suggested that the soil moisture could be assumed to limit evapotranspiration when PET is greater than 4mm d^{-1}, and the ratio of the difference between θ and θ_{pwp},, and θ_{fc} and θ_{pwp} is less than 0.3. This form of relative water content is similar to the form used in the simplified Denmead and Shaw relationship (1962) in which the soil moisture function is a ratio of the actual soil moisture to a parameter representing the soil moisture capacity.

In the study by Spittlehouse (1989), a model was proposed that estimated the actual evapotranspiration as the lesser of the potential evapotranspiration and the limiting evapotranspiration, and defined as a function of the soil moisture. The potential evapotranspiration was calculated as the Priestley-Taylor evapotranspiration with a locally calibrated value for the α coefficient. The limiting evapotranspiration was calculated as a linear function between zero and the potential evapotranspiration as the product of the soil moisture deficit, and a regressed coefficient. In order to fully define the soil moisture deficit relationship, the full range of soil moisture values, with upper and lower limits corresponding to actual evapotranspiration equal to the potential evapotranspiration, and actual evapotranspiration equal to zero, were utilized.

Arp and Yin (1992) limit the actual evapotranspiration to the lesser of the potential evapotranspiration and the proportion of soil moisture above the permanent wilting point if the value is less than the potential evapotranspiration and the soil moisture is less than the field

capacity. The permanent wilting point and field capacity soil moistures are estimated using a relationship between volumetric clay fraction and volumetric water fraction, based on studies completed by Forbes (1955) and Brady (1990).

Methods of calculating actual evapotranspiration as a function of soil moisture are readily suited to hydrologic applications since there are many good accounting methods for tracking infiltration.

Temperature

Low air temperatures have been shown to limit plant growth, where a reduction in temperature below 5 degrees Celsius will halt the growth. Low soil temperatures have also been shown to limit evapotranspiration (Turner and Jarvis, 1975). Anderson (1992) used a function of measured air temperature to reflect the soil temperature, and indexed the actual to the potential evapotranspiration. Some different functions of the air temperature were tested. One of the methods accumulated the number of days that the temperature rose above the threshold value of 5 degrees Celsius. The index used to reduce the potential evapotranspiration to the actual evapotranspiration was set at 0 until 5 days had accumulated. The function varied linearly to a value of 1.0 after 28 days had accumulated. Another model that was tested was based on the Thornthwaite equation, which incorporates long time-averages of temperature and potential evapotranspiration, shown as

$$PET = \left(1 + C_2\left(T - T_{avg.m}\right)\right)PET_{avg.m} \qquad \text{for } 0 < PET < 2 \cdot PET_{avg.m}, \quad [67]$$

where C_2 is a calibrated coefficient, T is the air temperature, and $T_{avg.m}$ and $PET_{avg.m}$ are the long-term monthly averages of temperature and potential evapotranspiration, respectively. This last model provided the largest, though only a marginal, improvement to the model simulations.

The input variable temperature is more accurately interpolated spatially than variables such as wind speed or radiation (Anderson, 1992). This is the reason why index models based on temperature (e.g. snowmelt models) generally produce good results; wind speed and radiation variables are more likely to have locally extreme values than temperature. Spatially stable variables are recommended for use in the development of empirical relations to relate actual evapotranspiration to potential evapotranspiration (Anderson, 1992).

The potential transpiration of a mountain grassland was estimated using the Penman combination equation with different models to index the rate to the actual transpiration (Wright and Harding, 1993). During the early (cooler) part of the year when the grass was dormant, the Penman equation overestimated the transpiration. A linear equation was used to index the transpiration as a fraction (between 0 and 1.0) of the potential transpiration, varying between a minimum and a maximum threshold temperature. The model that produced the best approximation provided for the optimization of both threshold temperatures. Because of the vegetation type studied in this experiment, ground surface temperatures were utilized. The researchers concluded that indexing, based on reduced temperatures, is useful in estimating actual transpiration.

Biomass

Evapotranspiration from common types of agricultural vegetation has been thoroughly investigated. The abundance of information surrounding these crops enables the development and application of seasonal factors as an indexing method to incorporate the effects of the growth stage on the actual evapotranspiration rate. Usually, these factors would be applied to the potential evapotranspiration rate in conjunction with a soil water restriction function. CLASS is another example of a model which utilizes seasonally varied canopy parameters (Verseghy *et al.*, 1991).

In the mountain grassland experiment (Wright and Harding, 1993), another indexing method was tested. The method utilized a simple sinusoidal function of the time of year to reduce the potential transpiration. The researchers concluded that the sine function was not the best curve to fit the actual relationship, and that some function based on actual biomass measurements would have produced better results.

2.3.3.6 Direct Measurements of Evapotranspiration - Atmometers

An atmometer is defined by Livingstone (1935) as an instrument measuring evapotranspiration where there is an unlimited water supply. The rate of evaporation is related to the vapour pressure deficit near the surface which is a function of the circulation, the radiated energy, and other factors. Atmometers incorporate all of these factors into a single measurement (the loss of water).

Evaporation Pans

The most common method for measuring evaporation directly is through the use of an Evaporation Pan. A simple water balance is maintained for a cylindrical reservoir open to the atmosphere:

$$E = W - \left(Volume_2 - Volume_1\right). \qquad [68]$$

Pan evaporation is considered to be the amount of evaporation that would occur if the source of moisture was unlimited. Evaporation pans are free-water surfaces which are physically similar to natural bodies of water being modelled. Good approximations of evaporation can be provided when the pans are located in an environment which resembles the lake environment being simulated.

Errors occur because of the reduced heat capacity of the pan in comparison to that of the larger bodies of water being emulated. Evaporation estimates are elevated during the warmer seasons when the average water temperature in the pan is relatively high compared to that of the larger local bodies of water, and reduced during the cooler seasons when the average water temperature is relatively low. Errors are further introduced by the conduction of stored heat energy through the sides of the pan. Similar to lakes and large bodies of water, the energy conducted through the bottom surface of pans is considered to be negligible. Evaporation pan measurements are most accurate for providing estimates of average annual potential evaporation from bodies of open water by averaging out individual seasonal errors. A simple reduction factor can be applied to reduce the potential evapotranspiration estimated by the evaporation pan to the actual evapotranspiration. For the temperate regions of North America, this factor is approximately 0.7 (Dingman, 1993).

Bellani Plate Atmometers

This type of instrument incorporates the factors affecting transpiration from plants by attempting to simulate the actual structure and physical process. The evaporating surface is a porous ceramic plate permitting the transmittance of water and simulating of the stomatal resistance. Covered by a green canvas, it provides a similar albedo and surface texture. The ceramic bowl has a small volume and therefore a small heat capacity, such as a leaf. The reservoir is drained through capillary action similar to water being drawn through a plant's vascular system.

Bellani plate atmometers have been shown to provide accurate estimates of potential evapotranspiration for short vegetation and crops (Fontaine and Todd, 1993). Estimates from the atmometers were about 0.71 of the estimates provided by independent evaporation pan observations in the study. This provides further proof of the instrument's accuracy since evaporation pans typically have reduction coefficients of about 0.70. The study was inconclusive with regards to the effectiveness of the instrument in estimating potential evapotranspiration from taller vegetation.

2.3.3.7 Evapotranspiration from Forests

Evapotranspiration rates from forests have not been as exhaustively studied as those rates from agricultural areas. The evaporation rate from forests can be significantly increased when the interception storage is at least partially filled (Shuttleworth and Calder, 1979; Lindroth, 1993). In comparison to low vegetation and water bodies, forests tend to have a higher stomatal resistance, possibly in compensation for the higher atmospheric conductance. These characteristics result in lower evapotranspiration rates during dry conditions, and higher rates after precipitation events.

The use of some equations for estimating potential evapotranspiration (such as the Priestley-Taylor equation) to model the actual evapotranspiration from forests should be used with discretion (Shuttleworth and Calder, 1979). Shuttleworth and Calder noted that the primary control on evapotranspiration was the vegetation surface wetness where the Priestley-Taylor value of potential evapotranspiration could easily be exceeded with a wet canopy. In contrast, the actual evapotranspiration is less than the potential evapotranspiration for conditions when there was no interception storage, even during periods with no soil moisture deficit. An approximation of these conditions is

$$AET_{forest} = Transpiration + Interception\ Evaporation, \qquad [69]$$

or

$$AET_{forest} = (0.72 \pm 0.07) \cdot PET_{forest} + \alpha_{storage}, \qquad [70]$$

where $\alpha_{storage}$ is some function of interception storage (Shuttleworth and Calder 1979). Values similar to these coefficients (0.72 and 0.07) have been calculated in other studies, with estimates ranging from 0.6 to 1.05 and a tolerances of ± 0.10, for Douglas Fir stands of varying ages (Price, 1987; Black *et al.*, 1984; Giles *et al.*, 1985; Spittlehouse and Black, 1981; McNaughton and Black, 1973).

Researchers have shown that, when locally calibrated, the Priestley-Taylor function provides good estimates of potential evapotranspiration from forested areas where a soil moisture deficit does not exist (Stagnitti *et al.*, 1989); 14% of the site on which this research was conducted was covered in standing water, and local conditions precluded advective effects. Under conditions of extreme moisture stress on the vegetation ($\theta \leq \theta_{pwp}$), evapotranspiration has been estimated at approximately 60% of the equivalent net radiation (Stagnitti, 1989):

$$AET_{forest} = 0.60 \cdot \left(K_n + L_n\right) \cdot \frac{1}{\rho_w \lambda_v}, \qquad [71]$$

Physiological factors constrain the rate of evapotranspiration in regions under moisture stress (Shuttleworth and Calder, 1979), and therefore, a reduction should be made as some function of these constraints. In the absence of wind and advective conditions, functions of plant physiology, such as those used in the calculation of the canopy resistance for Penman-Monteith equation, control the transpiration (Stagnitti *et al.*, 1989). Physiological controls, such as the vapour pressure deficit, and implicit controls such as temperature have some dependence on net radiation and are reflected in a radiation based model.

Munro (1986) concluded that using the Priestley-Taylor equation with an α value of 1.26 for a wet canopy and 1.0 for a dry canopy in forested wetlands is appropriate, provided that there is knowledge of the wetness of the canopy and that the value is not necessarily fixed for an entire day. Proviso was given against the general assumption that evapotranspiration from forest wetlands occurs at the potential rate.

2.4 Modelling Evapotranspiration

2.4.1 Operational Models

In many rainfall-runoff models, an estimate of the potential evapotranspiration is used as an estimate of the actual evapotranspiration. These approximations are frequently equated to published mean monthly evaporation pan estimates or long-term averages of actual evapotranspiration. This is a very simplistic approach used to approximate this complicated process.

2.4.1.1 Monthly Water Balance Methods

An accounting method for keeping a monthly balance of the water budget was developed by Thornthwaite and Mather (1955). The actual evapotranspiration is taken as the minimum of two values. If the precipitation is greater than the potential evapotranspiration, then

evapotranspiration occurs at the potential rate, otherwise, the evapotranspiration rate is a function of the soil moisture deficit which is calculated as a function of the monthly potential evapotranspiration deficit (the difference between the potential evapotranspiration and the precipitation).

2.4.1.2 Average Monthly Evaporation

Some hydrologic models maintain a very simple method for estimating evapotranspiration losses. Standard values of average monthly evapotranspiration estimated using the Penman combination model, as in the HBV/Pulse model (Bergstrom, 1985), or from published average values as in WATFLOOD are applied to the required time intervals. Utilizing values of the long-term average evapotranspiration rate can lead to systematic errors during periods of atypical meteorological conditions. As the size of the basin being studied decreases and the period of anomalous meteorological conditions increases, the adverse effects on the hydrologic simulation become more pronounced. Uncharacteristically low air temperatures and low total hours of sunshine affected the HBV/Pulse model simulations in this way (Anderson, 1992).

2.4.2 Research Models

The operational models discussed above do not attempt to precisely characterize the stomatal resistance. The stimuli affecting the stomatal openings differ somewhat from those governing evaporation from and open water surface. The degree of added complexity to accurately model the stomatal response to the environment is significant.

In a research environment, evapotranspiration models tend to evolve from more elaborate experiments designed for measuring the variables which affect the stomatal response. The extensive use of elaborate instrumentation allows for the application of more complex formulae and precision in estimating transpiration rates.

CLASS Model

The CLASS model (Verseghy, 1991) is an example of a vertical one-dimensional combined water and energy budget model. The latent heat flux is calculated with an equation based on the aerodynamics theories in the form of the Dalton equation. The equation is a function of the air temperature within the canopy. The air temperature is solved for implicitly in order to balance the energy budget of the canopy; in this way, evapotranspiration is solved for implicitly.

When the canopy is covered with intercepted precipitation, evaporation (latent heat flux) is assumed to occur at the potential rate according to

$$LE = \frac{\lambda_v \rho_a \cdot \left[q_a - q_{sat}\left(T_c\right) \right]}{r_{at}}. \qquad [72]$$

Similar to the aerodynamic equations, the driving gradient is calculated as the difference between q_a, the specific humidity, and $q_{sat}(T_c)$, the saturation specific humidity at the temperature of the canopy. The atmospheric resistance (r_{at}) in m s^{-1}, is a function of the wind velocity distribution.

Under dry conditions, the CLASS model incorporates the stomatal resistance by adding a second resistance factor in series with the atmospheric resistance:

$$LE = \frac{\lambda_v \cdot \rho_a \left[q_a - q_{sat}\left(T_c\right) \right]}{r_{at} + r_s}. \qquad [73]$$

The stomatal resistance (r_s) is calculated as the product of the ratio of the current leaf area index to the maximum leaf area index under mature growth conditions (LAI_{max}), and a typical value of minimum resistance r_{Smin}, so that

$$r_s = \frac{LAI_{\max}}{LAI} r_{s_{\min}}. \qquad [74]$$

Textbook values of r_{Smin} are used and are dependent on the vegetation type. CLASS recognizes that the physiologically controlled stomatal resistance is affected by environmental factors. The combined stomatal resistance of the different types of vegetation (r_c) is adjusted for the incoming short-wave radiation, vapour pressure deficit, leaf water potential which is related to the soil moisture suction ($\Psi_{s,r}$), and air temperature. The stomatal resistance is defined as a function of the parameters as

$$r_s = r_c \cdot f\left(K_{in}\right) \cdot f\left(e_{sat} - e\right) \cdot f\left(\psi_{s,r}\right) \cdot f\left(T_a\right), \qquad [75]$$

where the following empirical relations are used to define the individual functions:

$$f(K_{in}) = \max\left(1.0, \frac{500.0}{K_{in}} - 1.5\right)$$

$$f(e_{sat} - e) = \max\left(1.0, \frac{e_{sat} - e}{5.0}\right)$$

$$f(\psi_{s,r}) = \max\left(1.0, \frac{\psi_{s,r}}{40.0}\right) \qquad [76]$$

$$f(T_a) = 1.0 \qquad 40^\circ\text{C} > T_a > 0^\circ\text{C}$$

$$= \frac{5000.0}{r_c} \qquad 40^\circ\text{C} \leq T_a \geq 0^\circ\text{C}$$

In essence, CLASS applies a factor to the potential evapotranspiration rate to obtain an estimate of the actual evapotranspiration rate. CLASS defines this factor as a function of the atmospheric conductance and the canopy resistance. CLASS is categorized in the sub-group of research-oriented models because of its requirements for large amounts of input data and the use of the theoretical mass transfer approach for estimating the potential evapotranspiration.

2.5 Hydrologic Modelling using WATFLOOD

WATFLOOD is a fully distributed hydrologic model. The current version recognizes up to six different land classes in a watershed, two of which are pre-defined as urban and water classes. The use of distributed land cover information significantly improves the simulations (Tao and Kouwen, 1990). Attached to the land classes are various hydrologic parameters affecting the different hydrologic sub-processes. By discretizing the watershed into small elemental areas and specifying the percent of each type of land class in each element, the model preserves the distribution of the hydrologic properties and the land classes throughout the watershed. The model also utilizes fully distributed meteorological inputs. The runoff from each element is calculated as the sum of the runoff from each type of land cover weighted by the percentage of the elemental area covered by that type. The aggregate area of a particular land cover within an element is called a Grouped Response Unit (GRU).

Most hydrologic models differ from WATFLOOD by permitting only one type of land cover to be defined per element, a hydrologic response unit (HRU), as in the SHE (Systèm Hydrologique Européen) model, (Abbott *et al.*, 1986). In WATFLOOD, each pixel of land cover type in a land cover image is considered to be a separate HRU within each discretized element in the model. A GRU is comprised of many similar hydrologic response units.

A element is defined as a parcel of land that has a small enough routing time that the precise location of each piece of a certain land cover type within the element does not significantly affect the timing of streamflow. Thus, the average routing time of each GRU can be used instead of calculating a different routing time for each pixel within an element. Throughout the watershed, all of the land classes are modelled using the same hydrologic sub-processes, although, each of the land classes can have different values for parameters in the relations that define the hydrologic sub-processes. Implicit in the use of the GRU is the assumption that there is a strong correlation between the land cover and soil type. This is an adequate approximation, supported by the findings of other researchers who have shown that the hydrologic effects of land cover dominate over the effects of soil type (Kouwen *et al.*, 1990).

The size of an element must be limited by the lesser of the following: the largest area which receives uniform meteorological inputs (dependent on the type of precipitation events common to the region), or the largest element in which the storage time is much less than the basin storage time or the event duration (Kouwen *et al.*, 1993). The optimum size of the element is dependent on the total basin size. Guidelines suggest that the area of each element be constrained to maximums of 4% of the total basin area for basins less than 3000km^2, and 100% of the total basin area for basins less than 100km^2 for time steps of one hour (Tao and Kouwen, 1989).

Using a grid of square elements simplifies and expedites mass calculations. The use of grouped response units expedites the calibration of land cover parameters and improves the transferability of the parameters to regions of similar physiography (Kite and Kouwen, 1992).

2.5.1 Land Classification

Based on the definition of the GRU, it is necessary to determine the percent of the total area of each element covered by each land class. The five land class covers typically defined are water, wetland, tall vegetation, low vegetation, and barren areas. The most precise method for providing this input data is to utilize some form of satellite imagery. Without the assistance of a satellite image, topographic maps or aerial photography provide an alternative. Land cover classification using LANDSAT-5 TM imagery enables transferability of land cover parameters between basins with different land use characteristics, provided that they have similar physiography (Kouwen *et al.*, 1990). The use of satellite imagery is advantageous over the other classification methods because it is less time consuming and the model can easily be updated with recent images. For large regions, the use of imagery may be the only feasible method.

2.5.2 Hydrologic Processes

The following hydrologic processes are considered by WATFLOOD: precipitation, interception, surface storage, snowmelt, infiltration, interflow, groundwater flow, groundwater discharge, and overland flow. In a typical simulation, an hourly time step is used for modelling these processes.

Precipitation can be entered into the model in three different ways. Rain can be measured with surface point observations (rain gauges) and distributed over each element in the watershed using the Reciprocal Distance Weighting Technique (Wei and McGuiness, 1973). An average of the measurements made at the four closest gauges to the element of interest (one in each quadrant) is weighted inversely to the distance from the gauge to the centre point of the element.

The second method for inputting precipitation data is the identification of locations where snow depths and snow water equivalents have been measured. By identifying the land cover in which the measurements were made, the snow water data are distributed to that specific land cover class.

Interception is calculated by using the relation developed by Linsley *et al.* (1949) (equation 32). The current method of modelling interception in WATFLOOD provides good results for short-term simulations -- the duration for which it was designed. The process is not adequate for modelling events of a longer period because a continuous balance of the interception storage is not maintained. Lack of interception loss is compensated for by artificially increased evapotranspiration losses.

Surface Storage is a function of accumulated rainfall excess and an optimized depression storage constant. The limiting depression storage is approached exponentially. A running balance of the ponded water is computed considering losses through net precipitation input, overland flow, and infiltration.

Infiltration is calculated with an equation based on the Philip formula. The initial moisture conditions, which inhibits infiltration, is an optimized parameter representing the moisture content in the upper soil layer. Infiltration occurs between the surface storage to the upper soil layer.

Evapotranspiration is currently estimated using published mean monthly values. It is possible to define different values for different land classes, provided that the data are available. Depending on the time step being used, appropriate fractions of the monthly averages are used as an estimate of the evapotranspiration loss. The water is depleted from the storage in the upper soil layer.

Interflow is depleted from the storage in the upper soil layer with a simple recession constant function. The flow is combined with the elemental channel flow.

Upper Soil Drainage to the lower soil layers is estimated as the product of a constant and the difference between the current and the minimum upper soil layer storage. The constant and the minimum storage are optimized parameters.

Groundwater discharge is calculated as the product of a groundwater flow parameter and the maximum groundwater storage, raised to some power. The groundwater flow parameter and the value of the power are optimized parameters. Groundwater discharge is added to the elemental channel flow.

Overland Flow is calculated using a relationship based on the Manning Formula. Overland flow occurs when infiltration and depression storage have been satisfied and is combined with the elemental channel flow. The total flows contributing to the channel flow are routed using the storage-routing technique.

2.6 Summary

Evapotranspiration is an important process, accounting for up to 60% of the total hydrologic budget. In some cases, interception evaporation may account for between one quarter and one third of the total budget; to provide accurate hydrologic simulations, these components must be considered. The transpiration process removes water from the soil layers, whereas, evaporation can take place from any open water surface, including storage on or in the ground and vegetated surfaces.

The evaporation of intercepted water precludes the normal transpiration process because of the lower evaporative resistance. Interception evaporation is a function of advection and not radiated energy. Tall vegetation is considerably rougher than short vegetation, thereby inducing more mechanical diffusion and capturing more advection energy. Interception loss can significantly increase the total evapotranspiration loss from tall vegetation. In contrast,

transpiration from tall vegetation is lower than the transpiration from short vegetation under similar environmental conditions.

Generally, it is assumed that evapotranspiration from small local areas occurs at the equilibrium rate, thus eliminating the complications arising from feedback affects resulting land cover incongruities. Regions of heterogeneous land cover can often be considered as a homogeneous mix of the land covers on a larger scale.

The following three different approaches are generally used for estimating evapotranspiration:

1. Analytical
2. Theoretical
3. Empirical

Analytical methods consist of measuring all of the fluxes to deduce the evapotranspiration from the remainder. Certain quantities are difficult to measure for the analytical methods. To provide an accurate water balance, the groundwater storage and seepage must estimated. Water balances cannot typically provide short-term estimates of the evapotranspiration loss. Energy balance calculations are hindered by the requirement for vast amounts of input data and instrumentation.

Theoretical models provide accurate estimates of evapotranspiration from water surfaces and short crops. These models recognize that evapotranspiration is a combination of both radiation and advection components. The radiation sources are somewhat simpler to measure than the advection components. Complex equations relating advection to advanced theories of turbulent flow have been necessary to describe the additional energy inputs of advection to the total evapotranspiration loss. Further complexities are introduced for taller vegetation, with the need to estimate complex parameters to accurately characterize the physiological resistance. All of these situations require significant data inputs.

Empirical methods typically index the actual evapotranspiration to a measure of the potential evapotranspiration, although in reality, the potential evapotranspiration is a function of the actual evapotranspiration (Complementary Relationship). Good estimates of the potential evapotranspiration have been made as a function of temperature or radiation.

The most desirable method for modelling the evapotranspiration depends on the use of the hydrologic model and availability of data inputs. Operational models tend to use simplified

approaches which require minimal data inputs. Some models use published mean monthly values of actual evapotranspiration. Typically, the estimated actual evapotranspiration is constrained by the lesser of the potential evapotranspiration and the total precipitation, or by some function of the soil moisture. Simply using air temperature has also proven to be a valuable method of indexing the actual evapotranspiration to the potential evapotranspiration.

2.7 Conclusions

The chosen evapotranspiration model must concurrently maximize accuracy and simplicity to maintain the ease of its application and minimize input data requirements. For this reason, a method of calculating the potential evapotranspiration and indexing it to the actual evapotranspiration will be utilized. The index will be a function of the variables affecting the physiological controls on transpiration. By utilizing these variables, the relation will maintain a connection with the stomatal processes. The process would be modelled best with the use of the Penman-Monteith equation (equation 49). However, under the constraint of minimizing input data requirements, the complexity with which the canopy resistance is defined in the Penman-Monteith equation eliminates the feasibility of its use.

In substitution for the Penman-Monteith model, a model estimating Penman's definition of potential evapotranspiration will be utilized. Some researchers have recommended against using the Penman definition of potential evapotranspiration in a tall vegetated environment and conditions of limited moisture availability; these conditions exist in the watersheds being modelled. However, the definition has supplied good results in many hydrologic models and provides an easily applicable method while maintaining accuracy and a relation to the physical process. Adjustments to the potential evapotranspiration are necessary as a result of the conditions being different from those necessary for the Penman evapotranspiration. The potential evapotranspiration will be reduced for periods with constraining soil moisture or soil temperature conditions and increased for periods with elevated advective conditions.

The Hargreaves equation (equation 57) has been rigorously tested with model inter-comparisons thus proving its adequacy. The use of a spatially stable parameter, temperature, for the empirical relation is an attractive feature. The similarities of the equation with the more complex and theoretical Penman formulae are reassuring. Another temperature-dependent model, useful for modelling remote locations with limited meteorological observations, is the Turc equation (equation 63); it has also provided good results in model comparisons. A vast amount of research has been completed on the Priestley-Taylor equation (equation 64). Inter-

comparisons with other models have proven its utility. The value of estimating evapotranspiration with these three models will be analyzed.

For simplicity, estimates made with any of the three equations are referred to as potential evapotranspiration estimates. This is somewhat of a misnomer for the estimates produced by the Turc equation and should be noted since this equation typically produces estimates which are closer to the actual evapotranspiration rates.

One other simplification made throughout the analysis is the use of a constant value of 1.26 for the Priestley-Taylor coefficient (α). Thus, the Priestley-Taylor equation has been used to estimate not the equilibrium potential evapotranspiration but the true potential evapotranspiration. The actual value of the α coefficient will vary temporally as a function of time and the method(s) used to index the actual to the potential evapotranspiration (soil moisture and soil temperature). Therefore, the actual value of α is not explicitly calculated, but remains as a function of the reduction parameters. For completeness, the net ground heat flux has been included in addition to the net radiation inputs in the calculations using in the Priestley-Taylor equation (equation 64).

The availability of published long-term monthly averages of evapotranspiration permits the current method of modelling to be compared with the above equations. Measured values of latent heat flux actual evapotranspiration, estimated using Licor instruments, are also available for the testing these index methods. These values of latent heat flux (W m^{-2}) have been converted values of evapotranspiration (mm), by taking the quotient of the latent heat flux and the mass density of water and the latent heat of vaporization. The complete hydrologic model will be tested using the water balance data that were collected during the 1994 and 1995 BOREAS field programs.

The starting point for the revision of the model will be with the interception evaporation subroutine in recognition of its importance to the overall water balance. The three selected evapotranspiration models will then be applied to the interception evaporation and transpiration loss subroutines. Through this methodology, the general vertical water budget of the model will be revised to more precisely simulate the actual hydrologic process.

Chapter 3
Hydrologic Modelling with WATFLOOD

The hydrologic responses of the NSA and SSA watersheds have been modelled using WATFLOOD. The primary data requirements of the hydrologic model are meteorological and streamflow observations. The first streamflow measurement is used for initializing the simulated flows. The remaining measured flows are used for calibration and validation purposes. The other inputs to the model are defined using a geographically referenced database. This database contains the spatial characteristics of the watershed delineation, land cover and topography, and provides a system with which to reference the meteorological and streamflow inputs.

The NSA and the SSA watersheds have been defined on a Universal Transverse Mercator (UTM) coordinates system of reference. The UTM grid provides a convenient system for mapping WATFLOOD's grid of square elements. Use of the UTM references also assists with the compatibility of different data sets, including the LANDSAT-5 TM imagery, used for land cover classification.

3.1 Data Collection

A considerable amount of the scientific thrust for BOREAS was to study the conditions related to the separate dominant species in the boreal forest biome. Data were gathered from these different regions using meteorological and flux towers by an multinational interdisciplinary group of scientists. This thesis focuses on the hydrologic component of the experiment, but utilizes some of the information collected by other scientists specifically for the estimation of evapotranspiration. With a few small exceptions, all of the hydrologic data were collected by the author and a scientific team from the author's institution.

Stream gauges consisted of a float on a cable attached to a counterweight lying over a rheostat-pulley assembly. Voltage measurements across the moveable rheostat resistor were recorded by a data-logger every 15 minutes, thereby documenting the elevation of the float (stage of the water surface). Regular manual flow measurements were made using a velocity meter. By establishing the gauge locations upstream of a stable stream section providing a flow control, the relationship between stage and the flow remained constant. The resulting relationship between stage and manually measured discharges has been regressed at each gauging station (stage-discharge relationship), as shown for a typical gauge, SW3, in Figure 3.1. The regression enables the simple conversion between the 15-minute interval stage data and volumetric flows, as shown for the SW3 Gauge in Figure 3.2.

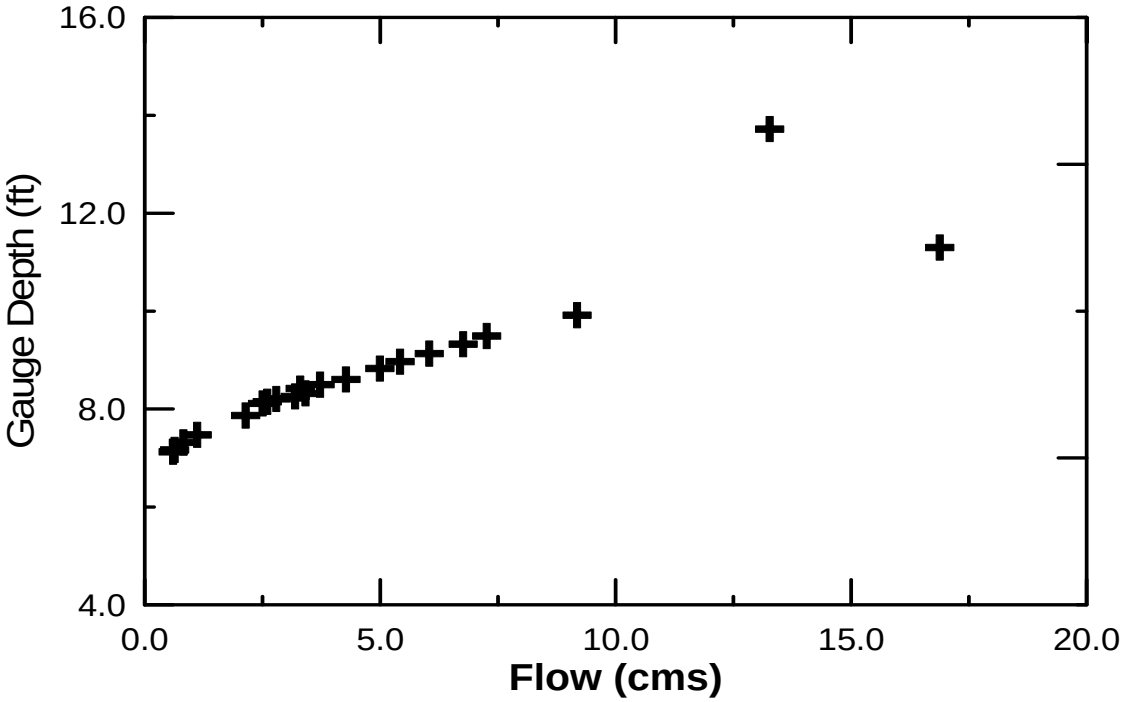

Figure 3.1: Stage-Discharge Curve - SW3 (Typical)

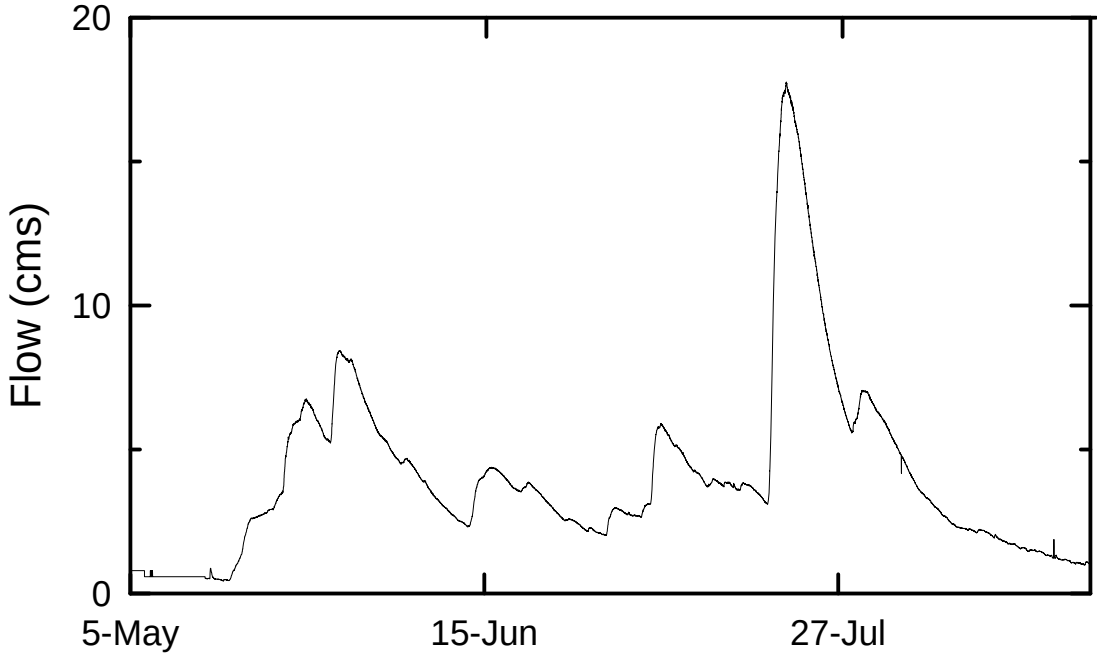

Figure 3.2: Discharge at SW3 - 1994

Flow data at each station were analyzed for any shift in the flow control. In instances where there was a shift, a new stage-discharge relationship was developed for subsequent flows. More than one stage-discharge curve was required at each of the NW2 and NW3 stream gauge locations. Scour during high flows and vegetative growth during the low summer flows affected the control at each of these two stations.

Precipitation data were collected through a network of rain gauges in both the SSA and the NSA. The network in the SSA consisted of seven tipping bucket and five Belfort rain gauges. The sum of the precipitation recorded at a typical gauge for the 1994 period is shown in Figure 3.3, plotted with respect to time. The network in the NSA was composed of five tipping bucket and five Belfort rain gauges. The rain gauges were located in areas which represented the surrounding local physiography and vegetation. To reduce the errors introduced by turbulent air movement around the gauge openings, the gauges were deployed in clearings protected by vegetation. The openings in the canopy around the gauges approximated an inverted conical section with side angles of 45 degrees as recommended by Dingman (1994).

As a result of the extensive wetlands in the lower-elevation interior portions of the basins, roads did not exist, thus making those areas inaccessible. Logging roads provided access to the full perimeter of the SSA watershed, so gauges were located evenly along its boundary. Periodic access to a gauge in the centre of the basin was made possible by a dry weather road.

Fewer roads in the NSA provided much less opportunity for access. The NW2 and NW3 basins are relatively small. This permitted the establishment of a very dense line of gauges along the northern boundary which is delineated much of the distance by the only road through the area. Off-road trails provided all-terrain vehicle access into a hydroelectric corridor. The gauges were positioned adjacent to the corridor, which runs along the southern fringe of the NW2 and NW3 basins. One gauge was positioned in the interior of the NW1 basin and was accessible only by helicopter. Therefore the gauge was serviced only once between the time of installation and the time of removal.

The inaccessibility of the NSA site eliminated the problems of vandalism sometimes associated with automated data collection equipment. In contrast, a number of gauges in the SSA were disturbed. Fortunately, only one gauge was tampered with, but it was not discovered until a significant portion of data had been lost. At both sites wildlife interfered with some observations. In general, significant data losses were prevented by following a rigorous service schedule which expedited the discovery and repair of unserviceable apparatus.

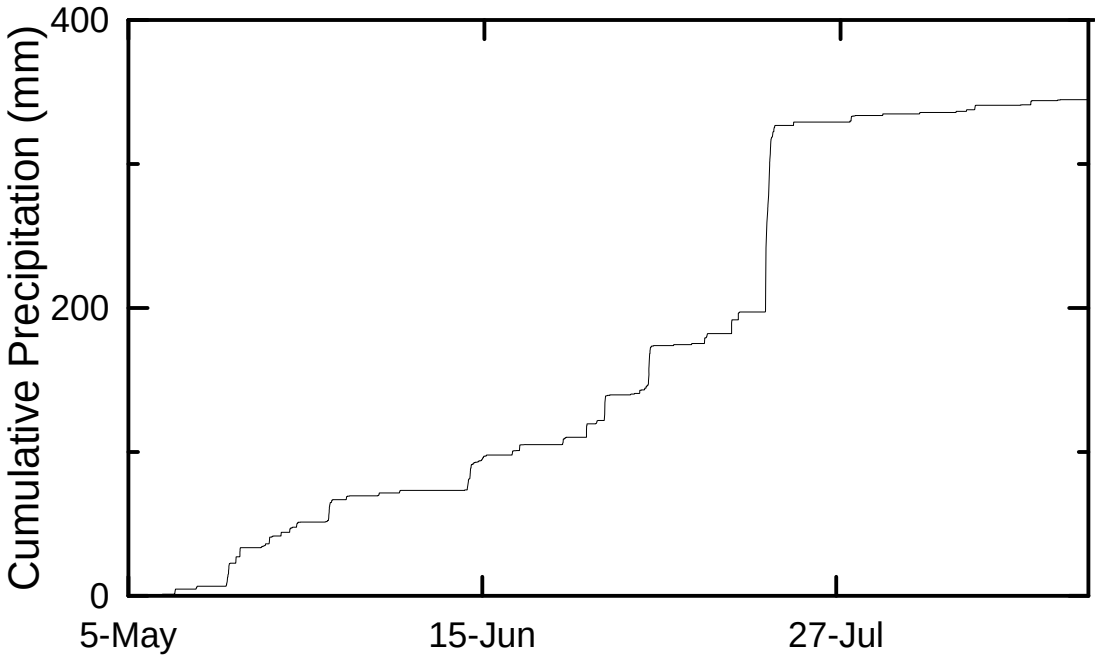

Figure 3.3: Cumulative Precipitation - SSA 1994 - (Typical)

Tipping Bucket No. 7

The data collection equipment was set up to provide continuous monitoring throughout the 1994 and 1995 growing season. Readings were taken every 15 minutes from late April to mid-October. In addition to these stations, meteorological and atmospheric flux data were collected at a number of sites in the two study areas during the 1994 season as part of the BOREAS project. Additional meteorological stations in the region have been operated by Atmospheric Environment Services Canada (AES). Parts of these data sets have been utilized in this research.

3.2 Watershed Delineation

The basin boundaries have been defined in order to denote the WATFLOOD grid elements within the watershed for which the database has been developed. The lack of relief in the topography of both watersheds has impaired the accuracy of delineation of the watershed boundaries. The most recent editions of 1:50,000 scaled topographic maps were utilized to estimate the locations of the watershed divides. Some local regions of significant relief, such as those in the western sections of the SSA watershed, made the task of delineation relatively easy. Difficulties arose in the extensive wetland areas, such as those lying across the northern boundary of the SSA watershed. In these areas a detailed examination of the physiography and local drainage was made with the use of small scale (1:15,840) aerial photography to locate the drainage divides.

Personal knowledge and an investigation of the local region also assisted in the accurate delineation of the watersheds. In the NW3 basin, UTM map no. 63-O/16 denotes a small tributary of the Sapochi River, upstream of station NW1, which flows westward from the centre of the NW3 basin. This information is contrary to notes made during the field investigations which indicate that flow in the channel does not currently exist. The re-mapping of remote areas, such as these watersheds, is very infrequent, with the most recent editions printed in 1977 and 1987 for parts of the SSA and 1979 in the NSA. The vast wetlands, wide contour spacing and large beaver population, combined with infrequent mapping, provides an opportunity for significant changes in drainage systems to remain unrecorded. This is a very plausible explanation for the discrepancies in the observed and mapped flow paths throughout both watersheds.

Observations of flow direction were recorded along the road through the centre of the SSA watershed during field visits. Some limited sections of lowlands in the north western portion of the SSA watershed were also explored. Personal knowledge of the study sites has been advantageous in establishing a more accurate delineation of both watersheds.

As a result of the intense field investigations and the use of large scale aerial photography, the watershed boundaries have been well delineated. Some uncertainty still exists in the remote and inaccessible lowland areas of both watersheds, a northern section of the area gauged by SW3 and a western portion of the area gauged by NW2. These areas are small in relation to the entire area of the watershed, as shown by Table 3.1. The location of these uncertainties (at the boundaries far away from the outlet) and the type of land cover (wetlands with much detaining capacity) reduces the impact of these areas on short-term hydrologic events. There is some potential for the influence of these regions on the long-term hydrologic balance.

Table 3.1: Basin Drainage Areas

Basin	Drainage Area (km^2)	Uncertainty (%)
SW1	610	± 10
SW2	75	± 5
SW3	485	± 10
SW4	220	± 5
NW1	400	± 5
NW2	30	± 7
NW3	40	± 10

The boundaries of each watershed and its sub-basins are shown in Figures 1.2 and 1.3 for the NSA and SSA basins, respectively.

3.3 Land Cover Classification

LANDSAT-5 TM imagery obtained on August 6, 1990 from the SSA and August 20, 1988 from the NSA has been used for classifying the land types within each watershed. The raw imagery was georeferenced and classified by other researchers (Hall, 1995) into similar land classes for the NSA and the SSA. The original images were referenced to the BOREAS grid system, a system of coordinates developed specifically for BOREAS to minimize the distortion of geographic related information in and between both study areas. Distortion, resulting from the type of map projection, of the region between the NSA and SSA is not of concern in this study. In order to be more compatible with the WATFLOOD database, the image was re-referenced to the UTM coordinate system. The UTM projection produces reasonably accurate representations of the earth's surface for small areas such as the watersheds being studied.

The inexact compatibility between the WATFLOOD grid elements and the pixel size in the LANDSAT-5 TM image results in a small error when determining the percent of land cover type in each grid element. This error occurs because the image is sampled across an area of 2000m x 2000m. Each pixel in the image represents an area of 30m x 30m. In order to classify the entire area in each 2.0km x 2.0km grid element, an integer number of pixels must be analyzed, an area covered by 67 x 67 pixels. This area (4.04km^2) is approximately 1.0% larger than the actual area of the grid element (4.0km^2). This size of error is negligible and becomes even less significant if it is assumed that the distribution of land cover types along the edge of the elements is the same as the distribution within the elements.

As part of the BOREAS Project, detailed experiments were conducted by various investigators in areas covered predominantly by a single type of vegetation. The satellite image has been classified, to a certain extent, according to the different land covers at each of these small-scale study areas (tower flux sites). The NSA and the SSA were classified similarly into 11 land classes; a description of the 11 land classes follows.

3.3.1 Wet Conifer

This land class is composed primarily of coniferous trees existing in "non-dry" conditions. Black Spruce and Jack Pine growing on peat or poorly drained mineral soils make up the majority of the areal coverage. A significant percentage of the total area in both watersheds is covered by this land type. This further exemplifies the extent of wetness in the watersheds. A detailed study of this land cover type was made in both the NSA and SSA in areas covered by mature Black Spruce at the Old Black Spruce tower flux sites (OBS-SSA and OBS-NSA).

3.3.2 Dry Conifer

This land cover type is comprised mainly of mature conifers growing in well-drained sandy soils. A detailed study of this land class was completed in both study areas with experimental apparatus deployed in stands of mature Jack Pine at the Old Jack Pine tower flux sites (OJP-SSA and OJP-NSA). Meteorological measurements were also made in this land class at the AFM-SSA and AFM-NSA tower flux sites.

3.3.3 Deciduous

Regions covered predominantly by deciduous vegetation (at least 80% of the total coverage) were classified as deciduous. A detailed study of the common type of deciduous vegetation (Aspen/Birch) was made in the SSA at the Old Aspen tower flux site (OA-SSA) in a stand of mature Aspen.

3.3.4 Mixed

Tracts of land that were covered by a mix of deciduous and coniferous vegetation were classified as Mixed. In order to be grouped into this classification, the dominant species had to be covering less than 80% of the total area. Experimental work was completed by investigators at mixed sites, but tower flux and meteorological measurements were not made on a continuous basis.

3.3.5 Fen

Fens, being a significant part of the physiography of the boreal forest region, were studied in detail in both study areas (FEN-SSA and FEN-NSA). This classification includes both fens and bogs. Fens tend to be covered in moss, birch, and sparse to medium density tamarack, whereas bogs tend to be treeless. Both areas are saturated, with the water table being at or near the surface.

3.3.6 Regeneration (Young, Medium and Old)

In the SSA, some of the vegetation had been harvested for pulp. These areas exist in different stages of regeneration, depending on the length of time since cutting. In general, the areas have been reforested with Jack Pine or Aspen. In both study areas, much vegetation has been cleared by forest fires and has regenerated naturally with Jack Pine or Aspen dominating the new growth. A detailed study of regenerating Jack Pine sites was made at the Young Jack Pine tower flux sites (YJP-SSA and YJP-NSA).

The regeneration classification has been further sub-divided into three classes of regeneration growth, young, medium and old. Growth in areas of young regeneration has been occurring, on average, for about 3 to 4 years. Areas of medium regeneration have been growing for approximately 7 to 8 years since disturbance. Regions of older regeneration growth were disturbed some time between 12 and 20 years ago. In this classification there is some confusion between the older regeneration and the deciduous classification, showing the trend of regenerating areas to evolve towards the latter type of land class.

3.3.7 Water

Areas covered by standing or moving water make up this classification in the image.

3.3.8 Disturbed

This classification type includes bare soil, rock outcrops, and areas where human interference has eliminated the natural vegetative cover. Most of the image pixels classified as this type of land cover are rock outcrops in the NSA and logged areas in the SSA, with roads and their adjacent clearings being apparent in both study areas.

Logging activity has taken place recently since the SSA image was taken in 1990. Although most of these activities have occurred outside of the watershed boundaries, some trees were harvested during 1994 along the southern fringe of the basin south of White Gull Lake. Zones of vegetation between the cut areas and the waterways act as buffers to the hydrologic response of the cleared areas. The relative size of the cut area is small in comparison to the total size of the watershed. Together, these conditions should minimize the effects on the hydrologic response of the changes in land characteristics since the image was taken.

3.3.9 Burn

Areas where vegetation has been substantially or completely eliminated by intense forest fires make up the burn classification. Recent forest fires have affected the classification of the SSA since the time of acquisition of the LANDSAT-5 TM image. Fortunately, these changes have occurred outside of the watershed boundaries.

3.3.10 WATFLOOD Land Classes

Currently, WATFLOOD considers up to five different land classes plus a class defined as urban. An aggregation of some of the 11 land classes identified in the initial image classification was required to classify the total area within the watersheds. A large number of combinations of the 11 land classes was available. In WATFLOOD, parameters affecting the hydrologic processes are defined according to their land cover classification. Therefore, land cover types known to have similar hydrologic responses have been combined into one land class. A second criterion for the aggregation of land classes was to obtain a classification which utilizes the advantage of the distribution of parameters available in WATFLOOD.

Land within the urban classification is considered to be hard surfaced and has parameters affecting runoff which reflect this. An attempt was made to identify the disturbed classification as the urban classification. The results from these simulations were not satisfactory. The portions of the road surfaces within this classification could be simulated using the urban classification. However, this classification also contains some logged areas,

bare soil and rock outcrops, all of which can have significantly different parameters than those of a hard surface, which affect runoff.

An attempt was made to maintain some of the forest land cover types (e.g. deciduous, mixed, coniferous, and regeneration) as separate land classes. After some preliminary calibration of the model parameters, hydrograph simulations produced unsatisfactory estimates of actual flows. With the availability of only five land classes, and the use of four of these classes for forest types, the result was an aggregation of cover types in the fifth land class with hydrologic dissimilarities. This land classification produced poor hydrological simulations.

The best utilization of the distributive ability of WATFLOOD would be to classify the region into five different land covers with equal area. This classification would give equal weighting to the parameters for each land class and make the hydrologic simulation equally sensitive to each of the parameters. However, this would result in the aggregation of land classes with hydrologic dissimilarities. The combination of the Dry Conifer, Regeneration, Deciduous and Mixed forest types into one land class produced the best initial simulated hydrographs. The development of this classification was partly dependent on the correlation between evapotranspiration and land cover, as will be discussed in Chapter 5. The aggregation of land classes into the five classes used in WATFLOOD has been completed as follows:

1. Barren = disturbed + burn
2. Dry Conifer = dry conifer + mixed + deciduous + regeneration (young + medium + old)
3. Wet Conifer = wet conifer
4. Fen = fen
5. Water = water

This classification results in the most uniform arrangement of the percent of total land cover per classification, while maintaining the best similarity of land covers within each land class. The percent of the total area of each land cover within each of the grid elements for the SSA and NSA watersheds is shown in Figures B1 to B10 in Appendix B. The percent of the total area covered by each land cover in each sub-basin is displayed in Table 3.2.

Table 3.2: Percent of Land Cover Type per Sub-basin

Land Class	SW1	SW2	SW3	SW4	NW1	NW2	NW3
Barren	1.2	1.0	1.1	1.0	3.6	2.9	2.0
Dry Conifer	28.1	41.8	23.3	22.3	54.4	48.8	27.4
Wet Conifer	60.5	50.4	63.8	62.6	35.0	44.4	56.9
Fen	6.9	6.4	7.6	7.1	5.6	3.4	13.5
Water	3.3	0.2	4.3	6.7	1.3	0.6	0.0

The disturbed areas and the burns have been combined because of assumed similarities in the minimal amounts of vegetative cover, thereby having similar effects on interception and transpiration. The second class consists of various types of relatively dry forest cover. With reference to the LANDSAT-5 TM classification and topographic maps, the mixed and deciduous areas have been observed to lay generally on higher, drier terrain. The dryness of this terrain is the similarity focused on for the amalgamation of these classes with the dry conifer classification. The Dry Conifers are preferable for harvest over the Wet Conifers. The Regeneration classification should therefore have similar soil characteristics to the Dry Conifers. This assumption breaks down in the NSA where the Regeneration classification occurs as a result of historical burns. However, the documentation describing the classification acknowledges that there is confusion between the Mixed class and the Medium and Old Regeneration classes. This provides further support for the aggregation of these classes.

The current land classification used for modelling provides a good distribution of the total land cover between the five available classes. The advantage of this is the more efficient use of the distributive ability of WATFLOOD. Each of the parameters will have a more significant impact on the overall hydrologic simulation if the total areas that each of them affect is similar.

3.4 WATFLOOD Database Development

The grid of WATFLOOD elements has been defined using the UTM grid system for both the SSA and NSA watersheds, as shown in Figures 3.4 and 3.5, respectively. In both basins, the dimension of each element was established as 2km x 2km. This size was chosen to permit the satisfactory representation of the physiographic and channel distribution characteristics of the watersheds, while providing a reasonable number of elements for the ease of computations. This dimension of element falls within the suggested guidelines specified in earlier studies (Tao and Kouwen, 1989).

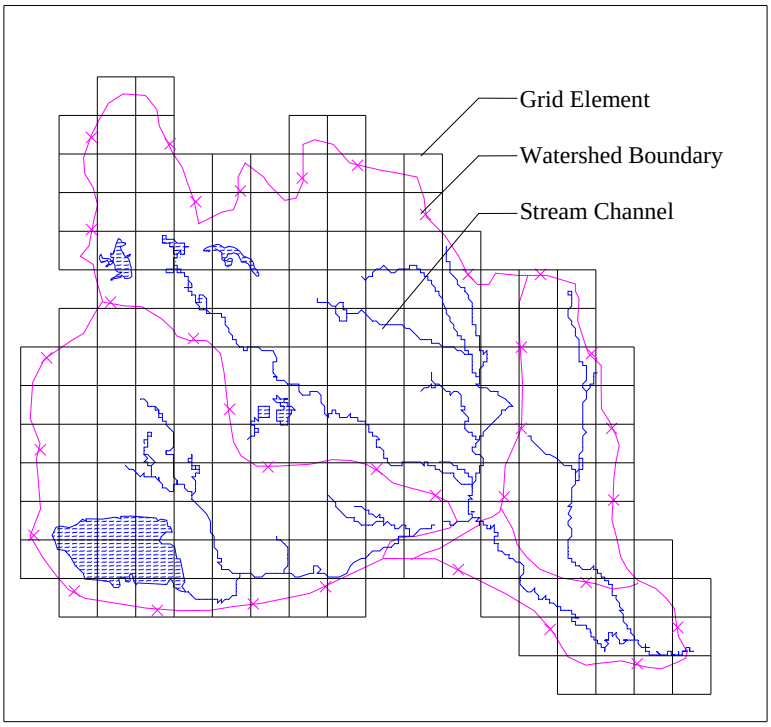

Figure 3.4: WATFLOOD Grid of Elements - SSA

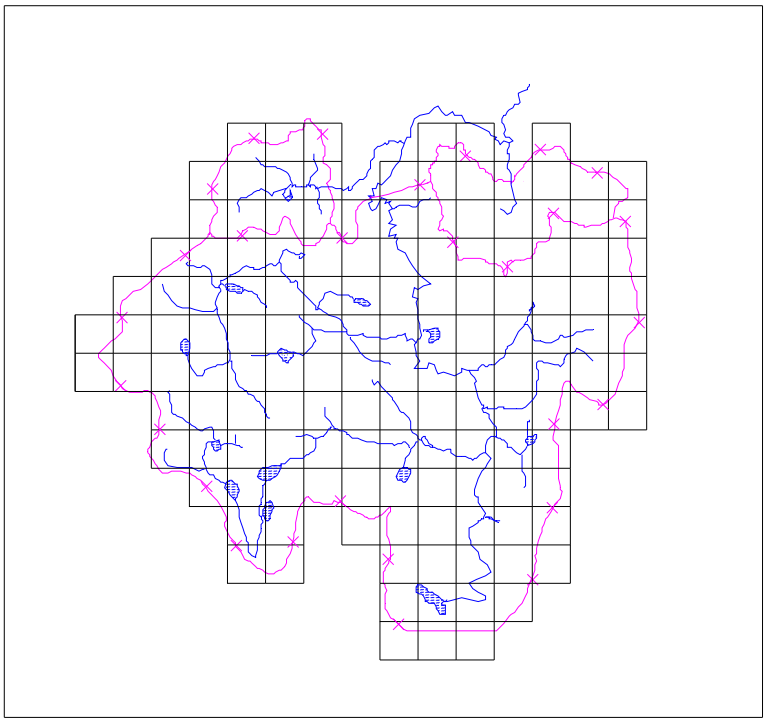

Figure 3.5: WATFLOOD Grid of Elements - NSA

The use of 1:50,000 scale UTM maps provide for a convenient mapping of the watershed database. The database contains information which is attached to each element, including the location, the percent of the total area of the element inside the watershed divide, a measure of terrain roughness based on the distance between contour lines, the existence of defined flow channels, the invert of the midpoint of the channel or the average terrain elevation for an element without channels, the general direction of elemental runoff, and the percent of area coverage by each land class in each element, based on the LANDSAT-5 TM image.

Most of the hydrologic parameters used in WATFLOOD are constant for each land class, regardless of the location in the basin . A sub-classification of the grid elements can be used to distribute the channel roughness parameters used for the hydraulic routing computations. This sub-classification can be used to represent different characteristics in a basin. In this study, each element was defined as one of the five following channel/terrain classes based on a qualitative analysis of the features shown on the topographic maps:

1. Winding channels
2. Wetlands or channels running through wetlands
3. Rolling terrain
4. Straight channels
5. Lakes, ponds or channels running through lakes and ponds

3.5 Data Inputs

For the simulations, a time step of one hour was chosen. This time step approaches the maximum step as a function of the element size, while providing a suitable time scale to control the consumption of computer resources.

Simulation of hydrologic events using WATFLOOD requires the input of certain meteorological conditions. Precipitation has been measured spatially with a network of rain gauges. The data have been integrated temporally to provide observations based on one hour periods corresponding to the simulation time step. Similarly, streamflow data have been estimated at the outlet of the seven sub-basins at 15 minute intervals and integrated to one hour intervals. Temperature data have also been provided at one hour intervals because of the requirements of the temperature-based evapotranspiration models.

3.6 Model Error Calculation

To provide a basis for quantifying the change in accuracy provided by modifications to WATFLOOD, initial simulations of the study periods have been made with the pre-study version of the model.

There are a number of different ways to evaluate the efficiency of the simulations. Donald (1992) also used hydrologic simulations to evaluate the efficiency of revisions the hydrological sub-processes of a model. In that study, the main focus was on simulating snowmelt -- somewhat different from the research in this thesis. However, the method of comparison between these two studies (hydrologic simulation) is identical. Methods suggested by the World Meteorological Organization were used for the evaluation of simulations in the work of Donald (1992). The most important criterion identified for comparing hydrologic simulations was that of a visual inspection of linear scale plots of simulated and observed flows (WMO, 1986). Another method identified as being useful was a comparison of the S criterion: the ratio of the root mean squared error (RMSE) of the estimated flows to the mean observed discharge for the simulation period:

$$s = \frac{\sqrt{\frac{1}{n}\sum_{i=1}^{n}\left(Q_{est_i} - Q_{obs_i}\right)^2}}{\frac{1}{n}\sum_{i=1}^{n} Q_{obs_i}}, \qquad [77]$$

where s is the ratio of the RMSE to the mean observed flow, Q_{est} is the simulated flow ($m^3 s^{-1}$), Q_{obs} is the measured flow ($m^3 s^{-1}$), i is the time period in the hydrograph, and n is the total number of periods. This criterion evaluates the difference in magnitude of flows throughout the period of the hydrograph. Although this estimate of error tends to weight differences in flow more heavily because of the exponent on the error, high flows tend to be of a shorter duration, thereby weakening the influence of these peaks. Use of the s criterion provides a more objective evaluation of the model efficiency.

Similar to the s criterion, the error of the simulated hydrographs (U) is often measured more simply as the total squared difference between the estimated and observed values of flow (Nash and Sutcliffe, 1970) given by

$$U = \sum_{i=1}^{n}\left(Q_{obs_i} - Q_{est_i}\right)^2 . \qquad [78]$$

During the automatic calibration of the model, the optimal solution is defined as the set of parameters that minimizes this measure of error. WATFLOOD uses a modified version of this estimate of error by incorporating the difference between the simulated and measured flows at each gauging station. The values of root of the mean of the squared error (RMSE) reported for the simulations have been calculated similarly to the s criterion. However, in contrast to the s criterion, the RMSE does not normalize the error with respect to the mean observed flow:

$$RMSE = \sqrt{\frac{1}{g \cdot n} \sum_{i=1}^{g} \sum_{i=1}^{n} \left(Q_{obs_i} - Q_{est_i} \right)^2} . \qquad [79]$$

3.7 Initial Simulation Results

There is a total of 29 parameters in the WATFLOOD model. Seven of these parameters are used in the runoff and melt processes of snow covered areas, while the remaining 22 parameters control the other hydrologic sub-processes. Of these, up to 13 can be distributed parameters for which different values can be defined for up to 5 different land classes. Up to 8 of these 13 parameters can be optimized using the automatic calibration. Of the remaining 9 lumped parameters, each of which have a single value for the entire basin, 3 can be optimized. In addition to these parameters is a table of maximum interception storage values which must be defined for up to five different land classes and 12 different months.

Wherever possible, textbook values have been used for these parameters. Most of the parameters in the hydrologic sub-processes do not have an explicit physical meaning and are a modification of a number of typically measurable parameters. As a result, textbook values do not exist for many of the parameters. As a starting point, the initial values for the parameters were established as those values proven during the calibration and validation of simulations produced by WATFLOOD for the Grand River basin in Ontario, Canada. The physiographical differences between river basins in southern Ontario and basins in the Boreal Forest are significant. However, these parameters merely provide an essential starting point for the calibration process.

The first calibration runs utilize the current version of WATFLOOD, which uses published monthly averages to estimate hourly evapotranspiration. In an environment such as Southern Ontario, this method may be more applicable since long-term averages are better known. Complications arise in the simulation of remote regions where there is a lack of long-term records. Published values of monthly pan evaporation (Fisheries and Environment Canada, 1973-82) were obtained for both of the SSA and NSA sites for the period from 1973 to 1982

and are shown in Tables C1 and C2 in Appendix C. Actual evapotranspiration rates will be different than those measured by an evaporation pan, and thus, will require some reduction value (such as the value of 0.7 typically used to reduce potential evaporation measured by Class A pans in temperate regions of North America). A consistent reduction of 0.7 is adequate for estimating evapotranspiration rates under average conditions. However, this reduction is not realistic for modelling atypically dry or wet periods where values of evapotranspiration may be significantly different from the long-term averages.

The initial hydrologic simulations of the SSA watershed, shown in Figure 3.6, use an unmodified version of WATFLOOD. Estimates of hourly evapotranspiration have been made from the published long-term average values of pan evaporation. The simulated flows show an excellent correlation with the measured flows. The most considerable discrepancies occur during the month of June and August. During June, the simulated flows tend to under predict the measured flows. The 1994 summer season was wetter than average. These cloudier, cooler, and wetter conditions would limit the energy available for evapotranspiration, thus explaining the larger than expected measured runoff. The month of August consisted of persisting hot, dry atmospheric conditions, with the occurrence of very little precipitation. These conditions would produce a greater than normal rate of potential evaporation, thus explaining the lower than normal flows not accurately simulated with the estimates made with the evaporation pan values.

A third observation of the simulation is the relatively high peak flows. If the receding limb flows (as simulated) matched the measured flows, many of the resulting peak flows would be higher than the actual flows. This suggests that not enough water is evaporated during the peaks, and too much is evaporated during the low flows.

The volumes of the simulated flows are approximately the same as the measured flows for the months of May and July. The volumes of flow for the month of June are underestimated and the volumes of flow for the month of August are slightly overestimated volume. Because of the variation from typical meteorological conditions, these volumes would be better predicted by using a model which is a function of the actual meteorological conditions. Throughout the simulation, the peak flows are slightly over predicted. The flows would be better predicted by increasing the interception rates during, and immediately, following precipitation events.

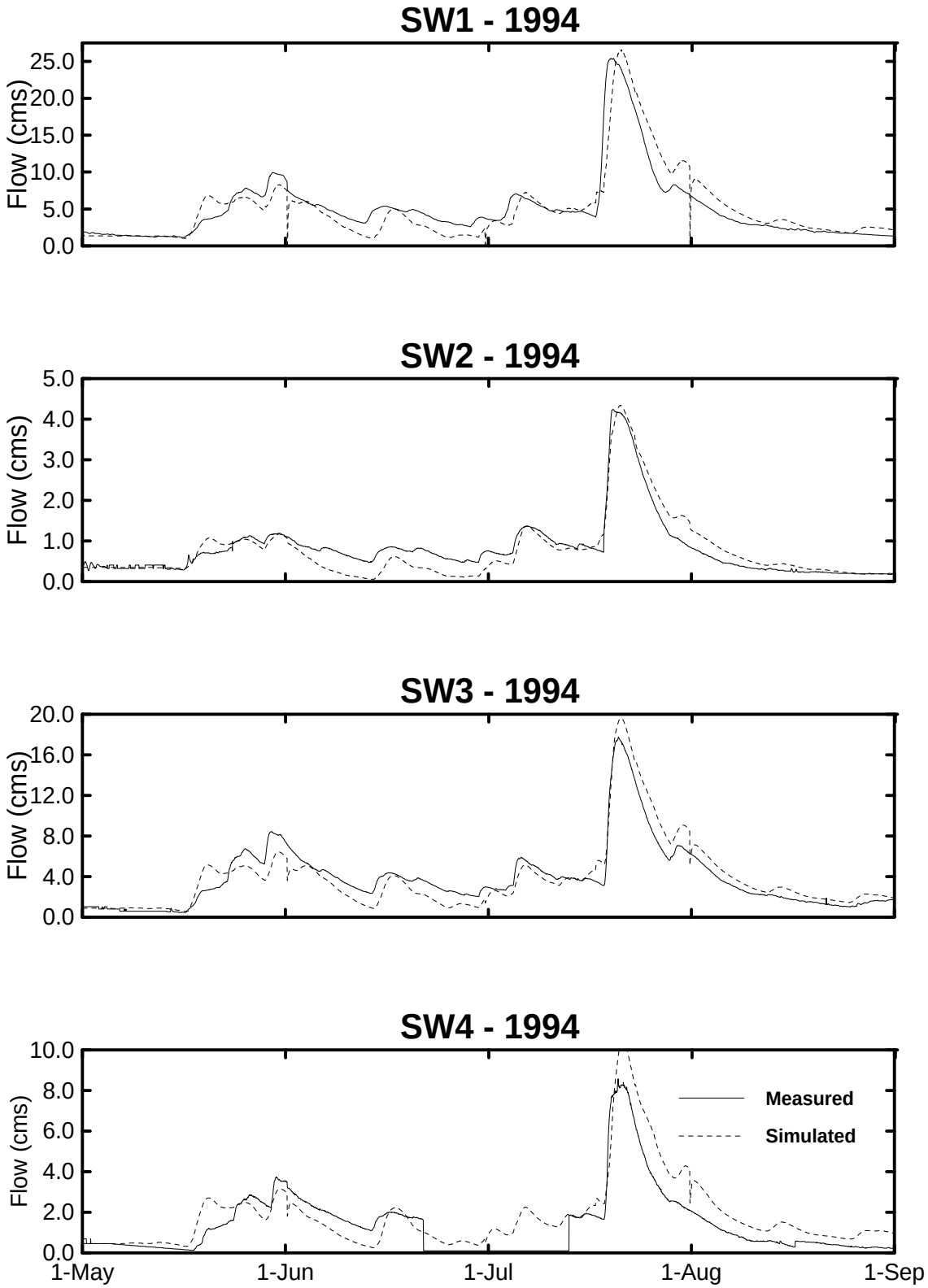

Figure 3.6: Hydrologic Simulation - SSA 1994 - Original Version of WATFLOOD

3.8 Incongruities in the Data

Some irregularities in the data are readily apparent in Figure 3.6. The gauge at SW4 was tampered with in late June/early July 1994, and as a result, the flow data were not recorded; the recorded hydrograph denotes this section of data as zero flow. Portions of data such as these have not been included in the error calculation for the simulations. Another portion of data that are unusable are the flow values recorded from September 1994 at SW3. A beaver dam interfered with the original flow control at this location resulting in a continuously changing stage-discharge relationship throughout this period of record. The new relationships could not be determined because of the lack of manual flow measurements at this location during this period.

Similar problems with beavers were prevalent throughout the 1995 season at the SW3 site, thus rendering the entire period of data to be of little use for calibration and validation purposes. Beaver problems also existed during some smaller time intervals at various other gauges during the 1995 season. The existence of low flows during periods of the 1995 season has potentially affected the accuracy of some flow records. The accuracy of the flow data record for the SW4 gauge during the 1995 season is questionable and is the subject of later discussion.

The SW3 gauge is located approximately 19 km upstream of the SW1 gauge. It would seem reasonable that, after most regional precipitation events, the peak flow should pass the SW3 gauge prior to passing the SW1 gauge. As shown in Figure 3.7 by the synchronized vertical reference bars, the peak flows at SW3 occur before the peak flows at SW1. The most reasonable explanation for this consistent attenuation in only this basin is that the data acquired from the Water Survey Canada gauge may not synchronized with the data obtained by the University of Waterloo. As shown in later simulations, all of the simulated peak flows at the SW1 gauge occur shortly after the measured peak flows. Regardless of the values of the roughness parameters used in the routing sub-routine, the simulated flows could not be attenuated for this extra period of time. The attenuation appears to be fairly constant throughout the simulation and is approximately one day.

The difference in the cumulative flow from the SW3 and SW1 basins should be similar provided that similar rainfall events occur over the basins. Similar precipitation inputs should exist between the two basins since the SW3 basin comprises approximately 80% of the SW1 basin. As shown in Figure 3.8, the difference between the cumulative flows from the two

basins is fairly constant, indicated by the constant slope of the line. However, there are some discontinuities in the slope. The large anomaly (6500, 8000) is most obvious, with smaller

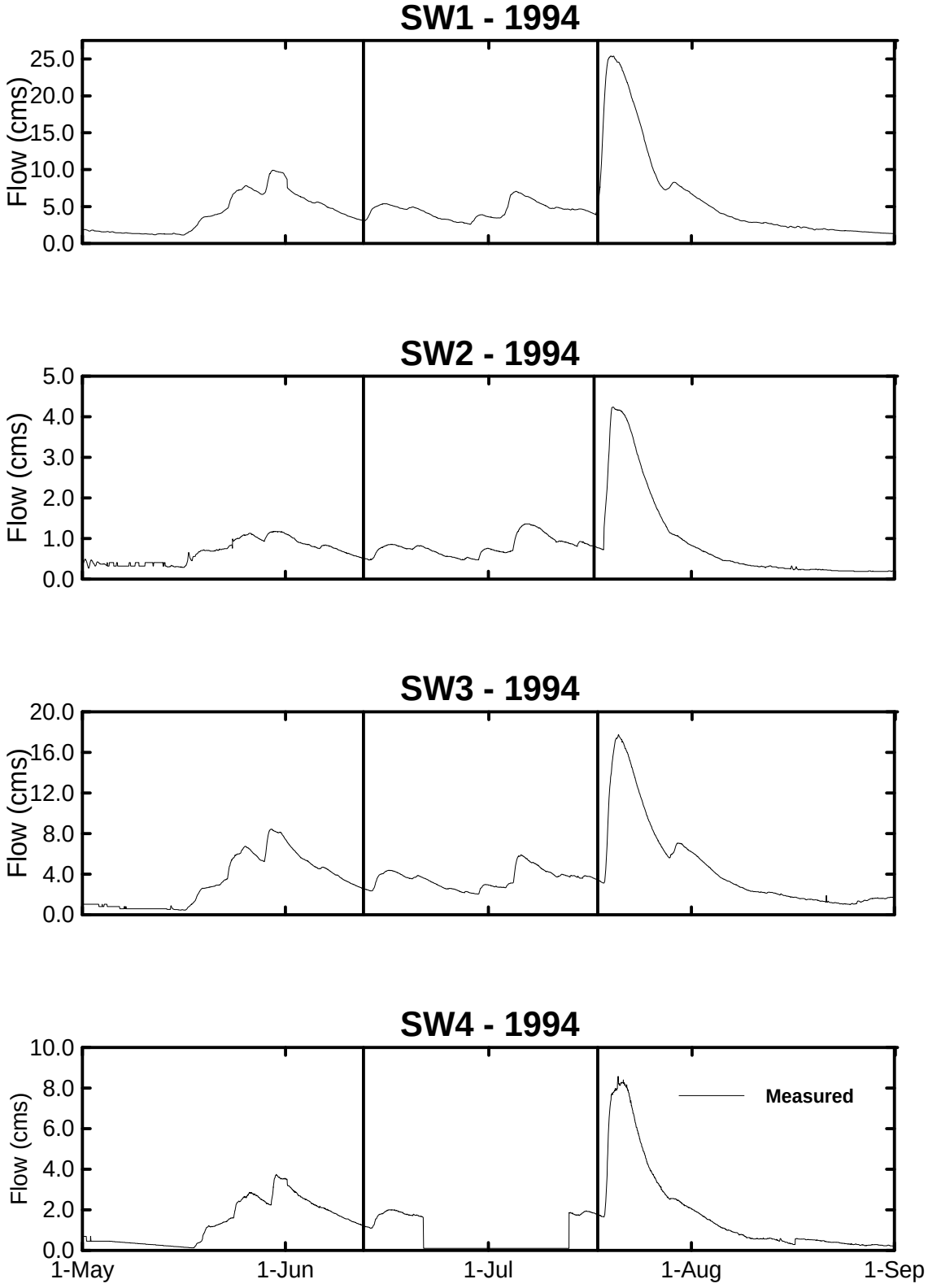

Figure 3.7: Lack of Attenuation in SW1 Peak Flows

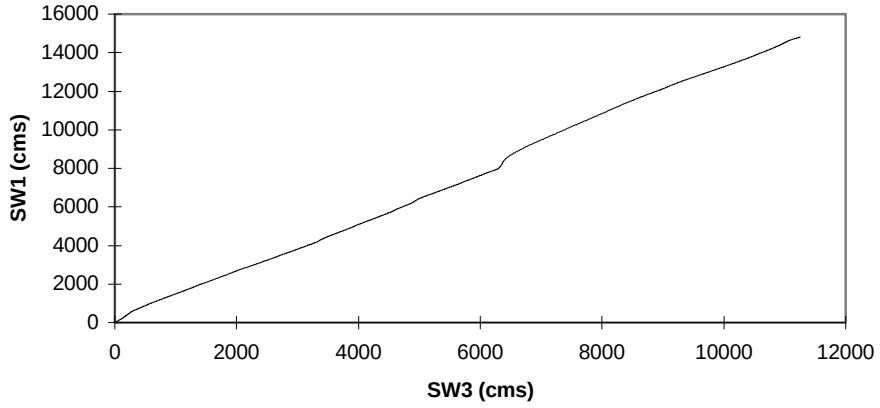

Figure 3.8: Cumulative Flows - SW3 vs. SW1

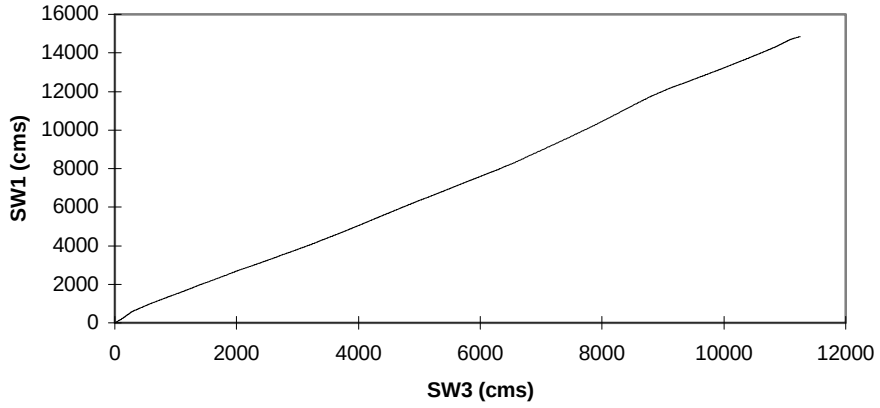

Figure 3.9: Cumulative Flows - SW3 vs. Adjusted SW1

ones being less apparent (3500, 4000). These discontinuities correspond to the lack of attenuation of the peak flows between SW3 and SW1. The correlation between the flows in Figure 3.8 has been improved by inserting one 24 hour period of data on June 12 in the SW1 flow record, shown in Figure 3.9. This point of insertion is most logical since there are a number of flows at this point in time that are similar and could have been confused during manual data entry. As well, this point corresponds to a low flow period just prior to a rising limb, immediately following the first vertical reference bar in Figure 3.7. It is after this period that the attenuation of flows exists.

Like the stream gauges, the Belfort rain gauges were built using rheostat devices to vary voltages. However, the Belfort gauges, unlike the stream gauges, used very light counterweights. The measurements in the rain gauges were sensitive to the deformation of mechanical components as a result of temperature variations. The temperature records maintained by the data loggers inside the rain gauges were correlated to the diurnal voltage variation of the gauged rain. By regressing a relationship, the noise in the rain data, as measured by the Belfort gauges, was mostly eliminated.

Chapter 4
Comparison of Evapotranspiration Models

The potential evapotranspiration models that have been chosen for further analysis are the Hargreaves equation, the Priestley-Taylor equation, and the Turc equation (equations 57, 64, and 63 respectively). Actual energy fluxes and meteorological data have been measured at the different tower flux sites by other BOREAS investigators. These measurements will provide the input data for the potential evapotranspiration models and a reference (the actual evapotranspiration) to which the estimated potential evapotranspiration values can be compared. Simultaneous measurements of soil moisture and temperature at these locations provide the data to support an investigation into a suitable method for indexing the actual evapotranspiration to the potential evapotranspiration.

4.1 Spatial Variability of Parameters

Watersheds that are the focus of future hydrologic studies may not be located in areas which have instrumentation deployed at such a high spatial resolution as in the BOREAS study. In particular, WATFLOOD has the ability to utilize distributed or non-distributed data. The use of non-distributed data significantly reduces the computational requirements to run the model, but these data can only be used if they are justified. For this reason, the spatial variability of the parameters used in calculating the evapotranspiration has been analyzed.

The variables required to make estimates of potential evapotranspiration using the Hargreaves, Priestley-Taylor, and Turc equations, are air temperature, relative humidity, net radiation, ground heat flux, and air pressure. The spatial variability of the daily average of these variables was analyzed, where the averages were calculated from the values of these measurements made at 15 minute intervals at the flux towers for successive 24 hour periods.

4.1.1 Temperature

Temperature is a spatially stable variable (Anderson, 1992). For the period between Julian Days 144 and 199, 1994, temperatures measured at tower flux sites have been plotted with respect to the day of year in Figures 4.1 and 4.2 for the SSA and NSA, respectively. Because a standard measurement height was not established, the temperature measured at the highest point on each of the towers has been used for consistency. For simplicity of comparison, only the line connecting the OBS-SSA data has been shown in the plot. All of the tower sites show the same general trend in air temperatures, with data values falling closely about the OBS-SSA trend line. The data values from the different tower sites tend to maintain the same relative magnitude, indicating the possible existence of small systematic differences between the sites.

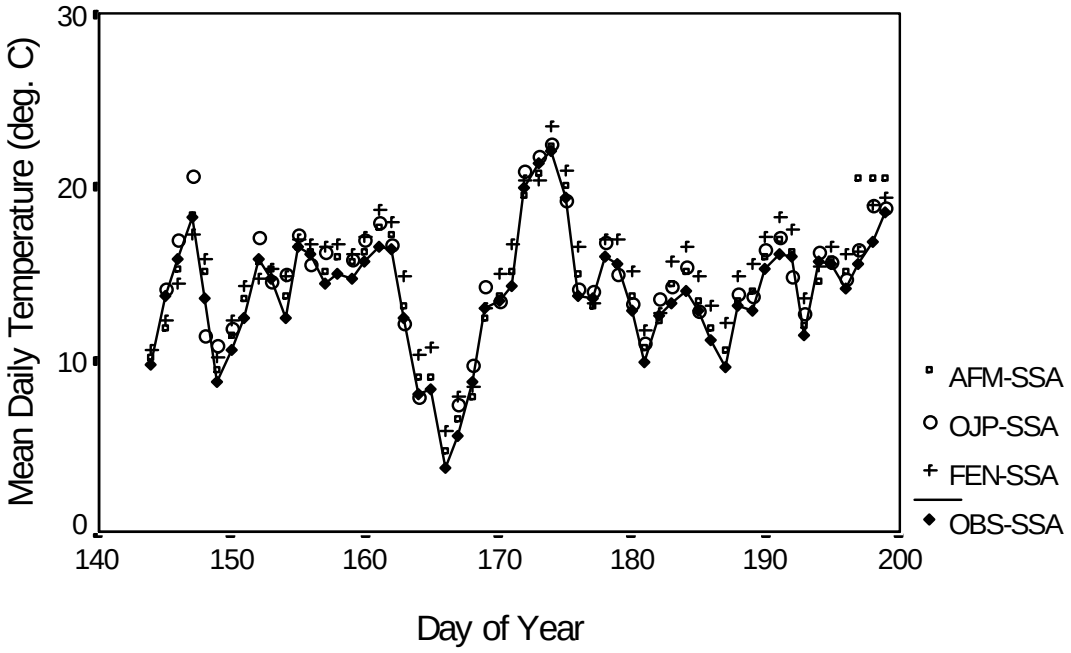

Figure 4.1: Temperature vs. Day of Year - SSA Flux Towers

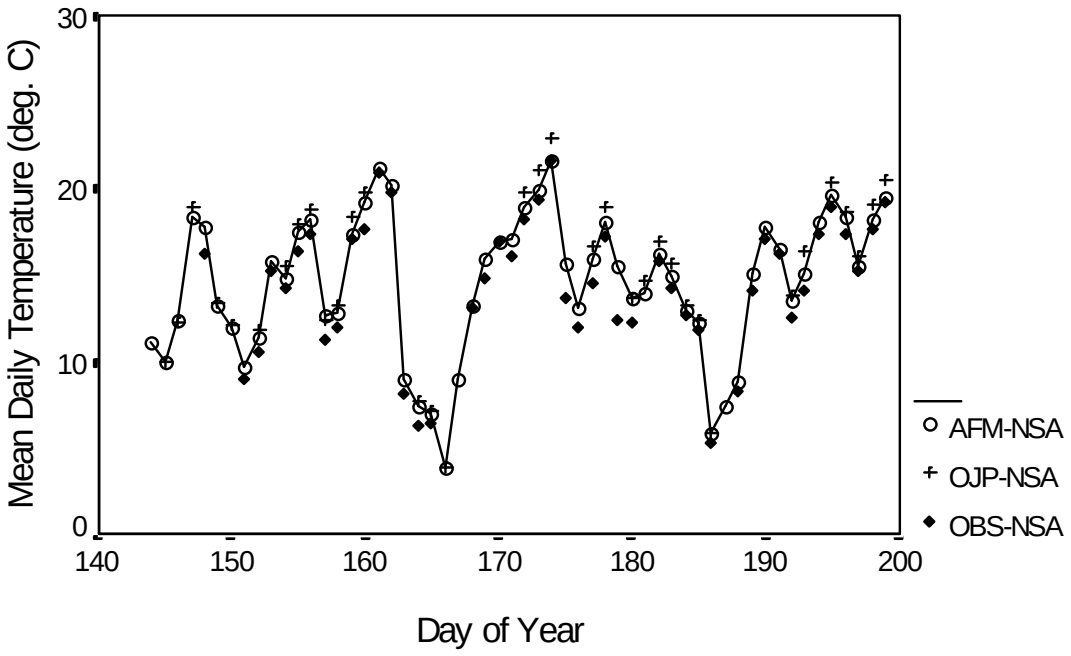

Figure 4.2: Temperature vs. Day of Year - NSA Flux Towers

Figures 4.3 and 4.4 show the correlation between the air temperature measured at the OBS and the AFM towers for the SSA and NSA, respectively. Both plots indicate a near perfect correlation, although some minor systematic differences exist. A comparison of the temperatures measured at each of the tower sites in both of the study areas is shown in Table 4.1. Between all but two flux towers the correlation between the measured temperatures is greater than 0.90.

Table 4.1: Comparison of Air Temperatures Measured at Flux Towers

Sites Compared	Correlation Coefficient R	t-test Significance	Daily Mean (°C)	Difference (°C)
OBS-SSA FEN-SSA	0.949	0.000	13.90 15.23	-1.33
OBS-SSA OJP-SSA	0.961	0.000	14.46 15.20	-0.74
OBS-SSA AFM-SSA	0.960	0.000	13.90 14.53	-0.63
FEN-SSA OJP-SSA	0.888	0.032	15.67 15.20	+0.47
FEN-SSA AFM-SSA	0.961	0.000	15.22 14.53	+0.69
OJP-SSA AFM-SSA	0.919	0.460	15.20 15.05	+0.15
OBS-NSA OJP-NSA	0.996	0.000	14.59 15.92	-1.33
OBS-NSA AFM-NSA	0.989	0.000	14.58 15.41	-0.83
OJP-NSA AFM-NSA	0.998	0.000	15.18 14.70	+0.48

A t-test has been used to analyze the significance of the difference between the pairs of observed values. A low value calculated with the t-test indicates a decrease in the probability of the null hypothesis being true. The null hypothesis for these analyses is that the difference between actual population means of the samples is zero. A level of significance of between 1 and 5% is generally considered to indicate that there is significant evidence against the null hypothesis. These values have been used for testing the null hypothesis within this thesis.

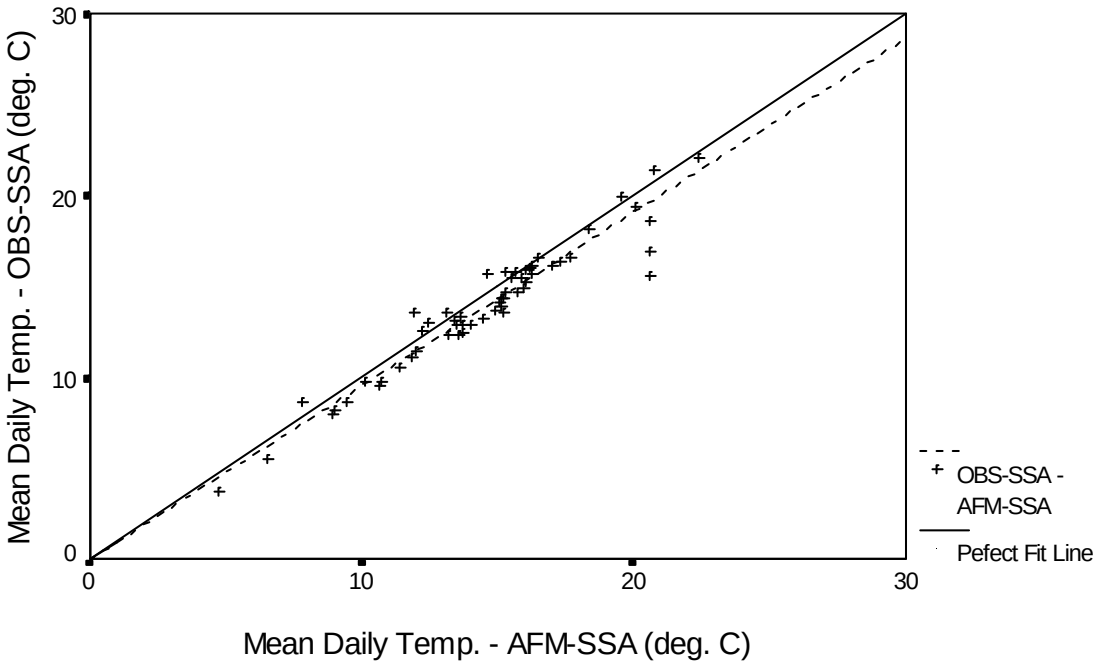

Figure 4.3: Temperature - OBS-SSA vs. AFM-SSA

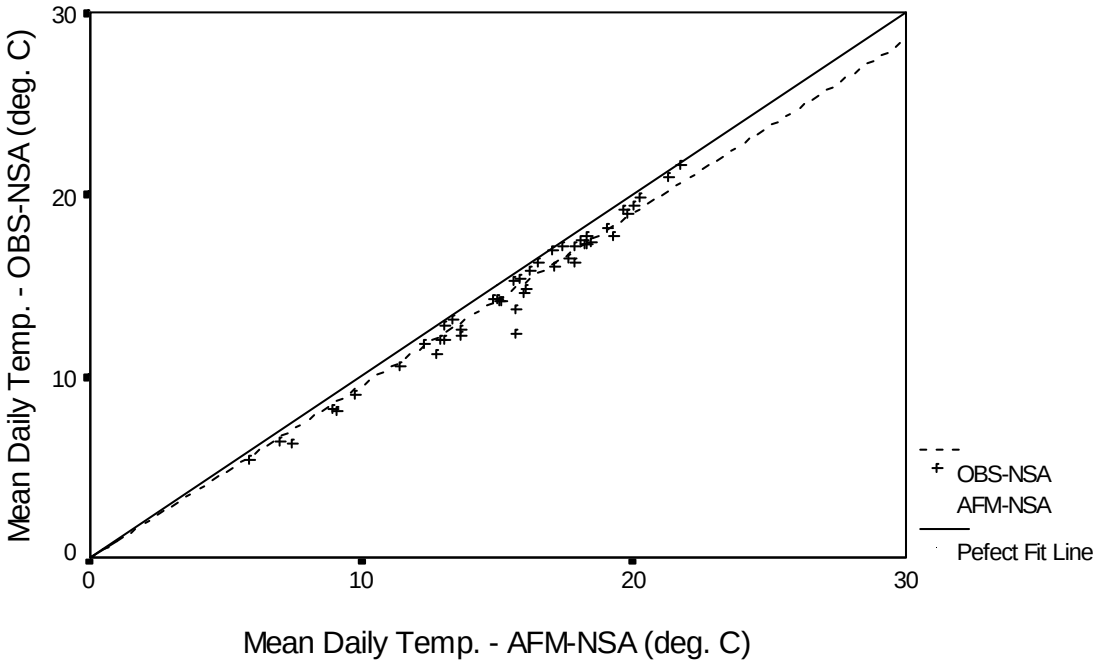

Figure 4.4: Temperature - OBS-NSA vs. AFM-NSA

The significance of the t-tests for the paired comparisons are shown and indicate that there is strong evidence against the null hypothesis in all but one of the comparisons. The daily variations are similar and the differences between towers are consistent. Together, these two results suggest that there is a systematic lack of fit between the temperatures measured at the different tower flux sites.

The difference between the temperatures is less than 1.33 ºC for all of the paired comparisons. This corresponds to a maximum error of ± 3.0% and ±2.0% in the estimates of the potential evapotranspiration made by the Hargreaves and Turc equations, respectively. After applying a reduction to the potential evapotranspiration values, typically of 0.6 to 0.7, these errors would be reduced to relatively insignificant values.

This systematic lack of fit may be a result of the different land covers or possibly because the temperature measurements were made consistently at a different height on each tower. Regardless of the reason for the systematic differences, the effect on the potential evapotranspiration estimates is small. Therefore, for simplicity the AFM tower measurements of temperature have been used as the standard temperature for estimating evapotranspiration throughout the basins. Although the paired comparison of the means suggest that the mean temperature measured at the AFM towers is not necessarily equal to the mean measured at the other towers, the strong degree of correlation suggests that the errors are systematic. Consistent errors can be significantly reduced or eliminated during the model calibration. The high degree of correlation in these comparisons provides further evidence of the spatial stability of temperature.

4.1.2 Net Radiation

The variable net radiation is utilized in the Priestley-Taylor model. This model calculates evapotranspiration as a direct function of the radiant energy fluxes. Typically, net radiation is significantly larger, from 10 to 100 times greater than the ground heat flux during daylight hours (Munro, 1979). As a result, the error in the final estimate of evapotranspiration during the daylight hours will be a direct reflection of the percentage of error in the net radiation input.

Net radiation is the total incoming radiation less the outgoing radiation. The incoming radiation will be a function of the sun angle (a function of the latitude, time of year, and time of day) and the obscuration created by the atmosphere, predominantly the cloud cover. Atmospheric disturbances tend to be relatively large when compared to the size of the NSA and SSA watersheds (40km across at the widest points). The typical speed at which these systems tend to

move means that on average, a single system would tend to affect the entire watershed during the course of a few hours. The average cloud cover associated with such a system will therefore be assumed to be constant throughout the basin for a one day averaged period. Similar cloud cover throughout the basin, coupled with a small variation in latitude of the basin, will result in a similar values of average incoming radiation for all areas of a small watershed.

The amount of energy reflected is a function of the surface albedo, which is governed by the ground cover and the sun angle. Outgoing long-wave energy, a component of the total outgoing energy, is a function of the temperature of the surface. The surface temperature will be related to the air temperature in the immediate vicinity, a variable previously shown to be spatially stable. Therefore, the total outgoing radiation will have some spatial variance related to the type of vegetation cover.

Values of net radiation were measured at each of the tower flux sites. The mean daily values of these measurements made between Julian Day 144 and Julian Day 199 in 1994 are plotted with respect to the day of year in Figures 4.5 and 4.6 for the SSA and the NSA, respectively. With a few exceptions, the net radiation from all of the sites follows the same general trend (shown by the line through the net radiation values at the FEN-SSA and the OJP-NSA). During a few of the days the OBS-SSA net radiation was consistently higher (between day 170 and 180) than the other the sites.

Figures 4.7 and 4.8 show the comparisons between the OBS and the AFM tower sites in the SSA and NSA, respectively. A very good correlation is apparent between the OBS-NSA and the AFM-NSA sites. Similarly, a good correlation is evident between the OBS-SSA and the AFM-SSA tower sites, although more systematic scatter about the perfect fit line is apparent at the southern sites. The net radiation of the OBS-SSA site increases more rapidly than the corresponding increase in the AFM-SSA net radiation. This type of systematic error would be explainable by a difference in the albedos of the two vegetation types.

Table 4.2 shows the statistical analysis from a comparison of the means of the daily net radiation measurements between the different tower flux sites in each study area. The net radiation is similar for all of the sites, with the exception that the net radiation at the OBS site in both study areas is slightly higher. In all of the comparisons the correlation coefficients are very high, being greater than 0.90. In all but one of the comparisons made in the SSA, there is overwhelming evidence against the null hypothesis. Three of these conclusions are a result of

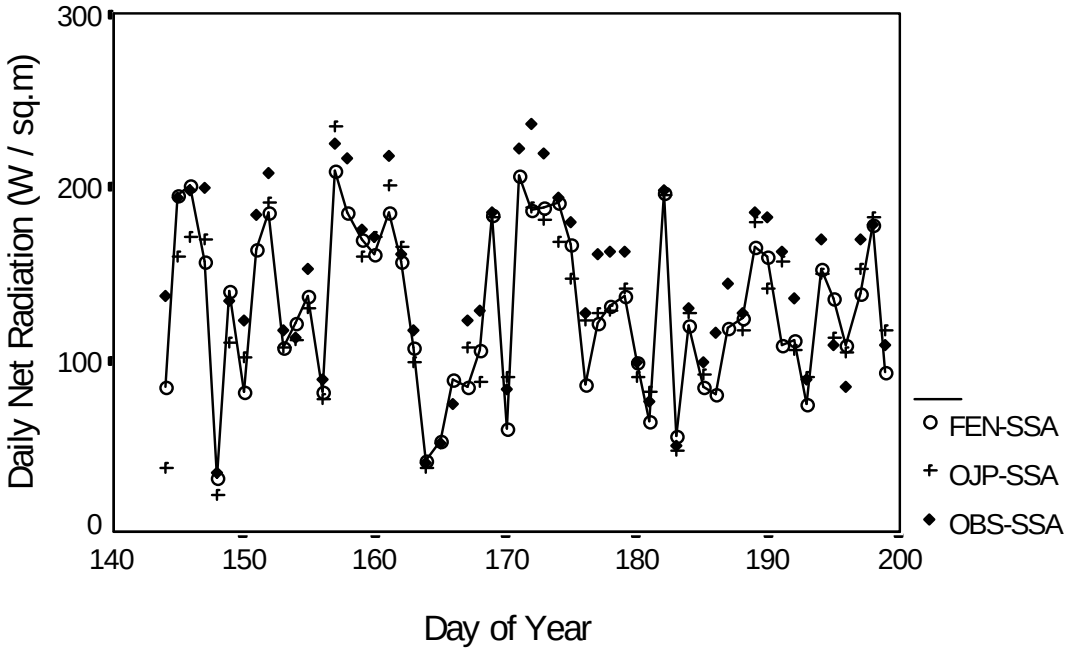

Figure 4.5: Net Radiation vs. Day of Year - SSA Flux Towers

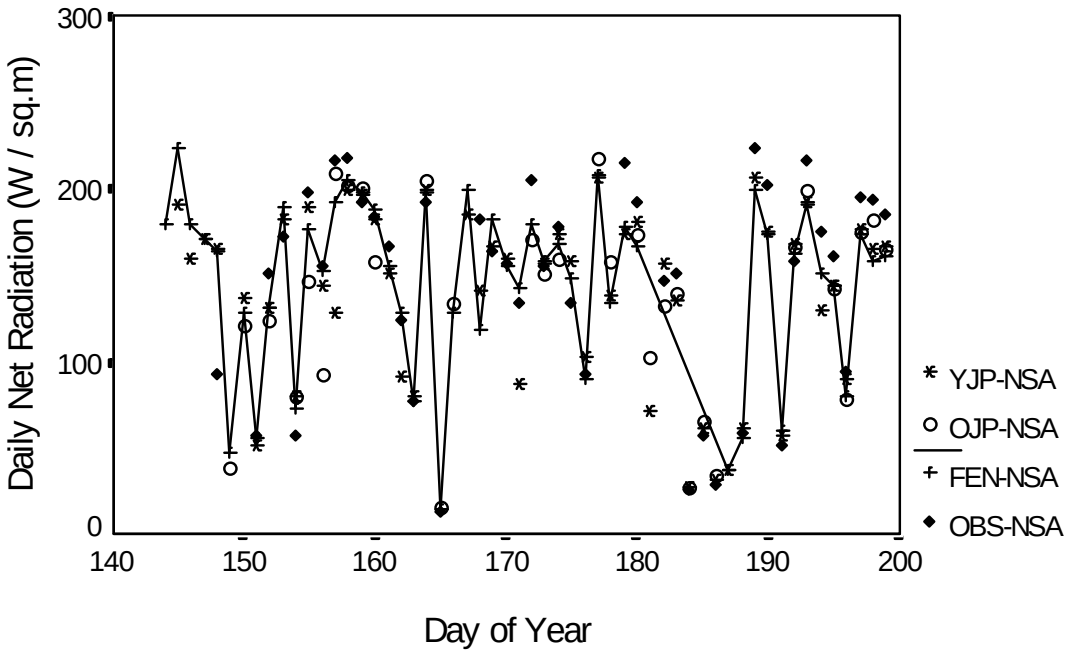

Figure 4.6: Net Radiation vs. Day of Year - NSA Flux Towers

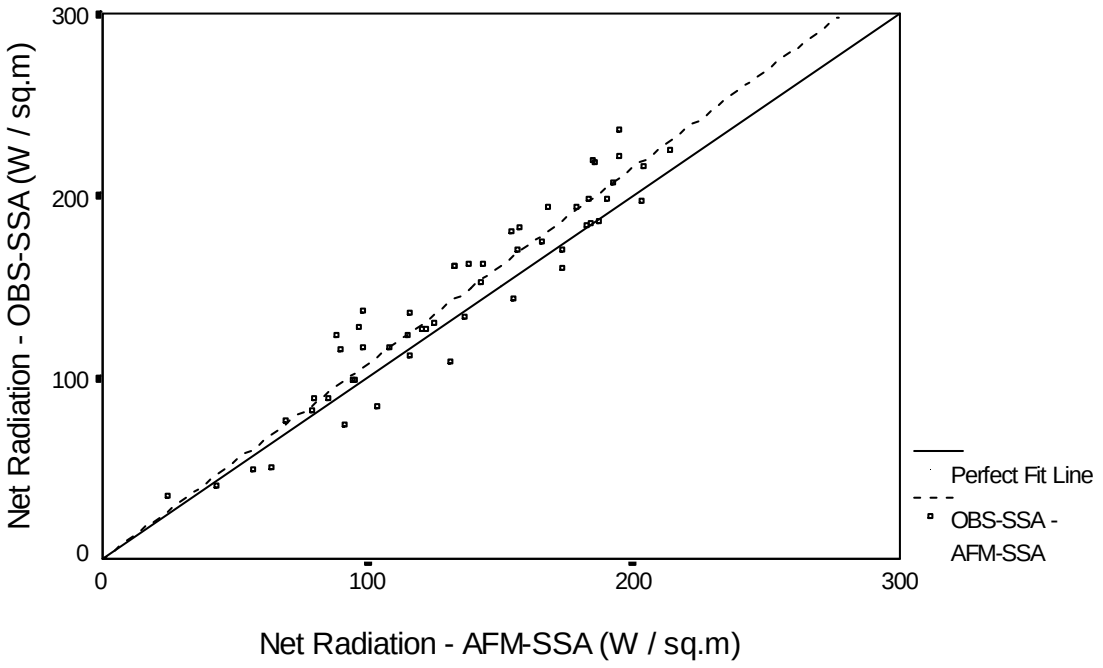

Figure 4.7: Net Radiation - OBS-SSA vs. AFM-SSA

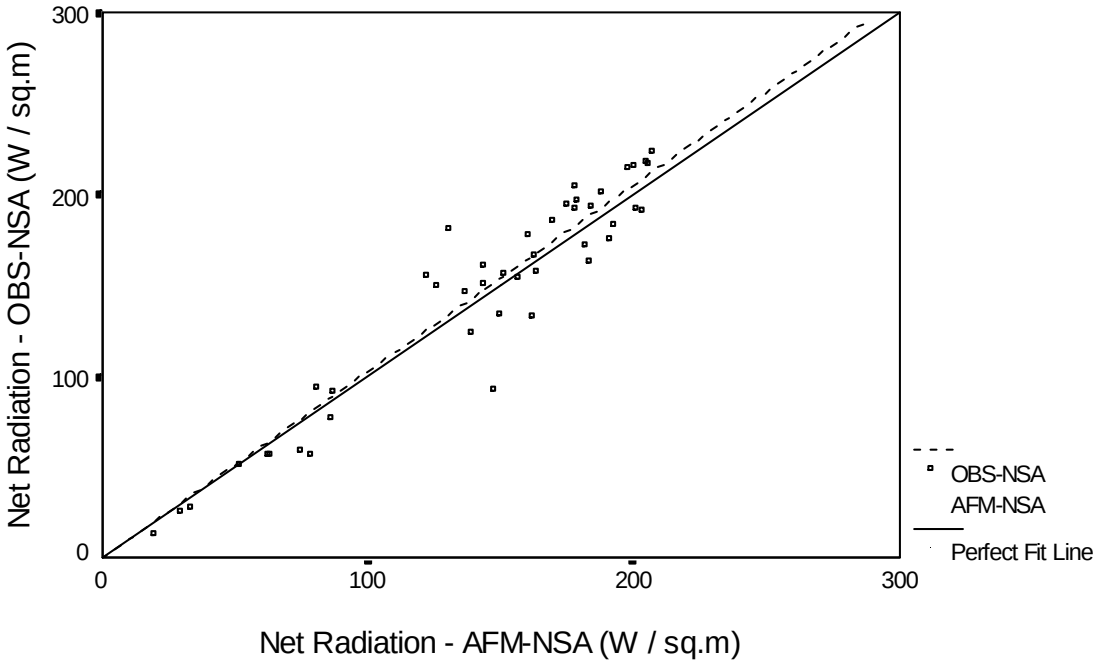

Figure 4.8: Net Radiation - OBS-NSA vs. AFM-NSA

Table 4.2: Comparison of Net Radiation Measured at Flux Towers

Sites Compared	Correlation Coefficient R	t-test Significance	Daily Mean ($W\ m^{-2}$)	Difference ($W\ m^{-2}$)
OBS-SSA FEN-SSA	0.935	0.000	145.4 130.0	+15.5
OBS-SSA OJP-SSA	0.916	0.000	145.6 130.3	+15.3
OBS-SSA AFM-SSA	0.957	0.000	145.0 134.4	+10.6
FEN-SSA OJP-SSA	0.921	0.982	130.2 130.3	- 0.1
FEN-SSA AFM-SSA	0.964	0.008	129.5 134.4	- 4.9
OJP-SSA AFM-SSA	0.963	0.018	128.9 133.5	- 4.6
OBS-NSA FEN-NSA	0.920	0.032	154.0 146.3	+ 7.7
OBS-NSA OJP-NSA	0.954	0.003	151.2 138.9	+12.3
OBS-NSA YJP-NSA	0.900	0.029	147.6 138.9	+ 8.7
OBS-NSA AFM-NSA	0.953	0.250	145.9 142.7	+ 3.2
FEN-NSA OJP-NSA	0.943	0.632	150.9 149.3	+ 1.6
FEN-NSA YJP-NSA	0.934	0.197	151.0 147.7	+ 3.3
FEN-NSA AFM-NSA	0.958	0.440	146.9 148.5	- 1.6
OJP-NSA YJP-NSA	0.896	0.921	143.8 144.2	- 0.4
OJP-NSA AFM-NSA	0.984	0.046	137.1 140.8	- 3.7
YJP-NSA AFM-NSA	0.910	0.090	139.9 145.1	- 5.2

the relatively high values of net radiation measured at the OBS-SSA tower. The sampled mean values at the remaining SSA sites differ by less than 4.9W m^{-2}, or about 5%.

In contrast to the SSA, all of the comparisons in the NSA (excluding those with the OBS-NSA), show that there is only some or weak evidence against the null hypothesis (that the difference population means of daily net radiation is zero). The mean values vary by less than 6%. Similar to the SSA, the OBS tower site has significantly higher values of net radiation.

There is a strong correlation between the values of the net radiation measured at all of the flux tower sites and an insignificant difference between their mean daily values. This implies that, for small watersheds, a measurement of the representative net radiation will provide sufficiently accurate data for the calculation of evapotranspiration from each land class. For watersheds with significant variations in land cover, a correction to the measure of the typical net radiation may be necessary; this correction could take the form of some function of the differences in albedo.

4.1.3 Pressure

Generally, it is assumed that atmospheric pressure remains constant over small horizontal distances and very minor elevation changes, characteristics of the NSA and SSA watersheds. In the Priestley-Taylor equation, the psychrometric constant is calculated as function of the atmospheric pressure, although the sensitivity of the constant to a change in pressure is very small. Throughout the 1994 study period, the atmospheric pressure in the SSA varied between 92.8 kPa and 96.5 kPa, as measured at the AFM-SSA site. The sensitivity of the psychrometric constant to a variation in pressure is very slight. Throughout the range of atmospheric pressures observed, the variation of the constant is relatively small, only ± 4.0%. Because of this low sensitivity, the published mean monthly values of atmospheric pressure for each of the regions have been used to calculate the psychrometric constant in cases where the actual values were not observed. For the simplification of future work in areas with minor changes in elevation, it would be appropriate to use the local average atmospheric pressure for this calculation.

4.1.4 Ground Heat Flux

Ground heat flux is a function of long-term temperature fluctuations and the properties of the underlying soil. Its spatial variability with respect to the long-term temperature variations will be minimal, but potentially significant as a result of typically heterogeneous soil and ground covers throughout watersheds. However, only a small amount of error is introduced by making

calculations with the Priestley-Taylor equation using non-spatially distributed values of ground heat flux. This parameter is usually assumed to be negligible. On average, it can be as high as 10% of the total energy budget (Munro, 1979). Even with an unlikely error in the estimation of this variable in the order of 50%, the overall error in the evapotranspiration estimate would only be 5%. An estimate of this parameter from a typically vegetated site is sufficient to provide a good approximation for the entire watershed.

The ground heat flux has been calculated from an approximation of the change in the heat stored in a unit volume of soil (equation 8). The change in storage is calculated as the product of the change in average temperature of a depth of soil and the specific heat capacity of the soil. A typical value for the specific heat capacity of soil, 2.1 $MJ \cdot m^{-3} \cdot °C^{-1}$ (Shuttleworth, 1993), has been used in the calculation.

4.1.5 Relative Humidity

Since relative humidity is a function of spatially stable variables, temperature and pressure, then it too, will be spatially stable.

4.2 Spatial Variability of Potential Evapotranspiration

The variables used to calculate potential evapotranspiration in the three models are all spatially stable. The value of using a single calculation of potential evapotranspiration for the entire watershed is apparent (e.g. for periods when all of the meteorological stations are not in operation, or for watersheds where data from more than one meteorological station are not available). In order to confirm the spatial stability of the potential evapotranspiration equations, the spatial variability of the estimates as a function of slight variations in the input parameters has been analyzed.

The AFM tower flux sites (located at the OJP-SSA and OJP-NSA tower flux sites) are a continuous source of meteorological data throughout the 1994 and 1995 study periods. Estimates of potential evapotranspiration, using the three models, have been made at the AFM-NSA and AFM-SSA sites for comparison with estimates made at seven of the tower flux sites in the NSA and SSA. The period used for comparison is from Julian Day 144 to Julian Day 199, 1994. Where temperature, relative humidity, and pressure have been measured at the flux towers, these values have been used for input into the evapotranspiration equations. Otherwise, values measured at flux towers within the same study area or local mean monthly values, shown in Tables C1 and C2 (Environment Canada, 1993) in Appendix C, have been substituted.

4.2.1 Hargreaves - Spatial Variability

In the Hargreaves equation [57], the extraterrestrial solar radiation has been estimated using equations [59] to [62], as shown in section 2.3.3.2. The correlation between the daily estimates of the Hargreaves potential evapotranspiration at each of the seven tower flux sites and at the AFM tower sites is shown in Table 4.3. Four of the five sites compared have correlation coefficients greater than 0.93. The null hypothesis, that population means of the two pairs are equal, is rejected at three of the four sites. Low variability in the evapotranspiration estimates reduces the probability that the actual means of the sampled populations are equal. However, the relative error in the actual daily means is small. Using the AFM sites to calculate the potential evapotranspiration tends to produce an estimate in error of less than 6.0%. As would be expected for the Hargreaves temperature-based equation, the difference in the mean potential evapotranspiration between sites varies directly with the difference in the mean temperature between the sites (calculated in section 4.1.1).

Table 4.3: Comparison of Mean Daily Hargreaves PET Calculated at Flux Towers and at AFM Tower

Sites Compared	Correlation Coefficient R	t-test Significance	Mean ($mm\ d^{-1}$)	Difference ($mm\ d^{-1}$)
OBS-SSA	0.957	0.000	3.94	+0.23
AFM-SSA			3.71	
FEN-SSA	0.933	0.000	3.93	+0.22
AFM-SSA			3.71	
OJP-SSA	-0.108	0.186	4.20	-0.20
AFM-SSA			4.40	
OJP-NSA	0.956	0.984	4.30	+0.00
AFM-NSA			4.30	

4.2.2 Priestley-Taylor - Spatial Variability

Daily potential evapotranspiration has been calculated with the Priestley-Taylor equation [64]. Values of net radiation and ground heat flux, as well as the meteorological variables measured at the flux towers, have been used for input into the equation. In the event of missing ground heat flux measurements, values measured at a site within the same study area were utilized. No substitutions were made for missing values of net radiation.

The values of the Priestley-Taylor potential evapotranspiration calculated at the AFM sites and the NSA and SSA tower flux sites have been analyzed for correlation and similarity of the

sample means, as shown in Table 4.4. All of the correlation coefficients are greater than 0.93, with the exception of one value being 0.85. In all of the pairs compared, the null hypothesis (that the population means are equal) must be rejected. The low variability of the estimated values about their means reduces the probability that the actual population means are equal. The difference between the means is typically less than 15%, with only two of the seven observations being greater than 15%. The observations of the OBS-NSA site are unusually high and are possibly the result of erroneous measurements. The differences in potential evapotranspiration between all of the towers corresponds to the differences in the net radiation.

Table 4.4: Comparison of Mean Daily Priestley-Taylor PET Calculated at Flux Towers and at the AFM Towers

Sites Compared	Correlation Coefficient R	t-test Significance	Mean ($mm\ d^{-1}$)	Difference ($mm\ d^{-1}$)
OBS-SSA AFM-SSA	0.932	0.029	3.85 4.03	-0.18
FEN-SSA AFM-SSA	0.937	0.000	3.70 4.03	-0.33
OJP-SSA AFM-SSA	0.854	0.002	3.65 4.03	-0.38
OBS-NSA AFM-NSA	0.931	0.000	6.40 4.40	+2.00
FEN-NSA AFM-NSA	0.942	0.000	4.03 4.73	-0.70
OJP-NSA AFM-NSA	0.984	0.000	3.87 4.31	-0.44
YJP-NSA AFM-NSA	0.926	0.000	3.60 4.53	-0.93

4.2.3 Turc - Spatial Variability

For the Turc equation [63], solar radiation has been estimated using the equations [59] to [62], as shown in section 2.3.3.2. Table 4.5 shows the values of correlation between the Turc estimates of daily evapotranspiration calculated at the NSA and SSA flux tower sites, and the corresponding AFM tower sites. In all but one of the five towers compared, the correlation is greater than 0.93. In three of the comparisons, there is insufficient evidence to reject the null

hypothesis, including the site with the lowest correlation (OJP-SSA correlation = 0.66). In all of these comparisons, the difference in the means is less than 6%.

Table 4.5: Comparison of Mean Daily Turc PET Calculated at Flux Towers and at the AFM Towers

Sites Compared	Correlation Coefficient R	t-test Significance	Mean (mm d^{-1})	Difference (mm d^{-1})
OBS-SSA AFM-SSA	0.956	0.220	1.40 1.41	-0.01
FEN-SSA AFM-SSA	0.925	0.762	1.41 1.41	+0.00
OJP-SSA AFM-SSA	0.656	0.612	1.43 1.41	+0.02
OJP-NSA AFM-NSA	0.948	0.000	1.42 1.51	-0.09

4.2.4 Conclusions - Spatial Variability

The above analyses indicate that there is a small but statistically significant difference between the estimates of potential evapotranspiration made at the tower flux sites and at the AFM tower sites. However, the differences in the potential evapotranspiration between the sites can be accounted for by the differences in the input variables. The generally high values of correlation and low values of standard deviation for the measured variables indicates that there is a systematic variation between the measurements.

At the time of writing, the tower flux measurements were not available for 1995 season. Data were available from the AFM tower sites located close to the OJP-SSA and the OJP-NSA tower flux sites. For the sake of consistency between modelling 1994 and 1995, for the purposes of simplification, and because of the standardization of measurements, the AFM meteorological tower measurements of air temperature, atmospheric pressure, net radiation, relative humidity, and ground temperature will be utilized for hydrologic modelling purposes.

The temperatures have been estimated as the average of the measurements made at the lowest and the highest elevations on the towers in order to estimate the within-canopy temperatures. For hydrologic simulation purposes, these values have been used to calculate the potential evapotranspiration rates from the Hargreaves and Priestley-Taylor models in both the NSA and SSA for all land cover classes. It has been shown that there are systematic differences between

the variables measured at the AFM sites and the tower flux sites. However, these differences are relatively small and will not have significantly adverse effects on the final estimates of actual evapotranspiration. The consistency in the variability will enable the calibration of parameters used to index the actual to the potential evapotranspiration rates to account for these systematic differences. A possible factor for adjusting the net radiation between sites is the difference in the albedo between land covers.

4.3 Temporal Variability of Potential Evapotranspiration

The equations used for calculating potential evapotranspiration were originally developed to provide estimates for periods of at least one day. The equations can be used for calculations of shorter periods, but are more accurate when averaged over longer periods. The version of the Turc equation that has been used was developed to provide estimates of evapotranspiration for 10-day periods. Similarly, the Hargreaves equation provides more accurate estimates for averaging periods of one week to one month. These periods are much longer than the river travel times within the basins being modelled, typically about one day, and are therefore too lengthy for use in a hydrologic model at this scale.

As a result of these short travel times, and even shorter travel times within each element, the time step in the hydrologic model has been established as one hour. Although it is possible to incorporate an evapotranspiration program with a different time step, it would be convenient to use the same period for calculations. To validate the use of these evapotranspiration models, which were developed for a different time scale than the one being used, the sensitivity of each equation to the time scale has been analyzed.

Half-hourly estimates of evapotranspiration have been made with each of the models, where all of the input variables have been provided at this interval. The half-hourly values have been summed to calculate the total daily evapotranspiration. The same models have been used with daily average values of the input variables. The daily averages of the input variables have been calculated as the average of the half-hourly values for each day.

Comparisons have been made between the daily potential evapotranspiration estimates made with the summed half-hourly data and the estimates made with the averaged daily data for each model. The period used for comparison is from Julian Day 144 to Julian Day 199, 1994. Comparisons have been made at seven of the tower flux sites.

4.3.1 Hargreaves - Temporal Variability

Figure 4.9 shows the relationship between the daily potential evapotranspiration (calculated from daily averages of temperature and humidity) and the total daily potential evapotranspiration (calculated with half-hourly measured data inputs). The plot is of the values calculated at the OBS-SSA tower flux site and is typical of the relationship found at the different sites in both study areas. A line indicating the perfect correlation (PET_{daily} equals $PET_{half\text{-}hourly}$) has been plotted for reference. The data points are well distributed about the line of perfect fit and do not show any systematic error. Table 4.6 shows the correlation between the values calculated with half-hourly data and the values calculated with daily averages.

Table 4.6: Comparison of Half-Hourly and Daily Calculated Hargreaves PET

Flux Tower	Calculation	Correlation Coefficient R	t-test Significance	Mean (mm d^{-1})	Difference (mm d^{-1})
OBS-SSA	Hourly Daily	0.993	0.000	3.75 3.94	-0.19
FEN-SSA	Hourly Daily	0.993	0.000	3.75 3.93	-0.18
OJP-SSA	Hourly Daily	0.999	0.982	4.80 4.81	-0.01
OJP-NSA	Hourly Daily	0.992	0.000	4.12 4.30	-0.18

At all of the towers, there is a very high correlation (greater than 0.990) between the values calculated half-hourly and the values calculated daily. However, the variance in each of the sets of values is so small that the null hypothesis, that the population means of the two groups are equal, is rejected at three of the five sites. The difference between the sampled means of each pair is less than 5.0%.

4.3.2 Priestley-Taylor - Temporal Variability

The relationship between the daily potential evapotranspiration (calculated from daily averages of the meteorological data and energy flux values) and the daily evapotranspiration (calculated from the sum of the values calculated from half-hourly data inputs), are shown in Figure 4.10. This plot is of the data measured at the OBS-SSA flux tower and is typical of the relationship observed at the tower flux sites in both study areas. A line indicating the perfect correlation (PET_{daily} equals $PET_{half\text{-}hourly}$) has also been plotted. The data points have only a very small

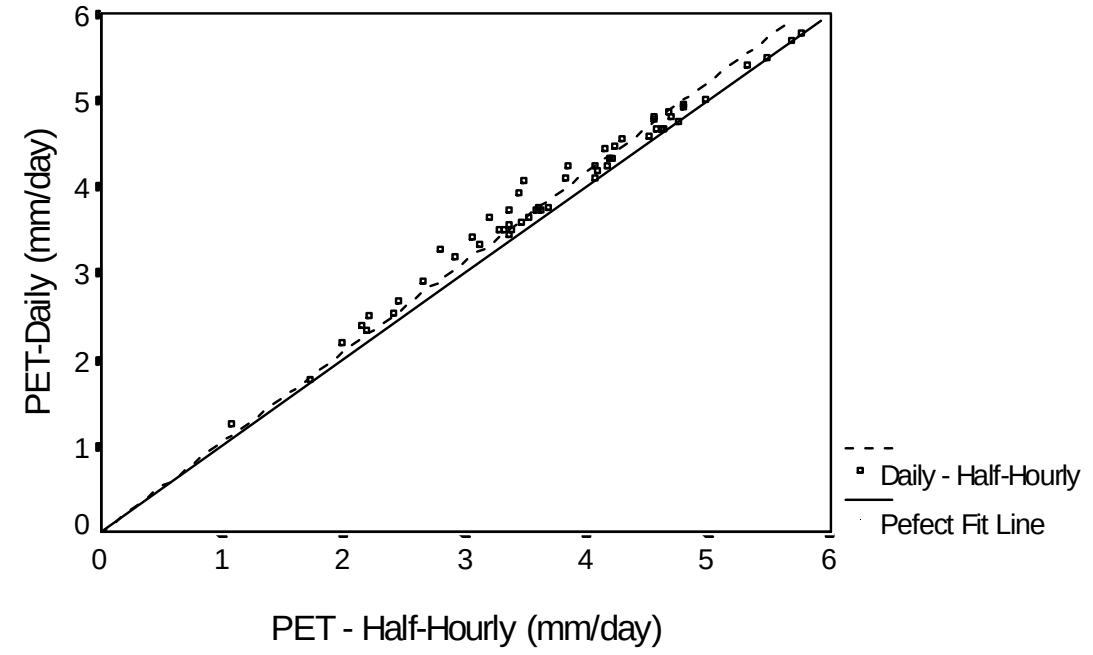

Figure 4.9: Hargreaves PET - Daily vs. Half-Hourly

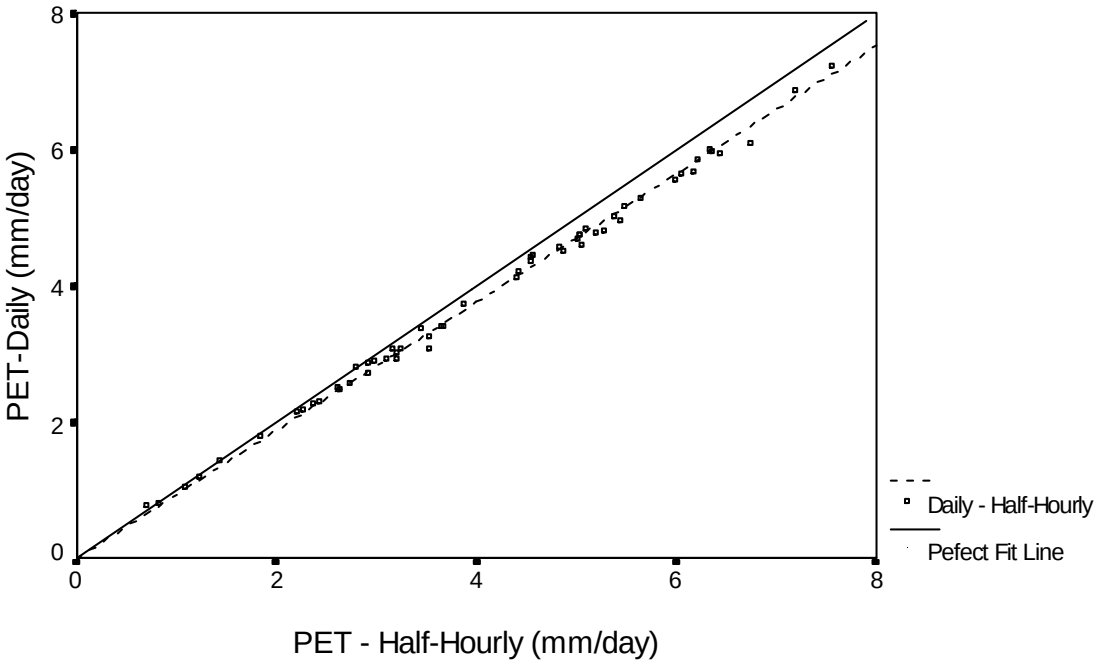

Figure 4.10: Priestley-Taylor PET - Daily vs. Half-Hourly

amount of scatter about the perfect fit line, which appears to be systematic. The rate of increase in the potential evapotranspiration calculated hourly compared to the potential evapotranspiration calculated daily is slightly greater than one.

The correlation between the half-hourly and daily calculated values of potential evapotranspiration is shown in Table 4.7. In all but one of the pairs the correlation is greater than 0.97. The variance in each of the sets of values is so small that the null hypothesis (that the population means of each of the two groups are equal) is rejected at six of the seven sites that have been compared. The actual difference between the sampled means of each pair is less than 6.0% in all but one of the eight comparisons. There is only weak evidence against the null hypothesis at the OJP-SSA flux tower. This location also has the lowest correlation (0.87), but has a relatively small difference between the means (3.4%). The FEN-SSA site has the highest difference between the means (8.4%). A higher rate of change in the diurnal temperature variation at the FEN-SSA site could result in a more dramatic difference between the daily and half-hourly calculated mean values of potential evapotranspiration using the Priestley-Taylor equation.

Table 4.7: Comparison of Half-Hourly and Daily Calculated Priestley-Taylor PET

Flux Tower	Calculation	Correlation Coefficient R	t-test Significance	Mean (mm d^{-1})	Difference (mm d^{-1})
OBS-SSA	Hourly Daily	0.998	0.000	4.08 3.85	+0.23
FEN-SSA	Hourly Daily	0.998	0.000	4.03 3.69	+0.34
OJP-SSA	Hourly Daily	0.871	0.215	3.78 3.65	+0.13
OBS-NSA	Hourly Daily	0.999	0.000	6.47 6.40	+0.07
FEN-NSA	Hourly Daily	0.978	0.014	4.15 4.03	+0.12
OJP-NSA	Hourly Daily	0.999	0.000	4.12 3.87	+0.35
YJP-NSA	Hourly Daily	0.981	0.002	3.77 3.63	+0.14

The Priestley-Taylor potential evapotranspiration is calculated as a function of the slope of the saturation-vapour pressure versus temperature curve, $s(T_a)$. Since the curve is an exponential function of temperature, time averaging of temperature values will not result in the correct time averaged value of the slope. The average of the slopes calculated from the half-hourly temperatures will be greater than the slope calculated from the average daily temperature. As the average temperature increases, the half-hourly calculated potential evapotranspiration will increase more rapidly than the daily calculated potential evapotranspiration. Therefore, with respect to Figure 4.10, as the temperature increases, the difference in calculated values will also increase, explaining the systematic scattering of the data.

The Priestley-Taylor equation has been developed to estimate daily average values. However, the slope of the saturation-vapour pressure versus temperature curve, $s(T_a)$, is better approximated with a smaller time step. Therefore, to estimate the true potential evapotranspiration, the smallest possible time step should be utilized, although using daily averages has been shown to introduce only small errors (Dingman, 1994). Priestley and Taylor (1972) developed the value of α in equation [64] based on daily mean values of input data. Using a time step of one hour will produce a slightly different estimate of the potential evapotranspiration. In order to equate the potential evapotranspiration estimates calculated with different time scales, a different value of the alpha parameter must be used in the equations.

As the temperature and the corresponding actual evapotranspiration rate increases, the value of the alpha parameter should decrease to a value lower than 1.26, as estimated by Priestley and Taylor. The systematic variation of the hourly versus daily calculated evapotranspiration is very small (with an approximate error of 10% at the maximum deviation from the perfect fit line). Therefore, the variation of the alpha parameter should be approximately 10% from the actual value at the highest point of deviation. The value of 1.26 was developed for saturated areas. This value must be optimized for local conditions, so the variation discovered here is not of concern. The variation of the potential evapotranspiration calculated with half-hourly values from the estimates calculated with daily averages is consistent, thus enabling the difference to be removed during calibration.

4.3.3 Turc - Temporal Variability

Figure 4.11 shows the relationship between the daily potential evapotranspiration (calculated from daily averages of temperature and humidity) and the total daily potential evapotranspiration (calculated with half-hourly measured data inputs). The plot is of the values

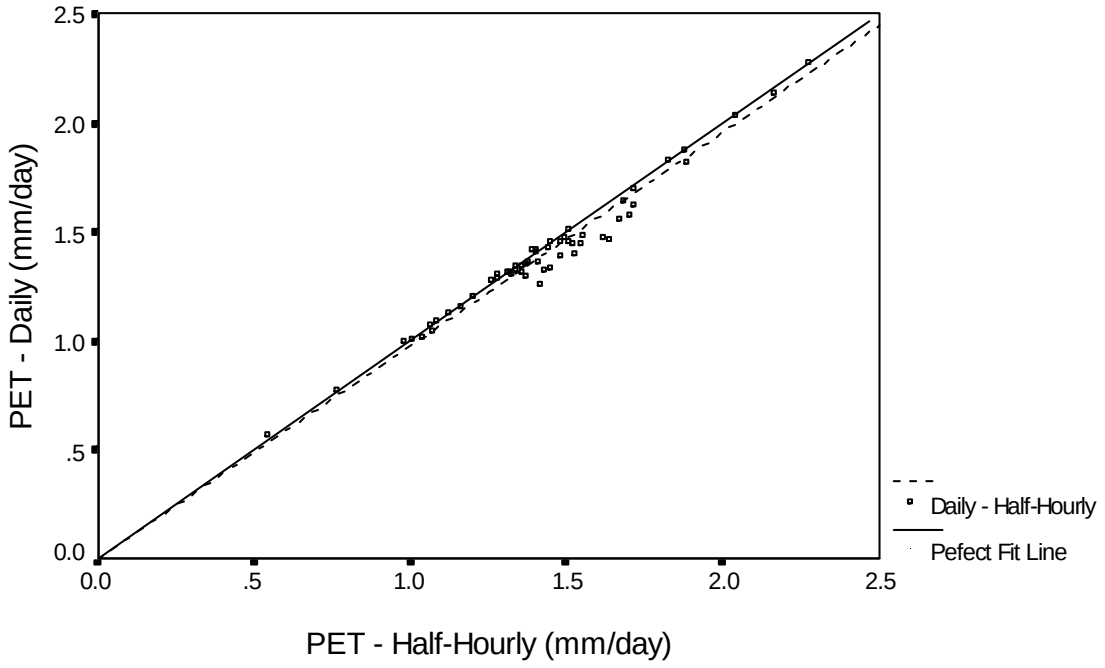

Figure 4.11: Turc PET - Daily vs. Half-Hourly

calculated at the OBS-SSA tower flux site and is typical of the relationship found at the different sites in both study areas. The line indicating a perfect correlation (PET_{daily} equals $PET_{half\text{-}hourly}$) has been plotted for a visual reference. The data points have only a very small amount of scatter and are well distributed about the perfect fit line. Table 4.8 shows the correlation between the values calculated with half-hourly data and the values calculated with daily averages.

Table 4.8: Comparison of Half-Hourly and Daily Calculated Turc PET

Flux Tower	Calculation	Correlation Coefficient R	t-test Significance	Mean (mm d^{-1})	Difference (mm d^{-1})
OBS-SSA	Hourly Daily	0.986	0.000	1.42 1.40	+0.02
FEN-SSA	Hourly Daily	0.973	0.653	1.41 1.41	+0.00
OJP-SSA	Hourly Daily	0.769	0.766	1.42 1.43	-0.01
OJP-NSA	Hourly Daily	0.481	0.000	1.55 1.42	+0.07

At two of the four towers compared, there is a high degree of correlation (greater than 0.97). The variance in these two comparisons is so small that the null hypothesis is rejected. The actual difference between the sampled means of each pair is less than 2.0% in all but one of the pairs. In at least one of the two pairs with a low correlation, the null hypothesis cannot be rejected because the standard deviation of the values in these pairs is large compared to the difference between the sample means; this accounts for the lack of correlation in this pair.

4.3.4 Conclusions - Temporal Variability

These models were originally developed to provide estimates of evapotranspiration for periods of one day or longer. Based on the standard deviation of the estimates about the sampled means, there is a statistical difference between the mean daily potential evapotranspiration estimated with daily averages and with the sum of half-hourly estimates. In essence, the estimates made with a different time step than the one used in the development of the original model are merely a slightly different estimate of the somewhat hypothetical value of potential evapotranspiration. The difference between the values (typically less than 5%) is insignificant in the context of the overall water budget.

Given the high values of the correlation and the systematic nature of the errors shown with the estimates for the Priestley-Taylor equation, the error in the estimates must be consistent. Consistent errors are easier to model because they can be reduced or eliminated in the calibration process. Provided that the error remains consistent, the validations will also be satisfactory. Because of the small differences in the estimates produced by using the different time scales, the effects on the final hydrologic simulation of calculating the daily potential evapotranspiration with either time scale are negligible.

4.4 Estimates of Actual Evapotranspiration from the Potential Evapotranspiration Models

Estimates of daily evapotranspiration have been calculated from the sum of the half-hourly calculated values. These estimates have been made for the period from Julian Day 144 to Julian Day 199, 1994. At most of the tower flux sites, the latent heat flux was measured with Licor instruments. These values of the latent heat flux will be considered to be the actual evapotranspiration rates from the surrounding vegetation in a comparison with the potential rates calculated with the three models.

It is important to realize that these measures of the latent heat flux are prone to error. More specifically, at the time of writing, the latent heat flux data measured by researchers at the OBS-NSA site was being revised and proviso was given about the possibility of significant errors existing in the current data (Wofsy, 1995). Included in some of the comparisons and regressions, are the published values of the mean monthly pan evaporation rates.

4.4.1 Comparison to Measured Actual Evapotranspiration Rates

The relationship between the potential and actual rates of daily evapotranspiration has been approximated at each of the tower sites. A relationship between the two values was sought using a linear regression approach without a constant in the expression. During a preliminary analysis, it was noted that there was strong statistical evidence that both a slope and an intercept parameter would improve the ability of the regressed relationship to predict the actual evapotranspiration. Through the range of data analyzed, it may be more accurate to estimate the actual evapotranspiration as the sum of some constant value and the product of the slope and the potential evapotranspiration. This relation does not pass through the origin, resulting in a value of actual evapotranspiration existing when the potential evapotranspiration is zero (the value of the intercept); this type of relationship would be accurate in the range of data collected. However, it will be necessary to extrapolate outside of the range of data used for the regression, particularly in instances when the evapotranspiration rate is low during the spring or autumn. In

this case, it is more logical to imply that the actual evapotranspiration is zero when the potential evapotranspiration is zero, as defined by an expression without a constant. The results of the regressions for the following relationship:

$$AET = B \times PET\,, \qquad [80]$$

are shown in Tables 4.9 and 4.10. Table 4.9 displays a summary of the regressed coefficients B for the relationship between AET and PET at each flux tower. Table 4.10 shows only the average values of the correlation coefficients R, the coefficients of determination R^2, and the standard error of the regression for each of the regressions. The complete list of the individual values of these coefficients for each regression are shown in Table C3 in Appendix C.

Table 4.9: Summary of Regression Coefficients (B) of Tower Flux AET and PET

Flux Tower / PET Model	SSA OBS	SSA FEN	SSA OJP	NSA OBS	NSA FEN	NSA OJP	NSA YJP	Average Coeff.
Hargreaves	0.50	0.68	0.17	0.45	0.63	0.12	0.33	0.41
Priestley-Taylor	0.49	0.67	0.42	0.27	0.58	0.13	0.34	0.41
Turc	1.42	2.12	1.15	1.36	1.92	0.37	1.01	1.34
Pan	0.28	0.45	0.24	0.32	0.50	0.09	0.26	0.31
Average Coefficients	0.67	0.98	0.50	0.60	1.00	0.18	0.49	

Table 4.10: Summary of Regression

PET Model	Average Coefficient of Determination R^2	Average Standard Error (mm d^{-1})
Hargreaves	0.85	0.60
Priestley-Taylor	0.59	0.52
Turc	0.90	0.51
Pan	0.87	0.57

4.4.1.1 Regressed Coefficients

The regressed value of B is actually the ratio of the mean daily actual evapotranspiration to the mean daily potential evapotranspiration at each of the tower flux sites for this period of data. The values of the regressed coefficients vary significantly between models and between tower

flux sites. In both study areas, the highest value for the average coefficient is at the FEN tower flux site (0.98 and 1.00); the next highest value is at the OBS tower flux site (0.67 and 0.60). The average value of the coefficients at the YJP tower flux site (0.49) is larger than the average at the OJP site (0.18) in the NSA. The average of the regressed coefficients for each of the tower flux sites varies in an expected manner. In general, the value of these coefficients decrease from site to site, corresponding to a decrease in the expected degree of saturation. The OJP-NSA was extremely dry during the 1994 period (Fitzgarrald, personal communication) and possibly uncharacteristic of the region. These conditions would account for the extremely low values of the regressed coefficients.

The values of the averages are similar between corresponding NSA and SSA tower sites, with the differences being 2% and 12% for the FEN and OBS sites, respectively. There is a marked difference between the average of the coefficients between the OJP-SSA and OJP-NSA sites.

The average of the regressed coefficients for each model has some similarities and differences. Both the Hargreaves and Priestley-Taylor equation tend to have approximately the same values for coefficients, at each tower site. The only significant difference is for the Priestley-Taylor equation at the OJP and OBS sites. The pan evaporation tends to highly over predict the actual evapotranspiration, and therefore has a high reduction value. The Turc equation tends to underestimate the actual evapotranspiration, and therefore requires a coefficient that is greater than one. At some tower sites (YJP-NSA), the Turc estimate approaches the measured value of the actual transpiration.

4.4.1.2 Coefficient of Determination R^2

All of the calculated R^2 values are reasonably high, being greater than 0.85 on average, for the each of the four regressed calculations of potential evapotranspiration, except the Priestley-Taylor equation. The correlation is low with this method because of some anomalous regression coefficients which are a result of irregularly high net radiation values.

4.4.1.3 Standard Error

The best measure of fit is the standard error of regression. If the standard error is less than the acceptable error the model is adequate. The average value of the standard error of all models is between 0.5mm and 0.6mm of evapotranspiration per day. Relative to the average daily actual evapotranspiration (1.5-2.0mm d^{-1}) this error is significant (25-30%). The Hargreaves and the pan evaporation regressions produce about the same standard error, approximately 0.6mm d^{-1}. The Priestley-Taylor and the Turc equation provide estimates with only slightly lower standard

errors of estimate, about 0.5mm d^{-1}. The relative magnitudes of the standard errors remain consistent with the relative magnitudes of the regressed coefficients (*i.e.* as the actual evapotranspiration increases, the error in the prediction also increases).

4.4.1.4 Ratio of Actual Evapotranspiration to Potential Evapotranspiration

Typical relationships between daily measured actual evapotranspiration and Hargreaves, Priestley-Taylor, Turc, and published mean monthly evaporation pan estimates of potential evapotranspiration are shown in Figures 4.12, 4.13, 4.14, and 4.15, respectively. Each plot shows a fairly uniform scatter of data about the regressed line with no systematic error.

The OBS sites in the NSA and the SSA have been utilized for comparison purposes because of the availability of an extended period of continuous data records at those sites. For the OBS tower flux sites during the period from Julian Day 144 to Julian Day 272, the AET/PET ratios have been plotted with respect to time in Figures 4.16 and 4.17, respectively. The trends shown in the plots of the SSA and the NSA show a high degree of correlation between all of the tower sites. In the SSA, there is a general long term trend of an increasing ratio until approximately day 185. In the NSA, at least one and a half separate cycles of increase and decrease are shown in the long-term trends. There is a gradual increase in the ratio until a downturn in the cycle occurs at approximately day 170 to 175. The increase begins again after a period of decrease on day 180 to 185 and continues to the end of the period shown.

4.4.1.5 Conclusions

Based on the expected variation in soil moisture, the variation in the coefficients is reasonable. The more saturated land covers tend to have higher values of the regression coefficient corresponding to lower reductions in potential evapotranspiration to the estimate of actual evapotranspiration. The reduction coefficients of the Hargreaves and Priestley-Taylor equations are similar, suggesting that, on average, these two equations produce similar estimates of potential evapotranspiration. All four methods produce similar standard errors in the estimate of evapotranspiration ±30%.

4.4.2 Correlation of AET/PET Ratio to Soil Moisture

The potential evapotranspiration must be reduced to provide an estimate of the actual evapotranspiration. The variation in the AET/PET ratio is dependent on the time scale; both short-term and long-term variations exist. Longer term reductions are related to seasonal variations in factors affecting evapotranspiration, such as biomass or ground temperature.

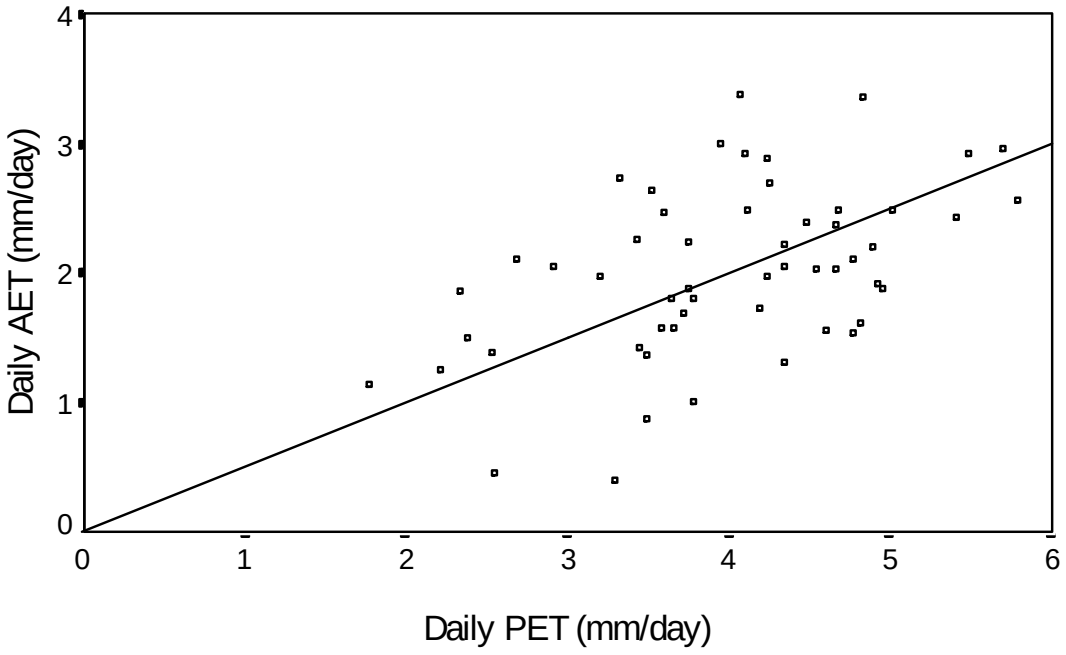

Figure 4.12: Measured AET vs. Hargreaves PET (Typical)

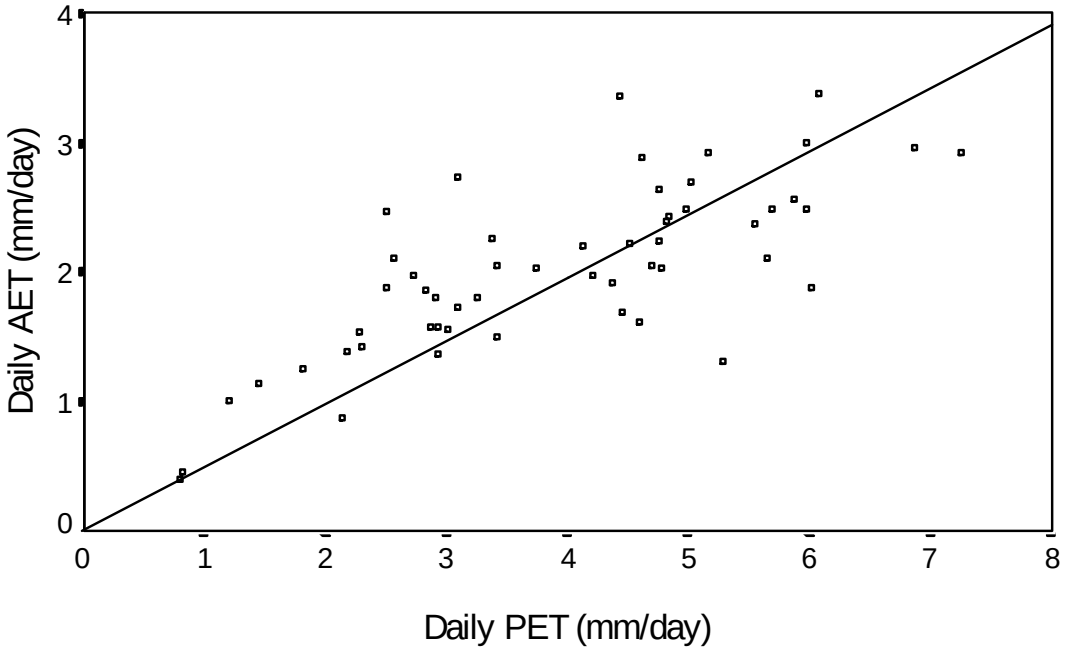

Figure 4.13: Measured AET vs. Priestley-Taylor PET (Typical)

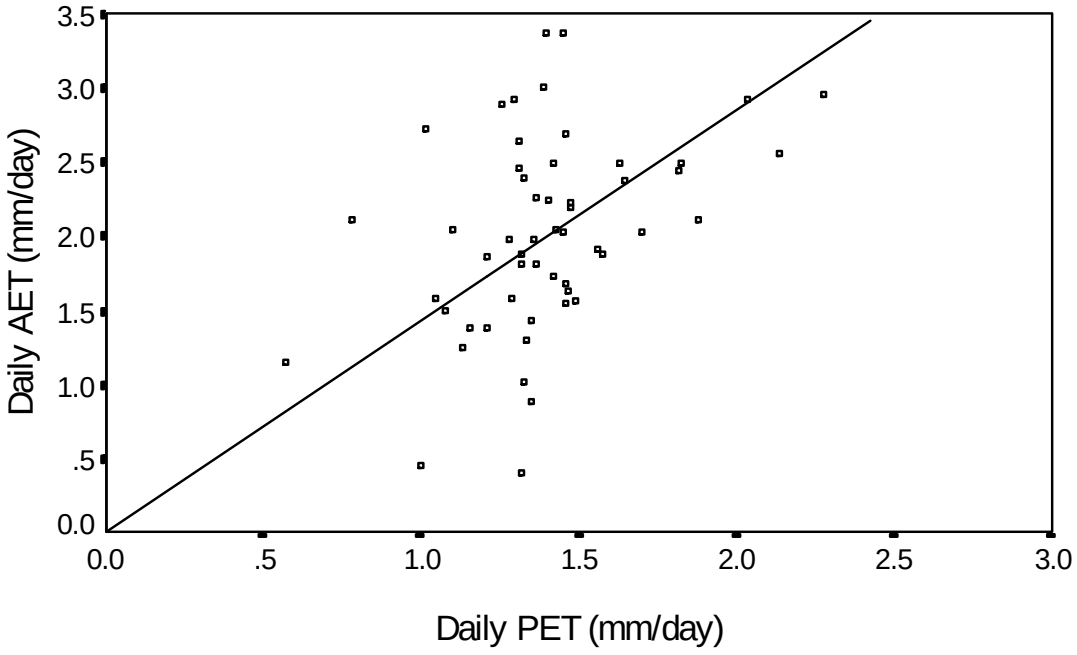

Figure 4.14: Measured AET vs. Turc PET (Typical)

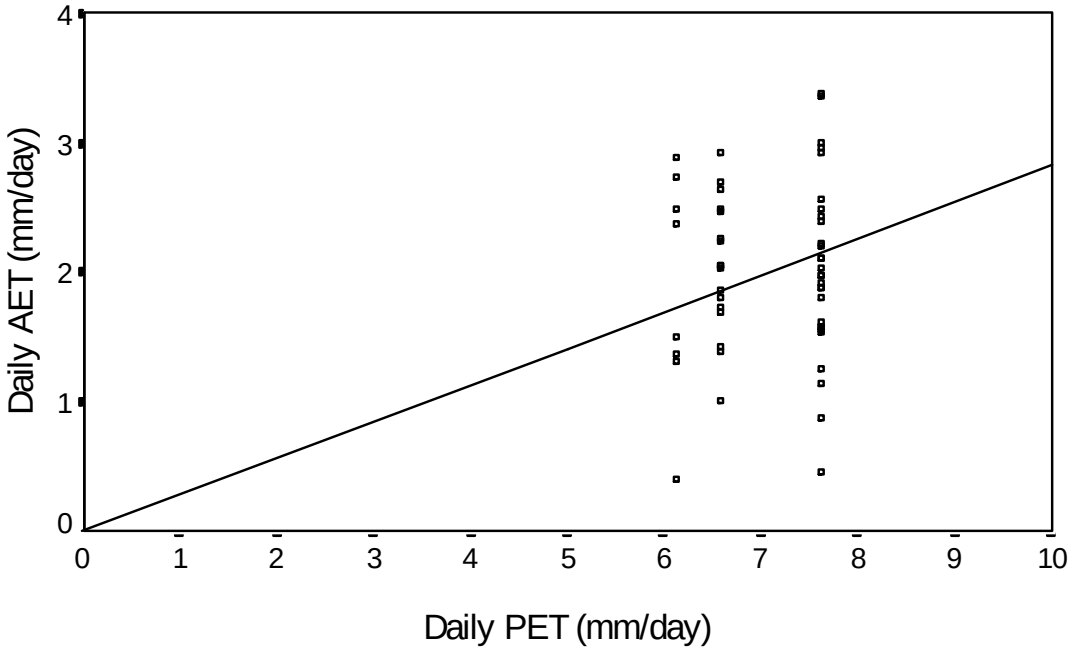

Figure 4.15: Measured AET vs. Evaporation Pan PET (Typical)

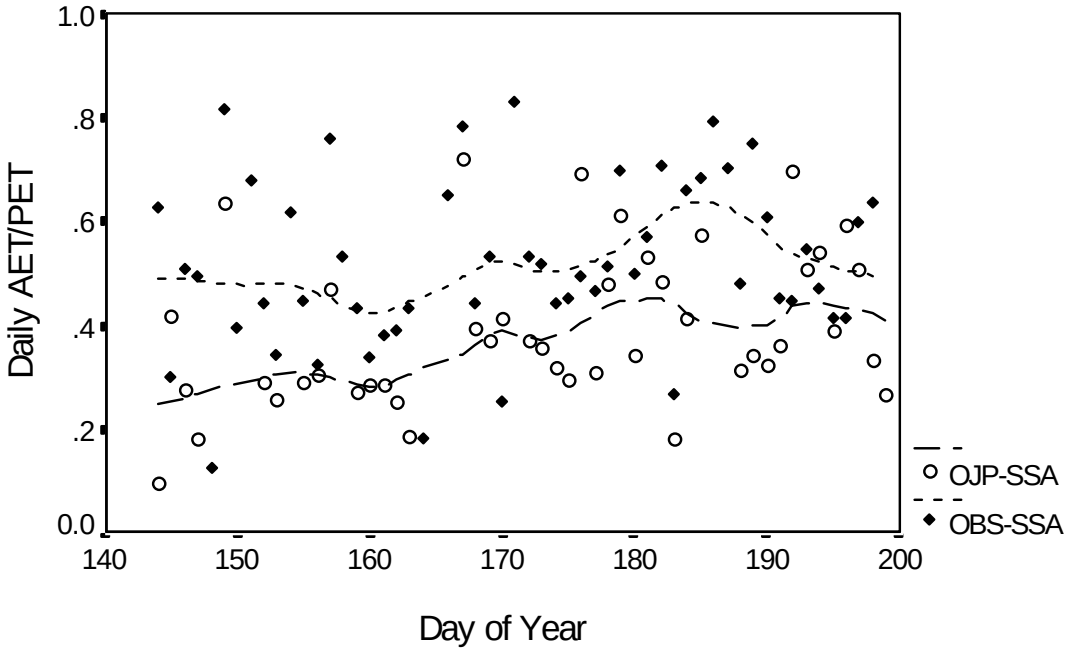

Figure 4.16: AET/PET vs. Day of Year - SSA

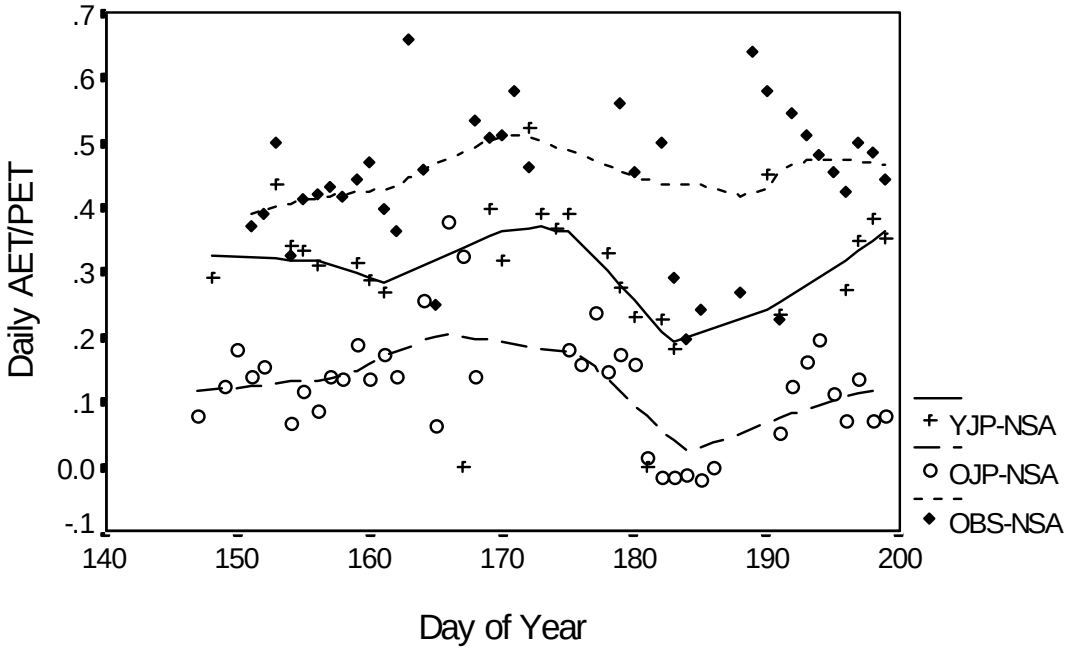

Figure 4.17: AET/PET vs. Day of Year - NSA

Factors affecting short-term variations include soil moisture, temperature, wind, radiation, relative humidity, and physiological constraints. Some of these factors have complex interactions, such as radiation and temperature. The vegetal physiological constraints are particularly complex and are a function of most of the meteorological factors. Therefore, by developing a reduction method as a function of these meteorological variables, the physiological constraints are indirectly considered. Some of these factors (e.g. relative humidity, radiation, temperature) are already considered in the evapotranspiration equations.

Many models have established the level of the soil moisture as the constraint on the actual rate of evapotranspiration, including the following: the Thornthwaite water budget model (Thornthwaite and Mather, 1955), CLASS (Verseghy, 1991), the Pulse model (Bergstrom *et al.*, 1985), the Broughton model (Broughton, 1966), and HYDROLOG (Porter and McMahon, 1971; Arp and Yin, 1992). The actual evapotranspiration is indexed to the potential evapotranspiration as a function of the soil moisture. A similar relationship has been sought to provide a method of reducing the values of potential evapotranspiration to the actual evapotranspiration.

The soil moisture was measured at several locations and depths around each tower flux site. In order to exaggerate the relatively small changes in average soil moisture, only measurements made within the top 0.5m of soil were used to calculate the averages.

Figures 4.18 and 4.19 are plots of the measured actual evapotranspiration versus soil moisture. There is no obvious correlation between these two variables. The paucity of data in Figure 4.19 reduces the value of conclusions drawn from it. A faint relationship between the two variables may exist in the SSA as shown in Figure 4.18. There is a dramatic scattering of the data during the prevalent periods of high soil moisture. As the soil moisture decreases, there is a slight curvature and increase in the slope of the relation at soil moistures of less than 31%. This could indicate the point below which there is a soil moisture deficit. The single datum point, where soil moisture is 32.5% and actual evapotranspiration is 0.0mm d^{-1}, does not follow the same trend as the remaining points and is an extreme outlier. It is probably the result of an error in the measurement of the latent heat flux or some other component of its calculation. Table 4.11 contains the values of correlation between the latent heat flux and the soil moisture. The latent heat flux in the SSA has a small correlation with the soil moisture. The correlation in the NSA is negative.

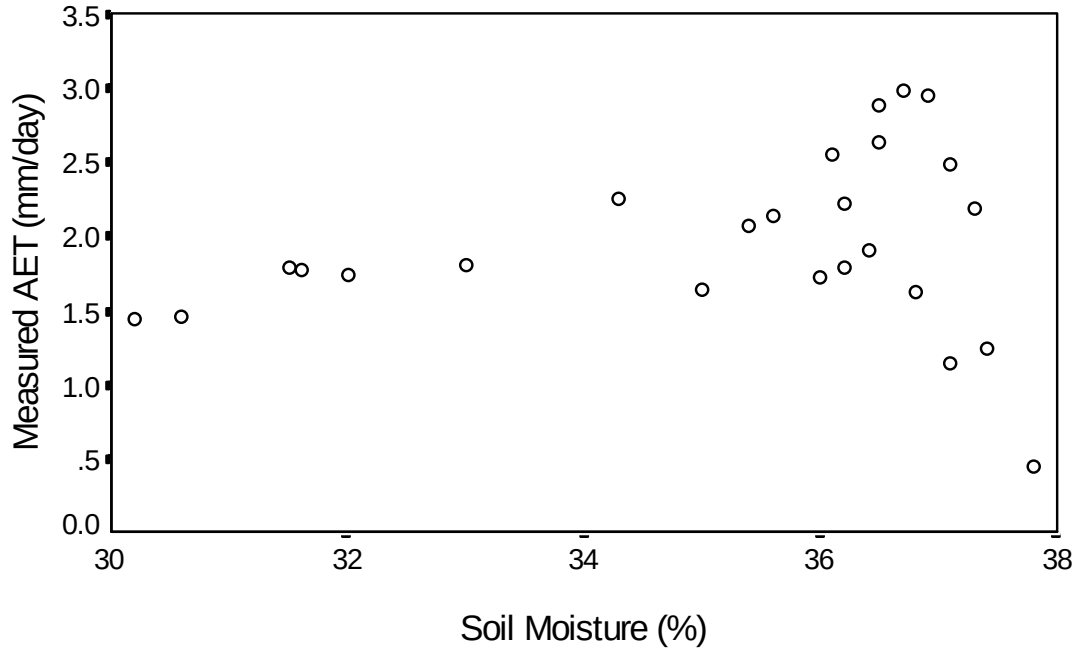

Figure 4.18: Measured AET vs. Soil Moisture - SSA

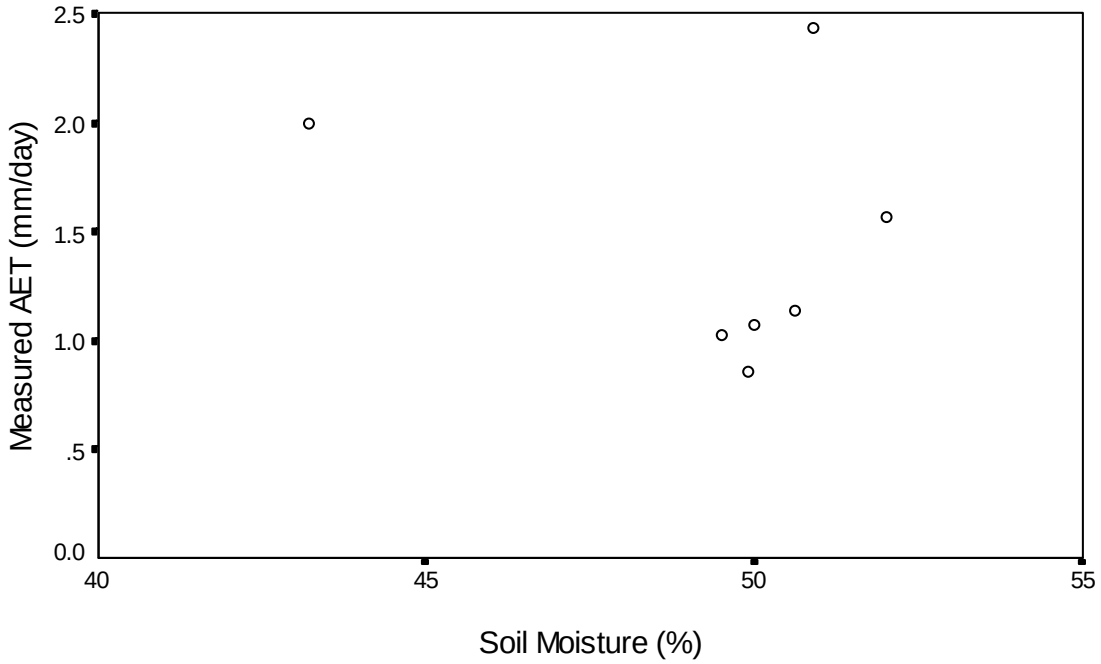

Figure 4.19: Measured AET vs. Soil Moisture - NSA

Table 4.11: Correlation of Measured AET to Soil Moisture

Location of Soil Moisture and Measurement of AET	Correlation Coefficient R
OBS-SSA	0.290
OBS-NSA	-0.252

The transpiration of plants is only constrained when the soil moisture is below the field capacity. A second relation between the AET/PET ratio and the soil moisture was analyzed. The difference between the measured soil moisture and a base constant, A_1 (similar to the permanent wilting point in percent), over the difference between the second base constant, B_1 (similar to the field capacity in percent), and the first base constant, was used as the soil moisture indicator (SMI):

$$SMI = \frac{\theta - A_1}{B_1 - A_1}. \qquad [81]$$

This Soil Moisture Indicator was applied to the potential evapotranspiration as a reduction to obtain the actual evapotranspiration. The results of the regression of the actual evapotranspiration to the product of the potential evapotranspiration and the Soil Moisture Indicator is shown in Table 4.12. By allowing the regression to continue unconstrained, the lower base point in the Soil Moisture Indicator tended to go to zero. This implies the existence of an unrealistic condition where all of the soil moisture is removed from the soil by evapotranspiration. Similarly, the upper base point tended to values of soil moisture beyond the maximum field capacity for any known soil. Similar values for the upper base point, ranging between 60% and 90%, were obtained for the Priestley-Taylor and Hargreaves potential evapotranspiration. Correspondingly, lower values for the upper base point were obtained for the Turc equation, because it requires little or no reduction to estimate the actual evapotranspiration. The value of the coefficients of determination indicate that the regressions are modest in their ability to predict the actual evapotranspiration.

Plots of the actual versus the predicted values of evapotranspiration are shown in Figures 4.20 and 4.21 for the Priestley-Taylor and the Turc equations, respectively, in the SSA. The predicted values for Priestley-Taylor regression fall closely around the line of perfect fit. The results are similar for the Turc regression.

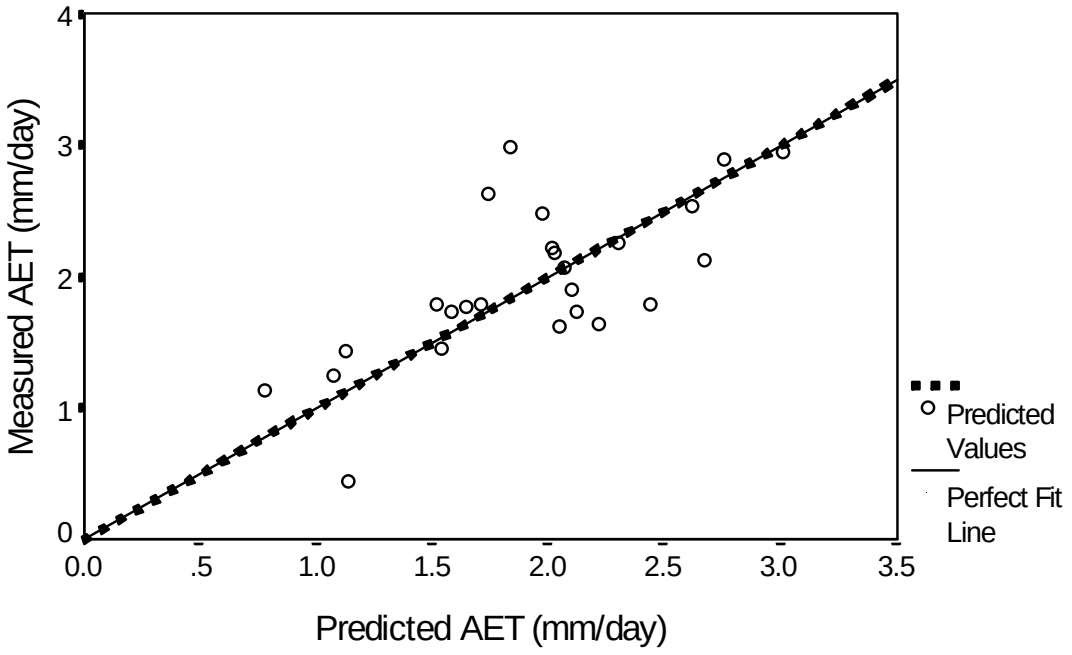

Figure 4.20: Measured AET vs. Predicted AET using Priestley-Taylor PET and Soil Moisture Indicator Models

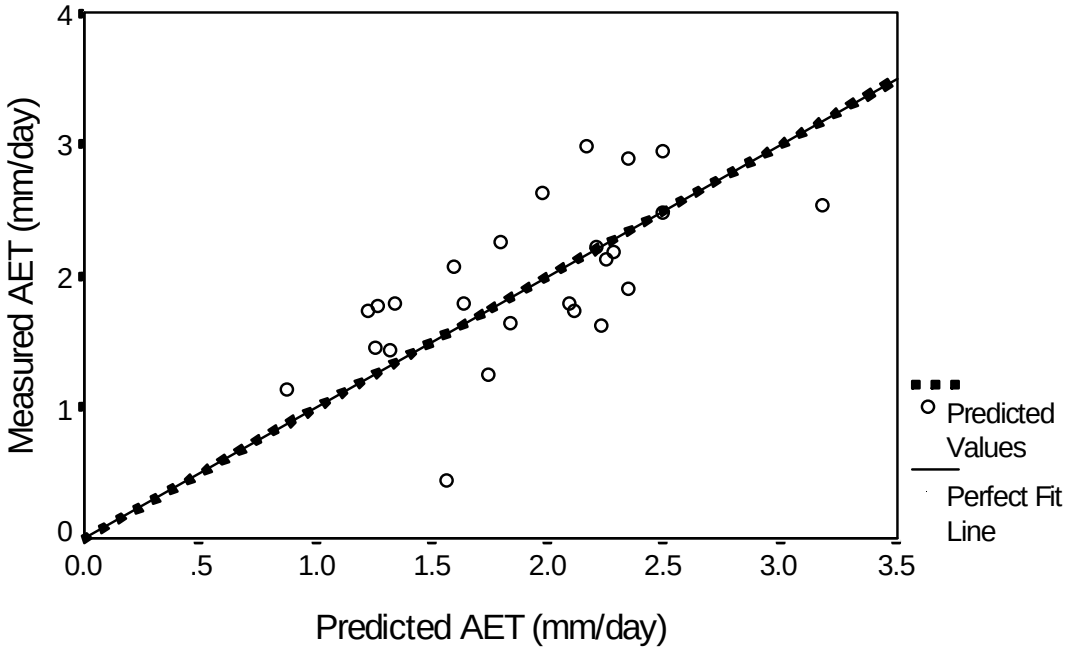

Figure 4.21: Measured AET vs. Predicted AET using Turc PET and Soil Moisture Indicator Models

Table 4.12: Summary of Regression of AET to PET and SMI

Measured AET	PET Model	Parameter A_1	Parameter B_1	Coefficient of Determination R^2
OBS-SSA	Hargreaves	0.0	70.4	0.402
OBS-SSA	Priestley-Taylor	0.0	70.3	0.639
OBS-SSA	Turc	10.0	27.5	0.414
OBS-NSA	Hargreaves	0.0	88.8	0.207
OBS-NSA	Priestley-Taylor	0.0	148.3	0.146
OBS-NSA	Turc	0.0	56.8	0.118

4.4.3 Correlation of AET/PET Ratio to Soil Temperature

The summary of the preliminary analysis of the BOREAS data concludes that the low soil temperature is a limiting factor in the rate of evapotranspiration (Sellers *et al.*, 1995). This conclusion has been noted by other researchers in separate experiments (Turner and Jarvis, 1975; Anderson, 1992).

To reflect the long-term variation in the soil temperature, the moving sum of the degree-days has been calculated (DD). The sum of the degree-days is calculated on a daily basis as the accumulation of the mean daily temperatures since the start of the simulation. The correlation between the degree-days and the actual evapotranspiration has been calculated for the OBS tower flux sites in the NSA and the SSA, with the values shown in Table 4.13. As calculated, the degree of correlation is practically non-existent, with both values being negative.

Table 4.13: Correlation Between Measured AET and Degree Days

Measured AET	Degree Days	Correlation Coefficient R
OBS-SSA	DD > 0	-0.246
OBS-NSA	DD > 0	-0.543
OBS-SSA	0 < DD < 1000	0.286
OBS-NSA	0 < DD < 450	0.486

The values of the degree-days have been plotted with respect to the values of the actual evapotranspiration for the SSA and NSA in Figures 4.22 and 4.23, respectively. Evident in the plot of the SSA are two trends, shown by a regressed parabolic fitting line. The first trend is a gradual increase in the actual evapotranspiration with an increase in degree-days. A maximum

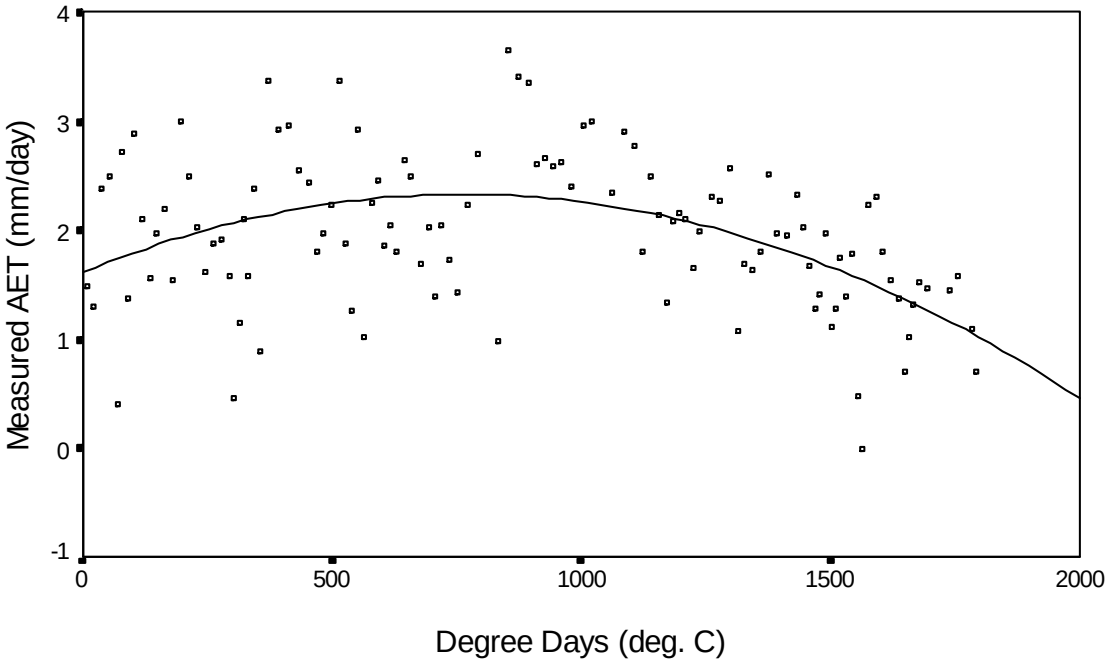

Figure 4.22: Measured AET vs. Degree Days - OBS-SSA

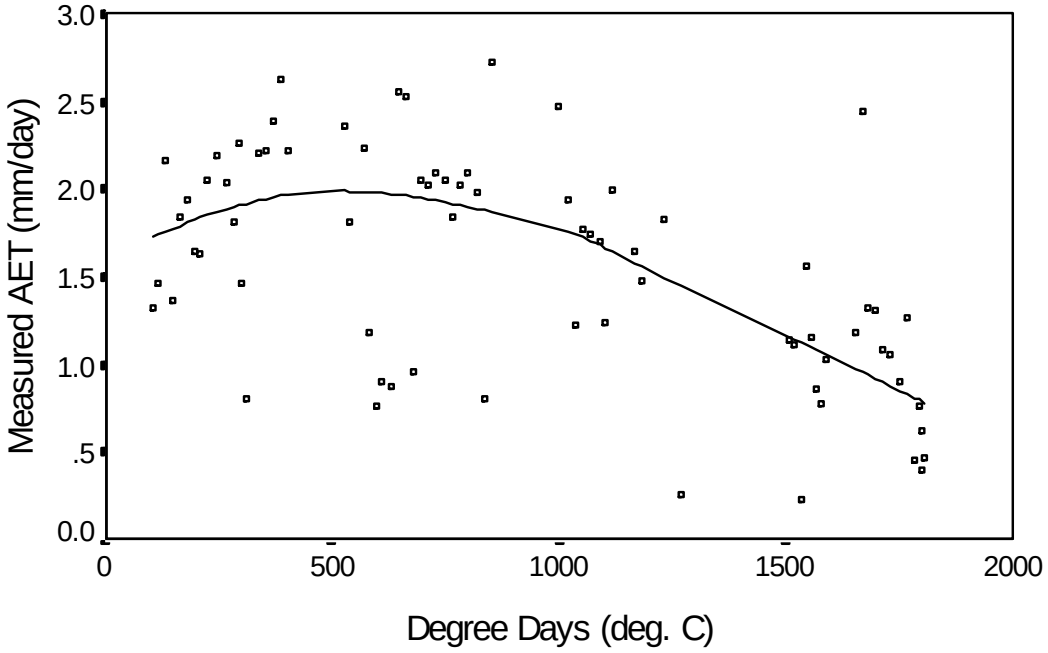

Figure 4.23: Measured AET vs. Degree Days - OBS-NSA

value is achieved and followed by a more rapid decrease in the actual evapotranspiration. There is wide scattering of the data. It is postulated that the initial increase in the actual evapotranspiration is a result of the thawing of the soil (a corresponding increase in the total degree-days) until the soil temperature is no longer a constraint to the evapotranspiration. At this point in time, other physiological and meteorological factors become more constraining on the rate of evapotranspiration. To a much lesser extent, the relationship is validated in the plot of the NSA degree-day data. In this plot, there is a much wider scattering of the data. The correlation between the actual evapotranspiration and the degree-days would be more pronounced for the analysis limited to the first portion of the curve.

Similar to the work done by Anderson (1992), a reduction in the potential evapotranspiration to the actual evapotranspiration has been made by multiplying by a fraction calculated as a function of the degree-days. The fraction is calculated as the ratio of two differences, as follows:

1. The difference between the current total of degree-days and a calibrated lower base value, and
2. The difference between the calibrated upper and lower base values.

A regression analysis has been applied to the actual evapotranspiration as a function of the soil moisture and the degree-days. The degree-day function has upper (D_1) and lower (C_1) base values (°C) similar to the base values (A and B) in the soil moisture function. The upper and lower base values have been regressed, as in the following equation:

$$AET = PET \times SMI \times \frac{DD - C_1}{D_1 - C_1}. \qquad [82]$$

The equations have been regressed on all three models at the OBS tower flux site in both study areas. Reasonable values of the constants were obtained only at the OBS-SSA site. The values of the four constants in the equations are similar for the two potential evapotranspiration models regressed (Hargreaves and Priestley-Taylor), as shown in Table 4.14 (regressions 1 and 2). The values of the coefficient of determination, shows that the regressed equations predict the actual evapotranspiration reasonably well (R^2 greater than 0.58). Plots of the predicted versus observed values are shown in the Figures 4.24 and 4.25 for the Hargreaves and the Priestley-Taylor regressions, respectively. The data on both of these plots fall closely about the perfect fit line; there is no systematic lack of fit evident in the plots. A comparison of the plots with Figures 4.20 and 4.21 indicates a slight improvement in the prediction of the lower and mid-

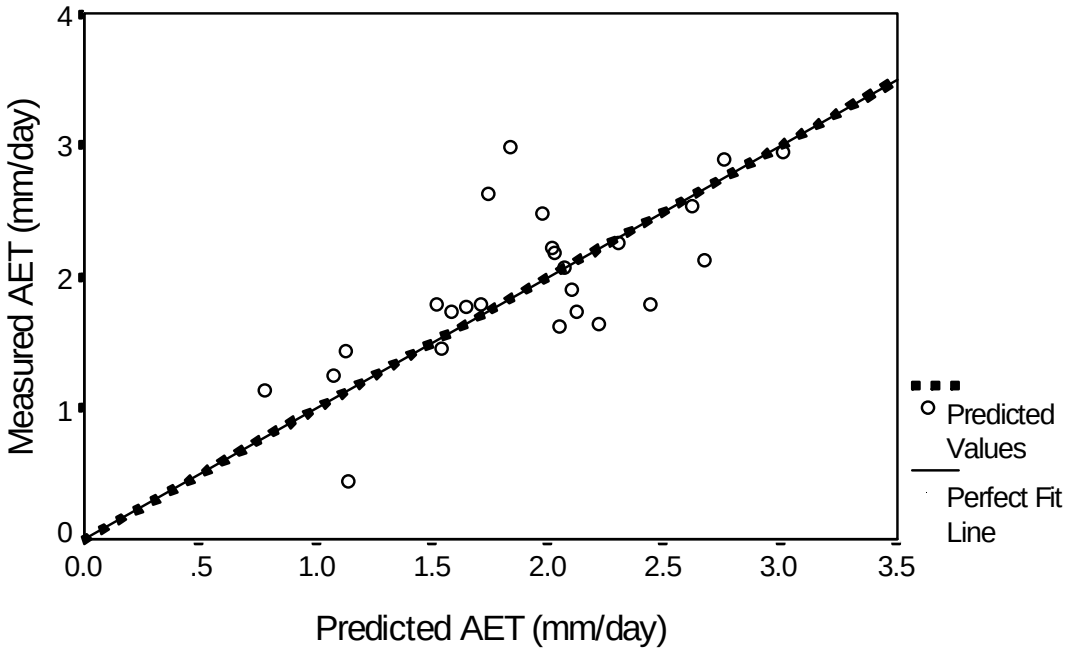

Figure 4.24: Measured AET vs. Predicted AET using Hargreaves PET, Soil Moisture Indicator and Degree Day Models

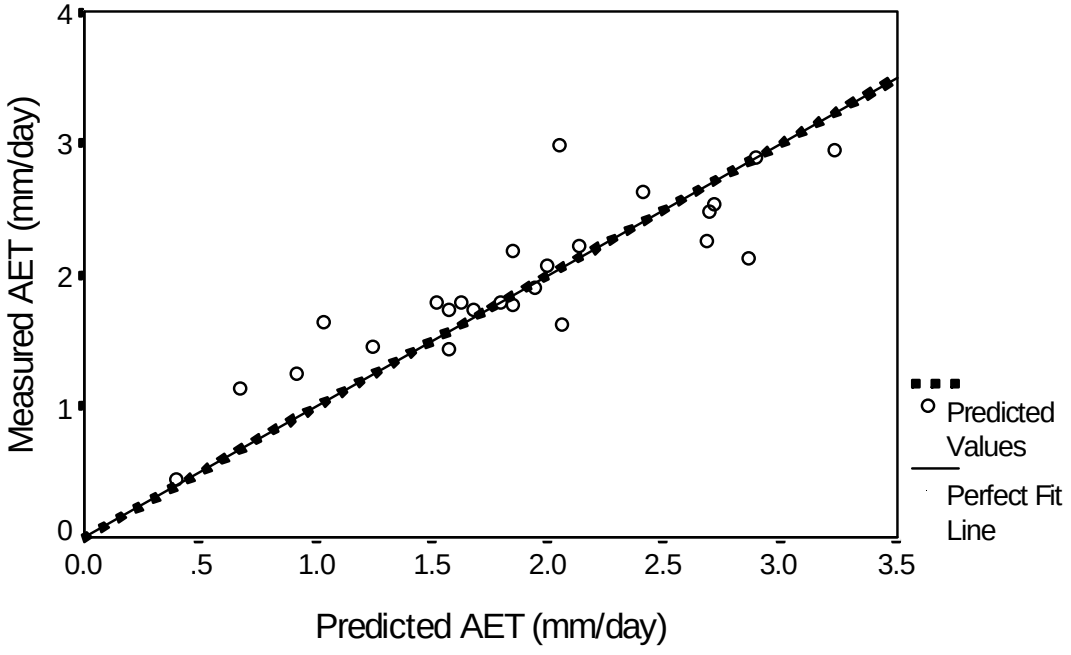

Figure 4.25: Measured AET vs. Predicted AET using Priestley-Taylor PET, Soil Moisture Indicator and Degree Day Models

range values. The prediction of the higher values is not necessarily improved, probably because of an insignificant amount of soil existing in a frozen state during the periods corresponding with these estimated data points.

Table 4.14: Regression of Tower Flux AET with PET, SMI, and DD

Regression	TF	PET	A_1	B_1	C_1	D_1	Coefficient of Determination R^2
1	OBS-SSA	Hargreaves	10.0	60.6	-2000	801	0.589
2	OBS-SSA	Priestley-Taylor	14.3	56.4	-2577	786	0.790
3	OBS-SSA	Hargreaves-Taylor	-	-	-2570	3288	0.344
4	OBS-SSA	Priestley-Taylor	-	-	-4833	5874	0.510
5	OBS-SSA	Turc	-	-	-4020	-933	0.202
6	OBS-NSA	Hargreaves	-	-	-900	1890	0.505
7	OBS-NSA	Priestley-Taylor	-	-	-635	2785	0.370
8	OBS-NSA	Turc	-	-	-855	496	0.490

A second set of regressions involving only the degree day function was performed on the portion of data prior to the local maximum in Figures 4.22 and 4.23. The set of degree-day values used in the regression consisted of only those points corresponding to degree-days of less than approximately 1000 and 450 for the SSA and NSA, respectively. These regressions produced modest R^2 values in the regressed data, as shown in Table 4.14 (regressions 3 to 8). Reasonable values of the base constants were regressed for each of the potential evapotranspiration models. These values were comparable between the Hargreaves and Priestley-Taylor equations.

4.4.4 Conclusions

The estimates of daily potential evapotranspiration, produced by all three equations are highly correlated. Both the Priestley-Taylor equation and the Hargreaves equation produce similar values for the hypothetical value of potential evapotranspiration. The Turc equation produces estimates which are generally in the vicinity of the actual measured values, but with the occurrence of some significant under and over predictions. The soil moisture shows some potential for indexing the estimate potential evapotranspiration to the actual evapotranspiration. Preliminary results from other BOREAS investigators have suggested that soil moisture is not a significant constraint on the evapotranspiration in this region (Sellers *et al.*, 1995), or at least not in the 1994 study period when the soil moisture levels do not constrain until August (Kimball et al, 1995). The degree-day measurement also shows potential for indexing the actual

evapotranspiration to the potential evapotranspiration. This parameter will be particularly important in regions where the soil takes longer to thaw. Using a combination of these parameters has produced good predictions of the actual evapotranspiration with the use of the Hargreaves and Priestley-Taylor equations in the SSA.

Chapter 5
Hydrologic Balance

As part of BOREAS, a primary objective of the hydrologic study of the NSA and SSA watersheds was to estimate the evapotranspiration losses using an analytical/water balance approach. Based on equation [34], the evapotranspiration losses are calculated as being equivalent to the inputs less the outputs less the change in storage of water in a closed system. The water budget analysis is a valuable tool because it provides an estimate of the evapotranspiration independent of other methods of investigation such as those used at the flux towers. This chapter analyzes the water budget for the SSA and NSA watersheds during the 1994 BOREAS field season in order to provide a means of comparison with the flux tower estimates of evapotranspiration.

5.1 Calculation of the Water Budget

The water budget has been completed for each of the sub-basins gauged in the SSA and NSA watersheds. Rainfall was measured using a network of rain gauges. The integration of the measured rainfall over a period of time gives an estimate of the total incoming precipitation for the area. To calculate the total precipitation over each sub-basin, the measured precipitation was distributed using the same method as that used in WATFLOOD (the Reciprocal Distance Weighting Technique (Wei and McGuiness, 1973)). The sum of the precipitation falling in each element in a sub-basin is the estimated total inflow for that basin. The total loss from each sub-basin is calculated as the integral of the hourly outflows over the entire period of interest. The evapotranspiration is calculated as the difference between the inflow and the outflow for a time integral that has no net change in storage.

The underlying assumption when using the water balance approach is that there are no significant groundwater outflows bypassing the basin outlet. Another assumption inherent in this method is that the storage term is the same at the start and at the end of the time integral. This last assumption is usually valid for annual and semi-annual balances. Similar quantities of basin storage typically exist at similar times from year to year, such as after spring-runoff and just before freeze-up.

If the basin is idealized as a large reservoir with a defined outlet, then, as the storage increases, the flow through the outlet will also increase. If it is assumed that there is some monotonic function defining the storage-discharge relationship, then at any point where the discharges are equal, the storage will also be equal.

This simplification breaks down in a number of situations. When vegetation conditions change in the basin the storage-discharge relationship will also change. The storage may be significantly different before and after leaf fall has occurred. The storage in a basin with and without snow, and before and after leaf opening will probably be different as well.

Large basins with longer response times will have storage-discharge relationships with some hysteresis. Because of the basin size, a significant amount of precipitation in the head waters of the basin may not affect the flow at the outlet for some time after the event has been recorded. An estimate of the storage based on the outflow at a time between the rainfall event and the travel time to the outlet will be in error. The effects on the water balances from any hysteresis in the storage-discharge relationships is minimized by utilizing points on the recession limbs of hydrographs that have similar slopes.

Points in time with similar outflows and similar hydrograph slopes will have similar amounts of storage. In order to visualize this concept, an analogy can be drawn to a wave passing a fixed location where the depth of the wave is measured. Waves with a similar shape will contain similar amounts of water and have similar slopes at corresponding depths. A wave with a steeper or shallower slope (a different shape) is more apt to contain a different amount of water behind it at the same depth as a shallower sloping wave.

A storage-discharge relationship can be assumed to be constant under the assumptions that no changes in vegetation occur, and that no precipitation events have occurred during the recent period (equal to the travel time from the most distant point in the basin). Under these conditions, and between two points in time with equal outflows, the change in the basin storage has been assumed to be negligible for the following analysis.

5.2 Evapotranspiration Loss Calculations

For each streamflow gauge, a number of points in time have been identified where the discharges were equal and the slope of the hydrographs were similar. At the points in time with similar discharges the storage in the sub-basins are assumed to be equal.

The integral of each flow, calculated for the period defined by the two points in time, has been subtracted from the total precipitation that fell within the same period to determine the quantity of water lost through evapotranspiration. To obtain the correct rainfall interval corresponding to the outflow interval, one day has been subtracted from the dates defining either end of the outflow interval. This adjustment has been used to account for the lag time between the

precipitation event causing the flow increase and the response at the sub-basin outlet. By using this method, the estimation of the precipitation will only be in error if a significant rainfall event occurs within the 24 hours preceding the start or the end of the interval. Estimation of evapotranspiration losses using this method are more accurate for longer periods of time because of the tendency for the magnitude of the any errors relative to the total budget to be reduced through averaging.

5.3 Temporal Variation of Water Balance Evapotranspiration

In order to compare the total depth of evapotranspiration losses during different time intervals, the depths must be normalized. The evapotranspiration data obtained through the water budget closure have been normalized by dividing by the period of the integral to yield an average daily rate. These average daily rates have been plotted separately for each of the SSA and NSA sub-basins with respect to the day of year in Figure 5.1 and in Figures D1 to D6 in Appendix D. When analyzing the plots it is important to understand that the lines represent the average rate for the entire period across which they run. The shorter lines more precisely represent the short-term average daily rates, but not necessarily with greater accuracy. Because of the inherent assumptions in the water balance analysis, the estimates made for shorter periods are more prone to error. There is a greater chance that the start and end of the short-term integrals occur within 24 hours of a precipitation event. As well, errors in the short-term balances are more noticeable because of the shorter period over which they are averaged.

Estimates of the actual evapotranspiration using the water balance approach produced negative values between the days 132 and 135. Errors in this specific calculation were due to the imprecise identification of the precipitation integral corresponding to the outflow integral. Therefore, this interval has not been used in the following analysis.

The preliminary estimates of actual evapotranspiration produced with water budget analysis are comparable to the measurements made at the tower flux sites. The evapotranspiration losses measured at the tower flux sites typically range from 1.5-2.0mm d^{-1} on average for the 1994 summer period (Sellers *et al.*, 1995). The long-term average rates for the SSA basins estimated using the water budget are approximately 1.6, 2.5, and 2.3mm d^{-1} for SW1, SW2, and SW3, respectively (long-term averages could not be estimated for SW4). Short-term rates fluctuate much more than these rates from 5.9mm d^{-1} at the highest rate to approximately 1.0mm d^{-1} at the lowest. The 0.4mm d^{-1} rate estimated with SW2 does not appear to follow the general trend of increasing rates during that period of time; the value likely contains some

error as a result of an inaccuracy in the estimation of the start and end of the interval. An overestimate of the

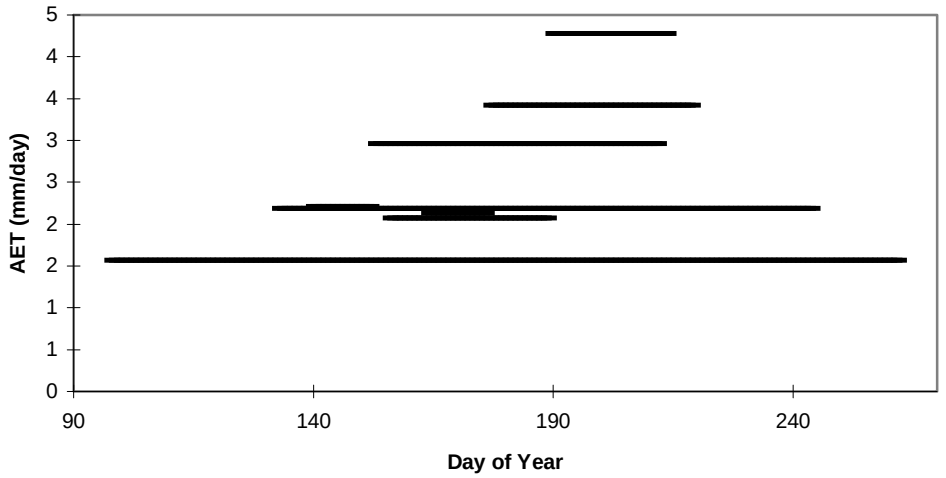

Figure 5.1: Mean Daily AET vs. Day of Year - SW1 (Typical)

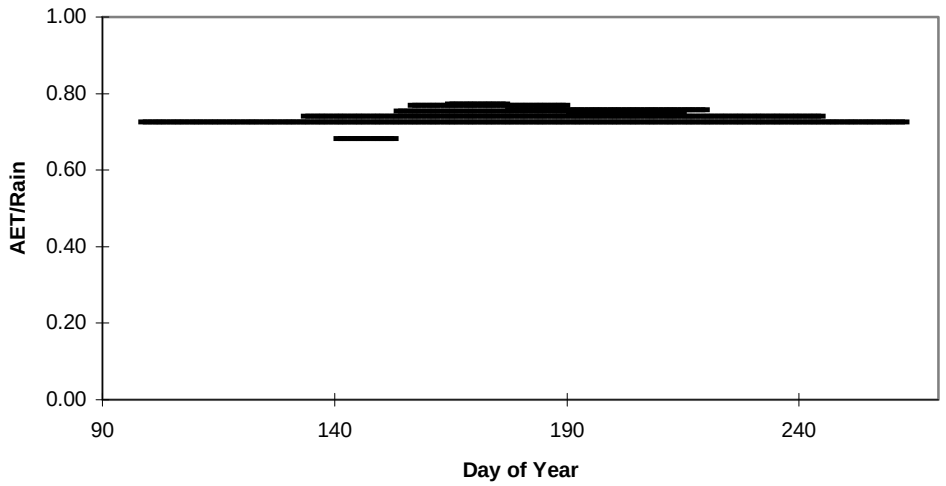

Figure 5.2: Total AET/Total Rain vs. Day of Year - SW1 (Typical)

precipitation contributing the flows for this duration would produce an erroneously low rate. The general trend of the average daily rates is to increase throughout the period until a maximum rate is attained at around day 200. This trend is similar to the trend of the AET/PET ratios in Figures 4.16 and 4.17. As can be expected from a preliminary analysis of this type, there is a considerable amount of variation in the rates. Improvements in these estimates are possible by defining the start and the end of the precipitation intervals that correspond to the flow intervals with more precision.

The paucity of hydrologic events that occurred during the 1994 season in the NSA has reduced the number of water balance intervals that could be defined. The average daily rates estimated for the NSA show less variation, but this is possibly a result of the fewer number of estimates. The range of estimated daily rates (from 1-3mm d^{-1}) corresponds well to the values observed at the tower flux sites by other researchers. There is no obvious temporal trend in the average daily rates.

The total depths evapotranspiration losses during the different lengths of time intervals have also been normalized by calculating the ratio of the evapotranspiration to the total rainfall. In this way, the percent of the gross precipitation lost through evapotranspiration is calculated. This ratio is useful for making a qualitative comparison with published typical evapotranspiration losses and for making a qualitative assessment of these losses and their temporal variations. These average daily ratios have been plotted separately for the SSA and NSA sub-basins with respect to the day of year as shown in Figure 5.2 , and in Figures D7 to 12 in Appendix D.

Throughout this period, all of the SSA sub-basins typically have short-term average ratios ranging from 0.7-0.8. The short-term ratios for the NSA also fall within this range of values. These ratios (varying from 0.65-0.75) are quite high compared to the mean global ratio of 0.60 (Brutsaert, 1986). However, the thick vegetated canopies, low relative humidity, and high sensible heat fluxes of the boreal forest regions (Sellers *et al.*, 1995) would result in high interception evaporation losses and higher than average gross evapotranspiration loss ratios, such as these values calculated here.

All of the plots of the SSA sub-basins show a similar trend. The trend of the ratio is to increase rapidly in the early part of the growing season, peak at the mid point, and gradually decrease in the latter part of the summer. This trend indicates that there is an increase in the percent of precipitation that is lost through evapotranspiration, to a maximum at the end of

June. The percent of rain lost through evapotranspiration slowly decreases throughout the remainder of the summer. This trend follows that which would be expected and is similar to the AET/PET plotted with respect to time (Figure 4.16) which also peaks at the end of June before decreasing. At the beginning of the growing season there is an increase in the amount of incoming solar radiation, the air temperature, the soil temperature, the rate of photosynthesis, and the leaf area index as the deciduous leaves open quickly. With an increase in leaf area, there is also a greater potential for interception evaporation. The peak rate of evapotranspiration may be constrained by the development of a soil moisture deficit.

The plots of the ratios for the NSA sub-basins are more difficult to interpret. In the NSA, the ratio of evapotranspiration to gross rainfall starts at a high value and then decreases. A minimum value is reached at around day 175 to 180 before a gradual increase in the ratio occurs. This trend is similar to that shown in the plot of AET/PET with respect to time (Figure 4.17), which also reaches a minimum at around day 180. These trends are somewhat different than what might be conventionally expected, as shown in the plots of the SSA.

In summary, the evapotranspiration estimates produced by the water budget follow the same seasonal trends as the ratios of actual to potential estimates of evapotranspiration made with the tower flux sites. The long-term average rates are similar to those observed by investigators using the flux tower data. Significantly higher estimates of the daily rates have been calculated with the short-term averages. However, these values are more prone to error because of the shorter duration used for averaging. The average ratios of evapotranspiration to precipitation calculated with the water balances are quite high (ranging between 0.65 and 0.80). These ratios are reasonable considering the relatively thick canopies and high sensible heat fluxes of these regions which increase the rate of interception evaporation.

5.4 Evapotranspiration Estimates - Water Balance versus Tower Flux

The total evapotranspiration losses for a number of separate time integrals in each of the seven sub-basins have been calculated by analyzing the water budget. For these same periods the total evapotranspiration losses measured at the corresponding flux tower sites have also been calculated. To normalize these values for comparison purposes, the ratios of the total evapotranspiration losses to the duration of the integrals have been calculated. This ratio is an estimate of the average daily rates of evapotranspiration. The comparison of these average daily rates is shown in Table 5.1.

Table 5.1: Comparison of Actual Evapotranspiration Estimates

AET Estimates Compared	Correlation Coefficient R	t-test Significance	Means ($mm\ d^{-1}$)	Difference ($mm\ d^{-1}$)	Standard Error of Differences ($mm\ d^{-1}$)
Water Balance OBS-SSA	0.321	0.05	2.81 2.38	+0.48	0.214
Water Balance OJP-SSA	0.146	0.42	2.08 1.93	+0.15	0.181
Water Balance SSA - Combined Towers	0.077	0.48	2.08 1.94	+0.14	0.190
Water Balance OBS-NSA	0.240	0.53	2.09 1.97	+0.12	0.182
Water Balance OJP-NSA	-0.045	0.00	2.09 0.61	+1.48	0.198
Water Balance YJP-NSA	-0.179	0.03	2.09 1.54	+0.55	0.196
Water Balance NSA - Combined Towers	0.118	0.01	2.09 1.39	+0.70	0.186

All of the pairs have low values of correlation. The NSA-OJP site, as noted above, has some irregularities in the measurements of latent heat flux which probably account for the low value of correlation shown.

In three of the comparisons the difference between the sampled means is small enough that the null hypothesis cannot be rejected. The OJP-SSA and OBS-SSA sites have a relatively low probability that the actual population means are not equal. The remaining comparisons show that there is some evidence for rejecting the null hypothesis. The differences in the sampled means of the OJP-SSA, OBS-NSA and the water balance estimates are less than 8%. The difference in the means of the other pairs varies from 18% for the OBS-SSA to 36% for the YJP-NSA. The measured values at the OJP-NSA are excessively low suggesting that the measurements at this site may not be characteristic of the region. Except for the OBS-SSA site, the standard error between the paired estimates in all of the comparisons is approximately 0.2mm. Based on the published typical values of this regions being 1.5-2.0mm d^{-1}, these standard errors correspond to errors in the daily estimates of approximately 10%.

The average daily actual evapotranspiration rate estimated using the water balance has been plotted with respect to the actual evapotranspiration rate measured at the flux towers, as shown in Figure 5.3 for the SSA. The lines of best fit through the origin compare well to the perfect fit line, although there is a large amount of scatter in the data. The water balance tends to overestimate the evapotranspiration measured at the flux tower sites.

The discrepancy in the estimate of the total evapotranspiration loss could be explained by an unaccounted loss in the water balance. An unidentified increase in the basin storage would account for this loss. According to the initial assumptions, with an increase in storage, an increase in the baseflow should also be observed. The beginning and end of the intervals used to integrate the flows were defined by points with identical values of baseflow; therefore, this explanation is unlikely. Another possibility is that too much water is being put into the balance because of an error in the delineation of the watershed. This would result in an overestimation of the area receiving precipitation which contributes to channel flow. The difference could also be explained by an unmeasured groundwater loss.

Another explanation could be that there is a long-term measurement error of the latent heat flux at the flux tower sites. Many of the sources of tower flux data contain the proviso with respect to the use of some periods of data.

The average daily actual evapotranspiration rates estimated using the water balance have been plotted with respect to the actual evapotranspiration rates measured at the flux towers for the NSA, as shown in Figure 5.4. The values in the NSA for the YJP and the OBS tower flux sites fall closely about the perfect fit line, although the values of the evapotranspiration from the YJP-NSA are slightly overestimated by the water balance. All of the measured values of evapotranspiration from the OBS-NSA are larger than the values measured at the YJP-NSA. The actual rate of evapotranspiration should be greater from the more saturated regions of Black Spruce (wet conifers). The watersheds are covered more predominantly by wet conifers. Therefore, to obtain the total composite runoff from the different land covers in the watershed, the total actual evapotranspiration from each land cover should be weighted according to the percent of the total watershed covered.

The estimates of the daily average rate of evapotranspiration produced by the water balance is the rate for the combination of land covers within the basin. These rates are compared to the estimates made for each of the land classes by the tower flux sites. To provide a more realistic comparison, the estimates made at the flux towers have been averaged and weighted according

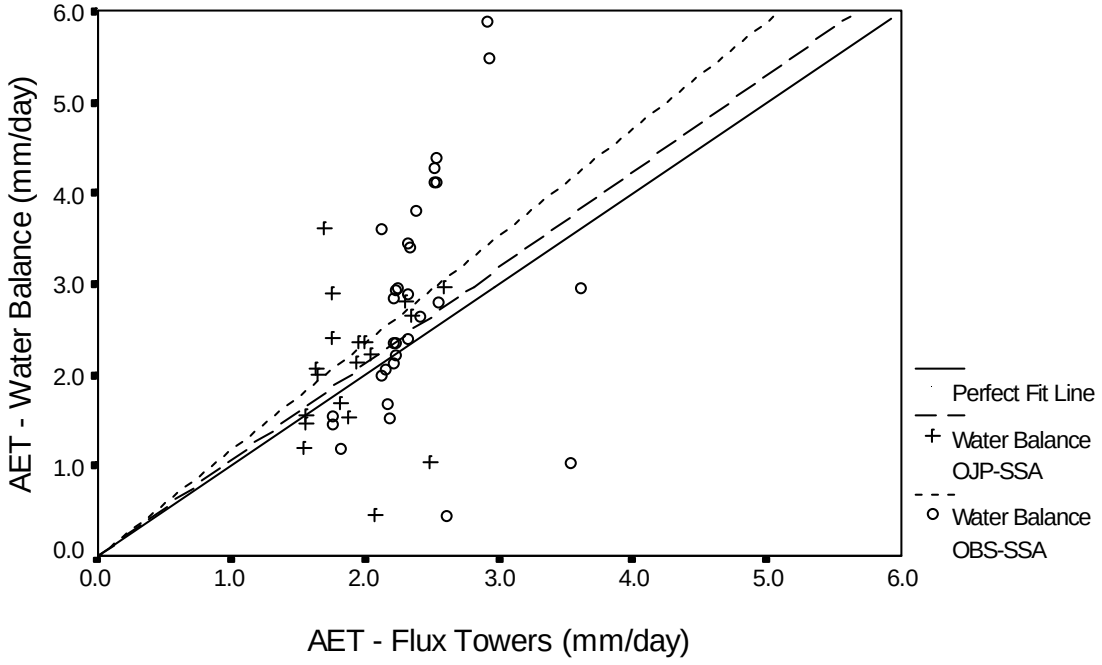

Figure 5.3: Mean Daily AET - Water Balance vs. Flux Towers - SSA

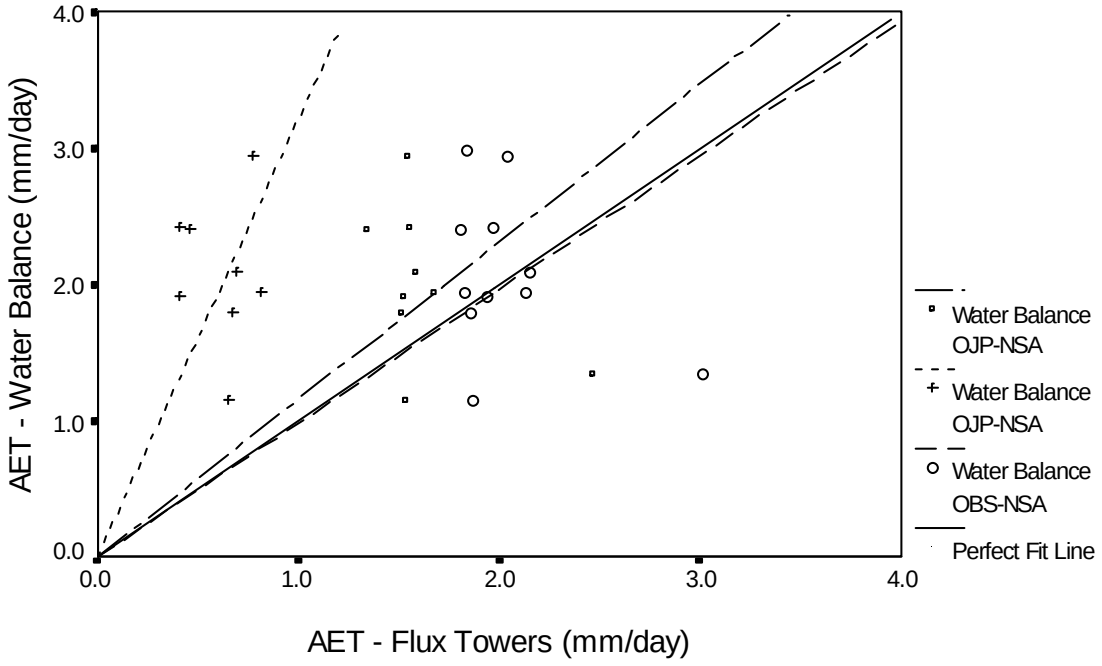

Figure 5.4: Mean Daily AET - Water Balance vs. Flux Towers - NSA

to the percentage of area covered by the corresponding land class in the basin with which the comparison is being made. In Figures 5.5 and 5.6, the average daily actual evapotranspiration rate estimated using the water balance has been plotted with respect to a weighted average of the actual evapotranspiration rate measured at the flux towers for the SSA and the NSA, respectively. For the SSA, the measured values at the OBS site have been weighted by the total area of the Wet Conifer classification in each sub-basin. The measured values at the OJP-SSA site have been weighted by the total area covered by Dry Conifers. The OBS-NSA site measurements have been weighted similarly to the OBS-SSA. The measurements at the NYJ-NSA and the OJP-NSA have been weighted by the total area covered by the Dry Conifer classification.

The line of best fit through the origin lies very close to the line of perfect fit in Figure 5.5. An improvement in the standard error (0.190) is realized for the OBS-SSA estimates (0.214) with only a very slight increase in the standard error from the estimates made at the OJP-SSA site (0.181). The significance of the comparison of the paired values (0.48) indicates that there is no evidence against the null hypothesis. The difference between the means is reduced slightly to 6%. The data are scattered uniformly about the perfect fit line. The agreement between the water balance-calculated evapotranspiration and the tower flux-measured evapotranspiration is improved by using a weighted average of the tower flux measurements in the SSA.

Similar results are apparent for the comparison between the water balance estimates and the weighted average estimates from the flux towers in the NSA. The improvement in the correlation between the estimates is more moderate in the NSA because of the use of the values measured at the OJP-NSA tower flux site. These values tend to have a large negative impact on the combined flux tower estimates.

In summary, there is a statistically significant difference between the sampled means of the estimates of evapotranspiration produced from the water budget and from each of the flux tower sites. In some cases, the difference is quite large. It appears that the actual evapotranspiration measurements made at the OJP-NSA site may not be characteristic of the evapotranspiration rates throughout this region. The values at the OJP-NSA site have significantly affected the weighted average of the tower flux site estimates of evapotranspiration relative to the difference in the water budget estimates. The OJP-NSA site also has a large difference, but when combined with the relatively good estimate from the OBS-NSA flux tower the average differences are significantly reduced. The difference in the estimates of the means in

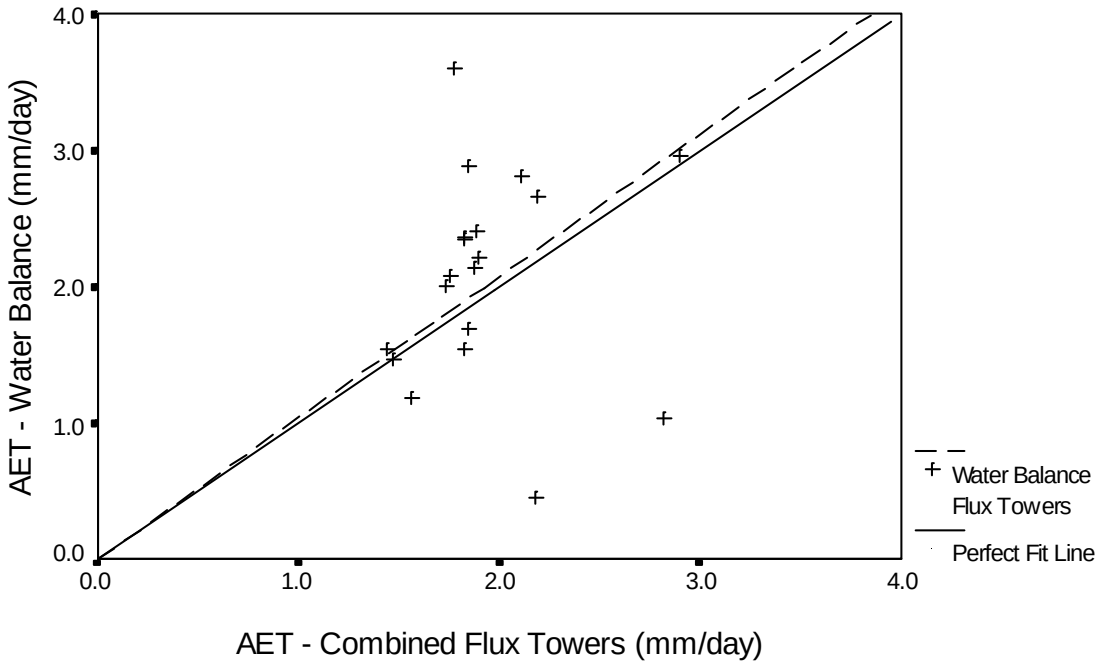

Figure 5.5: Mean Daily AET - Water Balance vs. Combined Flux Towers - SSA

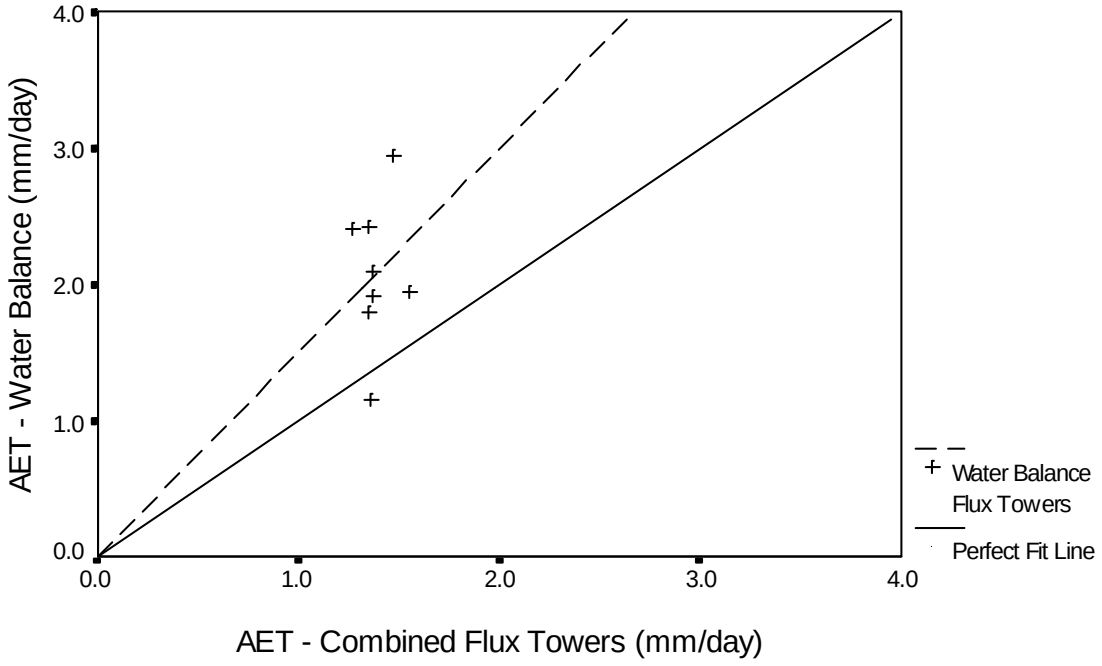

Figure 5.6: Mean Daily AET - Water Balance vs. Combined Flux Towers - NSA

the SSA are small, particularly when the estimates are weighted as a function of the areal coverage of each land class. The correlation between the evapotranspiration calculated by the water balance and measured at the flux towers is improved by using the average of the estimates made at each of the tower flux sites weighted by the areal coverage of each land cover type.

Standard errors between the water balance estimates and the flux tower estimates are generally about 10%. This value of standard error is reasonable, particularly for a preliminary analysis of this type of comparison. Improvements in the comparisons could be realized by refining the estimated time integrals for the water balance. A general overestimation of the evapotranspiration losses is made by the water balance in comparison to the flux towers. This discrepancy could be a result of erroneous tower flux estimates or possible deep groundwater flow which is unaccounted for in the balance. Some correlation exists between the land cover type and the evapotranspiration loss.

5.5 Comparison of Water Balance Actual Evapotranspiration to Potential Evapotranspiration

A regression between the potential and actual water balance measured evapotranspiration losses has been completed, similar to the regression with the flux tower measurements in section 4.4.1. A relationship between the two values was sought using a linear regression approach without a constant in the expression. Potential evapotranspiration has been calculated using the three models and input data from the AFM flux towers in both study areas. Table 5.2 shows the results of the regressions using equation [80] between the actual and the potential evapotranspiration, where the evapotranspiration is the mean daily rate (mm d^{-1}). The values of the regression constant B, the coefficient of determination R^2, the standard error of the regression and the mean of the sample estimates are displayed.

5.5.1 Regressed Coefficients

The regressed value of B is the ratio of the average of the actual evapotranspiration to the average of the potential evapotranspiration at the AFM tower flux sites for these periods of data. The values of the regression coefficients vary between the models and between the different study areas. The regression coefficients for each model have some similarities and dissimilarities. Both the Hargreaves and Priestley-Taylor equations tend to have approximately the same values for coefficients within each study area. In the SSA, the coefficients for the Hargreaves and the Priestley-Taylor equations are 0.65 and 0.59

Table 5.2: Comparison of AET - Water Balance to PET - Flux Towers

Water Balance AET	PET	Regressed Coefficient B	Coefficient of Determination R^2	Standard Error (mm d^{-1})	Mean AET (mm d^{-1})	Mean PET (mm d^{-1})
SSA	Hargreaves	0.65	0.84	0.21	2.72	4.11
SSA	Priestley-Taylor	0.59	0.83	0.23	2.72	4.53
SSA	Turc	1.74	0.83	0.10	2.72	1.54
NSA	Hargreaves	0.43	0.89	0.19	2.09	4.48
NSA	Priestley-Taylor	0.43	0.88	0.19	2.09	4.53
NSA	Turc	1.25	0.90	0.18	2.09	1.56

respectively. In the NSA, these values are both 0.43. The difference in the average value of the Hargreaves and Priestley-Taylor coefficients from the SSA to the NSA is 44%.

The value of these reduction parameters for all of the potential evapotranspiration equations are approximately (39%) higher in the SSA than in the NSA. A difference in the coefficients exists between the two sites since a larger reduction of the potential evapotranspiration to the actual evapotranspiration is necessary in the NSA. The NSA is typically drier than the SSA and would therefore tend to have lower total amounts of evapotranspiration constrained by available moisture. This difference is particularly noticeable for the 1994 season since the SSA experienced a wetter than normal year and the NSA experienced a drier than normal year. The NSA is typically colder and receives less incoming solar radiation than the SSA (as of function of the difference in latitude between the sites). Parameters in the potential evapotranspiration equations, such as temperature, in the Hargreaves and Turc equations, and net radiation in the Priestley-Taylor equation, should account for the differences in climate. Therefore, for normal meteorological conditions, the coefficients should be more similar between the two regions. Methods of indexing the actual to the potential rates which are a function of these climatic differences (such as soil moisture or soil temperature) would improve the spatial transferability of these equations.

5.5.2 Coefficient of Determination R^2

All of the calculated values of R^2 are quite high, being greater than 0.83 for each of the four regressed relationships of potential evapotranspiration. High R^2 values indicate that the application of the regressed reduction coefficients to the potential evapotranspiration produces satisfactory estimates of actual evapotranspiration.

5.5.3 Standard Error

The value of the standard error for all of the models is relatively constant at approximately 0.2mm d^{-1}, except for the Turc equation which is 0.1mm d^{-1}. This standard error is relatively low, being approximately less than 10% of the mean on average. The relative value of the standard error is significantly lower for the NSA because the mean values are also lower. Relative to the mean AET, the standard error is similar to the SSA, approximately 10%, on average. The standard error for each of the models in the NSA is fairly constant with an approximate value of 0.2mm d^{-1}.

5.5.4 Relationship of Actual Evapotranspiration to Potential Evapotranspiration

The average daily estimates of evapotranspiration calculated with the water balance have been plotted with respect to the mean daily estimates of potential evapotranspiration calculated at the AFM tower flux sites for the SSA and the NSA in Figures 5.7 and 5.8, respectively. In the plot of the SSA data, the Hargreaves and Priestley-Taylor equations significantly over predict the actual evapotranspiration, but the lines of best fit through the origin lay close to each other. There is a significant amount of scatter in the data about the line of best fit parallel to both axes. In contrast, for the Turc equation the line of best fit through the origin under predicts the actual evapotranspiration. The data have a significant scatter only about the line of best fit parallel to the water balance axis. However, little variation is shown in the estimates of the potential evapotranspiration.

In the plot of the NSA data (Figure 5.8), the best fit lines through the Hargreaves and Priestley-Taylor data lay even closer, although somewhat further from the perfect fit line. The line of best fit through the Turc data lays closer to the perfect fit line. In the NSA, all of the best fit lines have shifted lower, indicating an increase in the potential evapotranspiration estimates with respect to the actual evapotranspiration estimates from the SSA to the NSA. This shift is reasonable considering the relative increase in dry climatic conditions when moving from the SSA to the NSA during the study period. The scatter about the best fit lines is similar to that observed in the SSA.

The total actual evapotranspiration estimated with the water balance, and the potential evapotranspiration estimated with the Hargreaves, Priestley-Taylor, and Turc equations are shown in Figures D13 and D14 in Appendix D for the SSA and the NSA, respectively. The data in these figures are identical to the values in the Figures 5.7 and 5.8 except that the values have not been normalized with respect to time. Each plot has a linear portion throughout the lower values and a curved portion throughout the higher values. As the estimated values of

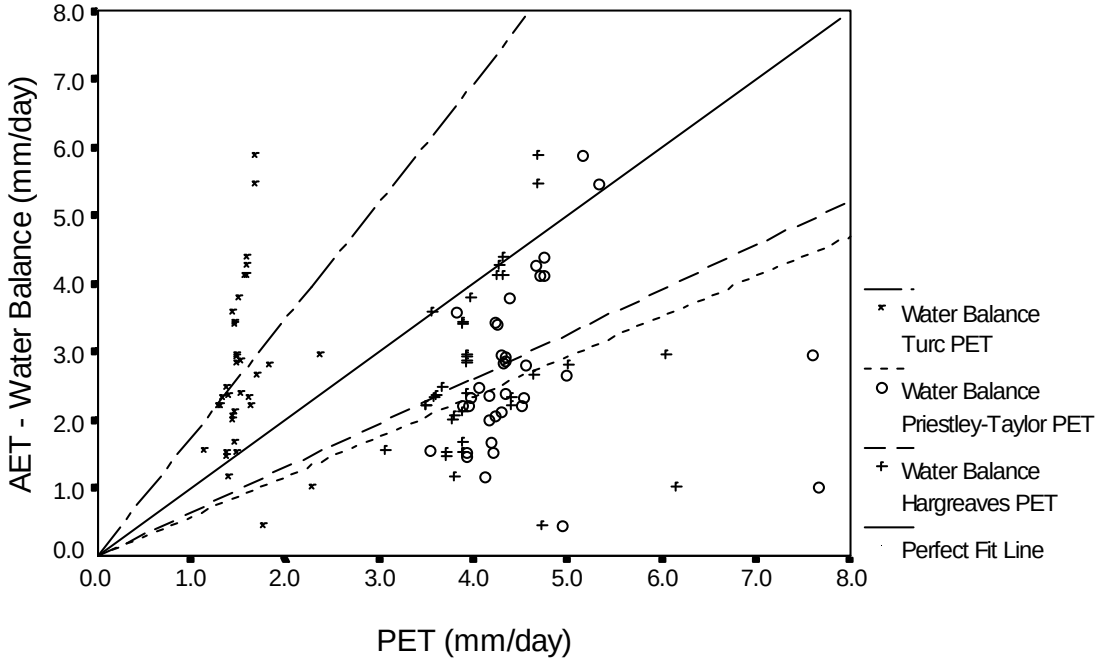

Figure 5.7: Mean Daily AET - Water Balance vs. PET - SSA

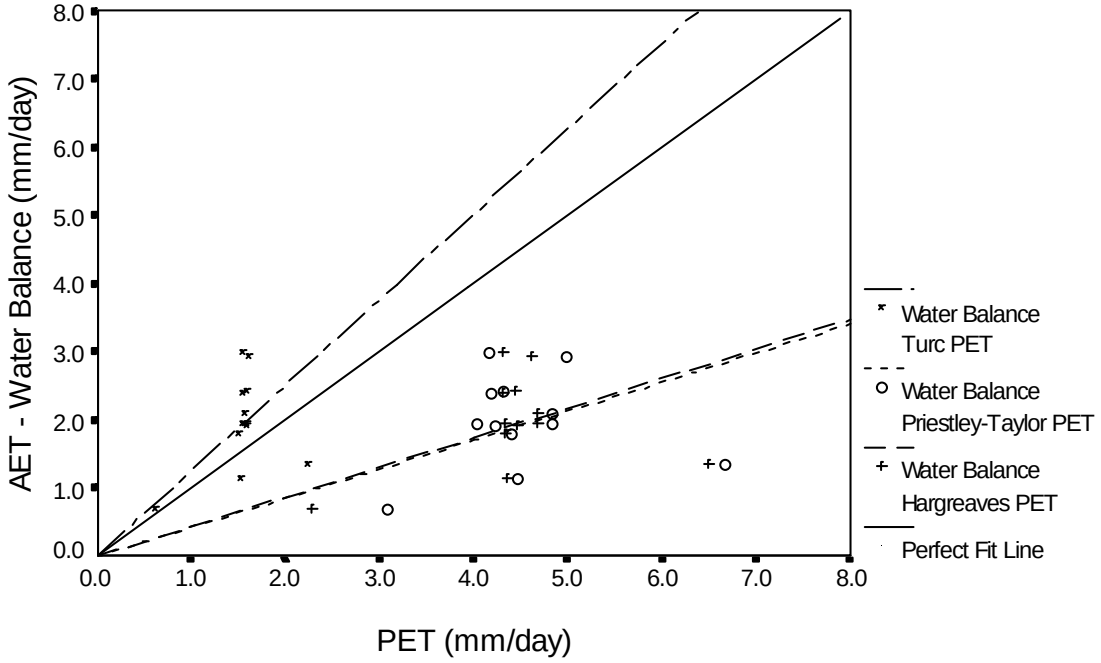

Figure 5.8: Mean Daily AET - Water Balance vs. PET - NSA

evapotranspiration exceed approximately 200-250mm, the calculated values of potential evapotranspiration do not increase proportionately. These data points correspond to the longer term estimates of actual evapotranspiration produced by the water balance. The values of the corresponding data points of the measured values of actual evapotranspiration at the tower flux sites are even lower than the water balance estimates of actual evapotranspiration. Therefore, substituting the flux tower measured values would exaggerate the lack of fit at the top end of these plots.

The non-linearity shows that with increased values of actual evapotranspiration, as measured for the long-duration periods, the potential evapotranspiration increases at a much greater rate. This implies that over the long-term, the constraint on the potential evapotranspiration increases. The total potential evapotranspiration continues to increase while the actual evapotranspiration is constrained and only increases moderately. This conclusion corresponds to a possible constraint on the actual evapotranspiration resulting from dry conditions late in the season, or cold soil conditions earlier in the season when no short-term calculations of actual evapotranspiration could be made from of the water balance.

Assuming that the actual evapotranspiration rates were constrained by a moisture deficit, the curvature in the top of the plot agrees with what would be calculated by the Complementary Relationship (Morton, 1978). As the existing conditions tend to dry, the potential evapotranspiration rate will continue to rise while the actual evapotranspiration rate will fall. In 1994, the SSA was unusually wet through the first half of the growing season (May - July); the period through August and September was significantly drier. The NSA did not experience the same meteorological trends as the SSA, in 1994. The NSA was relatively dry throughout the season and did not receive any significant amounts of precipitation to saturate the area.

5.5.5 Conclusions

In summary, the regression coefficients are consistent between study areas and between the different equations. The coefficients for the Hargreaves and Priestley-Taylor equations are similar for study areas. The estimates of potential evapotranspiration have only a modest correlation to the values of evapotranspiration calculated using the water balance. These low values of correlation can be explained by the fact that the value calculated with the water balance have very little temporal variation and reflect the longer term average, whereas the potential evapotranspiration estimates would tend to vary on a daily time scale. The fact that the Turc equation produces less variation in the estimates accounts for its higher correlation with the water balance estimates.

By applying the regression coefficients to the calculated potential evapotranspiration values, the resulting estimates of actual evapotranspiration correlate modestly to the water budget estimates of evapotranspiration. The coefficients of determination were greater than 0.83 for all of the potential evapotranspiration equations. The standard error of the estimates when using the reduction is relatively low and consistently about 10% of the measured mean values of actual evapotranspiration. All of the equations seem to be in error by approximately the same percentage, meaning that no single equation is significantly better than the others.

The plot of the actual to potential evapotranspiration indicates that over the long-term, there is some constraint placed on the evapotranspiration rate. These constraints appear to be prevalent during the early and latter parts of the growing season, as shown in the plots of the temporal variation of the percent of precipitation lost through evapotranspiration.

5.6 Conclusions

The use of the water balance is a valuable means for providing an independent check on other methods of estimating evapotranspiration. Certain assumptions with respect to basin storage and outflow must be made to facilitate short-term estimates of evapotranspiration. Normalizing the estimates of actual evapotranspiration by calculating the ratio of the evapotranspiration to the period of the time integral, or the total precipitation for the corresponding interval, enables a comparison of values calculated for different periods and different basins to be made. Values of the average long-term and short-term ratios show a good correlation to the seasonal variation of daily average actual evapotranspiration estimated by the tower flux sites. Correlation between the two estimates is improved by using the average of the tower flux estimates weighted as a function of the total area covered of the corresponding land cover type.

The estimates of evapotranspiration from the water balance do not correlate very well to the estimates of potential evapotranspiration. This is a result of the high temporal variation of the daily estimates of the potential evapotranspiration being compared to the lower temporal variation of the estimates of actual evapotranspiration produced by the water balance. When a simple regression coefficient is used to reduce the potential evapotranspiration to the actual evapotranspiration the standard error of final estimate of the actual evapotranspiration is approximately 10%.

The plot of the actual evapotranspiration calculated using the water balance with respect to the potential evapotranspiration, indicates that for longer time integrals the total potential

evapotranspiration increases more rapidly than the total actual evapotranspiration; however, there is a good correlation with the short-term estimates. These results, combined with the plots of the AET/Rain ratios with respect to time, suggests that there is some variable constraining the potential evapotranspiration during early and latter portions of the growing season.

Chapter 6
Modelling the NSA and SSA Basins using WATFLOOD

The flows in the SSA and NSA watersheds have been simulated for the 1994 and 1995 seasons using WATFLOOD with the revised evaporation and interception models. The 1994 data sets have been used for the purposes of calibrating the model parameters. Temporal validations of the calibrated parameters have been attempted by using the 1995 data sets.

6.1 Modifications to WATFLOOD

The original objective inspiring the development of WATFLOOD was the desire to simulate flows of a short duration. For each time step in the original version of the model interception is modelled using Linsley's method (1949). Evapotranspiration is calculated as the hourly fraction of the published monthly averages. Both of these sub-processes have been modified in order to more closely simulate the actual processes for periods of longer duration.

Figure 3.6 shows the measured flow records for summer period of 1994 in the SSA, and the hydrographs simulated by WATFLOOD using the original interception subroutine and monthly average values of evapotranspiration. The simulation record has been calibrated throughout the period shown. In the original version of WATFLOOD, interception is filled to capacity within the first few precipitation events and remains constant thereafter. In reality, the total amount of water evaporated from interception storage should continue to increase during subsequent precipitation events. As a result of interception evaporation, increased rates of total evapotranspiration should be evident following periods of precipitation (Stewart, 1977; Stewart and Thom, 1973). Constraints which reduce the rate of transpiration between events may also exist depending on the availability of water in the upper soil layers.

Diurnal variations in solar radiation constrain the rate of photosynthesis and transpiration; this results in variations in the inputs to channel flow by changing the rates of flow from the upper soil layers. These diurnal variations are not noticeable in measured hydrographs of 1994 in the SSA, as shown in Figure 3.7. For large basins with long times of concentration, such as in the SSA and NSA watersheds (approximately one day for the larger basins), the diurnal variations in transpiration losses are moderated and the use of daily averages is adequate. The diurnal variations become more evident during periods of low flow when changes in the interflow from the upper soil layers are a more significant percentage of the total flow.

The use of average monthly values of evapotranspiration is suitable for simulating average conditions. However, periods of extreme or atypical meteorological conditions will result in

inaccurate estimates of evapotranspiration. In these situations, an evapotranspiration model, which is a function of these meteorological variables, will more accurately characterize the actual evapotranspiration losses.

The evapotranspiration mass curve should be non-linear with time, increasing rapidly when moisture is available and becoming level during drier periods. The NSA and SSA watersheds are small enough that there is not much spatial variation in the temperature and radiation data. Future research will involve applications of the WATFLOOD in larger watersheds, such as the transect between the SSA and NSA basins (up to 25,000 km^2), and in areas with extreme variations in topography, such as the Columbia River basin. In areas such as these, spatial variability of these temperature and radiation parameters will exist. It is for this reason that the subroutines have been developed to utilize spatially distributed radiation and temperature data. Two significant modifications have been made to align the procedure for modelling interception and transpiration with the actual process.

6.1.1 Modified Interception Sub-process

Following Linsley's model (1949), the current version of WATFLOOD calculates the sum of precipitation from the beginning of the simulation to establish the decay exponent in the model. In the discussion of the model, Linsley identified typical values for interception evaporation and interception storage; these have been used in WATFLOOD.

The current version of WATFLOOD does not sufficiently reduce interception storage during long-term simulations to allow for the storage to be filled in subsequent events. The error in the estimation of interception losses is compensated for by increasing the total evapotranspiration loss. This results in too little water being removed from the budget during and immediately after precipitation events, when interception evaporation exists, and excess amounts being removed during dry periods between events. The imprecision in the simulation of interception could be compensated for by increasing the rate of infiltration to the groundwater storage and the overall rate of evaporation to remove excess volumes of groundwater discharge. A compensation such as this could result in a good hydrograph simulation, but the separate sub-processes would not be modelled correctly. These problems would likely result in poor validations of such a model.

The revised accounting procedure used for tracking interception storage and interception evaporation follows the model developed by Linsley (1949). The Linsley method calculates the total possible interception as the maximum canopy storage (h) plus the amount of

interception evaporation (IET) during the storm event (mm). In the new interception subroutine, a value of 1.6mm has been selected for the maximum canopy storage for the Dry and Wet Conifers classification during the growing season (June - September). These values are similar to the storage of the 1.2-1.5mm measured by Rowe (1983) for deciduous forests. During the dormant season (October - May) for the Wet Conifer classification the storage is reduced to 1.5mm to reflect the loss of leaf area from the deciduous under-story and any small amounts of deciduous over-story. Canopy storage for the Dry Conifer, Mixed/Deciduous, and Regeneration classification is set at a maximum of 1.5mm during the growing season, and 1.0mm during the dormant periods to reflect the leaf loss from the deciduous growth. The storage in the Fen class is established at a low value of 0.05mm during the growing season to simulate the interception by sparse tall vegetation and dense low vegetation. For dormant periods, the capacity has been reduced to lower values of 0.02mm to characterize reductions in leaf area of the low deciduous vegetation in the fens. Storage for the Barren class has been set to 0.0mm to reflect the lack of vegetation.

The amount of water in interception storage is reduced through evaporation which is estimated as a function of the potential evapotranspiration (PET) in mm. During a precipitation event, the rate of interception evaporation is assumed to equal the rate of potential evapotranspiration from a saturated surface because the interception surface is open to the atmosphere and is covered in water. Researchers have shown that, in fact, the evaporation rate of intercepted water can be well in excess of the potential rate (Stewart, 1977; Stewart and Thom, 1973). Therefore, after the precipitation event has ceased, the interception evaporation rate is set to the product of the potential evapotranspiration rate and a factor (FPET). For this analysis, FPET has been set at 3.0 times the potential rate. Interception evapotranspiration continues at this rate until the storage is reduced to zero, at which point IET is zero, or another precipitation event occurs and IET is reset to the potential rate. This increase in the actual rate of evapotranspiration is substantiated by the fact that with precipitation there can be considerable wind-producing advective conditions, which are not completely accounted for by the temperature and radiation-based equations. The FPET factor is not applied during the storm event because of the high humidity that usually exists concurrently with precipitation, which would not be considered when using longer term averages of humidity. Thus,

$$IET = FPET \cdot PET, \qquad [83]$$

where

FPET = 1.0 during a precipitation event, and
FPET = 3.0 after rainfall cessation.

The amount of precipitation removed by interception storage (V), in mm, is calculated as a fraction of the sum (X2) of the maximum storage and the interception evaporation, in mm:

$$V = fraction \cdot X2, \qquad [84]$$

and

$$X2 = h + IET = h + FPET \cdot PET. \qquad [85]$$

The value of the fraction is dependent on the total precipitation from the beginning of the storm. By defining the fraction as some function of the base of the natural logarithm to an exponent equal to the total precipitation since the beginning of the storm (P_i in mm), the rate of interception is established as an exponentially decaying rate. That is to say, the rate of interception decreases as water is intercepted as given by

$$fraction = e^{-P_i/X2}, \qquad [86]$$

and

$$V = X2 \cdot e^{-P_i/X2}. \qquad [87]$$

As a result of evaporating the intercepted water at the potential evapotranspiration rate, the amount of water lost from interception storage can exceed the maximum value of the storage. While under certain conditions it might be possible for the volume of interception evaporation to exceed the interception storage (periods of moderate precipitation and highly advective conditions), this does not seem reasonable for the typical situation. The interception evaporation has therefore been limited to the lesser of the maximum interception storage or the potential evapotranspiration. This constraint affects the interception evaporation for land classes with values of maximum storage that are less than the potential rate of evaporation (e.g. the Fen class). Thus,

$$X2 = h + FPET \cdot PET \qquad \text{if } PET \le h, \qquad [88]$$

or

$$X2 = X3 = h + FPET \cdot h \qquad \text{if } PET > h. \qquad [89]$$

For each time step in each element and in each land class, the throughfall is calculated as the precipitation less the amount of precipitation captured in the interception storage and the amount lost through evaporation of the interception storage:

$$\text{Throughfall} = \text{Precipitation} - (V_t - V_{t-1}) - PET\,, \qquad [90]$$

where t indicates the time step.

6.1.2 Modified Evapotranspiration Sub-Process

The current version of WATFLOOD uses published monthly average values for estimating evapotranspiration. Hourly estimates of the evapotranspiration are calculated by taking the appropriate fraction of the monthly value. A reduction of the published values of evapotranspiration is not necessary if values of actual evapotranspiration are used. However, if published evaporation pan measurements are used, these must be reduced to yield values of actual evapotranspiration. A reduction of these published values has been used for modelling long-term events, with the value of the reduction being dependent on the period of calibration. As a result of using long-term average values of evapotranspiration these reduction values will change from year to year. The modelling process currently does not incorporate a method for estimating the temporal variation of this reduction. The revision to the evapotranspiration subroutine makes available two other methods for calculating evapotranspiration.

6.1.2.1 Calculation of Potential Evapotranspiration

In the analysis of the potential evapotranspiration equations evapotranspiration estimates have been made using three different models, the Hargreaves, Priestley-Taylor, and Turc equations. The Turc model has been shown to provide significantly different estimates of evapotranspiration from those estimates provided by the Priestley-Taylor and Hargreaves equations. This inconsistency results in significantly different parameters than those used with the Hargreaves and Priestley-Taylor equations to calculate the actual evapotranspiration from the potential evapotranspiration (the Soil Moisture Indicator and degree-day parameters). The values of these parameters are not realistic for the Turc equation.

The significantly lower estimates of evapotranspiration produced by the Turc equation are usually, but not always, similar to the actual evapotranspiration equation. The ratio of the actual evapotranspiration to the Turc evapotranspiration varies significantly between 1.0 and 2.0, as shown in the regression coefficients in Table C3 Appendix C. The Turc estimates of evapotranspiration do not consistently require a reduction or an increase to provide an estimate

of the actual evapotranspiration. Thus, it is unclear whether the Turc equation provides a true estimate of the actual or potential evapotranspiration in these simulations. The Turc equation has a very low variability in the estimates of evapotranspiration, as shown in Figure 4.14 where there is little variation in the estimates with respect to actual evapotranspiration. Most of the Turc estimates of evapotranspiration lay in a narrow band in the vicinity of 1.0-1.5 mm, with few estimates falling outside of this range along the line of perfect fit in Figure 4.14.

Where radiation data are available, the Priestley-Taylor equation (equation 64) can be used to estimate the potential evapotranspiration. The similarity of radiation inputs throughout the basins justifies the use of non-gridded radiation data for the calculation of potential evapotranspiration. Values of Priestley-Taylor potential evapotranspiration have been calculated hourly and summed for the period of one day. Where only temperature data are available, the Hargreaves equation can be used to estimate the potential evapotranspiration using equation [57]. Gridded hourly temperature data currently exists for the SSA and NSA watersheds as a requirement of the snowmelt simulation. Therefore, these data have been utilized so that the Hargreaves evapotranspiration is calculated at a temporal resolution of one hour for each separate element.

The Priestley-Taylor and Hargreaves equations have been tested to determine if there can be any improvement in the evapotranspiration modelling process within WATFLOOD. Because of the similarity of the estimates of potential evapotranspiration that these two equations produce, no significant changes are necessary in the calculation of the actual evapotranspiration for the use of either equation. Estimates of potential evapotranspiration using the Priestley-Taylor equation have been adjusted as a function of the difference in albedo at the site where measurements of radiation have been made (albe), and the land classes with differing albedo (alb). In the adjustment, it is assumed that the ground heat flux contributes 5% of the overall energy. The remaining 95% of the potential evapotranspiration estimate is scaled as a function of the difference in albedo:

$$PET = 0.05 \cdot PET + 0.95 \cdot PET \cdot \frac{1 - alb}{1 - albe}. \qquad [91]$$

6.1.2.2 Potential Evapotranspiration Coefficient - Soil Moisture

Up to four coefficients have been applied to reduce the calculated potential evapotranspiration to the actual evapotranspiration. The first coefficient, the Upper Zone Storage Indicator (UZSI), estimates the evapotranspiration as a function of the soil moisture (θ).

Evapotranspiration is assumed to occur at the potential rate if the soil moisture is above the field capacity (FCAP). The rate of evapotranspiration is reduced to a fraction of the potential evapotranspiration for values of soil moisture below the field capacity down to zero at the permanent wilting point (PWP). The fraction is calculated by interpolating the soil moisture between the field capacity and the permanent wilting point at 1.0 and 0, respectively. That is

$$UZSI = \frac{(\theta - PWP)}{(FCAP - PWP)}. \qquad [92]$$

WATFLOOD does not calculate the percent soil moisture (θ); instead, the model calculates the moisture in the upper layer of soil as a depth of water, the Upper Zone Storage (UZS). During the calibration of the model, the value of the field capacity, called the retention factor (RETN), is optimized. Drainage from the upper zone storage is constrained to zero when the UZS is less than the RETN. Values of UZS below the RETN cannot be drained by the gravitational force, which is the driving force in the interflow and drainage to lower soil layers. Volumes of water in the Upper Zone Storage that are less than the RETN can only be drained by evapotranspiration.

The percent soil moisture is estimated by calculating the ratio of the UZS to the depth of water in the UZS at which saturation of the soil occurs. Since the RETN is the value of the field capacity in terms of depth, the equivalent depth at which the UZS is saturated can be obtained by calculating the ratio of the RETN to the FCAP. The percent soil moisture is the ratio of the current UZS to the UZS at saturation:

$$\theta = \frac{UZS}{\left(RETN / FCAP\right)}. \qquad [93]$$

The permanent wilting point is a function of the volumetric clay content. Arp and Yin (1992) have shown the relationship between volumetric water fraction and volumetric clay fraction. For modelling, an approximation of this relationship has been used to define the permanent wilting point as 50% of the field capacity. The fraction of the field capacity equal to the permanent wilting point is 0.5 (FFCAP) used in the following calculations:

$$PWP = FFCAP \cdot FCAP. \qquad [94]$$

An error in the approximated value of the field capacity will have only a very small effect on the overall simulation since it is the difference between the three parameters, θ, PWP, and FCAP, that are used in the calculations. The field capacity has been assumed to be half of the saturated capacity.

6.1.2.3 Potential Evapotranspiration Coefficient - Soil Temperature

The second coefficient (FPET2) applied to the potential evapotranspiration to reduce it to the actual evapotranspiration is based on the total number of the degree-days. The preliminary results from BOREAS have suggested that low soil temperatures constrain the actual evapotranspiration rate for the early part of the year (Sellers *et al.*, 1995). The degree-days are accumulated to emulate the seasonal heating of the soil, and the function is defined by three other values. Two values denote the upper (Temp3) and lower limits (Temp1) of the relationship corresponding to coefficients of 1.0 and 0.0. The third value (Temp2) is set between the upper and lower values to estimate a constant. Any total of degree-days (TTO) below Temp2 yields a constant for the coefficient equal to the ratio of the difference between Temp2 and Temp1, and the difference between Temp3 and Temp1. A total of degree-days between Temp2 and Temp3 yields the interpolated value of the coefficient between 0.0 and 1.0. A total of degree-days greater than Temp3 yields a coefficient of 1.0, indicating that there is no constraint on the transpiration due to soil temperature.

$$\begin{aligned} FPET2 &= \frac{Temp2 - Temp1}{Temp3 - Temp1} && \text{if } TTO < Temp2, \\ FPET2 &= \frac{TTO - Temp1}{Temp3 - Temp1} && \text{if } Temp2 < TTO < Temp3, \text{ and} \\ FPET2 &= 1.0 && \text{if } TTO > Temp3. \end{aligned} \qquad [95]$$

6.1.2.4 Potential Evapotranspiration Coefficient - Forest Vegetation

The third coefficient used to reduce the potential evapotranspiration is a function of the vegetation type. For tall vegetation, it has been shown that the evapotranspiration is significantly less than the potential rate (Price, 1987; Black *et al.*, 1984; Giles *et al.*, 1985; Spittlehouse and Black, 1981; McNaughton and Black, 1973). Typical values of actual evapotranspiration from tall vegetation range from 60-90% of the potential evapotranspiration. Stagnitti (1989) used a coefficient of reduction of 0.60 for the Priestley-Taylor evapotranspiration to estimate the actual evapotranspiration from tall vegetation. A reduction coefficient of 0.70 has been applied to the potential evapotranspiration rate for the Wet Conifer and the Dry Conifer classifications.

$FTALL = 0.70$ for Tall Vegetation, and
$FTALL = 1.00$ for Short Vegetation.

6.1.2.5 Potential Evapotranspiration Coefficient - Evaporation Pan Reduction

The fourth coefficient, ETP, is a general reduction coefficient. It has only been used for reducing the published mean monthly evaporation pan estimates. This coefficient has been applied to reflect the typical difference between the evaporation pan estimates and the actual evapotranspiration rates.

$ETP = 1.00$ for all classes using Hargreaves of Priestley - Taylor PET and for the Water class using Evaporation Pan PET, and
$ETP = (Optimized)$ for all classes except water using Evaporation Pan PET.

In the water class, evapotranspiration occurs at the potential rate, and as a result, no coefficients have been applied to reduce the potential evapotranspiration. However, the ratio of the actual to potential evapotranspiration from the Water class will vary considerably in time for this region. Simulation of spring events will overestimate the evaporation because of low water temperatures. Since these water bodies are relatively shallow, the heat capacities are small enough that there is a significant temperature change throughout the season. Mid-summer estimates of daily potential evapotranspiration may well underestimate actual evapotranspiration because of elevated water temperatures throughout the day, and lack of diurnal variation in actual evaporation rates. Nevertheless, the long-term average of the evaporation from the Water class should be relatively accurate with the coefficient set to 1.0.

6.1.2.6 Calculating Actual Evapotranspiration from Potential Evapotranspiration

The final reduction in transpiration is a function of the interception. Evaporation of intercepted water is assumed to occur preferentially to soil water transpiration. The sum of the atmospheric resistance and stomatal resistance to water evaporating from stomatal cavities is assumed to be greater than the atmospheric resistance to water evaporating from the surface of the vegetation. In each time step, the transpiration is reduced to zero during periods when interception evaporation (IET) is occurring. When the interception evaporation is less than the potential evapotranspiration the reduction coefficients are applied to the difference to determine the rate of transpiration. Finally,

$$
\begin{aligned}
AET &= PET && \text{if } PET < IET, \\
AET &= (PET - IET) \cdot UZSI \cdot FPET2 \cdot FTALL \cdot ETP && \text{if } PET > IET, \\
AET &= PET \cdot UZSI \cdot FPET2 \cdot FTALL \cdot ETP && \text{if } IET = 0, \text{ and} \\
AET &= PET && \text{for the Water Class.}
\end{aligned}
\qquad [96]
$$

This estimate of actual evapotranspiration is the combination of the water transpired from vegetation and the water evaporated from bare soils and open water.

6.2 Calibration of Parameters - 1994 Data

Certain model parameters cannot be explicitly defined based solely on qualitative information, background knowledge, or experience. Familiarity with the model will enable a reasonable initial estimate of these parameters to be made, but the final values that produce the best simulation must be found through an iterative fine tuning process. The parameters in each of the models (the original WATFLOOD model and the versions which incorporated the Hargreaves and Priestley-Taylor models) have been calibrated on the SSA and NSA watersheds for the 1994 season.

Some parameters have not been adjusted from the original values that have been established for similar land classes in simulations of the Grand River (Kouwen, personal communication). Instead, calibrations have focused on the optimization of the soil permeability and drainage parameters to which the simulations in these study regions were most sensitive. The specific parameters that were calibrated are discussed in section 6.2.3. The calibration of the parameters is the first attempt that has been made with the use of this modified version of the WATFLOOD. Improvement in the overall simulation may be possible by continuing the calibration process. Therefore, the exact values of specific parameters should not be considered to be the absolute optimum values. It is the relative values between land classes and between the northern and southern study that are significant and will be examined.

Of the three evapotranspiration models used in the simulations, the Hargreaves, Priestley-Taylor, and the published average evaporation pan values, the Hargreaves and Priestley-Taylor models most closely simulate temporal variations in the evapotranspiration. A more accurate simulation of the evapotranspiration processes have the least adverse effects on the calibration of the parameters for the other hydrologic sub-processes. For this reason, the parameters for the hydrologic sub-processes other than evapotranspiration and interception have been optimized using the version of WATFLOOD that incorporates the Priestley-Taylor equation.

6.2.1 Initial Parameter Values

For some of the simulations, many of the parameters have been held constant because of the insensitivity of the simulation to these parameters. The parameters for the Water and Barren classes were generally held constant using values used from simulations of the Grand River. Snowmelt parameters were not utilized since simulations were made for periods after snowmelt was complete and before snowfall occurred; the one exception to this occurred around day 140 in the SSA. A snowfall of approximately 2.0 cm occurred, but was subsequently measured by the rain gauges since the temperatures were around the freezing point and the melt occurred soon after the event.

The initial soil moisture conditions were established based on a qualitative analysis of the measured hydrographs prior to the simulation period, and to provide the best fit for each of the modelling periods. Table 6.1 lists the values of the initial conditions for the four different simulation periods, where 33% is assumed to represent saturated conditions.

Table 6.1: Initial Soil Moisture Conditions

Simulation	Initial Soil Moisture (%)
1994 - SSA	31.5
1994 - NSA	30.5
1995 - SSA	26.5
1995 - NSA	31.5

The degree-day parameters were calibrated for the Hargreaves equation to obtain the best simulation. The upper limit parameter has been set at 1000, which is similar to the value regressed in chapter 5. Personal knowledge of the existence of frozen soil conditions well into June 1994 in some areas of both the NSA and SSA provides justification for the use of the degree-day reduction coefficients, which affect the simulations well into June. Figure 4.23 indicates that there is a very low correlation between the degree-days and the evapotranspiration for the NSA during this period. In fact, there is a negative correlation. Therefore, the degree-day coefficients have been set to 0 for all of the NSA simulations. It is possible that the soil temperature in the north does not have a significant seasonal variation to produce a variation in the constraint on the transpiration process.

The land classes have been assigned values of albedo that are typical of the vegetation classes for this region. Values for land classes that are a combination of different land covers have

been assigned an average value of albedo. These values are shown in Table 6.2 and are the average values obtained by Sellers *et al.*(1995).

Table 6.2: Albedo Values for each Land Class

Class	Albedo (alb)
Barren	0.18
Dry Conifer	0.11
Wet Conifer	0.08
Fen	0.15
Water	0.15

The value of albedo for water varies throughout the day and is dependent on the angle of incidence of the solar radiation, ranging between 0.05 and 0.35 for incident angles of 60° and 0 ° respectively. This adjustment is only used with the simulations that use the Priestley-Taylor model, but the effects are minimal. The difference in the simulation error between the models with and without the adjustment was very slight and resulted in a small increase in the simulation error of 0.1%. The albedo adjustment factor will be more important in the simulation of areas that have large amounts of area covered by land classes with significantly different albedos. A complete list of the parameter values used in the evapotranspiration indexing functions is shown in Table E1 in Appendix E.

6.2.2 Discussion of Simulations

The Hargreaves model, Priestley-Taylor equation, and the published average monthly evaporation pan values (shown in Tables C1 and C2 in Appendix C) have been used separately to estimate the actual evapotranspiration in the following hydrologic simulations. The models have been calibrated on the 1994 data set in the SSA and NSA watersheds with some minor re-calibration being completed for the NSA 1995 data set. The simulations of the SSA 1994 data set are shown in Figures 6.1, 6.2, and 6.3 using the published average monthly values, the Hargreaves model, and the Priestley-Taylor equation, respectively. The simulations of the NSA 1994 data set are shown in Figures 6.4, 6.5, and 6.6 for the three evapotranspiration models. The root mean square error in each simulation for each sub-basin has been calculated using equation [79]. The RMSE is calculated in units of volumetric flow by this equation and has been converted into the average error in mm d^{-1}. The area weighted average of the error in each sub-basin has been calculated for each simulation, as shown in Table 6.3.

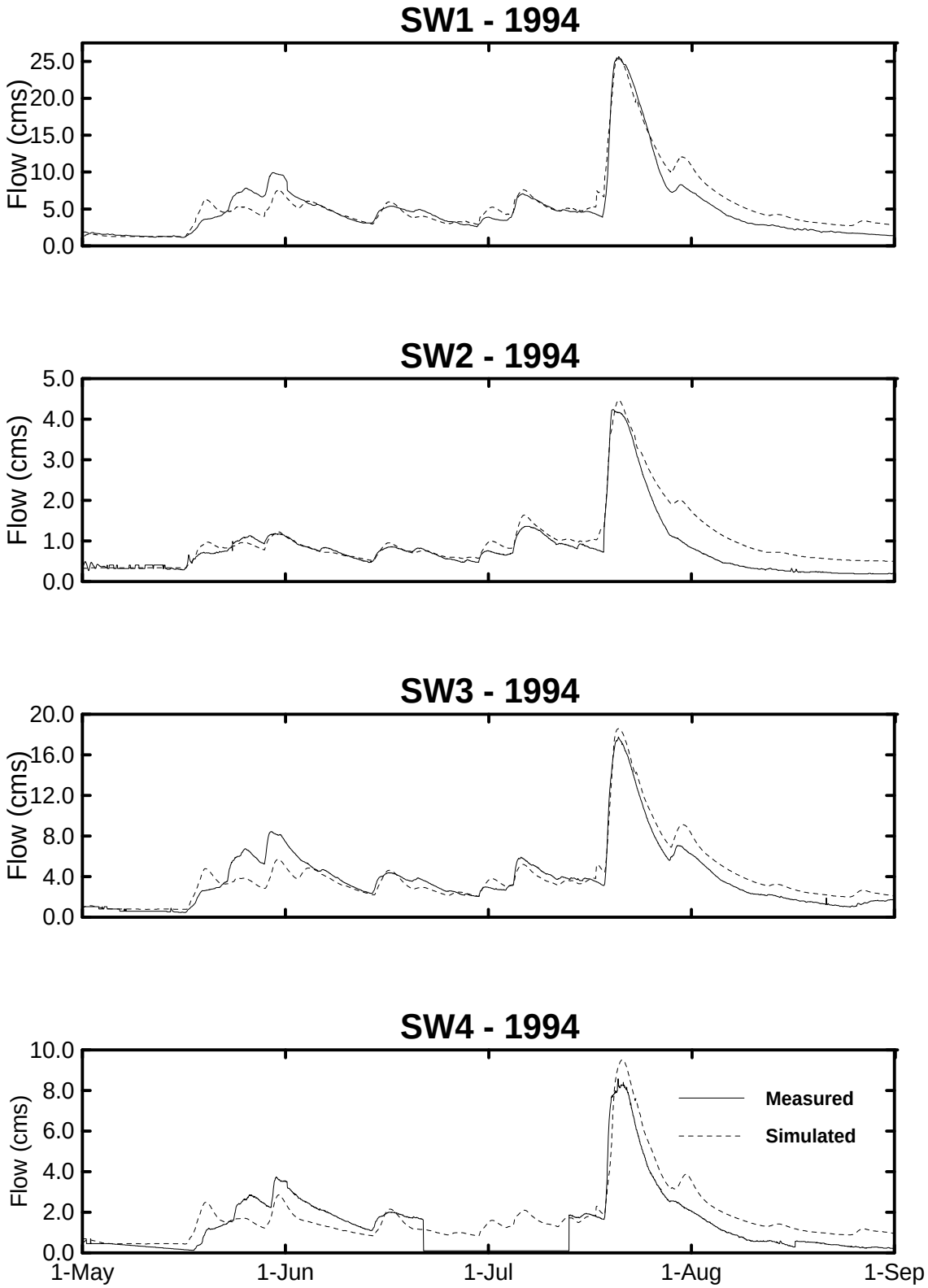

Figure 6.1: Calibrated Hydrographs - SSA 1994 - Evaporation Pan PET

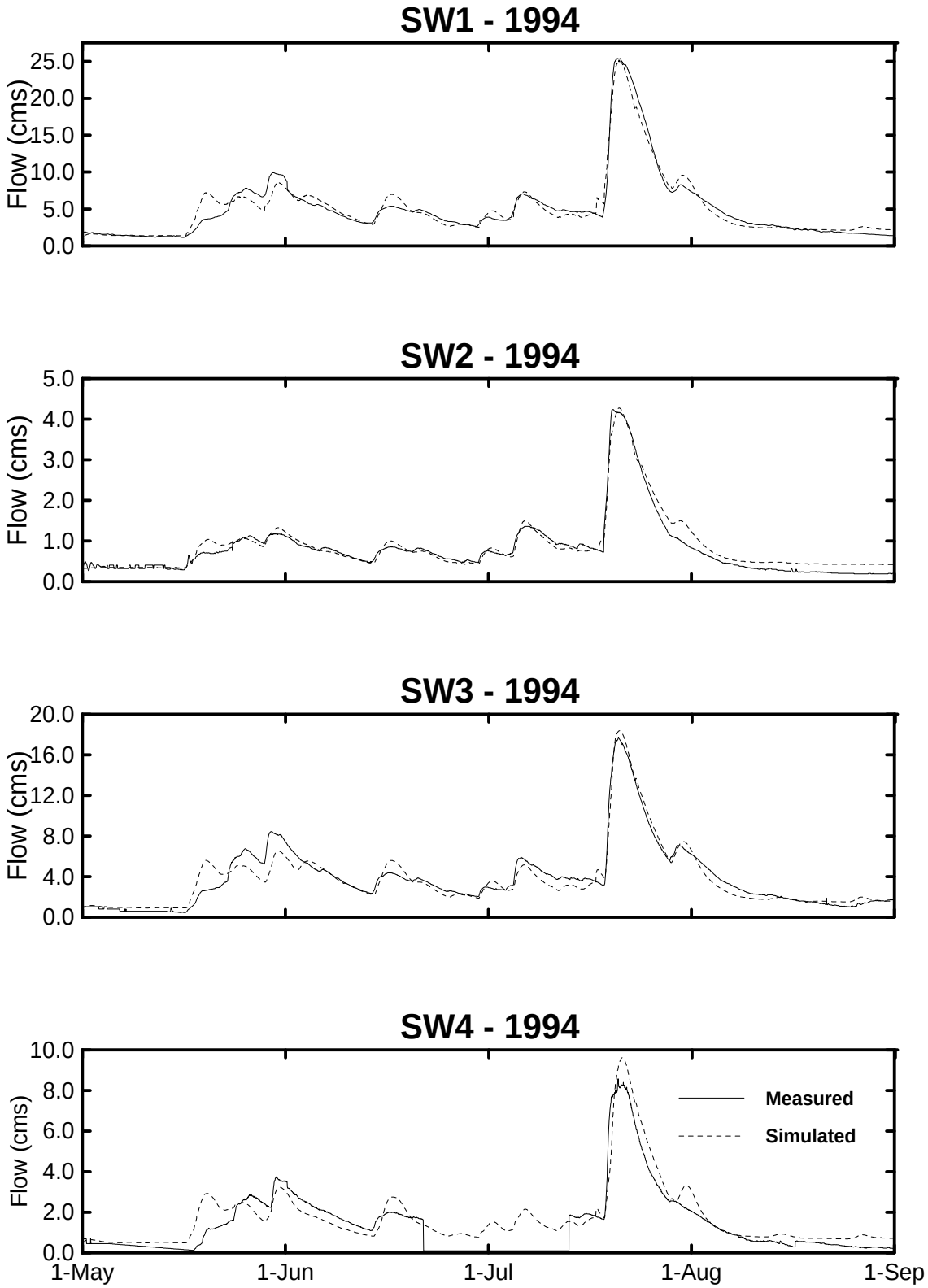

Figure 6.2: Calibrated Hydrographs - SSA 1994 - Hargreaves PET

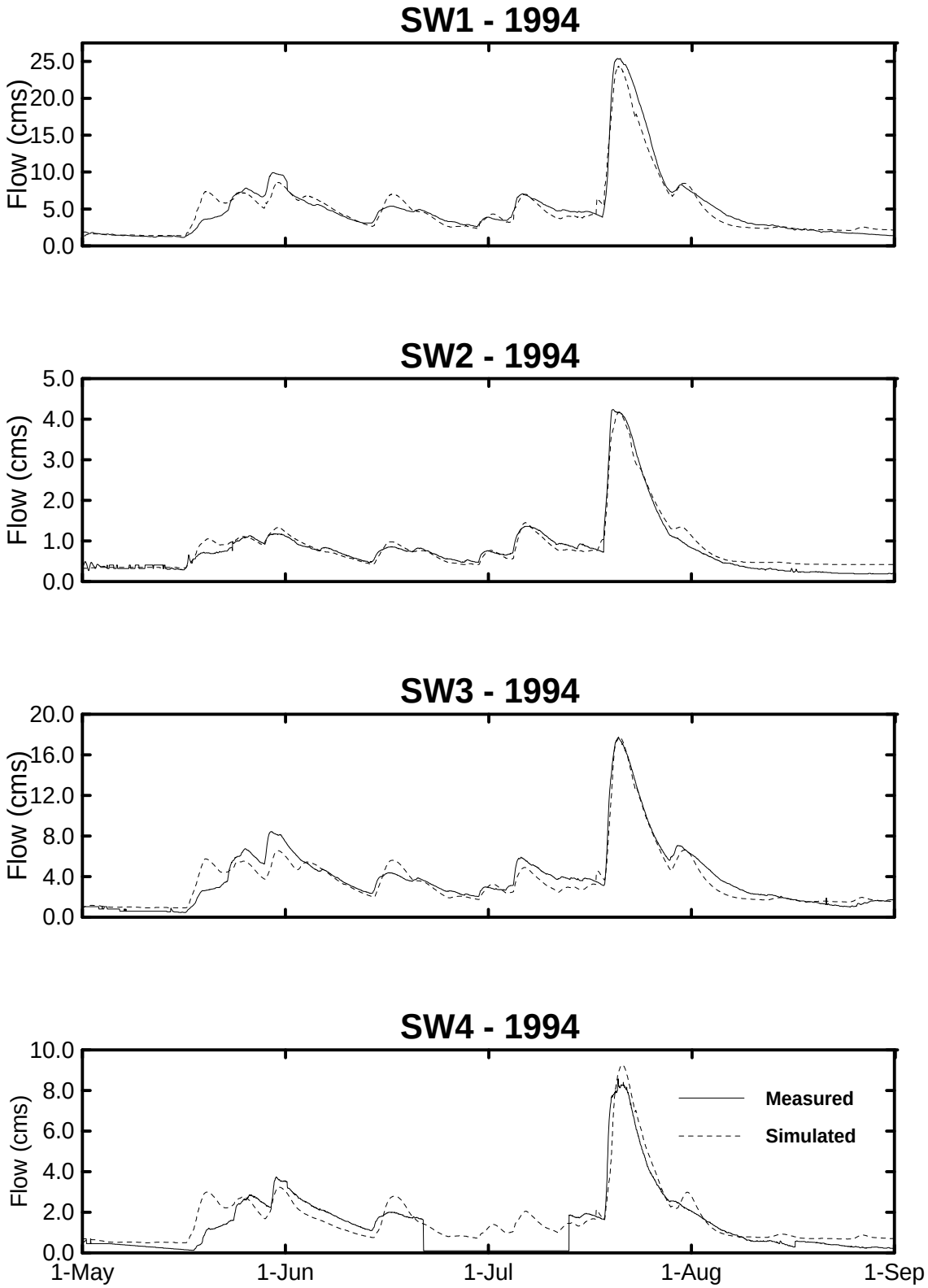

Figure 6.3: Calibrated Hydrographs - SSA 1994 - Priestley-Taylor PET

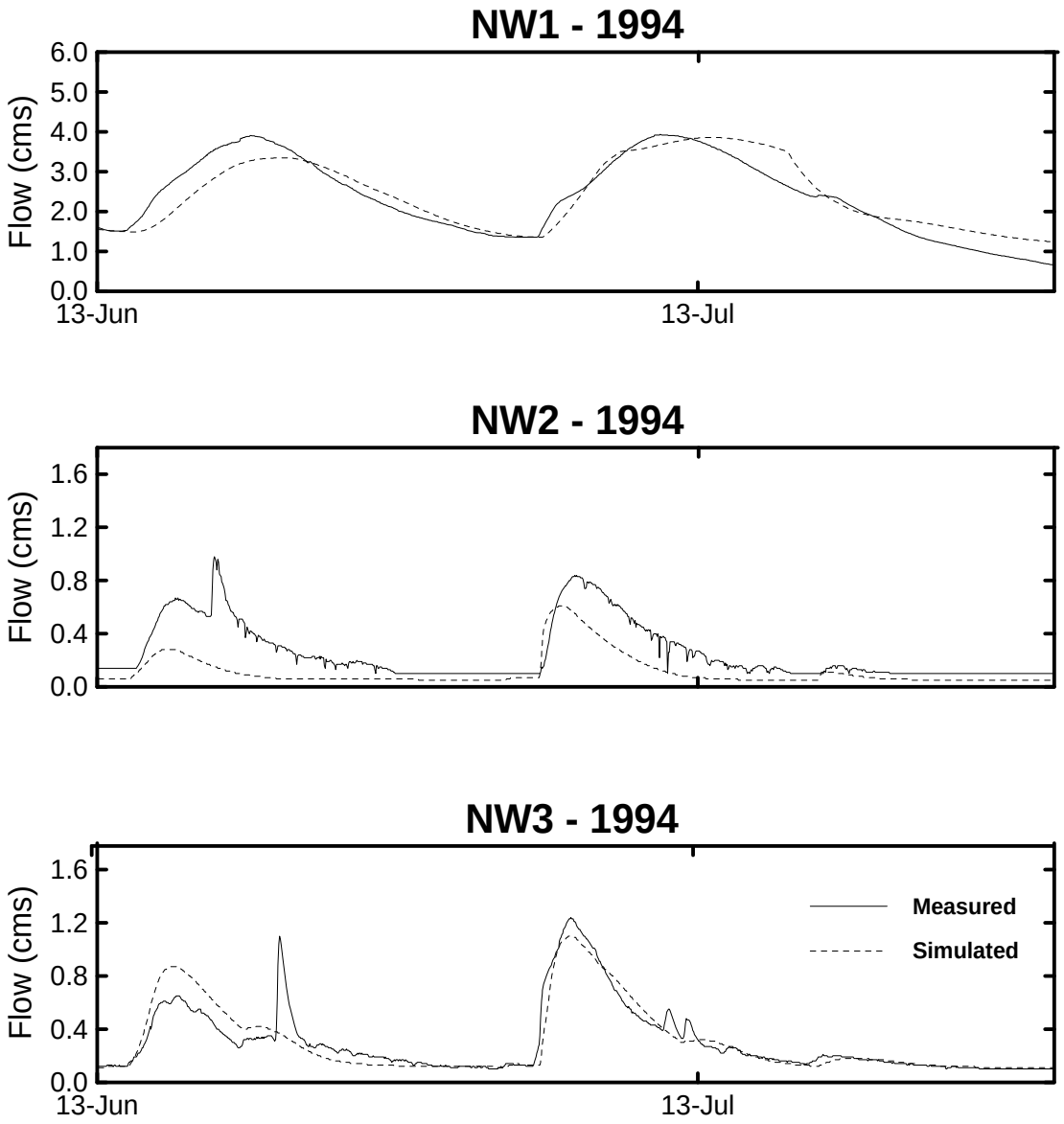

Figure 6.4: Calibrated Hydrographs - NSA 1994 - Evaporation Pan PET

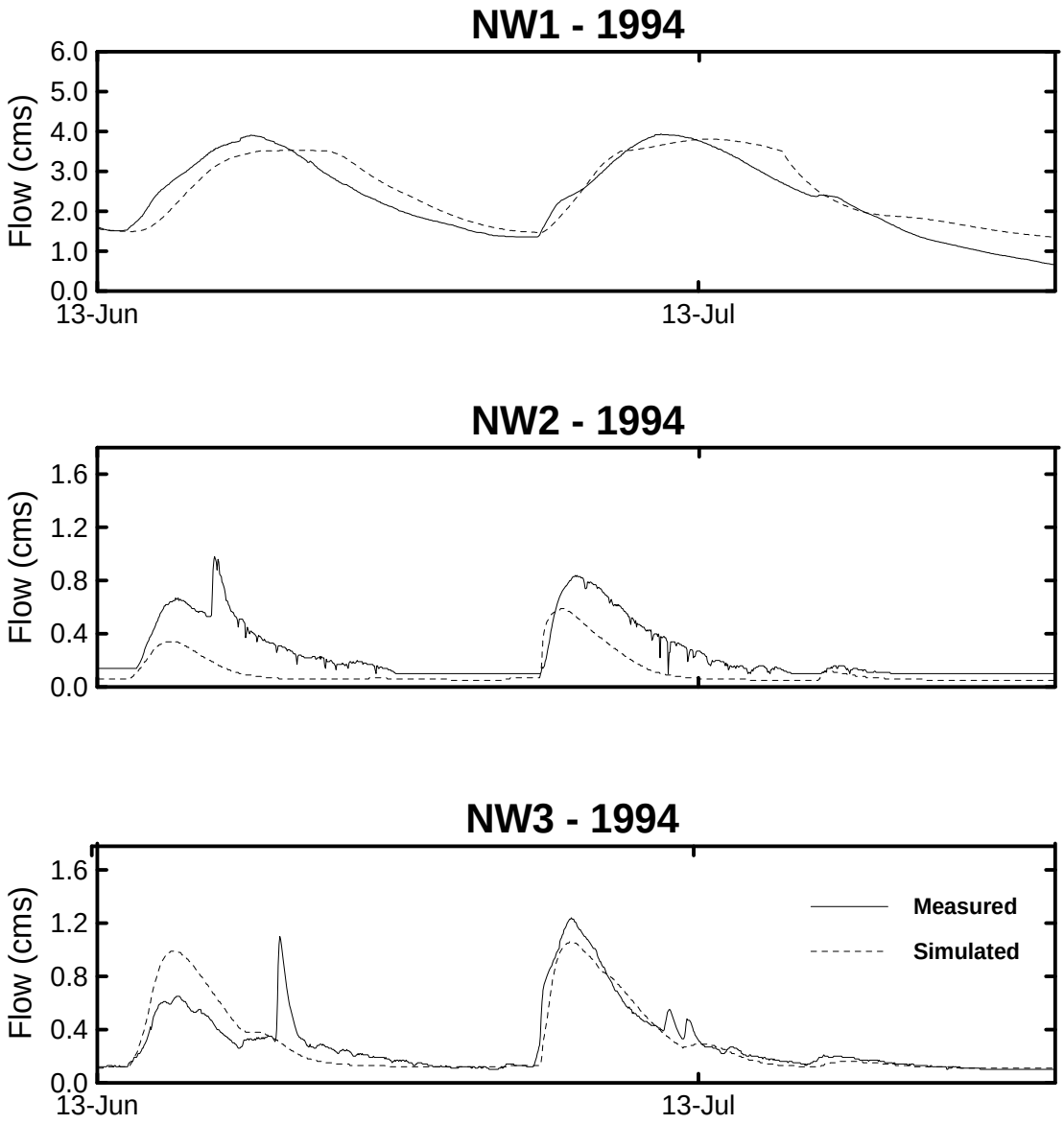

Figure 6.5: Calibrated Hydrographs - NSA 1994 - Hargreaves PET

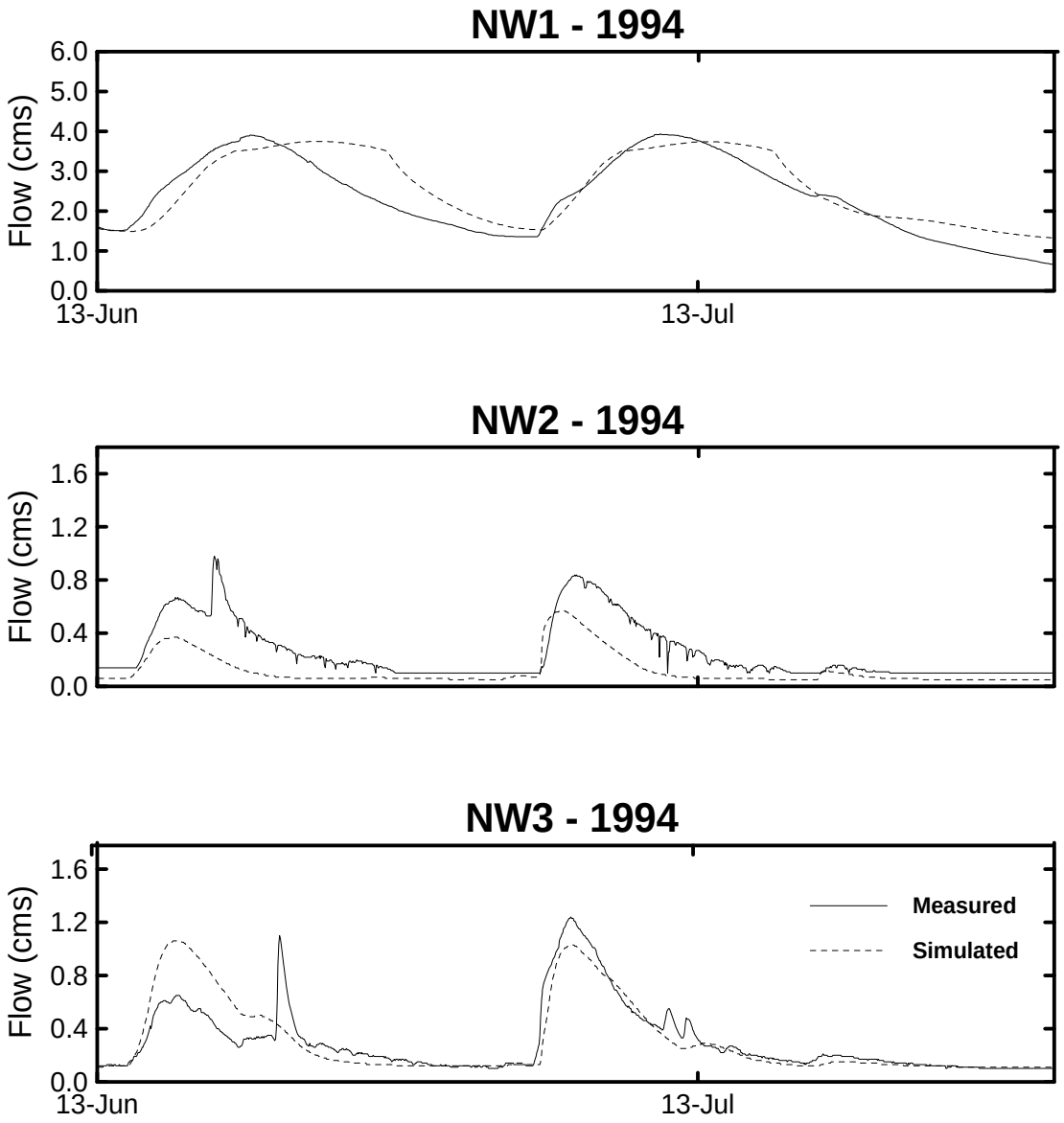

Figure 6.6: Calibrated Hydrographs - NSA 1994 - Priestley-Taylor PET

Table 6.3: Error of the Simulated Flows - Calibrations

Method	Year	Site	RMSE ($mm\ d^{-1}$)
Evaporation Pan	1994	SSA	0.06
Hargreaves	1994	SSA	0.04
Priestley-Taylor	1994	SSA	0.04
Evaporation Pan	1994	NSA	0.13
Hargreaves	1994	NSA	0.13
Priestley-Taylor	1994	NSA	0.15

All of the models produce an excellent simulation of the SSA 1994 data for each sub-basin. Most peak flows are closely approximated, as well as the rising and receding limbs. Some errors common to each model occur in the simulation of the peak flows in May. The simulated flows during the third week of May are in excess of the actual flows. However, the simulated volumes of runoff are approximately correct through this period because immediately thereafter the simulated flows underestimate the first measured peak flow. The baseflow at all gauges is slightly overestimated; this is evident in the simulations of the lowest flows at the end of August, particularly for the simulations using the published monthly averages.

The lowest simulation errors are produced by using the Hargreaves and Priestley-Taylor equations. Use of the published average evaporation pan values produces similarly good estimates of evapotranspiration with low values of error, although the error is approximately 25% larger. Use of the published average evaporation pan values tends to over predict the evapotranspiration losses during late May and early June, and under predict the evapotranspiration losses during August.

All three of the methods produce reasonable simulations of the NSA 1994 data. Each of the simulations produce approximately the same magnitudes of error during the same time periods. The simulations have similar magnitudes of error spaced temporally throughout the simulation with little difference evident between the models. Temporal estimates of peak flows are fair, with peaks being well approximated for the NW3 basin. The rising and receding limbs are fairly well approximated in all simulations, except for the final receding limb of the NW1 basin.

Based on the measured flows and the actual recession limbs of the hydrographs in the first hydrologic event, WATFLOOD establishes the value of the baseflow. In some simulations, the recession curve at the start of the simulation does not approach the lowest baseflow over the course of the entire simulation. As a result, some of the baseflows are established at higher values than they should be. This error is typical of the simulations of the 1994 NW1 data, and the overestimation of baseflows in the last portion of August for the SSA sub-basins.

For computational purposes, WATFLOOD does not recognize measured flows at volumes less than $0.1 m^3 s^{-1}$, and as a result, some of the measured baseflows exist in excess of the simulated baseflows since the simulated baseflows have been established at the values that are less than $0.1 m^3 s^{-1}$. This particular problem is predominant in the simulations of the NW2 watershed.

High flows of short duration (spikes) are evident in the NW2 and NW3 hydrographs in mid to late June. There is no increase in flow evident in either of the simulations of these basins at the corresponding times as these measured spikes. As well, during all of the calibration runs, a spike was never simulated that was even remotely similar to the ones measured. At least one of these spikes (NW3 - personal field notes) and probably both resulted from the removal of beaver dams upstream of the gauges by highway maintenance personnel.

In all of the simulations of the NW2 basin, the volumes are underestimated. One possible source of error is in the mapping of the watershed divide. Although measures have been taken to delineate the basin boundaries as accurately as possible (using small scale aerial photography), the potential for errors always exists in areas such as the NSA which have very little relief. In the event that a delineation problems exist on the boundary with the NW1 watershed, the flows in the NW2 watershed could be substantially increased, with a small decrease in the simulated flows from the NW1 basin. Such a change would improve the overall simulation and reduce the error since flows from the NW1 basin are generally overestimated, and flows from the NW2 basin are always underestimated.

Another problem with the calibration period in the NSA 1994 data is the limited duration of measurable flows. Significant flows occurred only during the summer months of June and July in the NSA. The meteorological conditions in the 1994 season were dry and therefore a lack of any significant precipitation events resulted in extremely low flows throughout the remainder of the growing season.

6.2.3 Calibration of Soil and Groundwater Parameters

Most of the parameters that have been calibrated affect the flow rates through the soil regime. The parameters that have been calibrated are shown in Table 6.4.

Table 6.4: Calibrated Parameters

Parameter	Name	Effects
REC	Interflow Recession Constant	Interflow is directly proportional to REC
AK	Permeability of Soil	Infiltration is directly proportional to AK
RETN	Upper Zone Retention	Upper zone soil water that cannot be drained by gravity - Identical to field capacity but is measured in depth (mm)
AK2	Upper Zone Drainage Constant	Constant affecting the drainage of water from the upper to the lower zone groundwater storage Drainage is directly proportional to the AK2
LZF	Lower Zone Drainage Constant	Constant affecting the discharge of water from lower zone groundwater storage Drainage is directly proportional to LZF
PWR	Lower Zone Drainage Function Exponent	Constant affecting the rate of change of discharge from the lower zone groundwater storage with respect to the total storage
R2	Channel Flow Roughness	Constant defining the resistance to channel flow Flow is inversely proportional to R2

The predominant land covers in the NSA and SSA are the Wet Conifer, Dry Conifer, and Fen classifications, with the forest classes covering significantly more area than the Fen class. Minimal amounts of area are covered by the Barren and Water classes. For these reasons, the model simulation error is most sensitive to the parameters affecting the Wet Conifer, Dry Conifer, and Fen land classes. Tables 6.5 and 6.6 display the calibrated values of the parameters for these three land classes.

The values of these parameters have been established to provide the least error between the simulated and measured hydrographs. Two other criteria were used in the calibrations. First, it is important to use parameters that are realistic in relation to the differences in land class and soil type and then to analyze the simulations in a qualitative sense.

Table 6.5: Values of Calibrated Parameters - Per Land Class

Parameter	Study Area	Dry Conifer	Wet Conifer	Fen
REC	SSA	0.0035	0.0010	0.0010
	NSA	0.0001	0.0090	0.0045
AK	SSA	45.0000	45.0000	2.2200
	NSA	9.0000	9.0000	1.4500
RETN (mm)	SSA	78.0000	84.6000	93.9000
	NSA	150.0000	63.0000	111.0000
AK2	SSA	0.0030	0.0030	0.0213
	NSA	0.0010	0.00001	0.00001

Table 6.6: Values of Calibrated Groundwater Parameters

Parameter	Study Area	Value
LZF	SSA	0.00087
	NSA	0.00001
PWR	SSA	1.58
	NSA	0.75

The parameters calibrated using the SSA 1994 data were used as an initial estimate of the parameters in the NSA 1994 calibration. With those parameters, the total measured volume of runoff was continually underestimated, and the recession of flows occurred too quickly. The initial calibrations attempted to simulate the gradual recession of measured flows in the NSA by changing the Lower Zone Storage constant (LZF) and the Power Function (PWR). These two parameters affect the amount of lower zone storage discharged to the channel flow in each time step and the rate of change of this release as a function of the storage to an exponent (PWR). These first simulations continued to underestimate the flow, and so adjustments were made to increase the volumes of flow through interflow.

The NSA is underlain with more sedimentary and finer soils than the SSA (Sellers *et al.*, 1994). The soils in the NSA contain more clay and are, therefore, less permeable than the soils in the SSA. The calibration of the NSA eventually produced significantly lower values of permeability (AK) than in the SSA. However, further perturbations showed the model to be insensitive to AK values above those values established in the calibration for the Dry Conifer,

Wet Conifer and Fen classes (9.0, 9.0, 1.45). In both watersheds, precipitation is infiltrated quickly into the ground with little or no overland flow occurring. The layers of moss that cover the ground in both regions are very permeable, allowing the water to infiltrate quickly. This conclusion corresponds with the insensitivity of the model to the overland flow roughness parameters.

The upper zone drainage constant (AK2) is higher in the SSA (45.0, 45.0, 2.22) than in the NSA (9.0, 9.0, 1.45) for all three classes. This is reasonable, considering that after permeating the moss, water would more easily drain through the sandy soils underlying all of the SSA region. The sedimentary soil layers in the NSA would tend to resist the deeper infiltration of moisture. Water remaining on top of the sedimentary layers would be able to move laterally through the moss layers. This correlates to the generally higher values of the Interflow Recession Constants (REC) in the NSA (0.0001, 0.0090, 0.0045) than in the SSA (0.0035, 0.001, 0.0009) for the more saturated land areas (Wet Conifer and Fen classes).

The upper zone soil water retention (RETN) is approximately the same for most of the land classes in both study areas. A thick layer of moss is the predominant ground cover in both study areas. After calibrating the NSA in the 1994 period and running the first validation in the 1995 period, it was discovered that the simulation significantly overestimated flows following long periods without precipitation. To compensate, the retention parameter was significantly increased to provide the necessary capacity which could be drained by transpiration throughout the drought period and then filled during a subsequent precipitation event. However, by increasing the retention parameters in all of the land classes, the peak flows for the NW2 basin were dramatically reduced. To compensate, the retention parameters in the Dry Conifer class were increased, with a similar magnitude of decrease being applied to the Wet Conifer class since the NW2 basin has approximately equal areas covered by these two covers.

The differences in the AK2, REC, and RETN parameters between the Dry and Wet Conifer classes in the NSA calibration have been established in an attempt to fit the simulations of all three watersheds to the measured values. The flows in the NW2 basin are consistently underestimated. In order to provide the best combined fit for all three of the NSA 1994 simulations, it is possible that some of the parameters may have been established beyond the true values. More specifically, the NW2 sub-basin contains more area covered by the Wet Conifer classification than the other basins. In order to increase the flows in the NW2 basin, the recession constant has been increased in the Wet Conifer class, with a corresponding

decrease in the Dry Conifer forest class to compensate for the increased flows in the NW1 and NW3 basins. Similar changes relative to these two land classes were made to the AK2 parameters to increase the flow in the NW2 basin. The effects of these changes were realized the most in the NW2 and NW1 simulations.

Figures 6.4 to 6.6 show that with this calibration the NW2 simulation still significantly under predicts the measured flows in the NW2 basin. The adverse effects to the NW1 simulation are somewhat evident in the sharpness with which the second simulated peak flow recedes in mid-July. The increased interflow from the Wet Conifer class produces this sharp recession, and is not completely compensated for by the decreased recession in the Dry Conifer land class.

The differences in the lower zone storage constant are significant between the SSA (0.00087) and the NSA (0.00001). Similarly, significant differences exist in the lower zone drainage function exponent (PWR) between the SSA (1.58) and the NSA (0.75). The high value of the LZF in the SSA simulates an initially faster draining lower zone storage in the SSA than the NSA. This is reasonable since the permeability of the sandy soils underlying the SSA would be greater than the permeability of the underlying sedimentary soils in the NSA. The drainage function exponent simulates the rate of change in lower zone drainage with respect to lower zone storage. The exponent is higher in the SSA and lower in the NSA, indicating the slow constant release of the NSA lower zone storage.

The channel roughness coefficients (R2) are different between the two study areas. The channel classes have been established based on the topographical information. Similar symbols may have been used on the maps which depict somewhat different land forms between the two sites. For example, the winding stream classification in the NSA may be somewhat different from the winding stream classification in the SSA. Therefore, the differences that exist in these parameters between the sites are not unusual. In general, the NSA coefficients tend to be higher than the SSA coefficients, as shown in Table 6.7.

Table 6.7: Values of Calibrated Channel Roughness Coefficients

Parameter	Study Area	Class1	Class2	Class3	Class4	Class5
R2	SSA	0.0500	1.000	0.899	0.326	1.970
	NSA	0.1450	1.270	1.800	1.020	0.055

The channels in the NSA tended to have more vegetative growth on the sides during the summer. This factor would tend to increase the roughness of the channel, making the differences between the two sites seem reasonable.

6.3 Validations of the Calibrated Models

The ability of the model and the new modifications to simulate actual flows must be validated after the calibration process. By introducing enough parameters (a complex polynomial), it should be possible to fit any continuous function. The validation procedure provides an unbiased test of the ability of the model to simulate flows.

Both a temporal and a spatial validation shall be completed to verify the adequacy of the model. A temporal validation attempts to simulate flows from the same watershed for a different time period than the period of calibration. A spatial validation is often considered a more rigorous test of the model in which the model and the calibrated parameters are used to simulate the hydrologic response of a region with similar physiography. Although the NSA and SSA are regions with dissimilar physiography, a spatial validation of parameters calibrated in each study area has been attempted using the parameters from the other basins to simulate the flows.

6.3.1 Temporal Validation using the 1995 SSA Data Set

A significant number of gaps exist in the streamflow data collected during the 1995 season. The continual cycle of rebuilding and removing beaver dams downstream of the SW3 gauge changed the flow control structure and altered the stage-discharge relationship on a continuous basis. As a result, the flows corresponding to the measured water levels cannot be explicitly calculated, and the entire season of data collected at this gauge cannot be used for validation. A similar situation existed at the SW4 gauge for the latter portion of the summer; this period of data at the SW4 location is noted as missing. The data for SW1 could not yet be obtained from the Water Survey of Canada and as a result, the validation with measured flows at this gauge could not be completed.

However, the data collected at SW2 contains its own discontinuities. These irregularities are probably the result of some electronic problems similar to those experienced previously with equipment of this type. Very slight discontinuities similar to those noticeable in the SW2 data are also perceptible in the data collected at the SW4 location. The relative magnitude of the average daily measured flows at the SW2 and SW4 gauges is significantly different between the 1994 and 1995 periods, as shown in Table 6.8.

Significantly less precipitation occurred during the 1995 season compared to the 1994 season. However, the basins should tend to have the same relative magnitudes in flows for the same year. The ratio of the average daily flow measured at SW4 to that measured at SW2 during the 1994 is 0.72. The same ratio for the 1995 period of data is 0.29. The difference in these ratios

Table 6.8: Average Daily Flows

	SW2 (mm d^{-1})	SW4 (mm d^{-1})	Ratio SW4/SW2
Measured 1994	1.02	0.74	0.72
Measured 1995	0.27	0.08	0.29
Simulated 1995	0.28	0.24	0.84

suggests that a significant change in the water fluxes in the hydrologic cycle occurred in one of these basins between the two periods of measurement, or an error in measurement or calculation of flows was made.

The ratio between the measured flows at the SW2 gauge and the simulated flows at the SW4 gauge have also been calculated for the 1995 data set using the Priestley-Taylor model for evapotranspiration. The ratios of these flows is 0.84. The ratio is slightly higher than the ratio calculated with the 1994 measured flow data, but it is more similar to the 1994 ratio than the ratio calculated with the measured flows from 1995. In conclusion, it is perceived that one of the two flow records (SW2 or SW4) are in error for the 1995 season.

All of the measured flows are relatively low in the 1995 season. Measurements of low flows are more prone to error than larger flows. As the values of measured flow decrease, the values approach the magnitude of error or uncertainty. As with any measurement, accuracy is decreased as the difference between the measured values and the tolerance approaches zero.

Together, these discontinuities, missing data, fewer maintenance visits to gauging equipment, and the noted possible sources of error leave very little data in the 1995 period with which to provide a reasonable validation. It appears that the measured flows from the SW4 gauge are more likely to be in error than the measured flows for the SW2 location. The SW2 gauge is the only remaining station unaffected by these problems and available for validation. Therefore, for the purposes of validation with the SSA 1995 data, the error has been calculated as the root mean square of the difference between the measured and simulated flows at the

SW2 gauge only. The errors in the simulations of the SSA 1995 data set using the parameters calibrated with the 1994 data are summarized in Table 6.9.

Table 6.9: Error of the Simulated Flows - Temporal Validations - SSA

Method	Year	1995 Validation RMSE (mm d^{-1})	1994 Calibration RMSE (mm d^{-1})
Evaporation Pan	1995	0.25	0.06
Hargreaves	1995	0.06	0.04
Priestley-Taylor	1995	0.08	0.04

The calibrated model using the published mean monthly evaporation pan values produces the largest validation error in the average daily runoff (0.25mm d^{-1}). The error in the initial calibration using this method was also the highest (25% higher than the other simulations), however, the relative validation error is 330% higher than the next highest value of error. The simulations produced by the model using the Hargreaves and Priestley-Taylor equations are significantly better, with errors 0.06mm d^{-1} and 0.08mm d^{-1}, respectively. Comparisons between the magnitudes of errors between years are not appropriate because of the different areas from which the errors have been calculated (*i.e.* the 1994 error calculations have been made using the errors from all of the basins, whereas the 1995 error calculations used only the errors from the SW2 gauge). As well, significantly lower flows were experienced during the 1995 season.

A qualitative analysis of the simulations shown in Figures 6.7, 6.8, and 6.9 indicates that the versions of WATFLOOD using the Hargreaves and Priestley-Taylor equations closely predict the peak flows, the receding limbs, and the baseflows throughout the period. The version of the model using the published average monthly evaporation pan values tends to significantly overestimate the peak flows. In contrast to the wet summer of 1994 in the SSA, the meteorological conditions in the 1995 period of data collection were relatively dry. Therefore, it is reasonable that the evapotranspiration parameters applied to the published means would be different for the two periods. These differences would explain the extreme overestimation of the peak flows in the simulation for the 1995 period using the parameters calibrated on the 1994 data set.

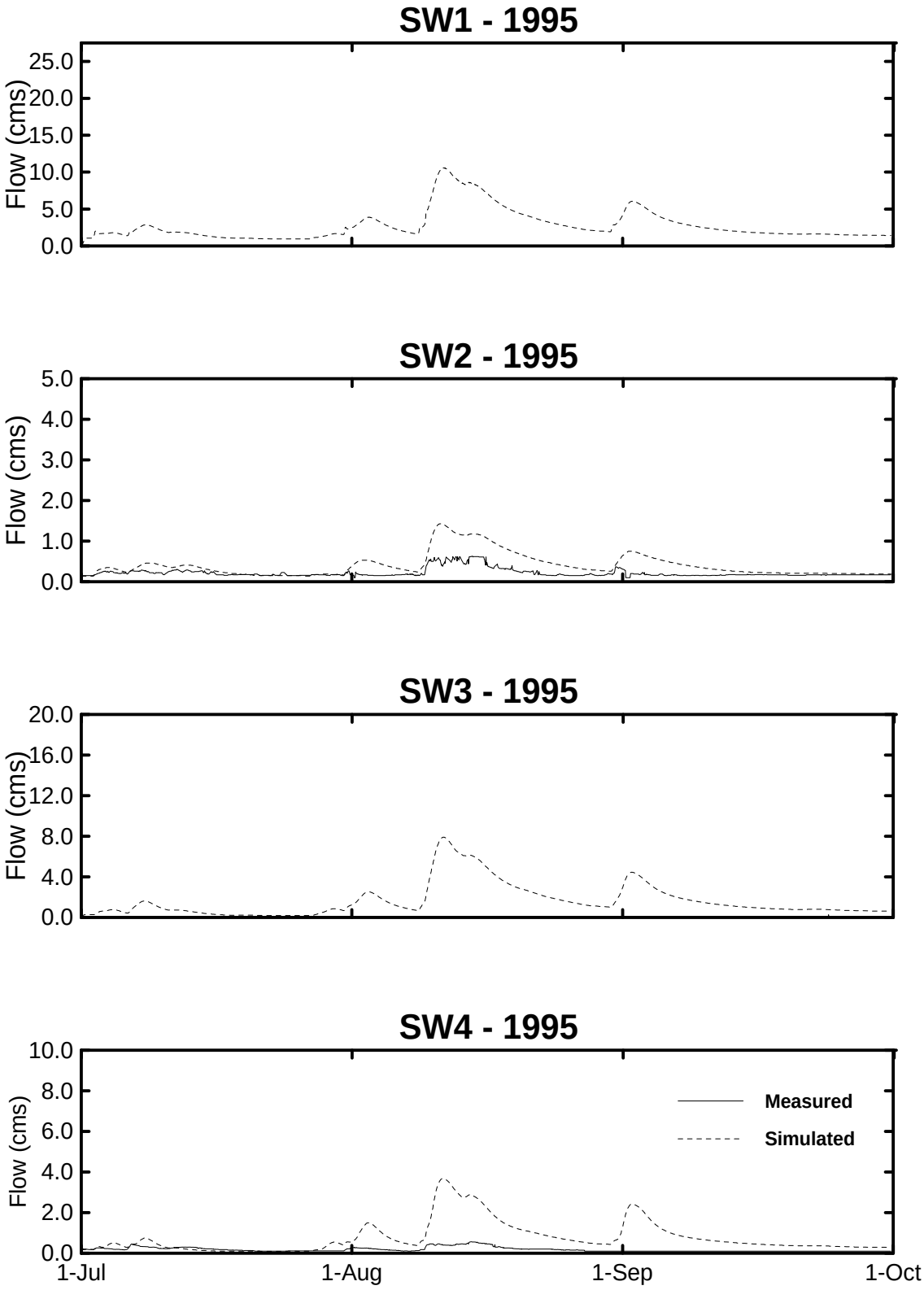

Figure 6.7: Temporal Validation - SSA 1995 Using Evaporation Pan Parameters from SSA 1994

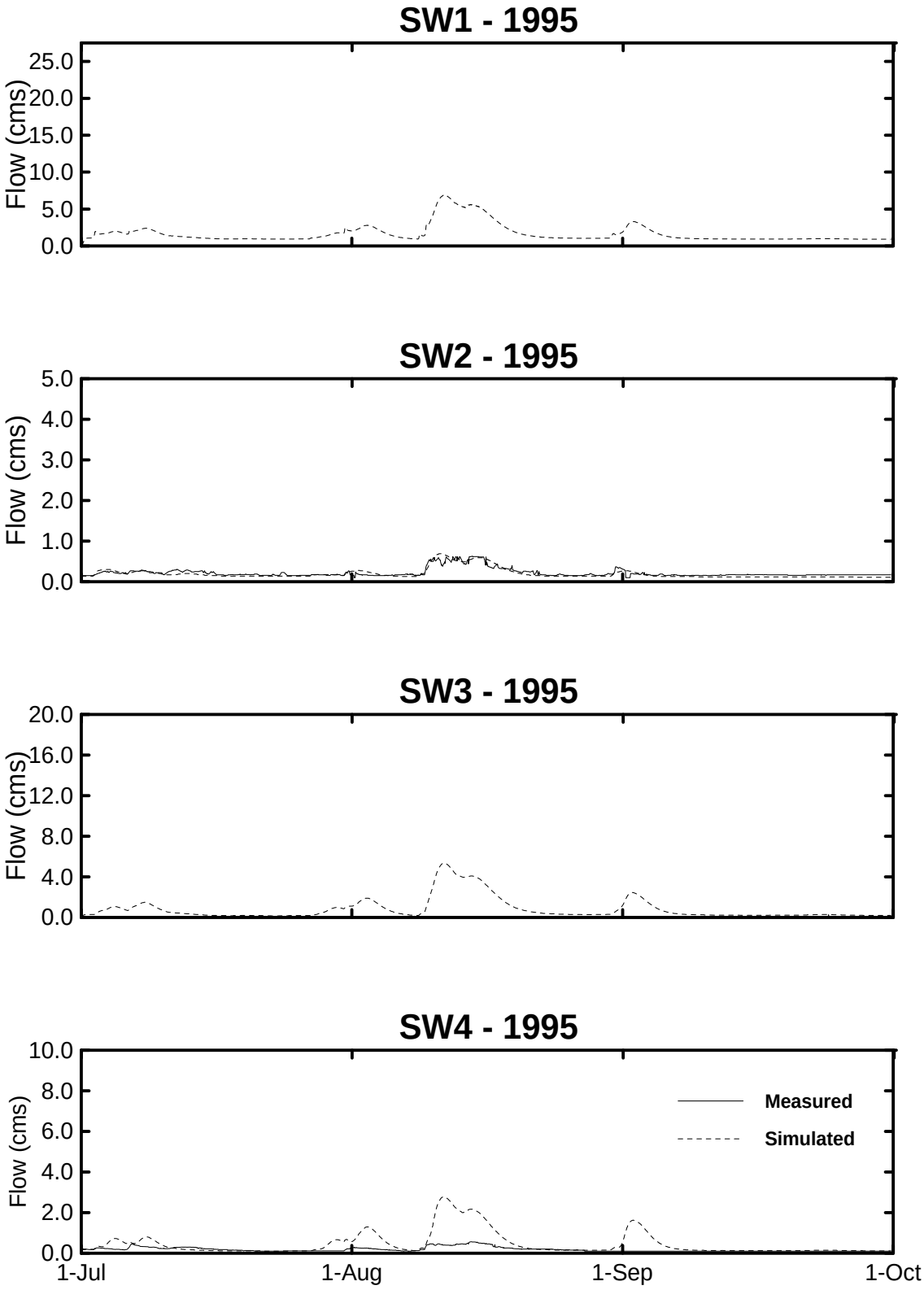

Figure 6.8: Temporal Validation - SSA 1995 Using Hargreaves Parameters from SSA 1994

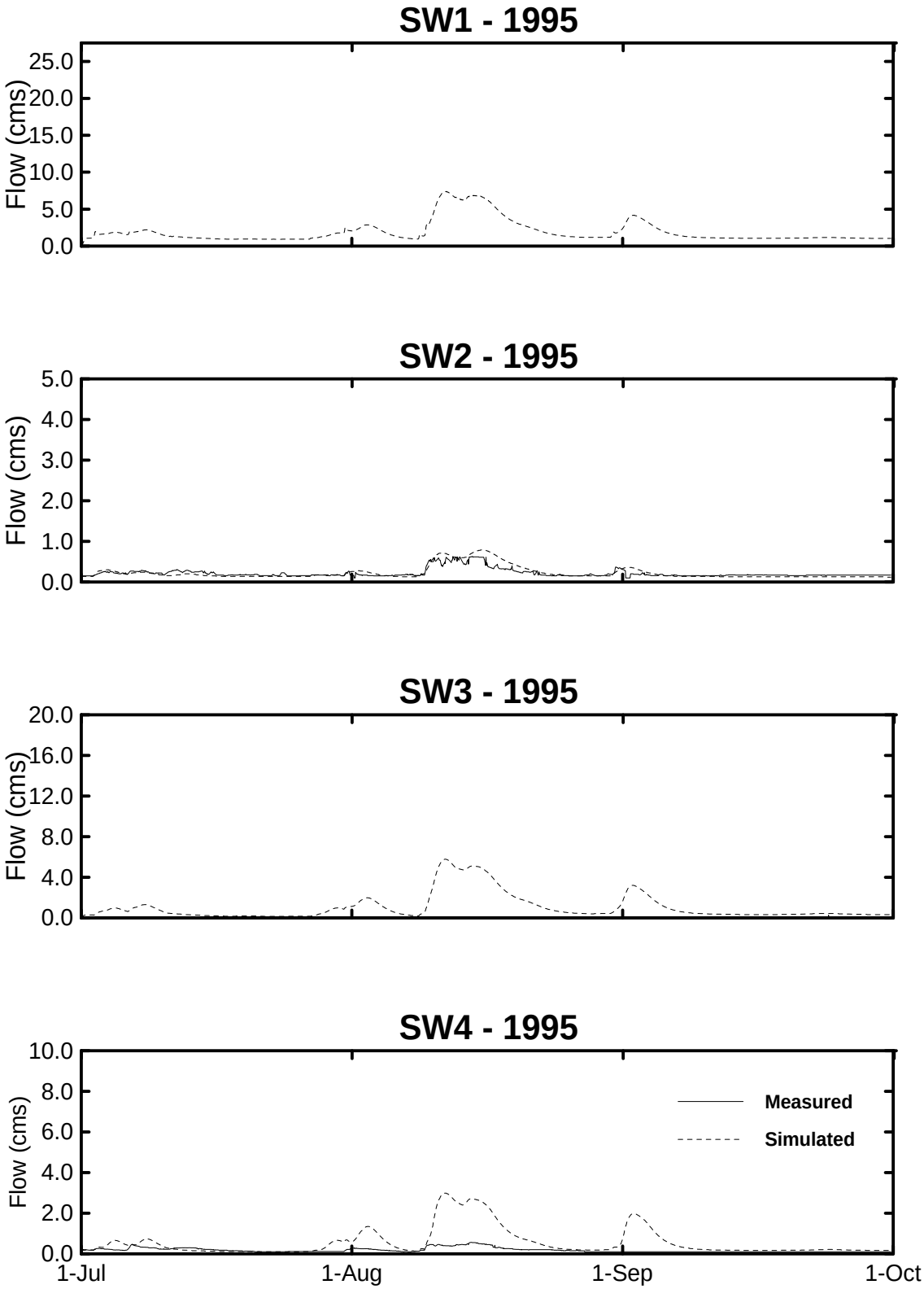

Figure 6.9: Temporal Validation - SSA 1995 Using Priestley-Taylor Parameters from SSA 1994

6.3.2 Temporal Validations using the 1995 NSA Data

Similar to the 1995 data set for the SSA, some problems exist with the 1995 flow data set in the NSA. The Water Survey of Canada data for the NW1 gauge could not be obtained for the 1995 period, and as a result, a validation using the NW1 gauge for the 1995 period could not be made. The validation simulations are shown in figures 6.10, 6.11 and 6.12. In order to provide a consistent a reasonable scale for plotting for both periods of simulation, some of the simulated flows in the 1995 period exceed the scale. The initialization of the baseflows of the NW2 and NW3 basins are slightly overestimated. During the first half of September the flows at NW2 slowly increase and then suddenly decrease. This portion of the flow record is typical of periods of data collected during the construction and subsequent removal of a beaver dam. These are the most apparent sources of error in the 1995 NSA data set. The errors in the simulations of the 1995 NSA data set using the parameters calibrated on the NSA 1994 data are summarized in Table 6.10.

Table 6.10: Error of the Simulated Flows - Temporal Validations - NSA

Method	Year	Validation RMSE ($mm\ d^{-1}$)	Calibration RMSE ($mm\ d^{-1}$)
Evaporation Pan	1995	0.39	0.13
Hargreaves	1995	0.43	0.13
Priestley-Taylor	1995	0.41	0.15
Priestley-Taylor - temporal variation of parameters	1995	0.32	N/A

All of the calibrated models produce approximately the same error in the validation, $0.4mm\ d^{-1}$. None of the methods appear to be superior in their temporal transferability. The fact that the evaporation pan estimates produce satisfactory simulation is likely a result of similar climatic conditions between the two years at this site. Comparisons between the magnitudes of errors between years are not appropriate because of the different basins from which the errors have been calculated.

A qualitative analysis of the simulated hydrographs indicates that all three versions of the model predict the peak flows with about the same accuracy. The version using the mean monthly evaporation pan values tends to produce higher estimates of flow than the other two versions. All of the versions predict the shapes of the receding limbs and baseflows fairly well throughout the period. The initial peak flows in early June are generally underestimated and the first peak flow in the mid-August, after an extensive dry period, is grossly overestimated.

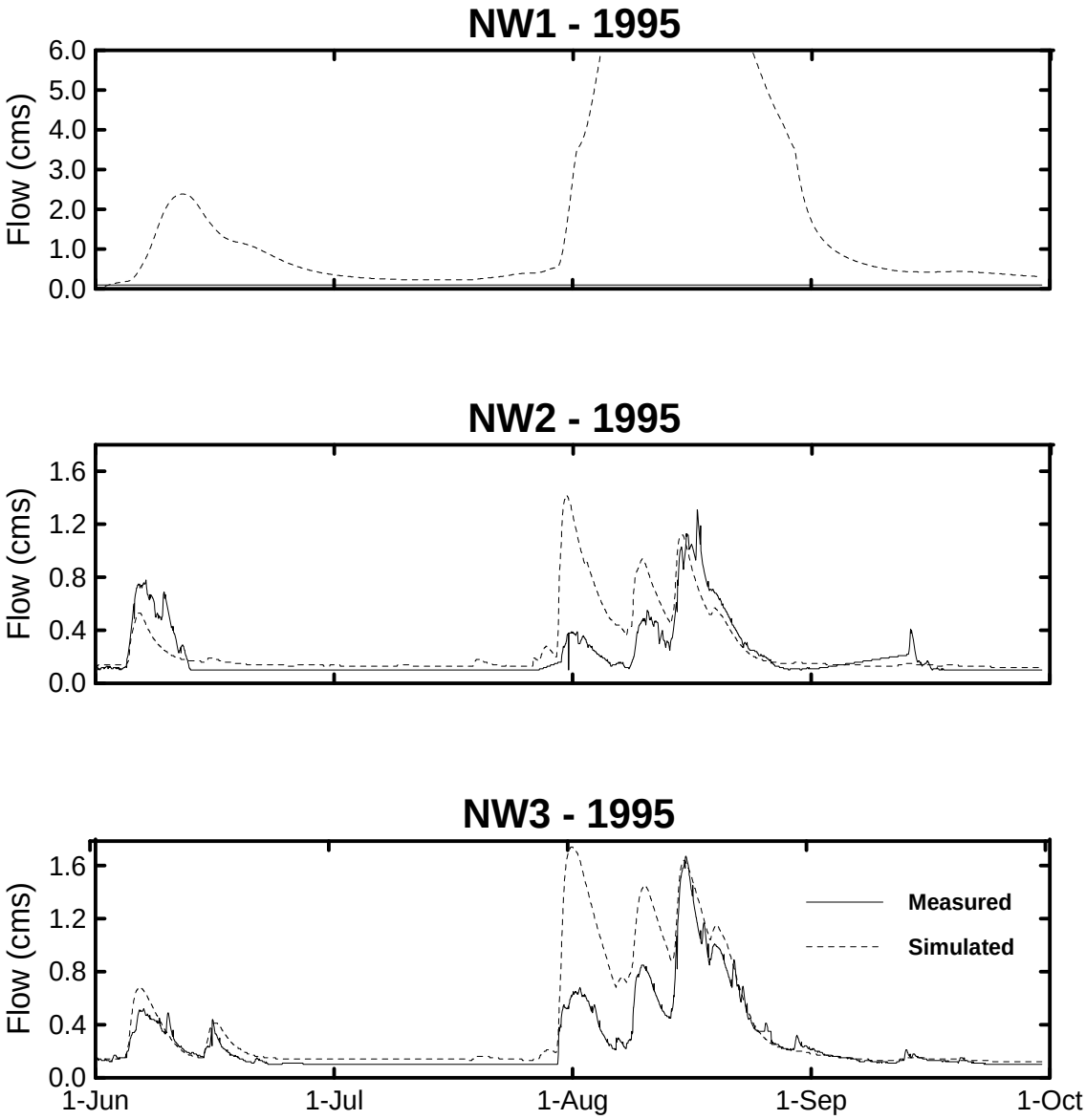

Figure 6.10: Temporal Validation - NSA 1995 Using Evaporation Pan Parameters from NSA 1994

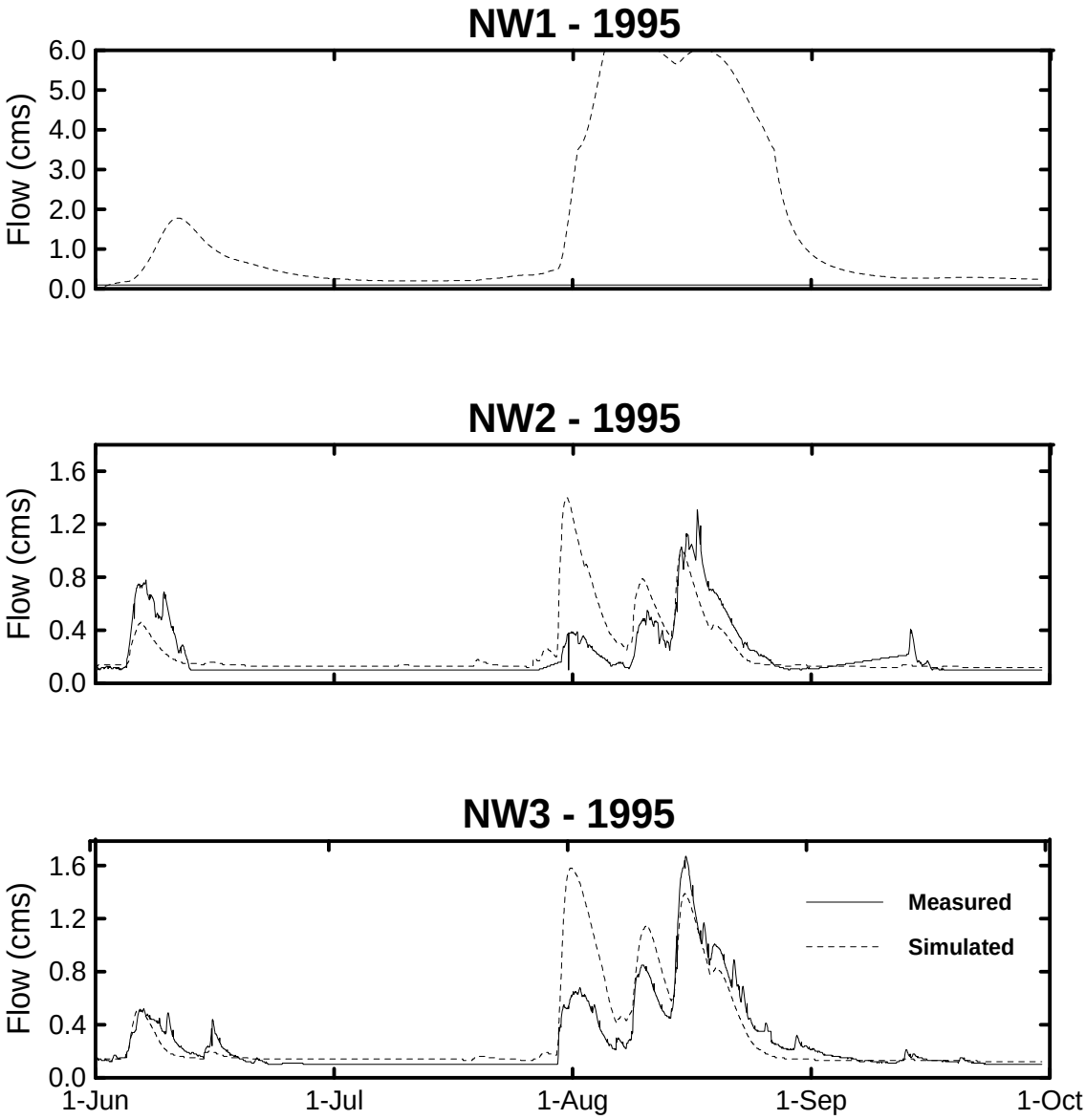

Figure 6.11: Temporal Validation - NSA 1995 Using Hargreaves Parameters from NSA 1994

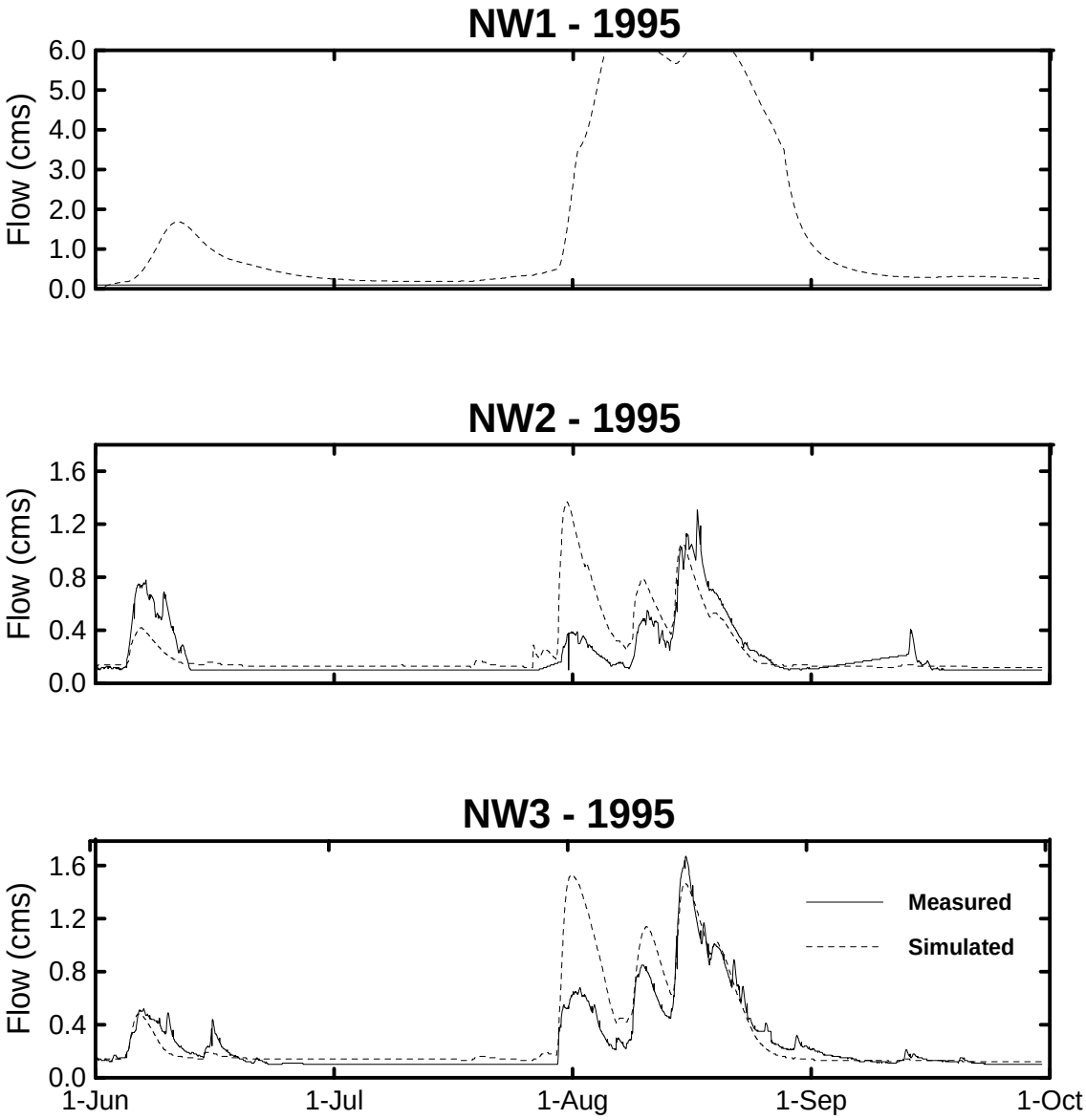

Figure 6.12: Temporal Validation - NSA 1995 Using Priestley-Taylor Parameters from NSA 1994

The parameters were calibrated using the 1994 data set in which the only significant flows occurred during June and early July. Initial validations of the 1995 data set (not shown) produced similar results as those shown here. To compensate slightly, the original calibrations were adjusted to incorporate greater values of upper zone soil water retention (RETN). This affects the simulation by providing more capacity for evapotranspiration losses throughout the dry period in the central portion of the 1995 simulation. A large portion of the first precipitation event in August is then able to be trapped by the large dry retention capacity, thereby producing low runoff flows during a subsequent precipitation event. The second storm event in August occurs before the retention capacity has been significantly reduced by drainage, or through evapotranspiration. This results in a decreased amount of precipitation retained in the upper soil zone from the second event, and an increase in the amount of runoff. The third event in August occurs soon after the second event while the retention storage is relatively full from the previous event. The results are similar to those of the second event in August. This calibration (Figures 6.10 to 6.12) produces the best simulation of those attempted with the 1995 flow period in the NSA although the accuracy is somewhat moderate. As well, the runoff from the events in early June and in July of the 1994 simulation are still underestimated.

The solution to the problems with these simulations would be a temporal variation in the retention and permeability parameters. It is postulated that this variation corresponds to the thawing of the frozen soil throughout the summer months. In northern regions, such as the NSA, permafrost and areas of discontinuous permafrost will produce temporal variations in the retention and permeability of the soil. In the early summer, frozen soil conditions will decrease the permeability and retention capacity of the soil thereby producing increased amounts of runoff. With the long-term thawing of soil throughout the summer, the permeability and the retention capacity of the soil will increase. Similar problems related to this ‘active layer’ exist in the hydrologic simulations of boreal watersheds in the tributaries of the Mackenzie River Basin (Hamlin, 1996).

To test this theory, a second validation of the parameters calibrated on the NSA 1994 data set was completed. The simulation uses the Priestley-Taylor model to estimate potential evapotranspiration. The model was modified to enable the adjustment of parameters to be made on a temporal basis. To provide a better simulation, the permeability and retention parameters in the Wet Conifer and Dry Conifer classes were decreased for the period after June. The drainage from the upper zone soil moisture storage to the lower zone storage was also reduced for the Dry Conifer class to the same value used for the Wet Conifer class. After

June, the permeability was significantly increased, and the retention parameters were increased by about 50% for the Dry and Wet Conifer classes. The changes to these parameters simulate an increase in porosity as the soil thaws during the early months of summer, and result in an increase in the permeability and the available water storage within the upper and lower soil zones. The effect of these changes are shown by the improvements in the simulated hydrographs shown in Figure 6.13. The peak flows during the June storm are slightly increased. The most significant improvement in the Priestley-Taylor model simulation is of the flows during the August period. The initial peak flows continue to be overestimated in the NW2 basin, and the third peak is slightly underestimated in both the NW2 and NW3 basins. There is a general improvement in the simulation of the three peaks and their receding limbs during the August period. The error of the simulation is reduced by 22% with these modifications.

6.3.3 Spatial Validations

As a more rigorous test of the calibrated parameters, a spatial validation has been attempted. The calibrations of the version of the model incorporating the Hargreaves model have been tested for spatial transferability, with the resulting RMSE shown in Table 6.11.

Table 6.11: Error of the Simulated Flows - Spatial Validations - NSA

Method	Calibration Data Set	Validation Data Set	Calibration RMSE (mm d^{-1})	Validation RMSE (mm d^{-1})
Hargreaves	1994 SSA	1994 NSA	0.13	0.19
Hargreaves	1994 NSA	1994 SSA	0.04	0.66

All of the parameters affecting all of the hydrologic sub-processes, except for the degree-day parameters, have been tested in these validations. The base temperature parameters that affect the degree-day function have been held constant for these validations. These parameters have been calibrated to the specific sites based on the climate of those sites. The difference in the climate between the two sites is apparent, with fewer degree-days accumulating in the northern site. Therefore, these base temperature parameters are not spatially transferable, unless the simulations are run from the same reference point with respect to average daily temperature (*i.e.* if the simulations were run from the beginning of the thaw period for the local climate).

In the validation of the parameters calibrated on the SSA 1994 data set using the NSA 1994 data set, the error is 0.19 mm d^{-1}. The parameters underestimate the measured volumes of flow significantly in the NW2 and NW3 basins, as shown in Figure 6.14. The peak flows are

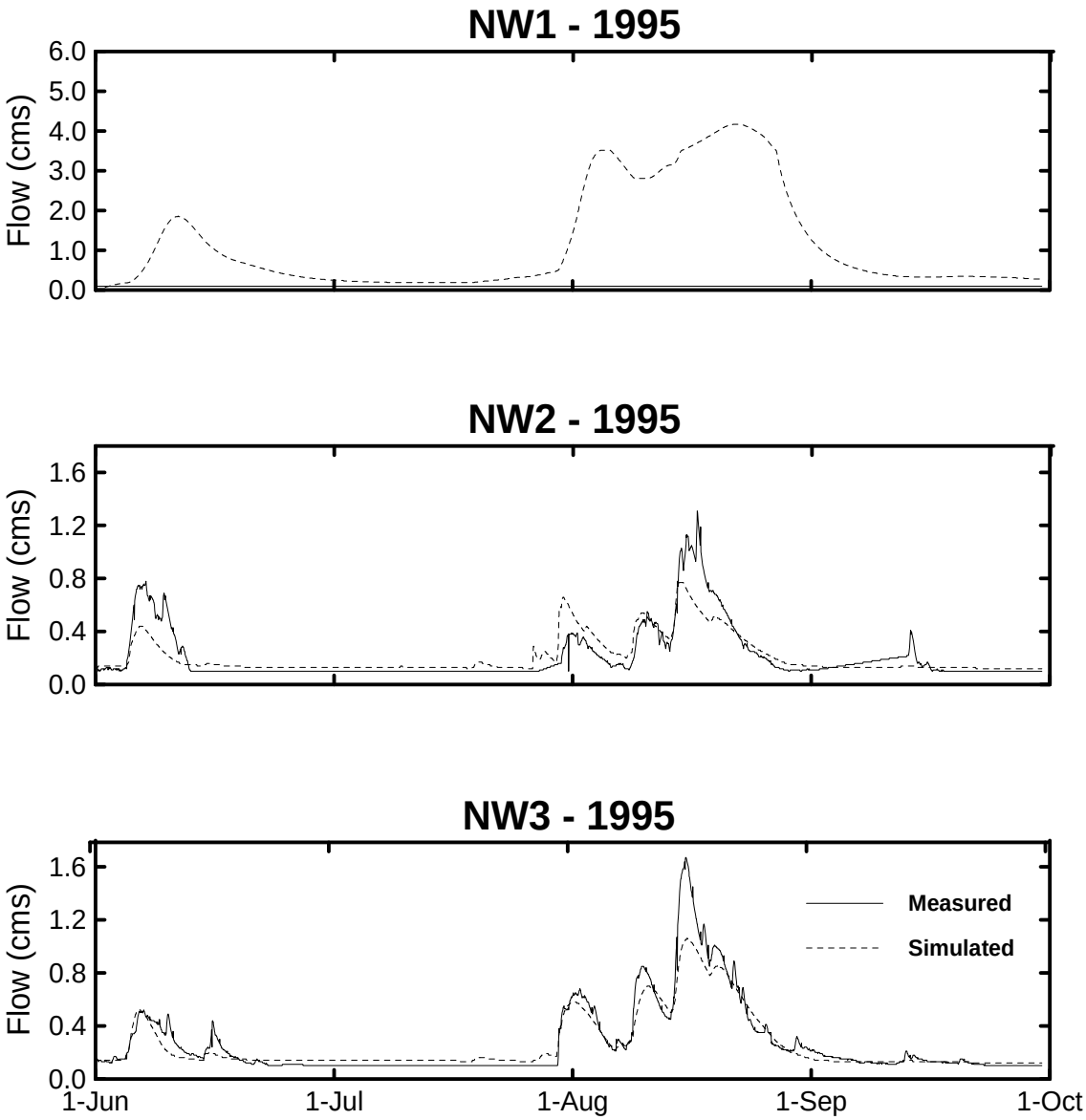

Figure 6.13: Temporally Variation in Soil Parameters - NSA 1995

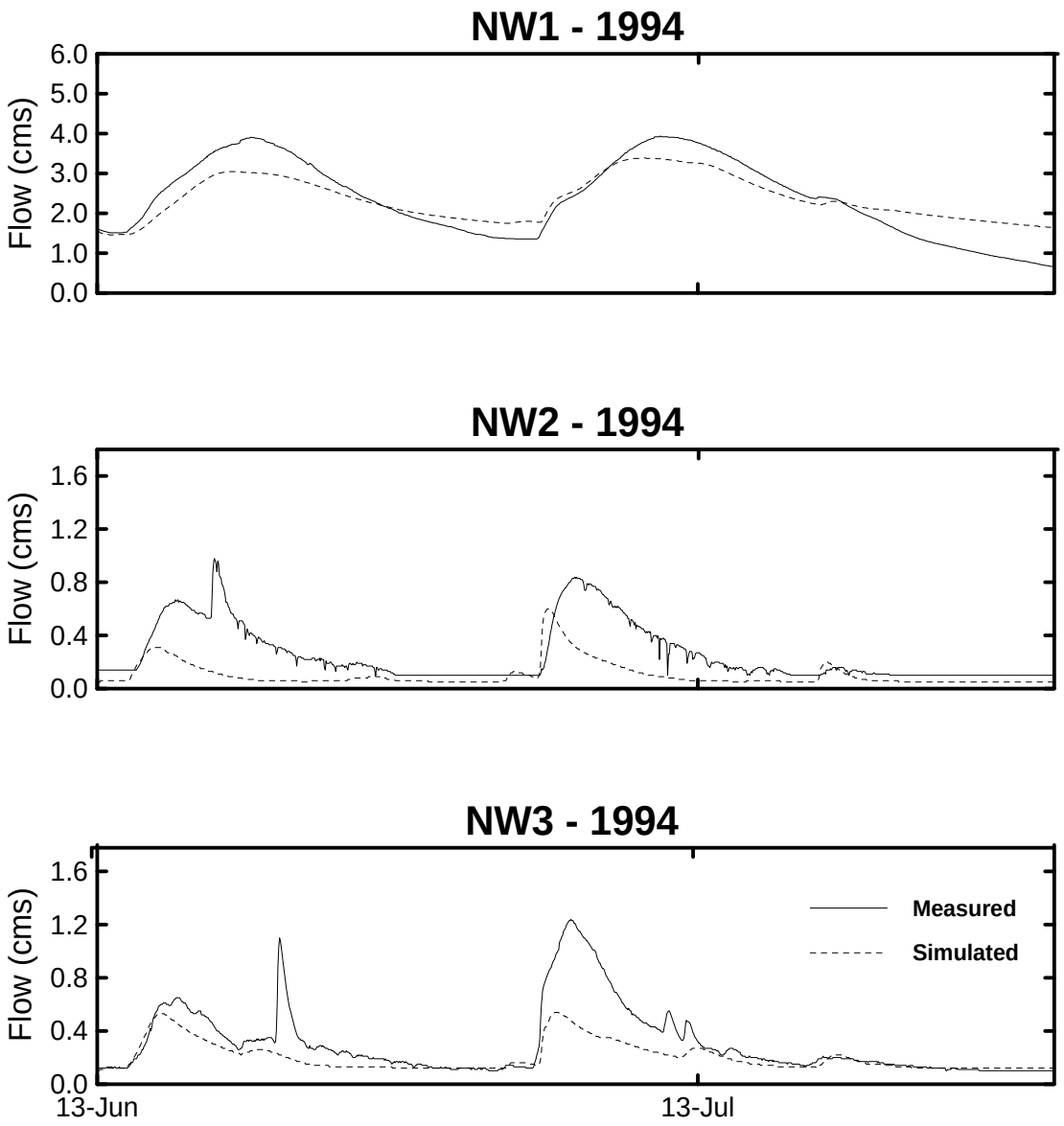

Figure 6.14: Spatial Validation - NSA 1994 Using Hargreaves Parameters from SSA 1994

estimated within approximately 20% for the NW1 basin, but the recession curve in the NW1 basin is not well approximated in contrast to the other two basins. The simulated flows are considerably different from the measured flows. However, the parameters calibrated on the NSA 1994 data set do not predict measured flows well either. The relative increase in the error above the value calculated for the calibrated parameters is relatively low, approximately 20%. The flows predicted by the parameters calibrated on the NSA 1994 data set tend to overestimate the flows measured in the SSA in 1994, as shown in Figure 6.15. There is a significant increase in the error above the value calculated for the calibrated parameters.

The parameters calibrated in the SSA are more transferable than those parameters calibrated on the NSA 1994 data set. This is reasonable since the calibration in the SSA yielded a very good simulation compared to the NSA. The differences in the physiography of the two regions also introduce problems into the validation. The SSA is predominantly underlain with porous sandy soils that promote drainage. The NSA is founded on less permeable glacial tills. As a result, infiltrated water in the SSA can be drained to the deep groundwater reservoirs and released slowly over a long period of time. The less permeable soils of the NSA do not permit the infiltration of upper zone storage. The high infiltration capacities of the moss coverage in both areas eliminates the potential for overland flow. In the NSA, the upper moss layers expedites the drainage of the infiltrated water, through interflow, along the surface of the less pervious glacial tills. This extends the period of runoff beyond that which would occur from overland flow dominated runoff, but reduces the baseflows because of the low volumes of water drained to the deep groundwater storage. Higher interflow and lower baseflow parameters in the NSA overestimate the initial runoff in the SSA. Conversely, the parameters calibrated in the SSA predict lower peak flows and higher baseflows in the validation on the NSA data. These processes explain the differences between the simulations using parameters calibrated on the different regions.

6.4 Simulated Water Balance

An analysis of the cumulative flows passing through the different hydrologic sub-processes provides a excellent diagnostic tool for the calibration of the model. By plotting these 'mass curves', it is easy to compare the water balance at any point during the simulation.

6.4.1 Typical Elemental Water Balance

In Figures 6.16, 6.17, 6.18 and 6.19 the cumulative simulated flows from the start of the simulation have been plotted with respect to time for each of the different land classes in a typical element (located at the centre of the SSA watershed). In these figures, the upper plot

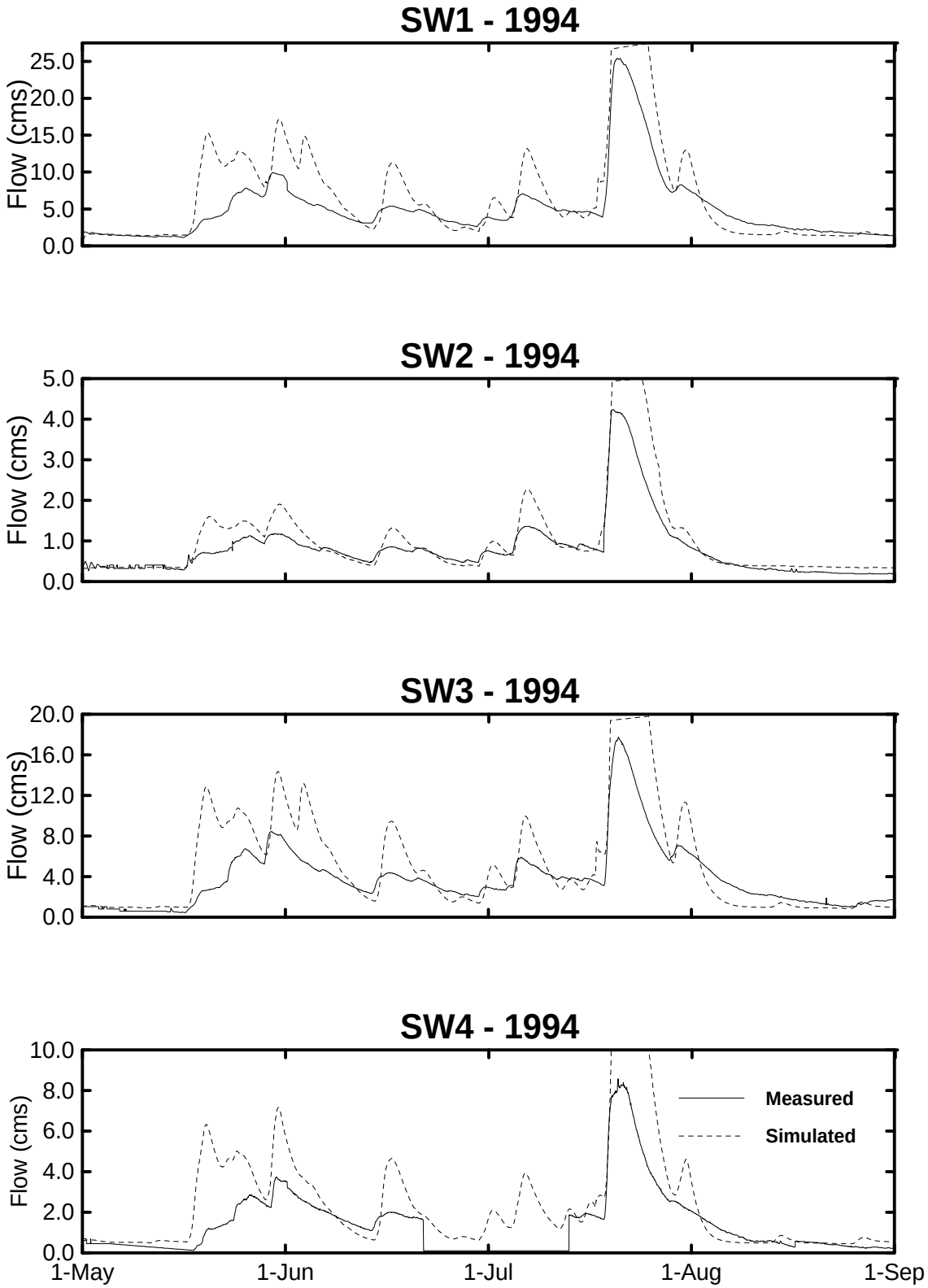

Figure 6.15: Spatial Validation - SSA 1994 Using Hargreaves Parameters from NSA 1994

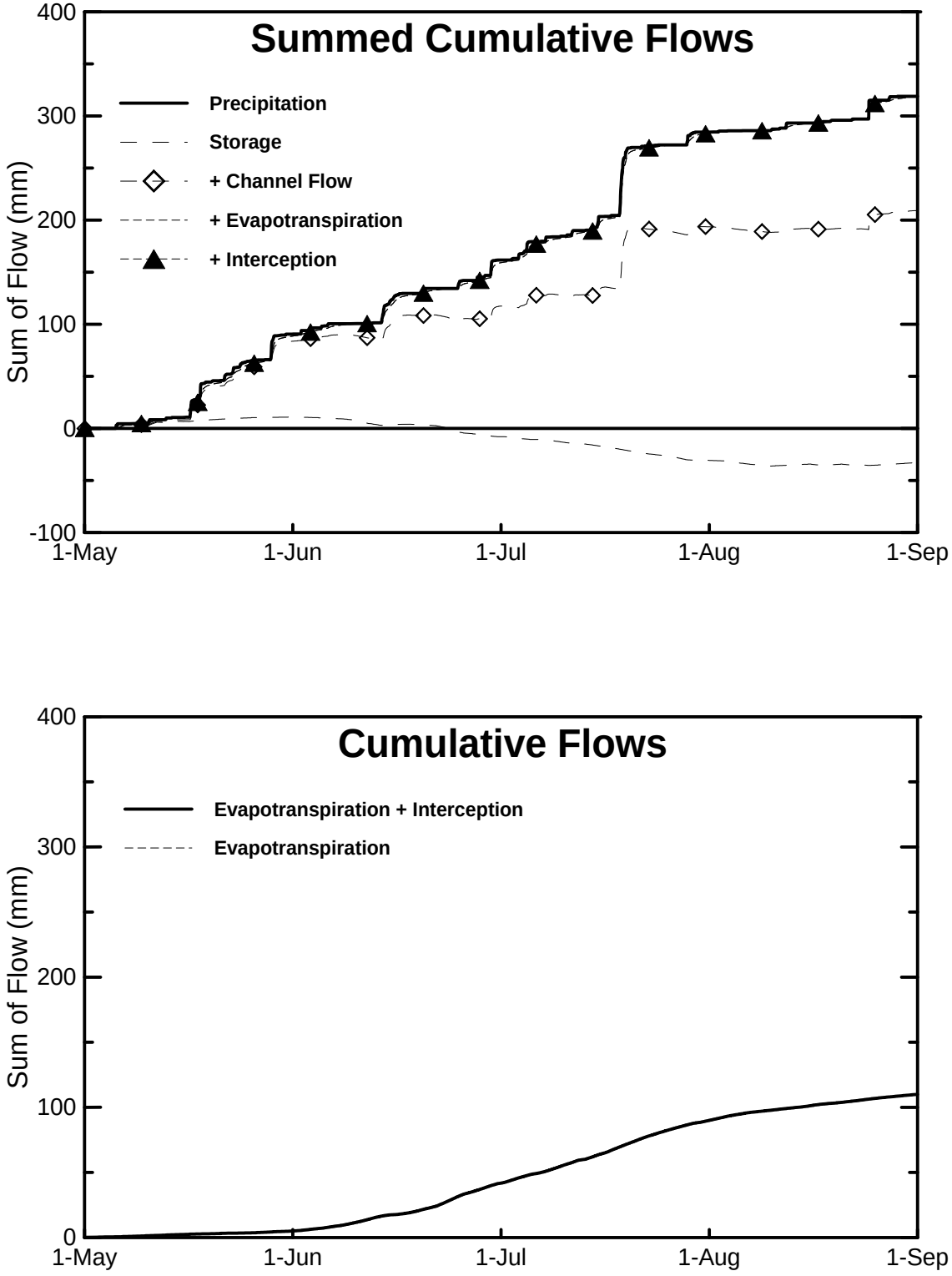

Figure 6.16: Simulated Water Balance

Barren Class - SSA 1994

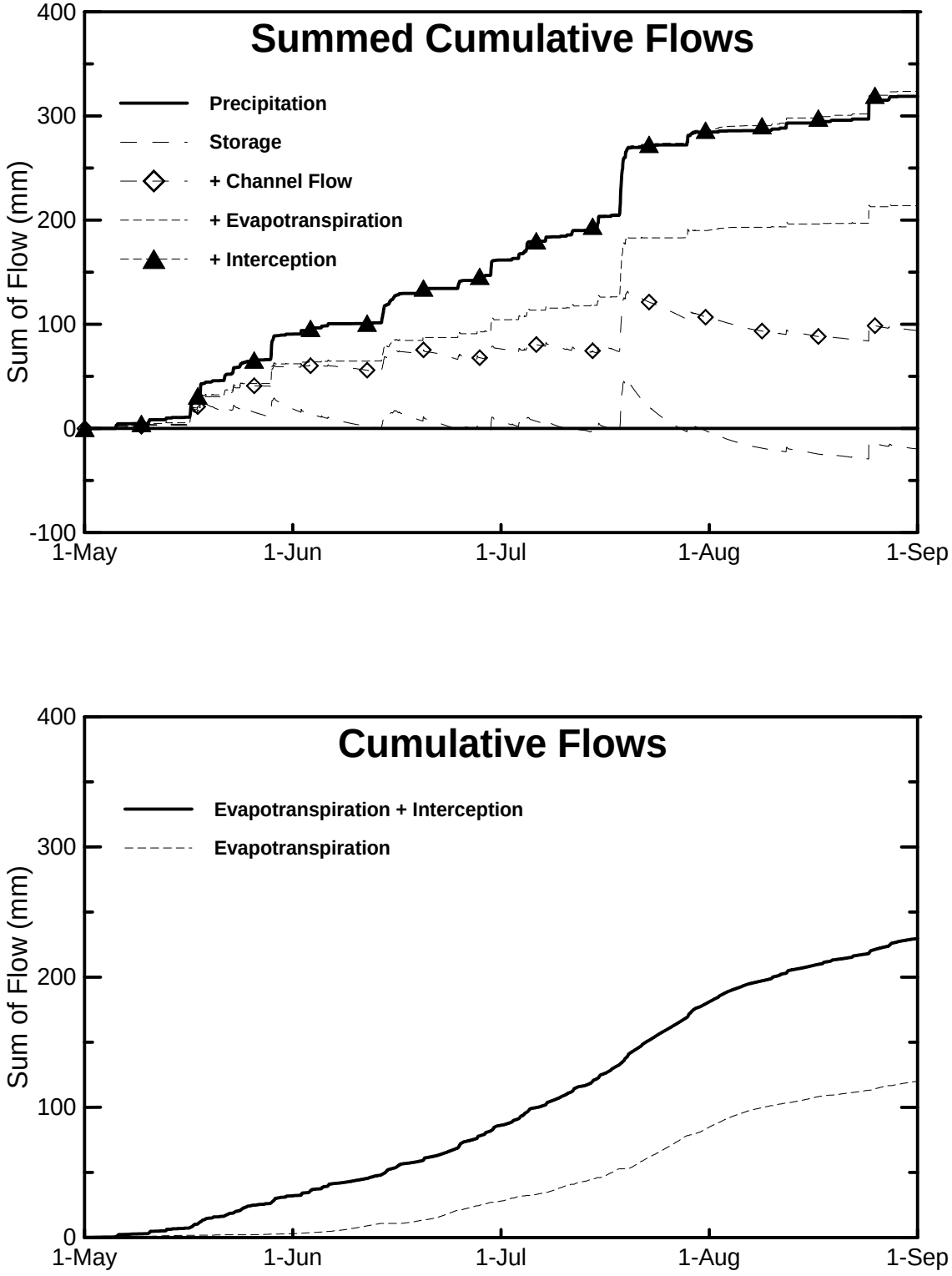

Figure 6.17: Simulated Water Balance

Dry Conifer Class - SSA 1994

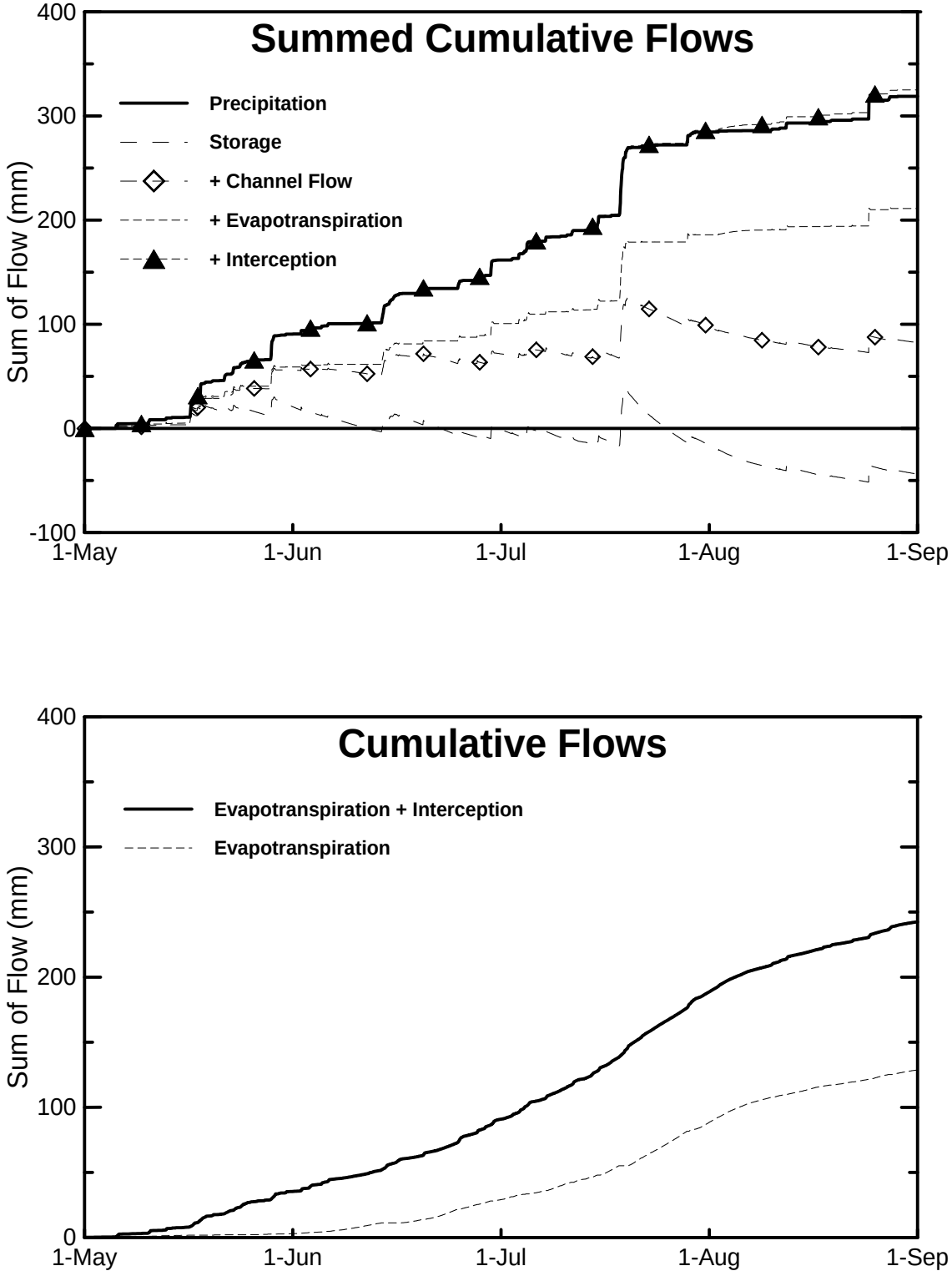

Figure 6.18: Simulated Water Balance

Wet Conifer Class - SSA 1994

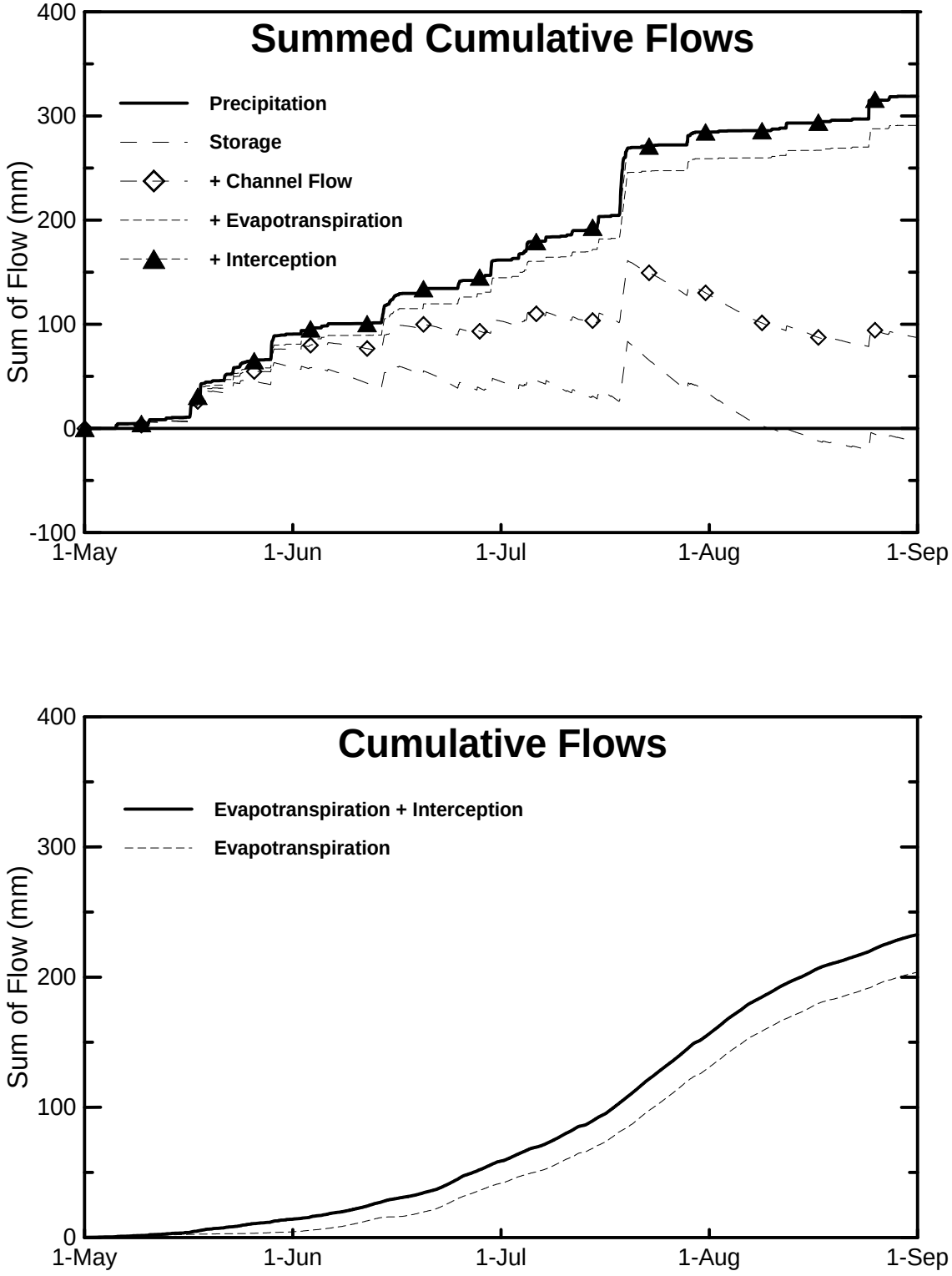

Figure 6.19: Simulated Water Balance

Fen Class - SSA 1994

depicts the sum of the cumulative flows through the different sub-processes. The lowest line of the curves show the net change in storage (the sum of the upper and lower zones). The line above that shows the additional sum of the losses from channel flow. The next line includes the additional losses from transpiration and soil evaporation. The next line includes the losses through interception. By summing the change in storage and the losses, the water balance is complete. For all of the land classes the final balance very closely approximates the total incoming precipitation. In order to more clearly display the changes in evapotranspiration and interception, the daily accumulation of the evapotranspiration, and the sum of the evapotranspiration and the interception are shown in the lower plot in each of the figures.

In the Barren class (Figure 6.16), the interception storage parameter has been set to zero so that the throughfall is equal to the total precipitation. In the barren class, bare soil evaporation and transpiration increase only very slightly during May. The increase is steady throughout June and July, and is reduced during August which corresponds to a reduced level of soil moisture. Both the Dry Conifer and Wet Conifer classes (Figures 6.17 and 6.18) show very similar mass curves throughout the simulation period. The total amount of intercepted water is slightly greater in the Wet Conifer class because of the larger interception storage parameter established for that class (0.1mm larger). Because of the relatively high values of permeability for the moss ground cover, the upper zone soil moisture increases sharply during precipitation events. Similar to the Barren class, a drop in the storage (in which the soil moisture is included) is evident during August. At this point, the rate of increase in the total volume of evapotranspiration slows indicating that a soil moisture constraint on the evapotranspiration has developed.

The mass curve for the Fen class (Figure 6.19) displays trends that have similarities to the Conifer classes and the Barren class. The total volume of intercepted water is low because of the low values established for the interception storage parameter. This volume represents the water intercepted by short deciduous shrubs, small amounts of tall vegetation, and high grass. The storage remains constant at a relatively high value throughout the summer until August when it is significantly reduced. The rate of increase in total evapotranspiration follows the same trend as shown in the other classes. Similar to the forest class, the storage increases quickly with the addition of precipitation. However, the poor drainage characteristics of the fen areas tend to maintain the high values of storage for longer periods by draining more slowly.

The simulated water balances for all of the classes are reasonable. With respect to interception, more significant increases occur in the more densely vegetated areas. Volumes of

interception are approximately 30-35% of gross precipitation. These ratios are similar to those observed (25-55%) previously (Johnson, 1990; Rowe, 1975,1979, 1983; Aldridge and Jackson, 1973; Pearce *et al.*, 1980). The simulated values are slightly higher than the normal values observed by these researchers (the normal values were at the lower end of the 25-55% range, typically between 25% and 30%). This slight increase in the simulated values corresponds to the relatively high values of interception loss as a result of the highly advective conditions, and the interception storage parameters established for the thickly vegetated canopies, both of which are characteristic to these regions (Sellers *et al.*, 1995).

Corresponding to the frozen soil conditions, the evapotranspiration is initially constrained during May, as shown by the low slope on the evapotranspiration mass curve. These conditions are consistent with the early reports from BOREAS (Sellers *et al.*, 1995). Soil moisture (storage) does not become limiting until later in the summer. Other researchers modelling this region during this time period (Kimball *et al.*, 1995) have noted that soil moisture conditions are close to field capacity at the start of the growing season. The general trend is a reduction in soil moisture beginning in late July and continuing until late September. These conclusions are consistent with the results from these simulations. Therefore, transpiration and soil moisture evaporation are not constrained by soil moisture until early August, as shown by the reduction in the difference between the runoff line and the sum of the runoff, evapotranspiration, and interception line. The storage and evapotranspiration mass curves show a reasonable simulation of the actual conditions and total volumes for the season.

The same mass curves for the land classes in a typical element in the NSA are shown in Figures E1 to E4 in Appendix E. These plots display some similarities to the plots shown for the SSA, particularly for the Barren and Fen classes. The ratio of the interception to the gross rainfall is approximately 30%. The most noticeable difference is in the total amounts of evapotranspiration and interception. The ratio of these losses to the total incoming precipitation is very close to 1.0. This implies that most of the runoff is a result of the net depletion of groundwater storage. At a first glance, the fact that the simulated evapotranspiration losses are so high could be the solution to the excessively low flows simulated in the NW2 basin. In fact, an attempt was made to reduce the total amount of evapotranspiration in order to increase the total simulated runoff in NW2 (Figure 6.4). The results of this perturbation did increase the flows but, as would be expected, a corresponding increase in the flows was simulated for the NW1 and NW3 basins thereby producing a net increase in the error of the simulation. The simulated water balance for the NSA appears to be

reasonable but a more detailed analysis may enable some improvement to be made in the overall hydrologic simulation of the NSA watersheds.

The level of the groundwater storage for the same element analyzed in the SSA is shown in Figure 6.20. There is a net increase in the storage throughout the summer. A significant increase occurs during the storm in late July after which there is a slight reduction for the remainder of the simulation. This explains the increase in the baseflow during the latter portion of the simulated hydrographs (Figure 6.1). However, if it is assumed that a definitive relationship exists between the groundwater storage and the measured baseflow, then this simulated increase in groundwater storage does not make sense when compared to the measured baseflow. Throughout the early part of the hydrologic simulation there is excellent correlation between the simulated baseflows (groundwater storage) and the measured flows except for the period in late August when the baseflows are overestimated. These results combined with the increase in simulated groundwater storage further suggest the possibility of the existence of a loss from the water balance system occurring through regional groundwater flow. However, the total change in net storage (combined upper and lower zone groundwater storage) shown in Figure 6.16 has been shown to be reasonable. It is possible that excessive amounts of water are being passed from the upper zone to the lower zone, thereby depleting the upper zone storage excessively, but resulting in a small net change in the total storage.

6.4.2 Validation of Evapotranspiration Estimates

The sum of the interception and the evaporation volumes simulated by WATFLOOD have been totalled for the same time integrals as the water balance and flux tower sums made in chapter 5. The totals for the WATFLOOD simulations have been calculated for the Wet Conifer class in the same element as the OBS-SSA tower flux site. The average daily rate of evapotranspiration has been calculated as the ratio of each of these integrated values to the corresponding time integral. Table 6.12 shows the results from a comparison of means between the three sets of estimates. All six of the comparisons show a moderate degree of correlation (correlation greater than 0.440). The two pairs with the lowest degree of correlation (comparisons with the OBS-SSA) are the only pairs for which the null hypothesis cannot be rejected. The other two comparisons yield overwhelming evidence against the null hypothesis.

Plots of the comparisons made in Table 6.12 are shown in Figures 6.21 and 6.22 plotted as simulated evapotranspiration versus measured actual evapotranspiration using the water balance and the OBS-SSA tower flux measurements. In both of the plots the simulations

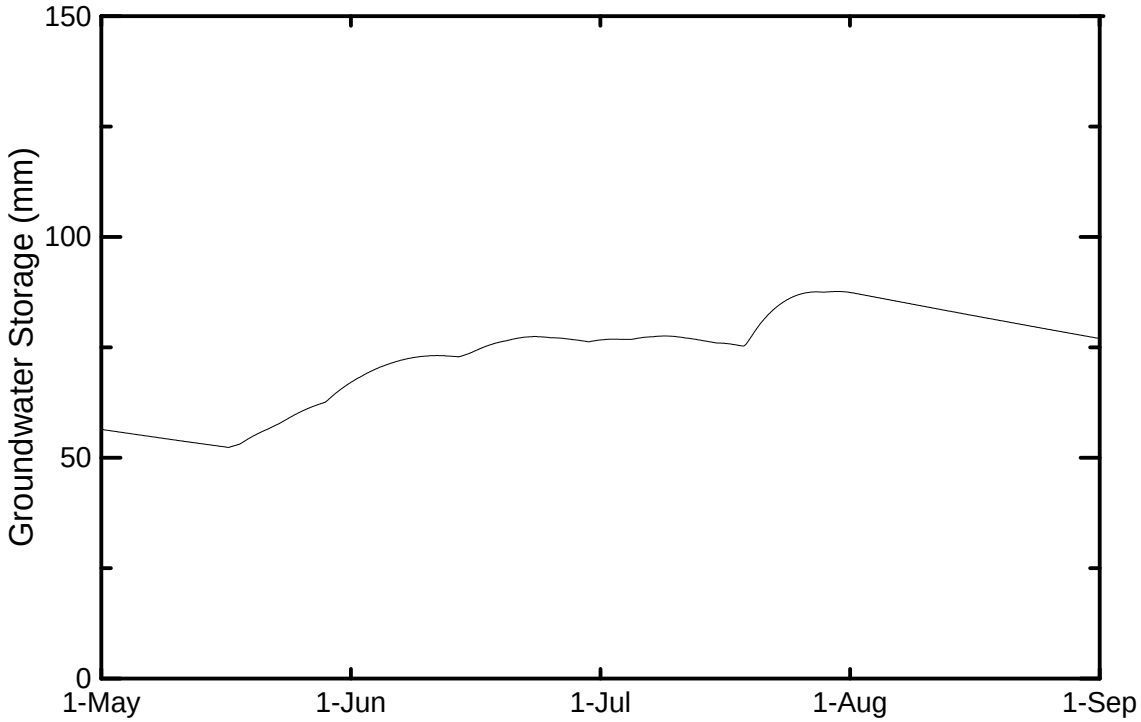

Figure 6.20: Temporal Variation in Groundwater Storage

Table 6.12: Comparison Between WATFLOOD-Simulated and Measured Actual Evapotranspiration

Method	Correlation Coefficient R	t-test Significance	Mean (mm d^{-1})	Difference (mm d^{-1})
Hargreaves	0.440	0.960	2.38	0.00
OBS-SSA			2.38	
Hargreaves	0.769	0.005	2.34	-0.43
Water Balance			2.77	
Priestley-Taylor	0.639	0.430	2.21	-0.15
OBS-SSA			2.36	
Priestley-Taylor	0.667	0.000	2.17	-0.80
Water Balance			2.97	

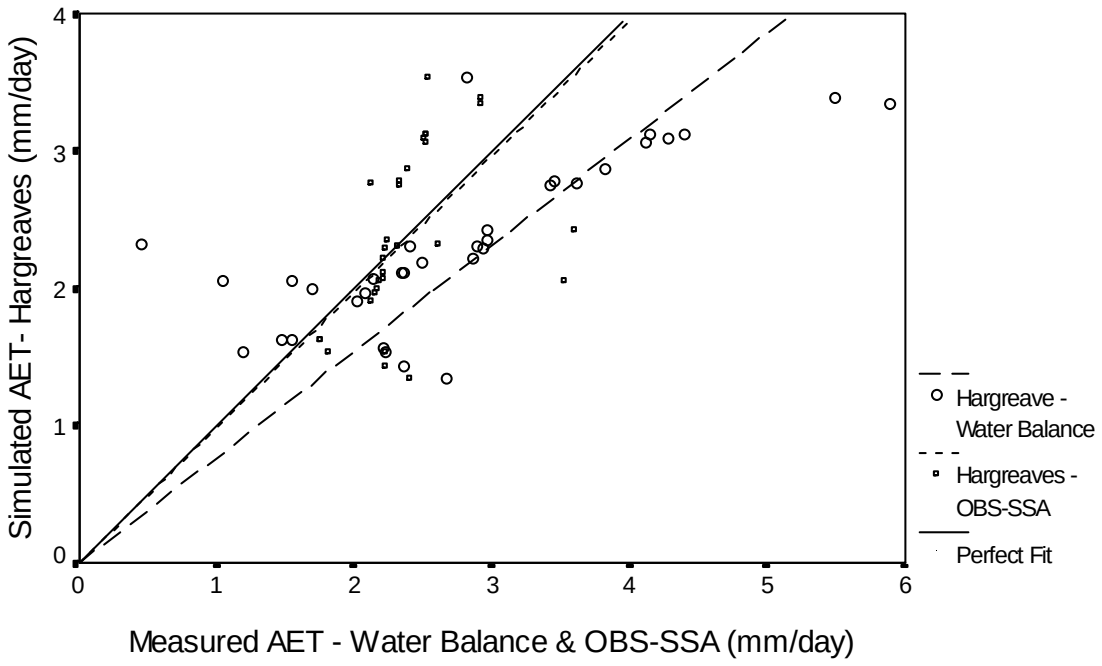

Figure 6.21: Simulated AET - Hargreaves vs. Measured AET - OBS-SSA - 1994

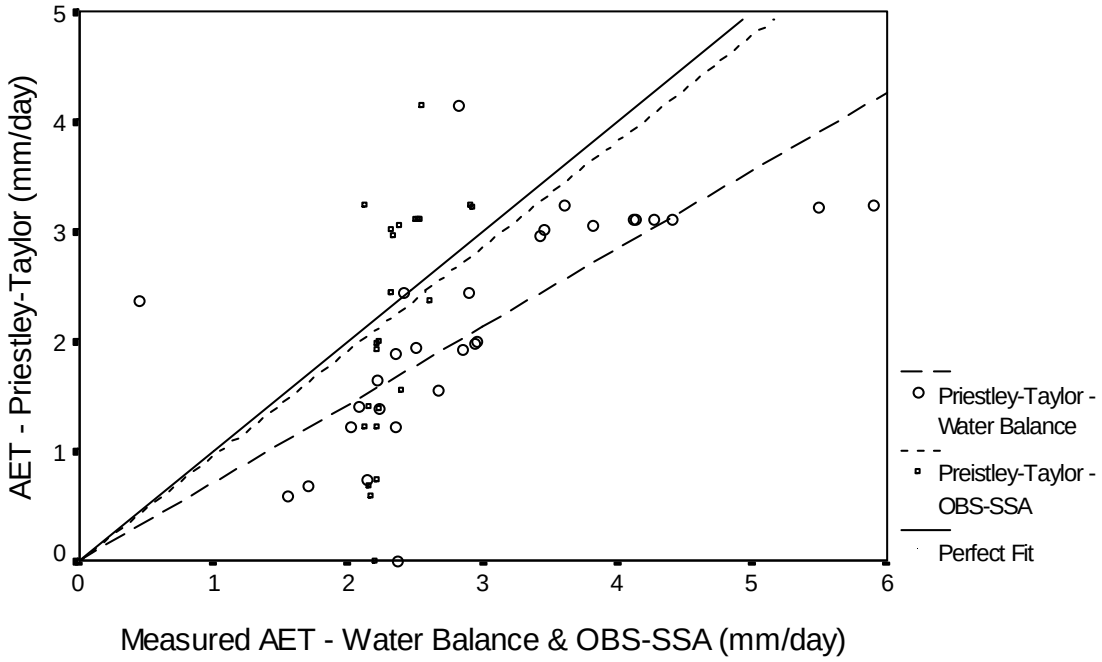

Figure 6.22: Simulated AET - Priestley-Taylor vs. Measured AET - OBS-NSA - 1994

underestimate the actual evapotranspiration measured using the water balance approach. The Priestley-Taylor and Hargreaves equations closely match the perfect fit line with the OBS-SSA tower flux site. The Priestley-Taylor equation has a higher amount of variation than the Hargreaves equation about the perfect fit line, and slightly over predicts the evapotranspiration. Both the Priestley-Taylor and Hargreaves equations produce reasonably good estimates of the actual evapotranspiration as measured by the tower flux sites.

In order to more closely compare the preliminary flux tower measurements and the simulated estimates, the two sets of values have been plotted temporally in Figure 6.23. The general trend of the evapotranspiration rate is more apparent by plotting the nine day moving averages in this figure. The simulation under predicts the measured values at the start and end of the simulation, whereas the measured values are overestimated during the central portion of the simulation. By comparing the daily mean estimates calculated from longer term average estimates, as in Table 6.12, the high and low differences compensate for each other.

At the time of publishing, a revised set of the flux tower measurements was being released. Similar to Figure 6.23, the revised OBS-SSA flux tower measurements have been plotted temporally in Figure 6.24 with the simulated estimates of actual evapotranspiration. The revised estimates show some improvement in their correlation with the simulated evapotranspiration, particularly during the central and latter portions of the simulation. However, some over prediction during the central portion and under estimation during the beginning and latter parts of the simulation is still evident.

The inaccuracies in the simulated evapotranspiration rates are probably the result of the method used for indexing the actual evapotranspiration to the potential evapotranspiration. The temporal variation of the reduction coefficients (Upper Zone Storage Indicator, UZSI; and the degree-day function, FPET2) used to index the actual to the potential evapotranspiration are shown Figure 6.25. The values in this figure are shown for the Wet Conifer Class in the SSA 1994 simulation and are typical of the values for the other classes. The value of the Priestley-Taylor coefficient (α) has been calculated as the product of the reduction coefficients shown in equation [96] and the standard value of 1.26 which has been applied throughout the analysis. The use of the degree-day function constrains the evapotranspiration during the early part of the simulation. At the end of the simulation, the evapotranspiration is constrained by the soil moisture deficit. During the centre period of the simulation, evapotranspiration is constrained only by the factor which is a function of the vegetation height (FTALL) and α is estimated as

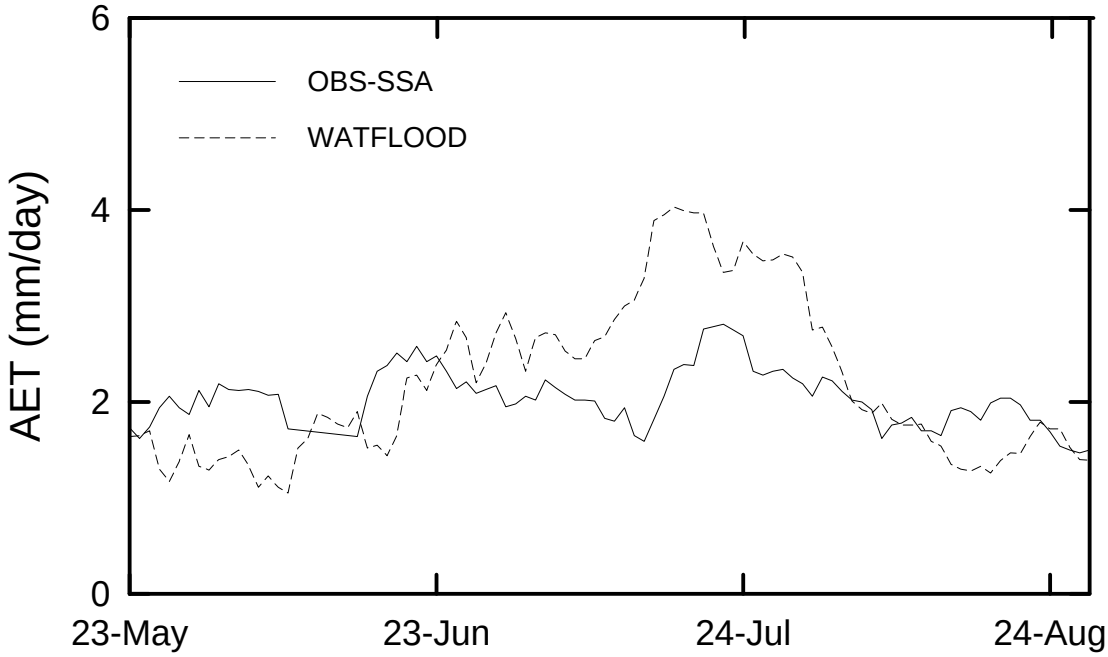

Figure 6.23: Temporal Variation of Simulated and Flux Tower Measured AET - SSA 1994

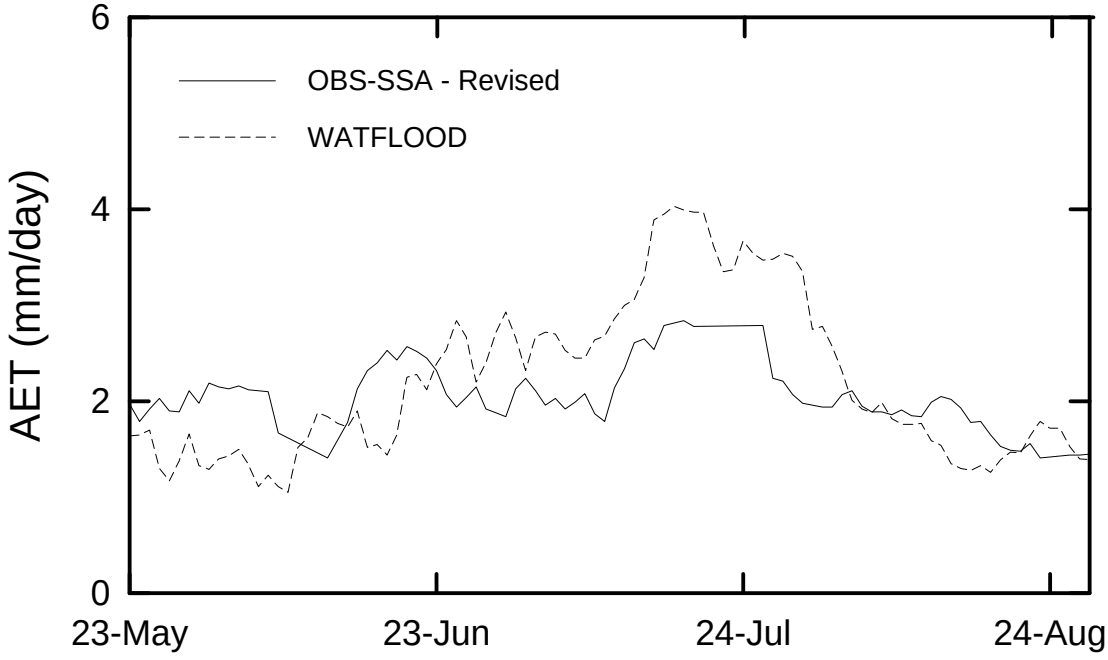

Figure 6.24: Temporal Variation of Simulated and Revised Flux Tower Measurements of AET - SSA 1994

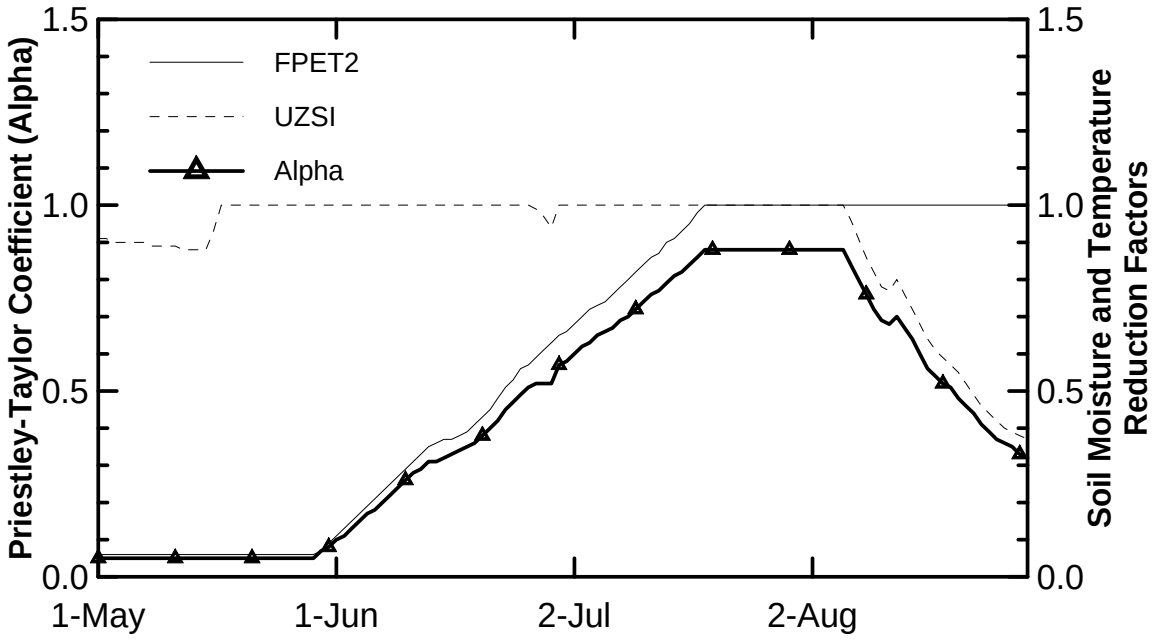

Figure 6.25: Temporal Variation of Priestley-Taylor α and PET Reduction Factors

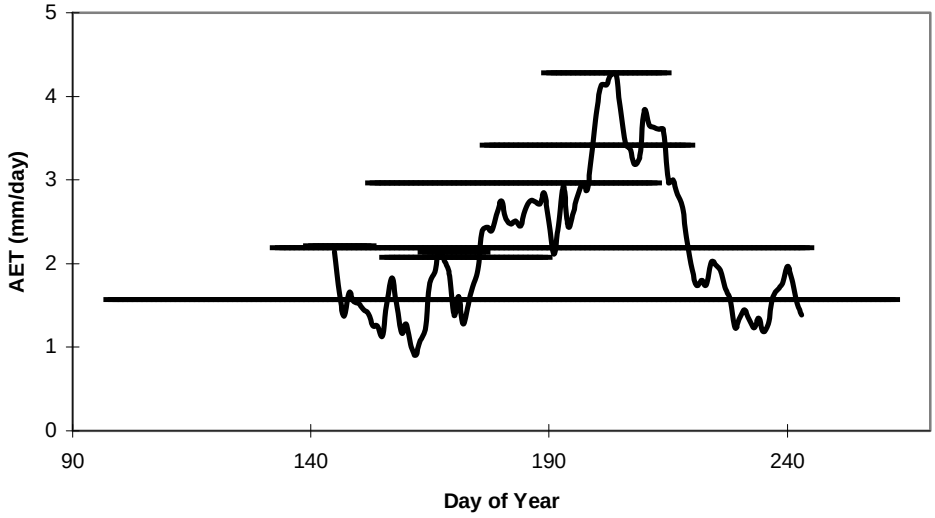

Figure 6.26: Temporal Variation of Water Balance Measured and Simulated AET

approximately 0.88 of the equilibrium potential rate. However, as shown in Figure 6.24, this rate is in excess of the measured rate.

The original objective in developing a method of indexing the actual to the potential evapotranspiration was to use physically-based functions, and not simply a reduction coefficient. By using a reduction coefficient (such as the ETP parameter), the overall potential rate will be reduced which will produce a better match to the mid-season measurements of actual evapotranspiration. However, the early and late periods of the simulation will also be reduced, and therefore, the degree-day and soil moisture function parameters will need to be adjusted to compensate.

The moving five day average of the simulated evapotranspiration has been plotted in Figure 6.26 along with the mean daily rates calculated from the water balance integrals for SW1 (originally shown in Figure 5.1). The simulated estimates more closely correspond with measured water balance values than the flux tower measurements. This is not an unusual outcome since the parameters defining the simulated values have been calibrated with the water balance.

A difference does exist between the flux tower estimates of evapotranspiration and the losses estimated by the water balance approach. In order to provide a closer fit with the flux tower measured losses, the use of the general potential evapotranspiration reduction coefficient (ETP) must be made. However, the parameters for the evapotranspiration functions when calibrated with the hydrometric data provide a good estimate of the actual water balance losses. This verifies that the new evapotranspiration model provides a satisfactory simulation of the measured evapotranspiration.

Chapter 7
Conclusions

7.1 Summary

Evapotranspiration is a significant part of the hydrologic cycle. It may account for up to 60% of the land surface water budget, where half of that may occur as interception evaporation. To provide accurate hydrologic simulations the evapotranspiration component of the hydrologic cycle must be considered. The primary objective of this thesis has been to incorporate a method for estimating evapotranspiration losses into the WATFLOOD hydrologic model. A more rigorous method for estimating evapotranspiration, particularly for the simulation of soil moisture conditions, is required for long-term hydrologic simulations. Since WATFLOOD is an operational hydrologic model, the method for calculating evapotranspiration losses must have minimal data requirements. At the same time, the new method must model the natural processes to maintain the validity and transferability of the model between regions. A second objective of this thesis has been to provide an initial analysis of the water budgets in the BOREAS NSA and SSA watersheds from the data obtained during the 1994 field season.

Evapotranspiration is a function of many environmental factors, which can be analogized to an electric circuit. The circuit is driven by a gradient (the vapour pressure deficit) and closed by two resistors, stomatal and atmospheric. These resistors are influenced by meteorological conditions, which are in a continual feedback relationship. The process is complex but has been simplified for operational purposes by making various assumptions.

Where extensive sources of meteorological data are available, as in a well equipped research environment, theoretical relations based on the physical processes can be used to provide estimates of evapotranspiration. However, in most situations meteorological data are scarce and empirical or semi-empirical models must be utilized. The analytical-water balance method has been used here for analyzing the use of the potential evapotranspiration equations and as an independent method of comparison with flux tower measured values.

Portions of the original WATFLOOD model have been modified to better simulate the physical hydrologic sub-processes. The introduction of a potential evapotranspiration model that is based on measured meteorological variables enables the more rigorous application of the model and enhances its temporal and spatial transferability. The original interception model has been modified so that water is evaporated from interception storage. Interception evaporation occurs at a rate equal to the potential rate during a rainfall event. Immediately following rainfall cessation, the rate of interception evaporation is increased by a factor of 3.0

to represent the increased advective conditions in areas of tall vegetation, which have a high atmospheric roughness. Interception evaporation occurs at this rate until either the storage is reduced to zero or another precipitation event occurs. This adjustment is necessary since the advective component of evaporation is not adequately considered with the radiation and temperature-based equations during highly advective conditions.

Interception evaporation precludes the transpiration of water from vegetation. Once the interception storage is reduced to zero, transpiration is approximated as a fraction of the potential evapotranspiration. Transpiration is reduced to 0.7 of the potential evapotranspiration for tall vegetation because of typically higher stomatal resistance.

The WATFLOOD geographical database has been established on a UTM grid system of coordinates for the White Gull Creek and the Sapochi River Basins in the BOREAS SSA and NSA, respectively. In order to classify the types of land cover, a classification developed from a LANDSAT-5 TM image has been used. The original classification identifying 11 different land cover types has been aggregated into five different classes that can be used by WATFLOOD. The land classes were combined based on hydrologic and geologic similarities, with importance also placed on the maximum distribution of the land area between the classes. Some uncertainty exists in the delineation of the watersheds as a result of very little relief in some of the headwater areas. Hydrometric data collected during the 1994 and 1995 growing seasons have been used for comparing the simulations.

7.2 Spatial and Temporal Variability of Potential Evapotranspiration Estimates

An analysis of the input variables to the potential evapotranspiration equations shows that there is little spatial variation in the measurements within the study areas. Meteorological measurements made at the different tower flux sites were used in the comparisons. Small systematic differences in temperature measurements existed between the sites. However, an explanation for these differences was inconclusive since the measurements at each of the towers were not made with reference to a common datum. The difference in temperature measurements was small enough that a common temperature measurement for each area has been used in the simulations. The difference in temperatures had a very small effect on the calculation of the evapotranspiration (e.g. for Hargreaves the difference is ±3 %).

Similar to the spatial variation in temperature, the variation in net radiation between land classes is small. The only significant difference in the measurements of net radiation (affecting

the Priestley-Taylor potential evapotranspiration estimate) occurred at the OBS sites. An adjustment of the final potential evapotranspiration estimate has been made to reflect the differences in net radiation as a function of the different values of albedo for the land classes.

It has been concluded that a common estimate of the potential evapotranspiration for each basin is adequate because of the very small spatial variation in net radiation and temperature. Therefore, for the hydrologic simulations these potential evapotranspiration estimates have been made using AFM tower data. At the time or writing, this data set contained the only continuous record for the 1994 season and was the only available record for the 1995 season.

The potential evapotranspiration models produce better estimates for longer time intervals for which they were originally developed, typically of at least one day. In order to validate the use of the models for periods shorter than those for which they were developed, a comparison of the estimates of evapotranspiration for different temporal scales was made. Generally, there was very little difference between the evapotranspiration estimates made with daily averaged input values and the daily values calculated by summing the half hourly estimates. Some systematic variation exists in the Priestley-Taylor estimate and can be explained by the errors introduced by averaging the slope of the saturation-vapour pressure versus temperature curve. However, these systematic errors are consistent and are therefore reduced during calibration.

7.3 Potential Evapotranspiration Equations

Researchers have shown both the Priestley-Taylor and Hargreaves potential evapotranspiration equations to provide reasonable estimates of the actual evapotranspiration when indexed using some other factor, such as soil moisture. Both of these equations provide consistent, and approximately the same, estimate of potential evapotranspiration. The models are therefore well suited for interchangeable use within WATFLOOD. The Turc equation produces estimates of evapotranspiration that vary from a fraction to some multiple of the actual evapotranspiration. As well, the difference of the estimate from this model with respect to the other two models detracts from the ease of its use. The Turc model did not tend to provide significantly better estimates of actual evapotranspiration than the other two models once they had been indexed. As well, the Turc model has no advantage over the other temperature-based equation analyzed (Hargreaves) in its ease of use or input data requirements. For these reasons, the modifications to WATFLOOD were constrained to the use and comparison of the estimates of evapotranspiration using the Priestley-Taylor and Hargreaves equations.

With the use of a calibrated reduction coefficient, the potential evapotranspiration models estimate the actual evapotranspiration within ±30%. Methods of indexing have been proposed to simulate the actual constraints on the potential evapotranspiration rates. Preliminary results from BOREAS have shown the soil temperature to be a significant factor in constraining evapotranspiration. The variation in soil temperature has been emulated as a the cumulative degree-days. When this method is combined with the constraints due to soil moisture, a model with reasonable accuracy results. This is the final version of the evapotranspiration model used in WATFLOOD. The soil moisture reduction does not have an effect until much later in the simulation of the 1994 season. This result is similar to the observations made by other researchers that are modelling this region (Kimball et al, 1995) and some of the preliminary results of BOREAS (Sellers *et al.*, 1995).

The parameters that define the soil moisture and degree-day functions are calibrated to provide the best hydrologic simulation. A preliminary investigation into the correlation of these functions and the values of their parameters show that these moisture functions are significant for indexing the actual to the potential evapotranspiration in the SSA. In contrast, there is no significant correlation between degree-days and the measured mean daily evapotranspiration rates is the NSA. Accordingly, the degree-day function has not been used in the hydrologic simulations of the NSA. Results from a regression of the parameters for the SSA indicates that the estimates of potential evapotranspiration produced by the Hargreaves and Priestley-Taylor equations can be indexed by these functions to closely predict the measured actual daily evapotranspiration rates.

7.4 The Water Balance and Estimates of Potential Evapotranspiration

A preliminary analysis of the water budgets in the SSA and NSA watersheds has been used to validate the measurements of evapotranspiration made at the tower flux sites. A good correlation is shown between the two independent measurements. As well, the water budget analysis shows that the potential evapotranspiration equations are useful for estimating actual evapotranspiration rates (measured by the water balance). A standard error of the daily estimates of approximately 10% results from the use of a simple calibrated reduction coefficient to index the actual to the potential evapotranspiration.

The relationship between the actual and potential evapotranspiration remains relatively constant for the short-term sums of daily values. However, for the long-term, a constraint is placed on the evapotranspiration rate. The constraint is apparent at the beginning and the middle of the growing season in the plots of the ratio of actual evapotranspiration to gross

rainfall with respect to time. These constraints can be explained by the low soil temperatures in the spring and the low soil moisture in the late summer. The ratios calculated with the water balance (60-75%) agree well with the global average annual losses (60%). The simulated ratios are somewhat higher than the global loss but this ratio would tend to be higher during the summer.

7.5 Measured Water Balance

The use of the water balance provides an independent check on the evapotranspiration losses calculated through other methods, such as the tower flux measurements. The long-term water balance provides very similar estimates to the tower flux measurements (within 10%) and an independent verification of the accuracy of both methods of measurements. The water balance for the SSA estimates evapotranspiration losses in excess of those measured at the flux towers. The long-term water balance estimates amplify the small errors in the balance and suggests that there are some additional losses not considered in the balance. Possible explanations for these differences include problems with the tower flux measurements or the existence of unaccounted losses through regional groundwater seepage. The correlation between the measured water balance and the tower flux estimates is improved by weighting the individual tower flux measurements with respect to the area covered by the corresponding land type in each basin. The most recent revisions to the flux tower measurements decrease the difference between the flux tower and the water balance estimates of evapotranspiration.

7.6 Hydrologic Simulations

The hydrologic simulation process consisted of two stages. First, the parameters affecting the hydrologic sub-processes were calibrated on the 1994 data set and then they were validated on the 1995 data set. The simulated flows were most sensitive to the groundwater and soil water parameters and, thus, these parameters were of the most use for calibrating the model.

In relation to the different land classes, the parameters that were yielded from the calibration were reasonable. The parameters affecting drainage into, through, and out of the soil layers qualitatively reflected the differences between the soils in wet and dry areas and between the geology of the SSA and the NSA.

The calibration of the parameters on the SSA 1994 data set produced an excellent simulation when using any of the three evapotranspiration models (published mean monthly evaporation pan values, the Hargreaves equation, or the Priestley-Taylor equation). Almost all of the peak flows and total volumes were very closely matched. The accuracy of the simulation of the

NSA 1994 data set using calibrated parameters was somewhat more moderate. The underestimation of the flows in the NW2 basin could not be alleviated. Reasonable simulation of the peak flows in the NW1 and NW3 basins was achieved. All three of the methods used for estimating evapotranspiration yielded approximately the same simulation error.

An attempt at a temporal validation of the calibrated parameters was made by simulating the 1995 data sets with the parameters developed on the 1994 data sets in the corresponding basin. Problems with the data collected during the 1995 period hampered the evaluation of the validations in the SSA. Low flows created similar problems. In general, the flows at the SW2 gauge were well simulated by the Hargreaves and Priestley-Taylor equations.

The accuracy of the validation on the 1995 flows in the NSA was more moderate, although this seems reasonable given the accuracy of the initial calibration. All three of the evaporation methods produced approximately the same error in the validation simulations. The parameters were initially calibrated on the 1994 data set which had measurable flows only during the start of the growing season. In contrast, the 1995 data set contained significant flows throughout the summer. Extreme error in the simulation of late season peak flows prompted the further investigation and calibration of the modelling parameters. It has been postulated that more significant amounts of frozen soil in the NSA result in temporal variations in the parameters affecting field capacity, interflow drainage, and drainage from the upper soil layer into the lower groundwater storage. By increasing the field capacity and drainage into and through the soil on a temporal basis throughout the simulation, the accuracy of the 1995 data set was dramatically improved.

An attempt was made to validate the calibrated parameters on a spatial scale. Differences in the physiography between the two study areas affect the values of the calibrated parameters and result in only moderate accuracy in the spatial validations. Parameters calibrated in the SSA underestimate peak flows in the NSA, and parameters calibrated in the NSA overestimate flows in the SSA. The less permeable glacial tills and rock outcrops in the NSA have a significantly different effect on the hydrologic sub-processes than the permeable sandy soils predominant in the lower soil layers of the SSA. The calibrated parameters are not transferable, in a spatial sense between the two study areas because of the significant differences in physiography. However, the parameters are temporally transferable.

The mass curve analysis using the simulated water balance has shown that the parameters established for the hydrologic sub-processes have yielded sensible water balances for all of the

land classes. The total percentage of the gross precipitation lost through interception evaporation (30%) approximates the percentages measured by other researchers. In a temporal sense, the soil moisture constraints placed on the evapotranspiration are also reasonable. The simulated mean daily rates of actual evapotranspiration from the Wet Conifer land class have been compared to independent estimates of evapotranspiration made at the OBS-SSA flux tower. This plot suggests that the soil moisture and degree-day constraints are slightly in excess of what they should be. However, in a comparison with water balance estimates of evapotranspiration loss, the constraints are reasonably accurate. The new method used to simulate evapotranspiration in WATFLOOD may require a further general reduction (use of the ETP parameter) in order to better predict the losses measured independently at the flux towers. The method is useful for simulating the evapotranspiration rates, particulary for the losses measured with the water balance.

Chapter 8
Recommendations

This thesis has illuminated a number of issues that require further analysis as well as possible modifications that could be made to improve WATFLOOD. If separate species of vegetation have distinctly different effects on the vertical water fluxes, a greater number of land classes must be made available in order to better characterize the land cover. Significant differences exist between some of the land classes that have been aggregated in this study (e.g. the differences between burns and roads, harvested areas and vegetated areas, etc.). However, the classification used in this analysis is adequate for these simulations since the percentage of area covered by the land classes with significantly different characteristics in the aggregated land classes is very low.

For the Priestley-Taylor equation, the potential evapotranspiration has been calculated on a daily time scale and the appropriate fraction of the daily estimate has been used as the average hourly rate. In contrast, the method using the Hargreaves equation calculates the evapotranspiration on an hourly basis. Future modifications to WATFLOOD should incorporate a calculation of the Priestley-Taylor evapotranspiration on an hourly time scale as well, since it has been shown that an hourly time step is applicable for use with the Priestley-Taylor equation. Although this modification will increase the computational requirements, it will be necessary for the estimation of losses from smaller watersheds where the diurnal variation in evapotranspiration losses is more apparent in the hydrographs. A further improvement to the Priestley-Taylor equation may be realized with the spatial distribution of net radiation data inputs. This modification will be necessary for modelling larger watersheds where the average incoming radiation will have significant spatial variation.

The level of soil moisture can be a significant constraint on the evapotranspiration losses. An attempt has been made to use parameters that have reasonable values and are commonly recognized, (field capacity and permanent wilting point). Further improvements could be made by defining these parameters according to the actual soil conditions. Improvements in these parameters and the tracking of soil moisture conditions would be achieved by including aseparate distribution of soil classes. However, it is obvious that introducing this additional classification would significantly increase in the computational effort required to run the simulations.

The modification of certain parameters to more closely resemble typically measured parameters would dramatically improve the ease of initializing the parameters. Such modifications would also improve to ability of researchers to analyze the validity of the calibrated parameters.

In northern climates, the temporal variation of frozen soil significantly affects the hydrologic processes. Even in southern regions this variation will be important, although for a somewhat shorter duration during the spring. The more accurate and precise simulation of the spatial and temporal variation of the active layer may provide significant improvements to the hydrologic simulation of watersheds in alpine and boreal climates.

An optimized parameter (ETP) , which has not been utilized in these simulations, has been incorporated into the model to index the actual to the potential evapotranspiration. For the Priestley-Taylor estimate of potential evapotranspiration a value of 1.26 for the α parameter has been utilized throughout this study. The value of α could be changed to values different than 1.26 by varying the value of the ETP accordingly. Values for α, other than 1.26, have been observed by various researchers in other studies. To maintain the overall seasonal water balance the parameters defining the other constraints on evapotranspiration, such as the degree-day or the soil moisture parameters, will require adjustment if a value different than 1.0 is used for the ETP parameters.

The variation in the total evapotranspiration losses with respect to the land cover type is prevalent. The analysis using the water budget and the flux tower measurements make this variation apparent. Future analyses could attempt to characterize the variation in evapotranspiration as a function of the total area covered by the different land cover types. The results from such an analysis would benefit by locating the watersheds for future studies so that each of the sub-basins contain significantly different amounts of each type of land cover, in contrast to the BOREAS watersheds.

An attempt has been made to produce a preliminary analysis of the water budget for both study areas on a short and long-term basis. The results of this analysis show that there is much more information to be obtained from these data. A refinement of the start and end of the rainfall intervals which more precisely correspond to the flow intervals should be incorporated into the further analysis of these data. As well, the final revisions to the flux tower measurements should improve the results of the comparison.

Plotting the simulated water balances in each of the land classes provides a powerful tool for analyzing the parameter calibrations. An analysis of the accuracy in the total simulated volumes of evapotranspiration and average daily evapotranspiration losses has been made in this study by comparing the losses to those measured independently at the flux towers. Comparison of other portions of the water balance would improve the understanding of those processes and the accuracy of their simulations.

Finally, the hydrologic modelling produced some excellent simulations of the measured flows, particularly for the SSA 1994 data set. Improvement in the temporal transferability of the model is apparent with the use of the new evapotranspiration models. The lack of confidence in the SSA 1995 data should inspire the further development of these calibrated parameters and their validation using the SSA 1996 data. In particular, it may be necessary to use a general reduction parameter to reduce the potential evapotranspiration rate closer to the actual evapotranspiration rate before applying the degree-day and soil moisture factors to characterize the shorter term variations. Further refinement and parameters and modelling in the NSA is required. Continuation of the detailed analysis of the flows through the sub-processes in the NSA should yield an improvement in the calibration and validation of the 1995 data set. A modification of the model to incorporate the processes affected by the active layer should also improve the simulations.

REFERENCES

Amiro, B.D. 1988. Evapotranspiration and surface water balance measurements at the Whiteshell research area, 1985 to 1987. Atomic Energy of Canada Limited. Technical Record 350. 31 pages.

Aldridge, R. and R.J. Jackson. 1973. Interception of rainfall by hard beech (*nothofagus truncata*) at Taita, New Zealand. *New Zealand Journal of Science* 16: 185-198.

American Society of Civil Engineers, Committee on Irrigation Water Requirements of the Irrigation and Drainage Division of the ASCE. 1990. Evapotranspiration and irrigation water requirements: a manual. The Society. 332 pages.

Andersson, L. 1992. Improvements of Runoff Models, Which Way to Go? *Nordic Hydrology* 23: 315-332.

Andrew, G.C. and J.D. Kemper. 1992. Canadian Professional Engineering Practice and Ethics. Holt, Rinehart and Winston of Canada, Limited. 395 pages.

Arp, P.A. and Yin, X. 1992. Predicting water fluxes through forests from monthly precipitation and mean monthly air temperature records. *Canadian Journal of Forestry Research* 22: 864-877.

Bardsley, W.E., and D.I. Campbell. 1994. A new method for measuring near-surface moisture budgets in hydrological systems. *Journal of Hydrology* 154: 245-254.

Bergstrom, S. and A. Forsman. 1973. Development of a conceptual deterministic rainfall-runoff model. *Nordic Hydrology* 4: 147-170.

Black, T.A., D.T. Price, F.M. Kelliher, and P.M. Osberg. 1984. Effect of overstory removal on seasonal growth of a young Douglas-fir stand. 1983-84 Annual Report, E.P. 855, Research Branch, B.C. ministry of Forests, Victoria, B.C.

Bouchet, R.J. 1963. Évapotranspiration réelle et potentielle, signification climatique. Gentbrugge, Belgium: *International Association of Scientific Hydrology* Publication No. 62: 134-142.

Brady, N.C. 1990. The nature and properties of soils. 10th edition. Mac-Millan Publishing Company, New York.

Brutsaert, W., and H. Stricker. 1979. An Advection-Aridity Approach to Estimate Actual Regional Evapotranspiration. *Water Resources Research* 15(2): 443-450.

Brutsaert, W. 1986. Catchment-Scale Evaporation and the Atmospheric Boundary Layer. *Water Resources Research* 22(9): 39S-45S.

Calder, I.R. 1977. A model of transpiration and interception loss from a spruce forest in Plynlimon, Central Wales. *Journal of Hydrology* 33: 247-265.

Chiew, F.H.S. and T.A. McMahon. 1990. Estimating groundwater recharge using a surface watershed modelling approach. *Journal of Hydrology* 114: 285-304.

Chiew, F.H.S., and T.A. McMahon. 1991. The applicability of Morton's and Penman's evapotranspiration estimates in rainfall-runoff modelling. *Water Resources Bulletin* 27(4): 611-620.

Davenport, D.C. and J.P. Hudson. 1967. Changes in evaporation rates along a 17-km transect in the Sudan Gezira. *Agriculture Meteorology* 4(5): 339-352.

De Bruin, H.A.R. and J.Q. Keijman. 1979. The Priestley-Taylor Evaporation Model Applied to a Large, Shallow Lake in the Netherlands. *Journal of Applied Meteorology* 18: 898-903.

Denmead, O.T. and R.H. Shaw. 1962. Availability of Soil Water to Plants as Affected by Soil Moisture Contents and Meteorological Conditions. *Agron. J.* 54(5): 385-389.

Dingman, S.L. 1994. Physical Hydrology. Prentice-Hall. 575 pages.

Donald, J.R. 1992. Snowcover depletion curves and satellite snowcover estimates for snowmelt runoff modelling. Ph.D. Thesis, Department of Civil Engineering, University of Waterloo. 233 pages.

Environment Canada. 1993. Canadian Climate Normals 1961-1990, Prairie Provinces. *Atmospheric Environment Service.* 266 pages.

Fisheries and Environment Canada. 1973-1982. Monthly Record Meteorological Observations in Western Canada. *Atmospheric Environment* Volumes 58-67.

Fontaine, T., and D. Todd. 1993. Measuring evaporation with ceramic Bellani plate atmometers. *Water Resources Bulletin* 29(5): 785-795.

Forbes, R.D. (editor). 1955. Forestry handbook. Ronald Press Company, New York.

Giles, D.G., T.A. Black, and D.L. Spittlehouse. 1985. Determination of growing season soil water deficits on a forested slope using water balance analysis. *Canadian Journal of Forest Resources* 15: 107-114.

Granger, R.J. 1989. An examination of the concept of potential evaporation. *Journal of Hydrology* 111: 9-19.

Granger, R.J. 1989. A complementary relationship approach for evaporation from nonsaturated surfaces. *Journal of Hydrology* 111: 31-38.

Hall, F.G. 1995. Landcover classifications of the SSA and NSA using the LANDSAT-5 TM, BOREAS group TE-18. BOREAS Information System (BORIS).

Hamlin, L.P.B. 1996. Snowmelt hydrologic modelling of northern wetland dominated river basins. M.A.Sc. Thesis, Department of Civil Engineering, University of Waterloo. 214 pages.

Hamon, W.R. 1961. Estimating Potential Evapotranspiration. *Journal of the Hydraulics Division, Proceedings of the American Society of Civil Engineers* HY3: 107-120.

Hargreaves, G.H. and Samani, Z.A. 1982. Estimating Potential Evapotranspiration. *Journal of the Irrigation and Drainage Division, Proceedings of the American Society of Civil Engineers* 108(IR3): 225-230.

Hope, A.S., and S.M. Evans. 1992. Estimating reference evaporation in the central valley of California using the Linacre model. *Water Resources Bulletin* 28(4): 695-702.

Iritz, Z., and A. Lindroth. 1994. Night-time evaporation from a short-rotation Willow stand. *Journal of Hydrology* 157: 235-245.

Jones, F.E. 1992. Evaporation of Water: with emphasis on applications and measurements. Lewis Publishers. 188 pages

Johnson, R.C. 1990. The interception, throughfall and streamflow in a forest in highland Scotland and the comparison with other upland forests in the U.K. *Journal of Hydrology* 118: 281-287.

Keulegan, G.H. 1938. Laws of turbulent flow in open channels. *Journal of Research* 21(6): 707-741.

Kimball, J.S., M.A. White, and S.W. Running. 1995. Simulating Interactions Between climate, Vegetation and Hydrologic Characteristics within the Boreal Forest. Submitted to: American Meteorological Society's 22nd conference on Agricultural and Forest Meteorology, September 5, 1995.

Kite, G.W. and L.E. Welsh. 1995. Research in the use of distributed meteorological data in the SLURP hydrological model for the Upper Columbia Basin. Progress Report No. 2. Submitted to the Hydroelectric Engineering Division, B.C. Hydro, May 30, 1995.

Kite, G.W. and N. Kouwen. 1992. Watershed Modeling Using Land Classifications. *Water Resources Research* 28(12): 3193-3200.

Kohler, M.A. and L.H. Parmele. 1967. Generalized estimates of free-water evaporation. *Water Resources Research* 3:997-1005.

Kouwen, N., F. Seglenieks, and E.D. Soulis. 1995. The use of Distributed Storm Rainfall Data and Distributed Hydrologic Models for the Estimation of Peak Flows for the Columbia River Basin. Submitted to the Hydroelectric Engineering Division, B.C. Hydro, July 12, 1995.

Kouwen, N., E.D. Soulis, A. Pietroniro, J. Donald, R.A. Harrington. 1993. Grouped response units for distributed hydrologic modeling. *Journal of Water Resources Planning and Management* 119(3): 289-305.

Kouwen, N., E.D. Soulis, A. Pietroniro, and R.A. Harrington. 1990. Remote sensing to assess vegetative cover effects for flood forecasting. International Conference on River Flood Hydraulics, 17-20 September, 1990. Paper M2: 437-446.

Kouwen, N. 1988. WATFLOOD Users manual. Water Resources Group, University of Waterloo. 125 pages.

Lemeur, R., and LU. Zhang. 1990. Evaluation of three evapotranspiration models in terms of their applicability for an arid region. *Journal of Hydrology* 114: 395-411.

Linacre, E.T. 1977. A simple formula for estimating evaporation rates in various climates, using temperature data alone. *Agricultural Meteorology* 18: 407-424.

Lindroth, A. 1993. Potential Evaporation - A Matter of Definition. *Nordic Hydrology* 24: 359-364.

Linsley, R.K. Jr., M.A. Kohler, and J.L.H. Paulhus. 1949. Applied Hydrology. McGraw-Hill. 689 pages.

Livingstone, B.E. 1935. Atmometers of Porous Porcelain and Paper, Their Use in Physiological Ecology. *Ecology* 16(3): 438-472.

Mailhot, J., R. Benoit, P. Pellerin, V. Lee, N. Kouwen, E.D. Soulis, G. Kite, and L. Welsh. Fine-scale modelling of intense orographic precipitation over the Columbia River Basin and coupling with distributed hydrology models.

Malmstrom, V.H. 1969. A new approach to the classification of climate. *Journal of Geography* 68:351-357.

McNaughton, K.G. and T.A. Black. 1973. A Study of Evapotranspiration from a Douglas Fir forest Using the Energy Balance Approach. *Water Resources Research* 9(6): 1579-1590.

Mohan, S. 1991. Intercomparison of evapotranspiration estimates. *Hydrological Sciences Journal 36(*5): 447-461.

Monteith, J.L. 1965. Evaporation and the Environment. *Symp. Soc. Exp. Biol.* 19: 204-234.

Morton, F.I., 1969. Potential Evaporation as a Manifestation of Regional Evaporation. *Water Resources Research* 5(6): 1244-1255.

Morton, F.I. 1975. Estimating Evaporation and Transpiration from Climatological Observations. *Journal of Applied Meteorology* 14: 488-497.

Morton, F.I. 1978. Estimating evapotranspiration from potential evaporation: practicality of an iconoclastic approach. *Journal of Hydrology* 38: 1-32.

Morton, F.I. 1983. Operational estimates of areal evapotranspiration and their significance to the science and practice of hydrology. *Journal of Hydrology* 66: 1-76.

Morton, F.I. 1983. Operational estimates of lake evaporation. *Journal of Hydrology* 66: 77-100.

Morton, F.I. 1986. Practical Estimates of Lake Evaporation. *Journal of Climate and Applied Meteorology* 25: 371-387.

Munro, D.S. 1979. Daytime Energy Exchange and Evaporation From a Wooded Swamp. *Water Resources Research* 15(5): 1259-1265.

Munro, D.S. 1986. On Forested Wetlands as Evaporators. *Canadian Water Resources Journal* 11(1): 89-99.

Nash, J.E. 1989. Potential evaporation and "The Complementary Relationship". *Journal of Hydrology* 111: 1-7.

Pearce, A.J. and L.K. Rowe. 1980. Nighttime, Wet Canopy Evaporation Rates and the Water Balance of an Evergreen Mixed Forest. *Water Resources Research* 16(5): 955-959.

Porter, J.W. and T.A. McMahon. 1975. Application of a catchment model in southeastern Australia. *Journal of Hydrology* 24(1/2): 121-134.

Porter, J.W. and T.A. McMahon. 1971. A model for the simulation of streamflow data from climatic records. *Journal of Hydrology* 13(4): 121-134.

Price, D.T. 1987. Some Effects of Variations in Weather and Soil Water Storage on Canopy Evapotranspiration and Net Photosynthesis of a Young Douglas-fir Stand. Ph.D. Thesis, University of British Columbia, Vancouver B.C.

Priestley, C.H.B. and R.J. Taylor. 1972. On the Assessment of Surface Heat Flux and Evaporation Using Large-Scale Parameters. *Monthly Weather Review* 100(2): 81-92.

Rowe, L.K. 1975. Rainfall Interception by mountain beech. *New Zealand Journal of Forest Hydrology* 5: 45-61.

Rowe, L.K. 1978. Rainfall Interception by a beech-podocarp-hardwood forest near Reefton, North Westland, New Zealand. *Journal of Hydrology (New Zealand)* 18: 63-72.

Rowe, L.K. 1983. Rainfall Interception by an evergreen beech forest, Nelson, New Zealand. *Journal of Hydrology* 66: 143-158.

Rutter, A.J., K.A. Kershaw, P.C. Robins, and A.J. Morton. 1971. A predictive model of rainfall interception in forests; 1. Derivation of the model from observations in a plantation of Corsican pine. *Agricultural Meteorology* 9:367-384.

Saeed, M. 1986. The Estimation of Evapotranspiration by Some Equations Under Hot and Arid Conditions. *Transactions of the American Society of Agricultural Engineers* 29(2): 434-438.

Sellers, P.J., W.J. Shuttleworth, J.L. Dorman, A. Dalcher, and J.M. Roberts. 1989. Calibrating the Simple Biosphere Model for Amazonian Tropical Forest Using field and Remote Sensing Data. Part I: Average Calibration with Field Data. *Journal of Applied Meteorology* 28: 727-759

Sellers, P.J., F.G. Hall, H. Margolis, R.D. Kelly, D. Baldocchi, G. Den Hartog, J. Cihlar, M. Ryan, B. Goodison, P. Crill, K.J. Ranson, D. Lettenmeier, and D.E. Wickland. 1995. The Boreal Ecosystem-Atmosphere Study (BOREAS): An Overview and Early Results from the 1994 Field Year. *Bulletin of the American Meteorological Society* 76(9): 1549-1577.

Sellers, P.J., F.G. Hall, D. Baldocchi, J. Cihlar, P. Crill, G. Den Hartog, B. Goodison, R.D. Kelly, D. Lettenmeier, H. Margolis, J. Ranson, and M. Ryan. 1994. Experiment Plan, Boreal Ecosystem-Atmosphere Study, Version 3.0. May 1994.

Sellers, P.J., Y. Mintz, Y.C. Sud, and A. Dalcher. 1986. A Simple Biosphere model (SiB) using point micrometeorological and biophysical data. *Journal of Atmospheric Sciences* 43(6): 505-531.

Shuttleworth, W.J. Chapter 4; Maidment, D.R. (editor-in-chief). 1993. Handbook of Hydrology. McGraw-Hill. 51 pages.

Shuttleworth, W.J. and I.R. Calder. 1979. Has the Priestley-Taylor Equation Any Relevance to the Forest Evaporation? *Journal of Applied Meteorology* 18: 639-646.

Silvestri, V., M. Soulie, J. Lafleur, G. Sarkis, and N. Bekkouche. 1990. Foundation problems in champlain clays during droughts. I: Rainfall deficits in Montreal (1938-1988). *Canadian Geotechnical Journal* 27: 285-293.

Spittlehouse, D.L. 1989. Estimating evapotranspiration from land surfaces in British Columbia. *International Association of Hydrological Sciences* 177: 245-255.

Spittlehouse, D.L. and T.A. Black. 1981. A growing season water balance model applied to two Douglas fir stands. *Water Resources Research* 17: 1651-1656.

Stagnitti, F., J.Y. Parlange, and C.W. Rose. 1989. Hydrology of a small wet catchment. *Hydrological Processes* 3: 137-150.

Stewart, J.B. 1977. Evaporation From the Wet Canopy of a Pine Forest. *Water Resources Research 13(6): 915-921.*

Stewart, R.B. and W.R. Rouse. 1976. A simple Method for Determining the Evaporation From Shallow Lakes and Ponds. *Water Resources Research* 12(4): 623-628.

Stewart, H.B. and A.S. Thom. 1973. Energy budgets in pine forest. *Quarterly Journal of the Royal Meteorological Society* 99: 145-170.

Tanguay, M., A. Robert, and R. Laprise. 1990. A semi-implicit semi-lagrangian fully compressible regional forecast model. *Monthly Weather Review* 118: 1970-1980.

Tao, T. and N. Kouwen. 1989. Remote sensing and fully distributed modeling for flood forecasting. *Journal of Water Resources Planning and Management* 115(6): 809-823.

Thornthwaite, C.W. and J.R. Mather. 1955. The water balance. Philadelphia, PA: Drexel Institute of Technology, climatological Laboratory *Publication No. 8.*

Turc, L. 1972. Indice climatique de potentialité agricole. *Science du Sol 2: 81-102.*

Turc, L. 1961 Evaluation des besoins en eau d'irrigation, évapotranspiration potentielle : fomule climatique simplifiée et mise à jour (ETp. f.60), *Ann. Agro.* pages 13-49.

Turner, N.C. and P.G. Jarvis. 1975. Photo Synthesis is Sitka Spruce (Pieca sitchensis (Bong.) Carr.) IV: Response to Soil Temperature. *Journal of Ecology* 12: 561-576.

Verseghy, D.L., N.A. McFarlane, and M. Lazare. 1991. CLASS - A Canadian land surface scheme for GCMS, I. Soil model. *International Journal of Climatology* 11: 111-133.

Verseghy, D.L., N.A. McFarlane, and M. Lazare. 1993. CLASS - A Canadian land surface scheme for GCMS, II. Vegetation model and coupled runs. *International Journal of Climatology* 13: 347-370.

Veissman, W. Jr., G.L. Lewis, and J.W. Knapp. 1989. Introduction to Hydrology, Third Edition. Harper Collins. 780 pages.

Wei, T.C. and. J.L. McGuiness. 1973. Reciprocal Distances Squared Method: A Computer Technique for Estimating Areal Precipitation. *USDA-ARS-NC-8* pages 1-23.

Winter, T.C. and D.O. Rosenberry. 1995. Evaluation of 11 Equations for determining evaporation for a small lake in the north central United States. *Water Resources Research* 31(4): 983-993.

World Meteorological Organization (WMO). 1986. Intercomparison of Models of Snowmelt Runoff, Publication No. 646, Geneva, Switzerland.

Wofsy, S. 1995. Old Black Spruce Flux Tower Data, BOREAS group TF-3 - 1994 field season. BOREAS Information System (BORIS).

Wright, I.R., and R.J. Harding. 1993. Evaporation from natural mountain grassland. *Journal of Hydrology* 145: 267-283.

APPENDIX A:

LIST OF VARIABLES

a, alb, albe	albedo
A_1	regressed coefficient for the soil moisture reduction function (% soil moisture)
AET	actual evapotranspiration (mm, mm hr^{-1}, or mm day^{-1})
AK	permeability - WATFLOOD parameter (mm s^{-1})
AK2	upper zone drainage constant - WATFLOOD parameter - affects drainage from upper to lower soil water storage
b_0,b_1	empirical constants in Dalton's Theory
B	Bowen ratio
B_1	regressed coefficient for the soil moisture reduction function (% soil moisture)
c_a	specific heat capacity of air (J m^{-3} °C^{-1})
c_p	ratio of vegetal surface area to projected area
c_s	specific heat capacity of soil (J m^{-3} °C^{-1})
C	concentration (mass $length^{-3}$)
C_{at}	atmospheric conductance (m s^{-1})
C_{can}	canopy conductance (m s^{-1})
C_{leaf}	leaf conductance (m s^{-1})
C_t	Hargreaves temperature reduction coefficient
C_1	regressed coefficient for the degree day reduction function (°C)
dr	relative distance between the earth in the sun
d_s	depth of soil contributing to heat storage (m)
D	diffusivity: D_H sensible heat; D_M momentum; D_{WV} water vapour
D_{hr}	number of hours of daylight per day
DD	total of the degree days since the start of the simulation (°C)
D_1	regressed coefficient for the degree day reduction function (°C)
e_a	actual vapour pressure (kPa or mb)
e_s	surface vapour pressure (kPa of mb)
e_{sat}	saturation vapour pressure (kPa or mb)
E	evaporation rate (mm, mm hr^{-1}, or mm day^{-1})
E_a	evaporation rate per unit area (mm m^2 m^{-2} hr^{-1})
ET	evapotranspiration rate (mm, mm hr^{-1}, or mm day^{-1})
ETP	an PET reduction parameter

F	flux rate (W m^{-2})
FFCAP	fraction of the FCAP equal to the PWP
FPET	a PET reduction parameter based on temperature
FPET2	a PET parameter increasing PET by 3.0 for interception evaporation
FTALL	a PET reduction parameter based on the vegetation height
G	ground heat flux (W m^{-2})
GW	groundwater flow (mm m^2 m^{-2})
h	maximum interception storage capacity per unit of projected area (mm m^2 m^{-2})
H	sensible heat flux (W m^{-2})
IET	interception evaporation (mm, mm hr^{-1}, or mm day^{-1})
J	Julian Day
k_1	Prandtl-von Karman dimensionless constant (0.4)
k_2	Linsley's decay coefficient (mm m^2 m^{-2})
K	short-wave radiation (W m^{-2})
K_E	mass transfer coefficient for evaporation
K_{ET}	mass transfer coefficient for evapotranspiration
K_H	mass transfer coefficient for sensible heat
K_{in}	incoming short-wave radiation (W m^{-2})
K_{LE}	mass transfer coefficient for latent heat
K_n	net short-wave radiation (W m^{-2})
ℓ	characteristic length used in Prandtl-von Karman equation (length)
L	long-wave radiation (W m^{-2})
L_{at}	incoming long-wave radiation (W m^{-2})
L_w	sum of emitted and reflected long-wave radiation (W m^{-2})
L_n	net long-wave radiation (W m^{-2})
LAI	leaf area index
LE	latent heat flux (W m^{-2})
LZF	lower zone drainage function - WATFLOOD parameter controlling discharge from lower ground water storage
M	momentum (kg m^2 s^{-2})

P	atmospheric pressure (kPa or mb)
P_s	energy consumed by photosynthesis (W m^{-2})
P_i	sum of precipitation per unit of projected area since the beginning of the storm (mm m^2 m^{-2})
PET	potential evapotranspiration (mm, mm hr^{-1}, or mm day^{-1})
$PET_{avg.m}$	long-term mean monthly potential evapotranspiration (mm $month^{-1}$)
PET_H	Hamon monthly potential evapotranspiration (cm $month^{-1}$)
PET_M	Malmstrom monthly potential evapotranspiration (cm $month^{-1}$)
PWR	exponent - WATFLOOD parameter controlling rate of lower zone discharge
q	energy (W m^{-2})
q_a	specific humidity
q_{sat}	saturated specific humidity
Q	stored energy (W m^{-2})
Q_{est}	simulated flow (m^3 s^{-1})
Q_{obs}	measured flow (m^3 s^{-1})
r_{at}	atmospheric resistance (s m^{-1})
r_c	composite stomatal resistance for different vegetation types (s m^{-1})
r_s	stomatal resistance (s m^{-1})
r_{smin}	stomatal resistance (s m^{-1})
REC	recession constant - WATFLOOD parameter controlling interflow
RETN	retention - WATFLOOD parameter, similar to the field capacity (mm)
R2	channel roughness - WATFLOOD parameter
R_a	water equivalent of extraterrestrial solar radiation (mm d^{-1})
s	s criterion - a measurement of error
$s(T_a)$	slope of saturation vapour pressure-temperature curve (kPa °C^{-1})
SMI	soil moisture indicator - soil moisture reduction function for PET
SW	surface water flow (mm m^2 m^{-2})
t	time (s, hr, or day)
t_R	duration of rainfall event (hr)
tto	total of the degree days since the start of the simulation (°C)
T	some base temperature (usually 0 °C)
T_a	air temperature (°C or K)

$T_{avg.d}$	mean daily air temperature (°C or K)
$T_{avg.m}$	long-term mean monthly air temperature (°C or K)
T_c	temperature of the canopy (K)
T_m	mean monthly temperature (°C or K)
T_s	surface temperature (°C or K)
$T_{1,2}$	temperature at time step 1 and 2 (°C or K)
Temp1,2,3	calibrated degree-day function parameters (°C)
u	measurement of error between Q_{est} and Q_{obs} used by WATFLOOD
u_*	shear velocity (m s^{-1})
UZS	upper zone storage - WATFLOOD parameter for water in the upper soil zone (mm)
UZSI	upper zone storage indicator - soil moisture reduction function for PET
v	volume of interception storage (mm)
v_a	wind speed (m s^{-1})
v_m	wind speed at measurement height (m s^{-1})
$v_{2.0}$	wind speed at 2.0 m (m s^{-1})
W	gross rainfall (mm, mm hr^{-1}, or mm day^{-1})
w_a	relative humidity
w_s	the sunset hour angle (radians.)
X2	sum of maximum storage and interception evaporation
z	depth of soil (m)
z_0	roughness height (0.1 $z_{veg.}$ m)
z_d	zero plane of displacement (0.7 $z_{veg.}$ m)
z_m	measurement height (m)
α	Priestley-Taylor PET_{eq} coefficient
$\alpha_{storage}$	an interception storage function
δ	solar declination (radians.)
δ_t	difference between the mean monthly maximum and minimum temperatures (°C)

ε	emissivity
ε_{at}	atmospheric emissivity
ε_w	emissivity of water
ϕ	latitude North
γ	psychrometric constant
λ_v	latent heat of vaporization
θ	soil moisture (%)
θ_{fc} or FCAP	soil moisture - filed capacity (%)
θ_{pwp} or PWP	soil moisture - wilting point (%)
ρ_a	mass density of air (g m^{-3})
ρ_{sat}	saturation absolute humidity (g m^{-3})
ρ_w	mass density of water (g m^{-3})
ρ_v	mass vapour density (absolute humidity) (g m^{-3})
ρ_a/ρ_v	0.622
σ	Stefan-Boltzmann constant (5.67×10^{-8} W m^{-2} s^{-1} K^{-4})
τ	shear stress (N m^{-2})
τ_0	shear stress at the surface (N m^{-2})
$\psi_{s,r}$	soil moisture suction

APPENDIX B:

LAND COVER CLASSIFICATION

FROM

CHAPTER 3

		6	7														
	4	9	4				0	0									
	0	1	4	0	1	4	0	0	0	0							
	0	0	4	6	4	8	1	0	0	0							
	1	1	3	0	0	1	1	0	0	0	0						
		4	4	1	0	0	3	0	0	0	0	0	0	0			
	1	4	2	1	0	0	0	2	0	0	0	0	0	1			
4	4	1	0	0	0	0	0	2	0	0	0	0	0	2	2		
3	0	0	0	0	0	0	0	2	1	0	0	0	2	0	1		
5	0	0	0	0	0	0	0	0	3	0	1	2	1	0	2		
5	1	0	0	0	0	0	0	0	2	1	0	3	0	0	6		
3	0	0	1	0	1	0	0	0	1	3	2	3	1	1	1		
3	2	1	1	0	0	0	0	2	3	0	0	1	3	1	1	1	
	11	6	4	3	2	2	2	0				0	0	9	3	2	5
													0	1	2	1	3
														1	5	1	3

Figure B1: Percent of Each Element in the Barren Class - SSA

		59	43														
	65	49	28				21	12									
	85	38	34	18	27	31	11	11	10	10							
	47	24	34	56	44	37	24	16	10	17							
	37	34	20	15	15	34	23	15	16	27	38						
		43	58	27	10	12	28	23	20	21	36	44	58	58			
	44	29	34	10	6	11	7	17	14	15	20	30	55	57			
30	15	14	8	8	7	14	7	15	8	13	21	28	25	36	37		
13	3	6	12	7	6	9	8	36	23	23	19	31	26	28	60		
30	8	11	22	13	3	8	11	11	36	25	39	47	41	17	70		
40	33	12	21	12	5	8	10	10	31	12	39	63	18	29	77		
33	20	6	29	53	17	21	10	8	18	15	38	46	41	38	41		
18	32	16	21	80	51	48	38	28	37	22	49	28	23	33	51	37	
	41	41	34	72	79	76	39	10				36	48	77	58	48	45
													11	36	63	65	54
														12	55	30	55

Figure B2: Percent of Each Element in the Dry Conifer Class - SSA

	47	34	49														
	24	38	66				70	70									
	15	55	55	72	60	62	77	76	81	82							
	49	62	44	35	47	52	72	72	79	61							
	34	34	62	65	48	53	65	76	80	59	56						
		46	32	53	72	83	66	56	78	72	61	55	40	28			
	54	57	61	82	92	68	81	73	81	80	73	68	39	38			
64	75	78	86	81	91	75	78	69	81	76	64	64	64	57	27		
73	91	86	81	80	83	56	65	57	66	57	73	63	71	57	36		
58	81	64	55	78	86	85	74	81	54	64	57	51	57	63	20		
51	65	83	60	78	81	84	81	77	62	85	61	34	76	49	13		
48	32	19	26	41	66	66	80	87	72	80	59	48	54	55	56		
75	45	11	14	12	40	44	54	62	57	73	49	71	72	63	47	57	
	41	47	58	21	16	18	54	80				63	51	14	37	49	47
													80	62	31	28	39
														87	37	64	40

Figure B3: Percent of Each Element in the Wet Conifer Class - SSA

		1	1														
	2	4	2				9	18									
	1	7	6	10	12	3	13	13	9	8							
	2	8	14	4	5	3	3	12	10	21							
	0	1	6	10	14	11	8	9	4	13	5						
		3	4	10	17	5	2	14	3	6	2	1	3	14			
	1	3	3	7	2	20	9	4	5	5	7	2	6	4			
2	6	6	4	12	2	11	13	13	11	11	15	7	9	4	2		
11	6	8	6	13	6	11	26	6	10	20	9	5	1	15	2		
5	10	25	18	7	7	7	15	8	7	11	4	0	1	20	8		
2	1	5	19	10	10	8	8	13	4	2	1	0	6	22	4		
4	1	0	3	7	15	12	10	5	10	2	0	3	4	5	1		
3	2	1	1	3	9	7	8	8	4	5	1	0	3	2	1	5	
	6	5	4	3	2	4	5	9				1	1	0	1	1	3
													8	2	4	6	4
														0	3	5	2

Figure B4: Percent of Each Element in the Fen Class - SSA

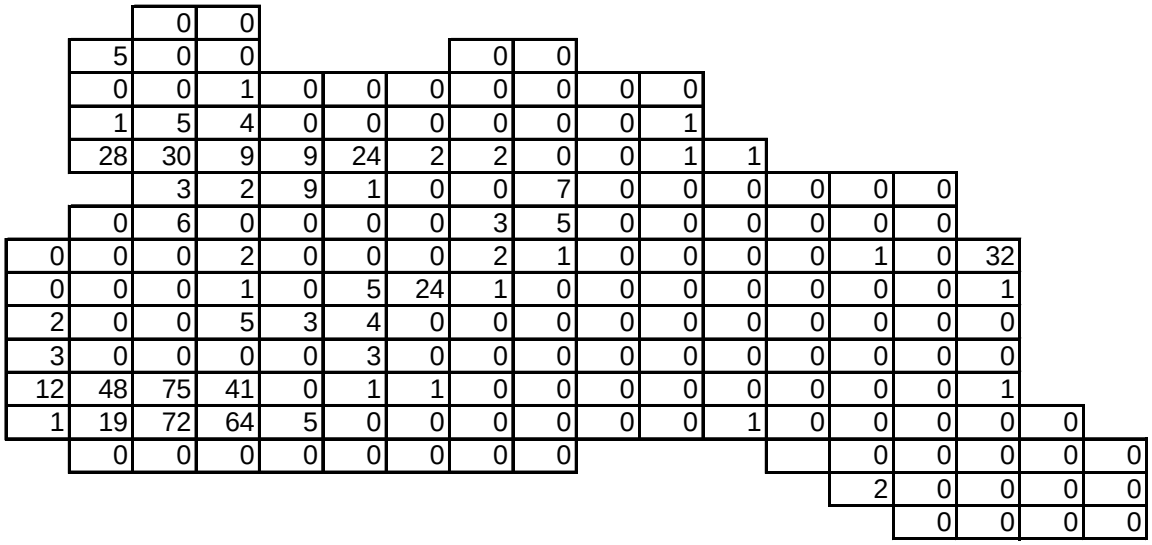

	0	0														
5	0	0				0	0									
0	0	1	0	0	0	0	0	0	0							
1	5	4	0	0	0	0	0	0	1							
28	30	9	9	24	2	2	0	0	1	1						
	3	2	9	1	0	0	7	0	0	0	0	0	0			
0	6	0	0	0	0	3	5	0	0	0	0	0	0			
0	0	2	0	0	0	2	1	0	0	0	0	1	0	32		
0	0	1	0	5	24	1	0	0	0	0	0	0	0	1		
0	0	5	3	4	0	0	0	0	0	0	0	0	0	0		
0	0	0	0	3	0	0	0	0	0	0	0	0	0	0		
48	75	41	0	1	1	0	0	0	0	0	0	0	0	1		
19	72	64	5	0	0	0	0	0	0	1	0	0	0	0	0	
0	0	0	0	0	0	0	0					0	0	0	0	0
												2	0	0	0	0
													0	0	0	0

Figure B5: Percent of Each Element in the Water Class - SSA

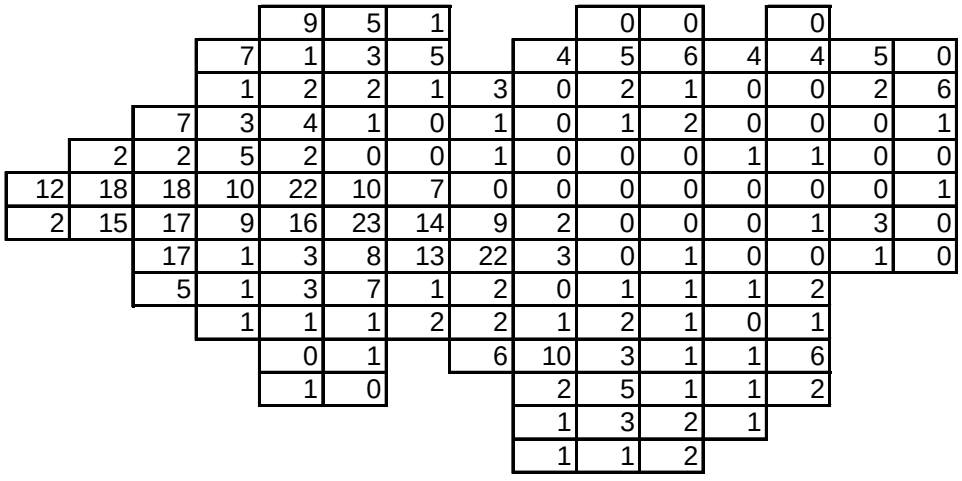

			9	5	1			0	0		0			
		7	1	3	5		4	5	6	4	4	5	0	
		1	2	2	1	3	0	2	1	0	0	2	6	
	7	3	4	1	0	1	0	1	2	0	0	0	1	
	2	2	5	2	0	0	1	0	0	0	1	1	0	0
12	18	18	10	22	10	7	0	0	0	0	0	0	0	1
2	15	17	9	16	23	14	9	2	0	0	0	1	3	0
		17	1	3	8	13	22	3	0	1	0	0	1	0
		5	1	3	7	1	2	0	1	1	1	2		
			1	1	1	2	2	1	2	1	0	1		
				0	1		6	10	3	1	1	6		
				1	0			2	5	1	1	2		
								1	3	2	1			
								1	1	2				

Figure B6: Percent of Each Element in the Barren Class - NSA

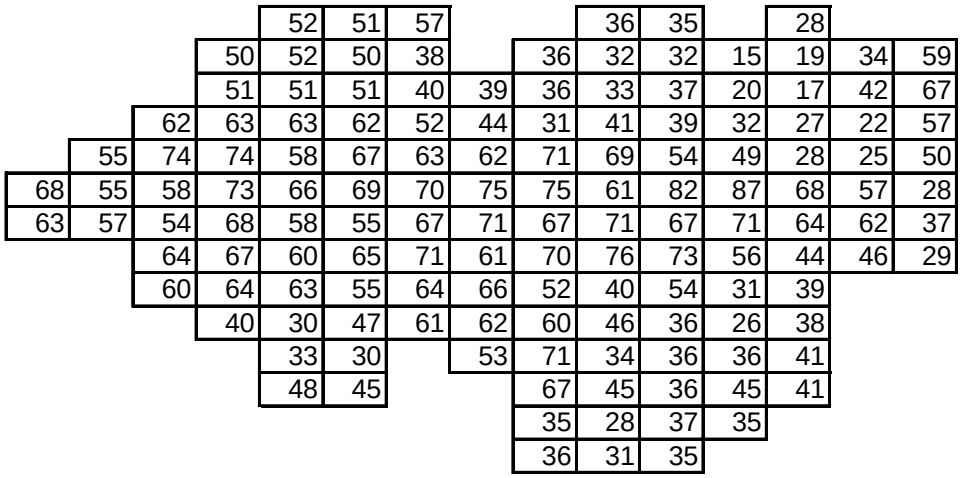

			52	51	57			36	35		28			
		50	52	50	38		36	32	32	15	19	34	59	
		51	51	51	40	39	36	33	37	20	17	42	67	
	62	63	63	62	52	44	31	41	39	32	27	22	57	
55	74	74	58	67	63	62	71	69	54	49	28	25	50	
68	55	58	73	66	69	70	75	75	61	82	87	68	57	28
63	57	54	68	58	55	67	71	67	71	67	71	64	62	37
		64	67	60	65	71	61	70	76	73	56	44	46	29
		60	64	63	55	64	66	52	40	54	31	39		
			40	30	47	61	62	60	46	36	26	38		
				33	30		53	71	34	36	36	41		
				48	45			67	45	36	45	41		
								35	28	37	35			
								36	31	35				

Figure B7: Percent of Each Element in the Dry Conifer Class - NSA

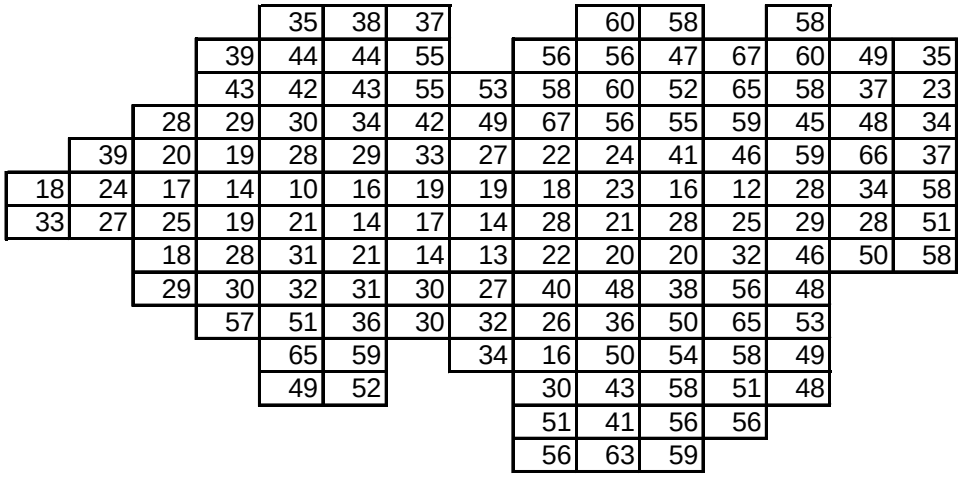

			35	38	37			60	58		58			
		39	44	44	55		56	56	47	67	60	49	35	
		43	42	43	55	53	58	60	52	65	58	37	23	
	28	29	30	34	42	49	67	56	55	59	45	48	34	
39	20	19	28	29	33	27	22	24	41	46	59	66	37	
18	24	17	14	10	16	19	19	18	23	16	12	28	34	58
33	27	25	19	21	14	17	14	28	21	28	25	29	28	51
	18	28	31	21	14	13	22	20	20	32	46	50	58	
	29	30	32	31	30	27	40	48	38	56	48			
		57	51	36	30	32	26	36	50	65	53			
			65	59		34	16	50	54	58	49			
			49	52			30	43	58	51	48			
							51	41	56	56				
							56	63	59					

Figure B8: Percent of Each Element in the Wet Conifer Class - NSA

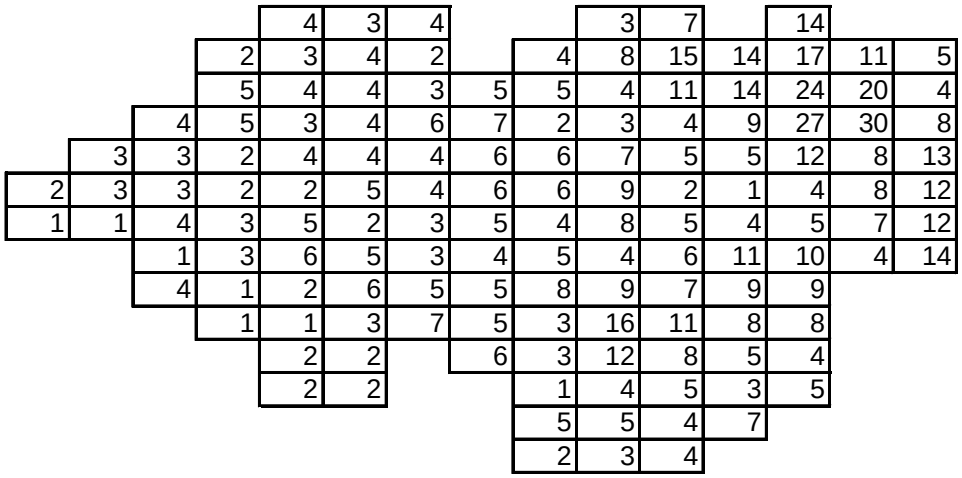

				4	3	4			3	7		14		
			2	3	4	2		4	8	15	14	17	11	5
			5	4	4	3	5	5	4	11	14	24	20	4
		4	5	3	4	6	7	2	3	4	9	27	30	8
	3	3	2	4	4	4	6	6	7	5	5	12	8	13
2	3	3	2	2	5	4	6	6	9	2	1	4	8	12
1	1	4	3	5	2	3	5	4	8	5	4	5	7	12
		1	3	6	5	3	4	5	4	6	11	10	4	14
		4	1	2	6	5	5	8	9	7	9	9		
			1	1	3	7	5	3	16	11	8	8		
				2	2		6	3	12	8	5	4		
				2	2			1	4	5	3	5		
								5	5	4	7			
								2	3	4				

Figure B9: Percent of Each Element in the Fen Class - NSA

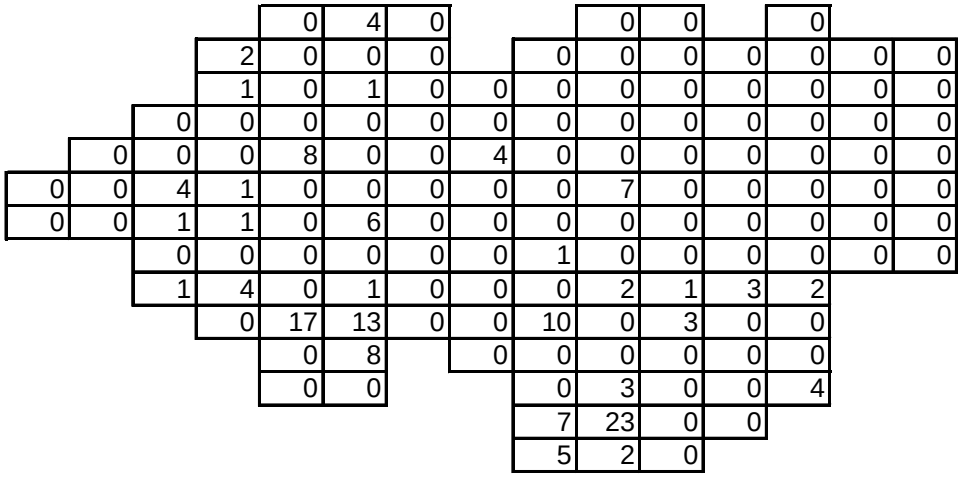

				0	4	0			0	0		0		
			2	0	0	0		0	0	0	0	0	0	0
			1	0	1	0	0	0	0	0	0	0	0	0
		0	0	0	0	0	0	0	0	0	0	0	0	0
	0	0	0	8	0	0	4	0	0	0	0	0	0	0
0	0	4	1	0	0	0	0	0	7	0	0	0	0	0
0	0	1	1	0	6	0	0	0	0	0	0	0	0	0
		0	0	0	0	0	0	1	0	0	0	0	0	0
		1	4	0	1	0	0	0	2	1	3	2		
			0	17	13	0	0	10	0	3	0	0		
				0	8		0	0	0	0	0	0		
				0	0			0	3	0	0	4		
								7	23	0	0			
								5	2	0				

Figure B10: Percent of Each Element in the Water Class - NSA

APPENDIX C:

METEOROLOGICAL MEANS

AND AET/PET REGRESSION

FROM

CHAPTER 4

Table C1: Published Meteorological Means - Prince Albert, Saskatchewan

	Minimum Temp. (deg.C)	Maximum Temp. (deg.C)	Pressure (kPa)	Relative Humidity @600 hrs (%)	Relative Humidity @1500 hrs (%)	Evaporation Pan (mm)
January	-25.1	-14.9	96.48	72	67	N/A
February	-21.8	-9.5	96.53	75	66	N/A
March	-14.2	-2.1	96.40	79	65	N/A
April	-3.9	8.4	96.33	80	51	N/A
May	3.5	17.8	96.20	78	42	190
June	8.0	22.2	96.02	81	48	229
July	10.4	24.2	96.21	76	52	204
August	9.0	23.0	96.25	87	50	173
September	3.6	16.7	96.28	86	43	106
October	-1.8	8.8	96.19	82	54	81
November	-12.3	-4.1	96.27	80	69	N/A
December	-21.6	-12.3	96.38	75	70	N/A

Table C2: Published Meteorological Means - Thompson, Manitoba

	Minimum Temp. (deg.C)	Maximum Temp. (deg.C)	Pressure (kPa)	Relative Humidity @600 hrs (%)	Relative Humidity @1500 hrs (%)	Evaporation Pan (mm)
January	-30.6	-19.5	99.02	N/A	64	N/A
February	-27.9	-14.4	99.21	69	59	N/A
March	-21	-5.6	99.12	70	51	N/A
April	-9.5	4.6	99.08	74	47	N/A
May	-0.6	13.2	98.93	74	45	103
June	5.2	19.3	98.57	79	49	168
July	8.8	22.6	98.57	85	50	187
August	6.9	20.7	98.63	88	52	136
September	1.7	12.6	98.76	88	59	66
October	-4.2	4.2	98.70	86	67	N/A
November	-16.5	-7.2	98.84	80	73	N/A
December	-27.3	-17.1	98.98	72	70	N/A

Table C3: Regression of AET and PET

PET	AET	Regressed Coefficient B	Coefficient of Determination R^2	Standard Error (mm)
Hargreaves	OBS-SSA	0.50	0.93	0.59
	FEN-SSA	0.68	0.98	0.49
	OJP-SSA	0.17	0.59	1.20
	OBS-NSA	0.45	0.95	0.44
	FEN-NSA	0.63	0.94	0.73
	OJP-NSA	0.12	0.75	0.31
	YJP-NSA	0.33	0.95	0.35
Priestley-Taylor	OBS-SSA	0.49	0.94	0.51
	FEN-SSA	0.67	0.97	0.60
	OJP-SSA	0.42	0.81	0.81
	OBS-NSA	0.27	0.91	0.51
	FEN-NSA	0.58	0.95	0.67
	OJP-NSA	0.13	0.82	0.25
	YJP-NSA	0.34	0.94	0.36
Turc	OBS-SSA	1.42	0.92	0.62
	FEN-SSA	2.12	0.97	0.61
	OJP-SSA	1.15	0.88	0.64
	OBS-NSA	1.36	0.95	0.44
	FEN-NSA	1.92	0.95	0.70
	OJP-NSA	0.37	0.72	0.33
	YJP-NSA	1.01	0.95	0.35
Evaporation Pan	OBS-SSA	0.28	0.90	0.67
	FEN-SSA	0.45	0.96	0.76
	OJP-SSA	0.24	0.84	0.75
	OBS-NSA	0.32	0.93	0.53
	FEN-NSA	0.50	0.93	0.72
	OJP-NSA	0.09	0.71	0.34
	YJP-NSA	0.26	0.93	0.42

APPENDIX D:

ADDITIONAL FIGURES

FROM

CHAPTER 5

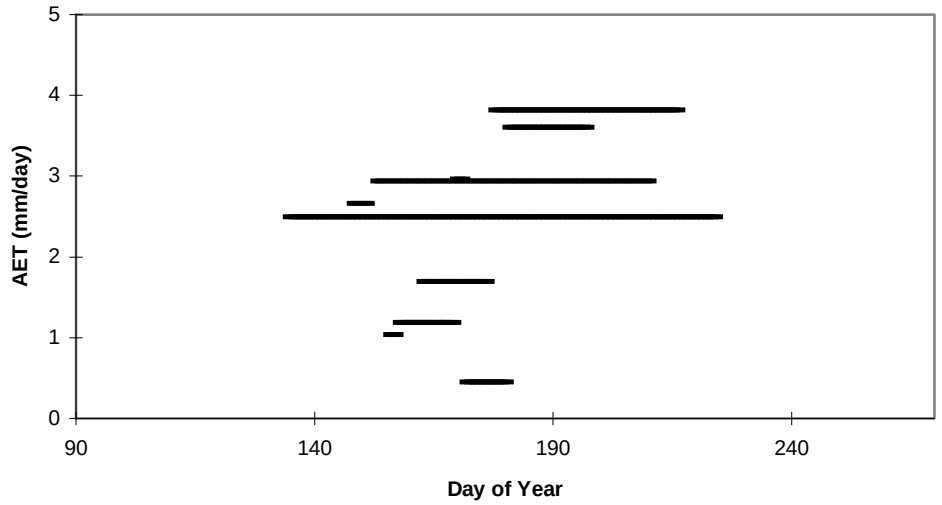

Figure D1: Mean Daily Water Balance AET vs. Day of Year- SW2

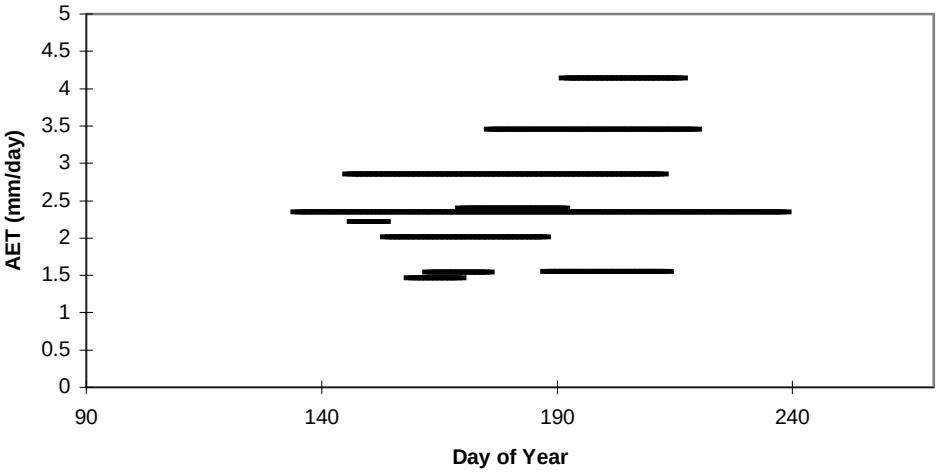

Figure D2: Mean Daily Water Balance AET vs. Day of Year- SW3

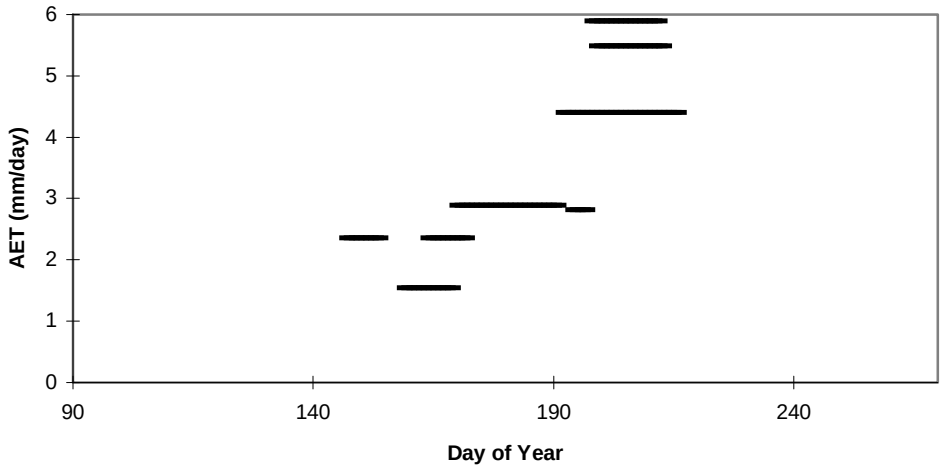

Figure D3: Mean Daily Water Balance AET vs. Day of Year- SW4

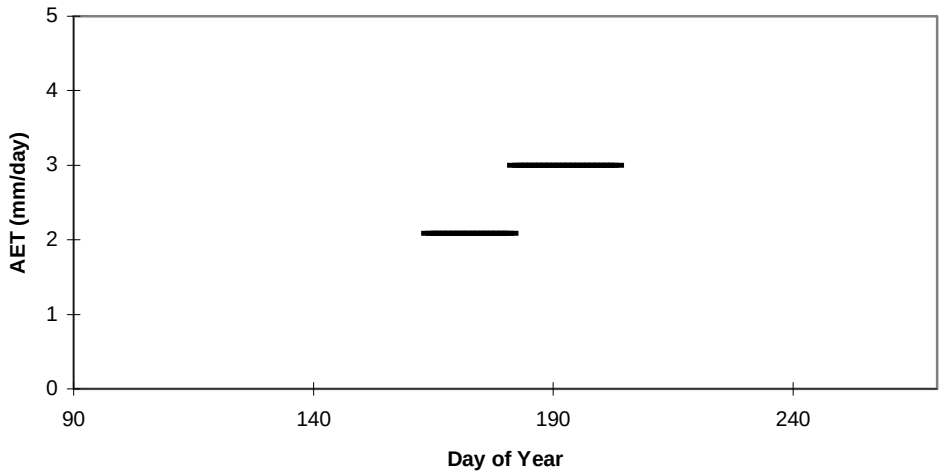

Figure D4: Mean Daily Water Balance AET vs. Day of Year- NW1

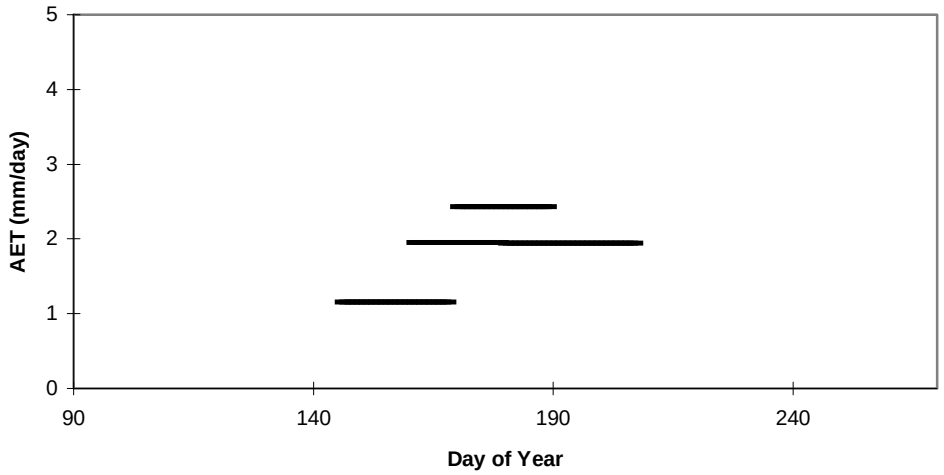

Figure D5: Mean Daily Water Balance AET vs. Day of Year- NW2

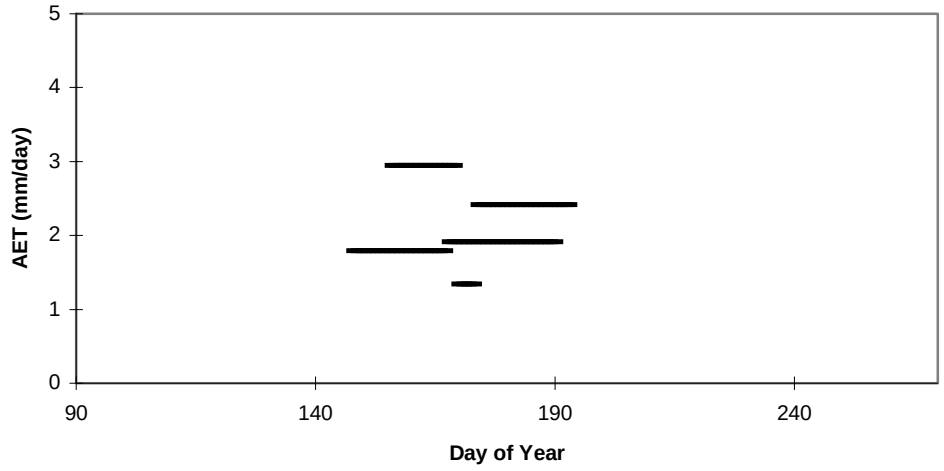

Figure D6: Mean Daily Water Balance AET vs. Day of Year- NW3

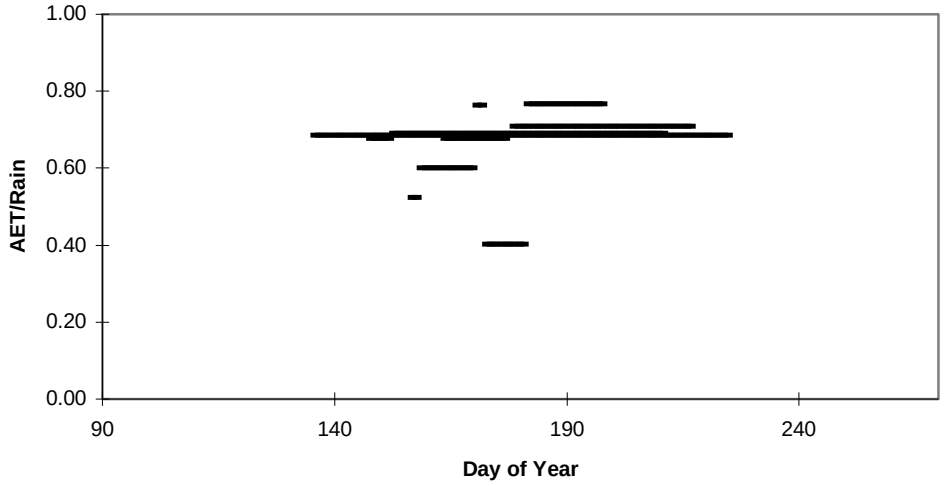

Figure D7: Total Water Balance AET/Total Rain vs. Day of Year- SW2

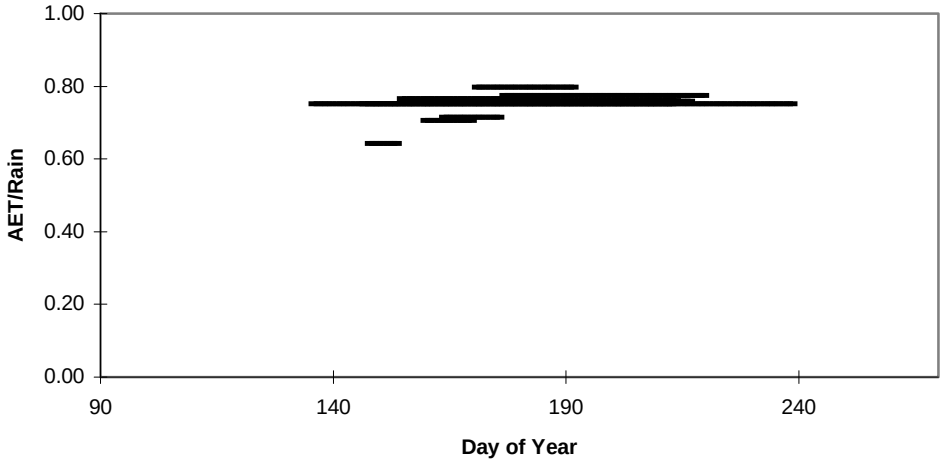

Figure D8: Total Water Balance AET/Total Rain vs. Day of Year- SW3

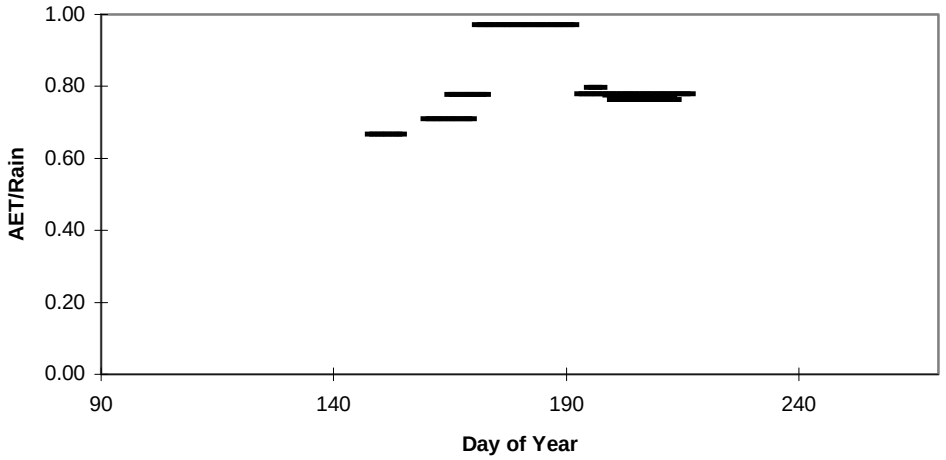

Figure D9: Total Water Balance AET/Total Rain vs. Day of Year- SW4

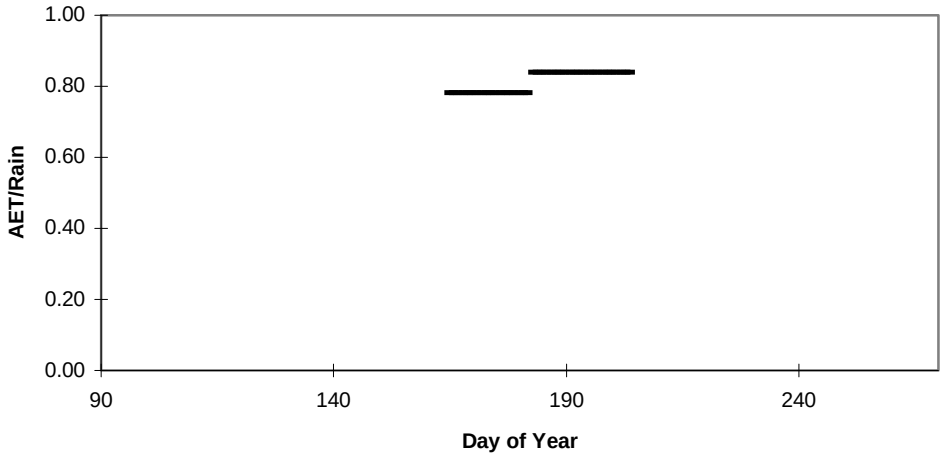

Figure D10: Total Water Balance AET/Total Rain vs. Day of Year- NW1

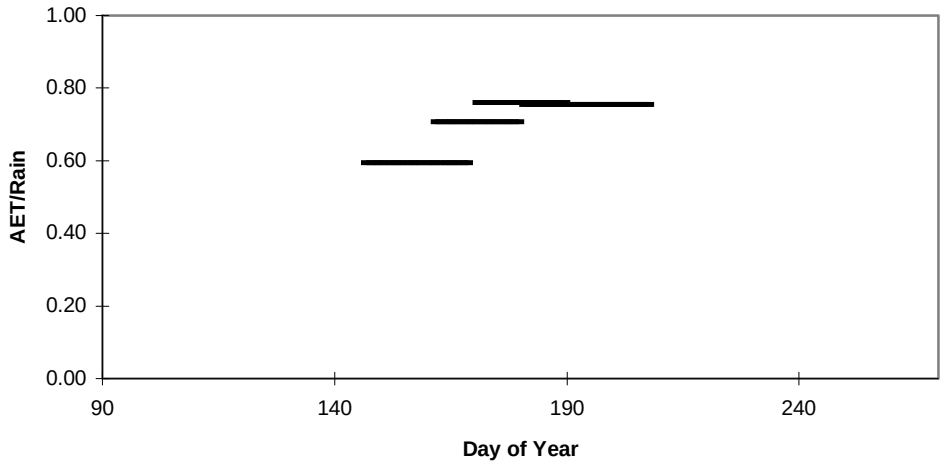

Figure D11: Total Water Balance AET/Total Rain vs. Day of Year- NW2

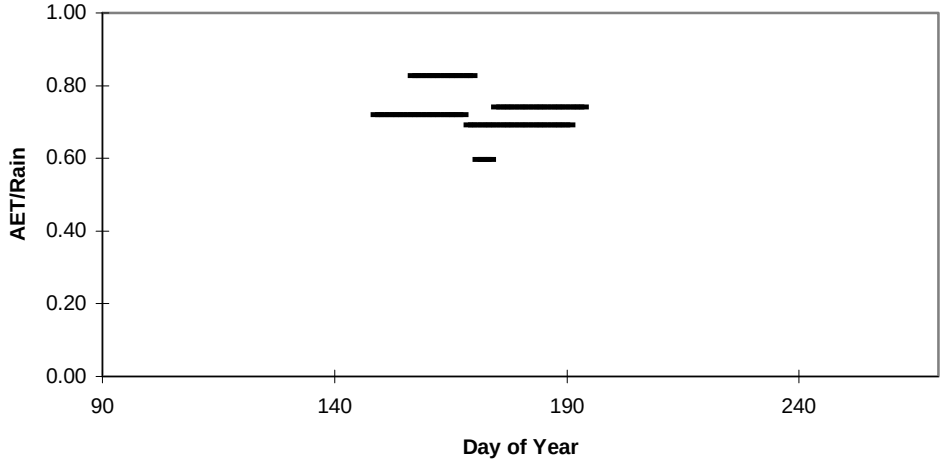

Figure D12: Total Water Balance AET/Total Rain vs. Day of Year- NW3

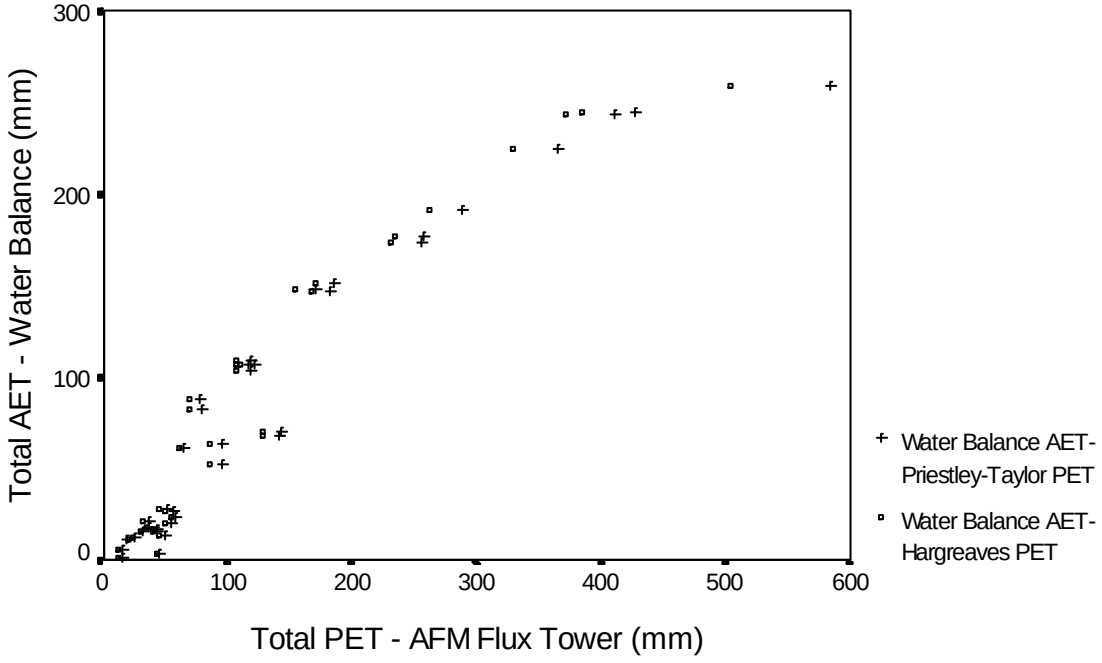

Figure D13: Total Water Balance AET vs. Total PET - SSA 1994

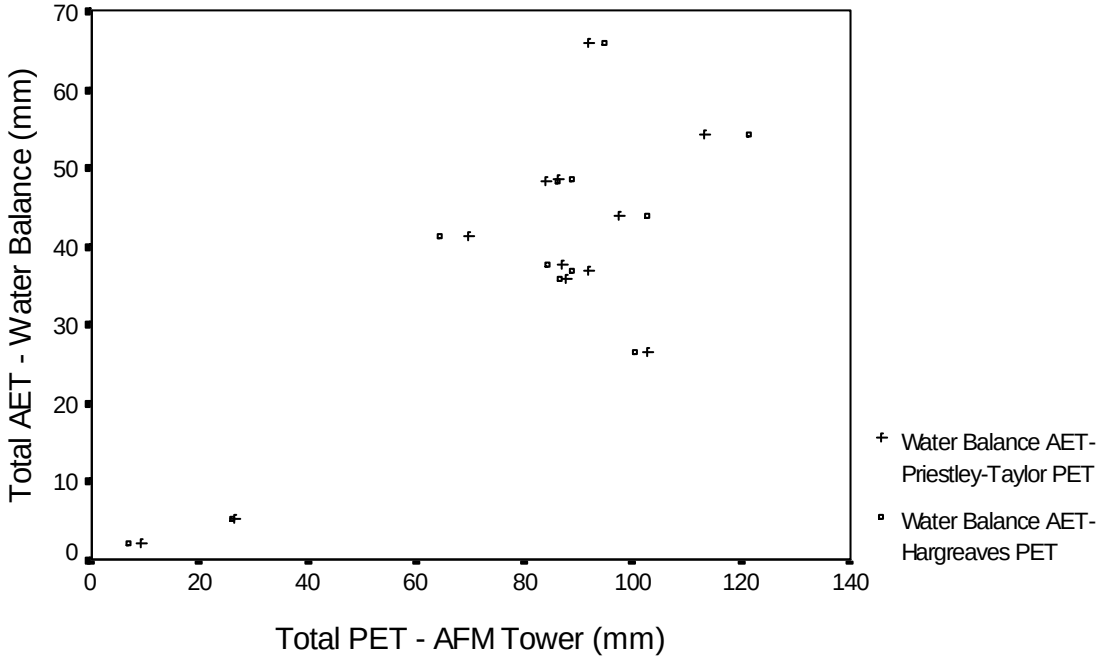

Figure D14: Total Water Balance AET vs. Total PET - NSA 1994

APPENDIX E:

EVAPOTRANSPIRATION INDEXING FUNCTIONS

PARAMETER VALUES AND

SIMULATED WATER BALANCE - NSA

FROM

CHAPTER 6

Table E1: Evapotranspiration Indexing Parameters

Class	alb	h	ETP	Evap. Pan ETP SSA 1994	Evap Pan ETP NSA 1994	FPET	FTALL
Barren	0.18	0.00	1.0	0.35	0.7	n/a	1.0
Dry Conifer	0.11	0.16	1.0	0.12	0.7	3.0	0.7
Wet Conifer	0.08	0.15	1.0	0.14	0.7	3.0	0.7
Fen	0.15	0.05	1.0	0.22	0.7	1.0	1.0
Water	0.15	0.00	1.0	1.00	0.7	n/a	1.0

	SSA-1994	SSA-1995	NSA-1994	NSA-1995
Temp1	200	0	0	0
Temp2	250	0	0	0
Temp3	1000	0	0	0

albe	0.11
FCAP	0.30
FFCAP	0.50

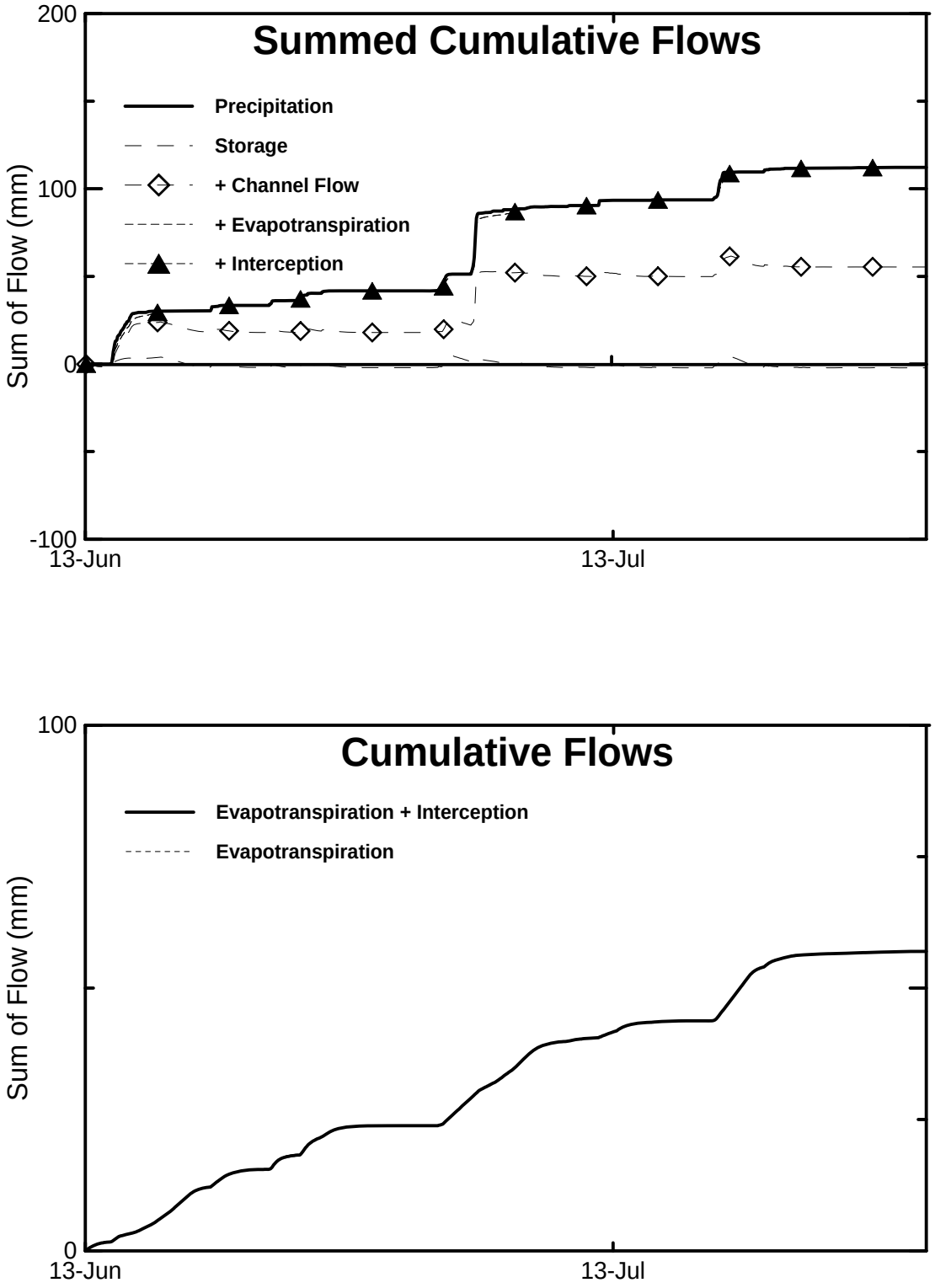

Figure E1: Simulated Water Balance

Barren Class - NSA 199

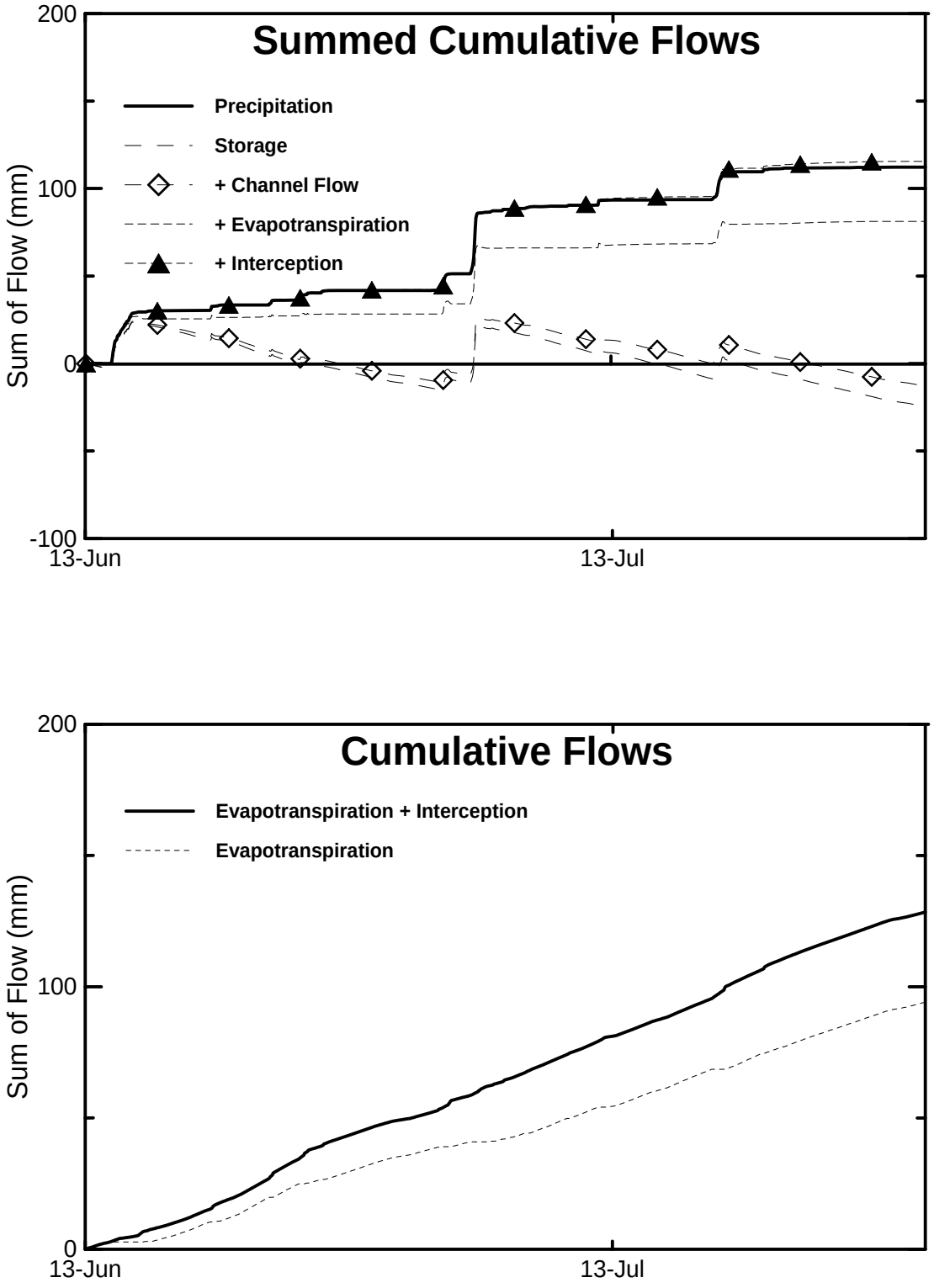

Figure E2: Simulated Water Balance

Dry Conifer Class - NSA 1994

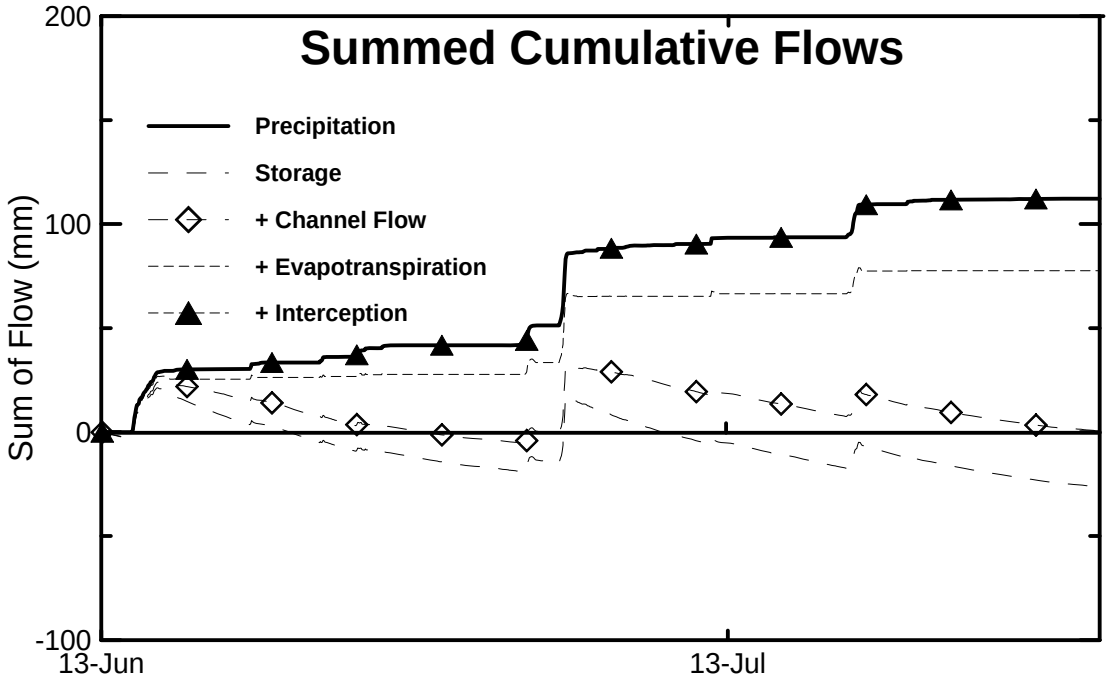

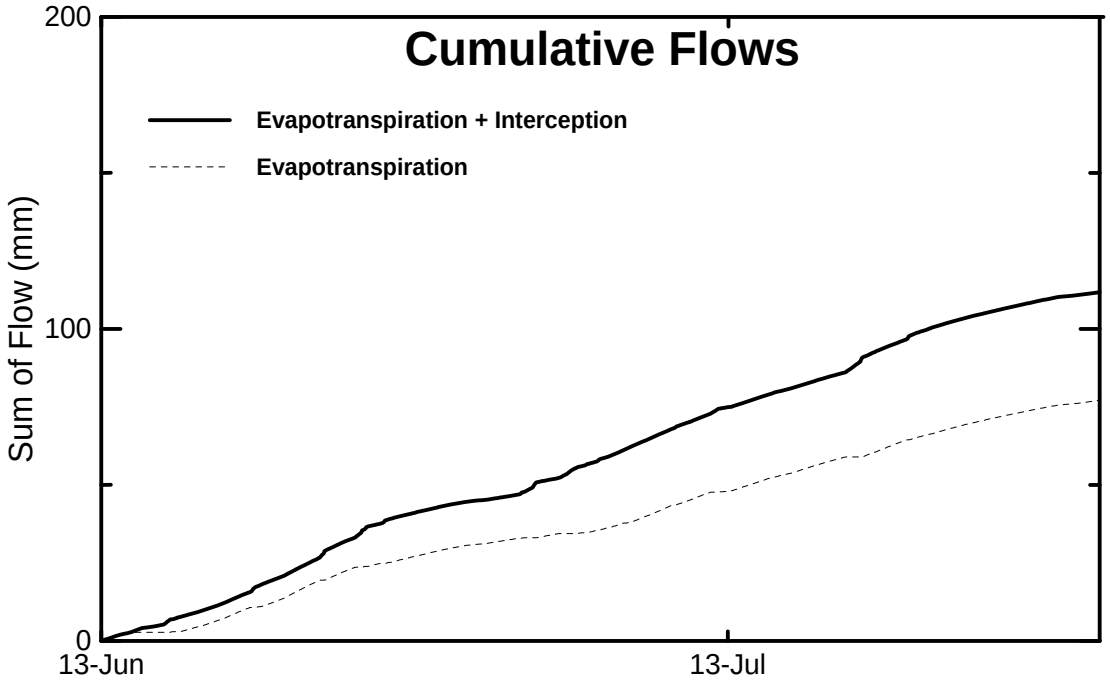

Figure E3: Simulated Water Balance

Wet Conifer Class - NSA 1994

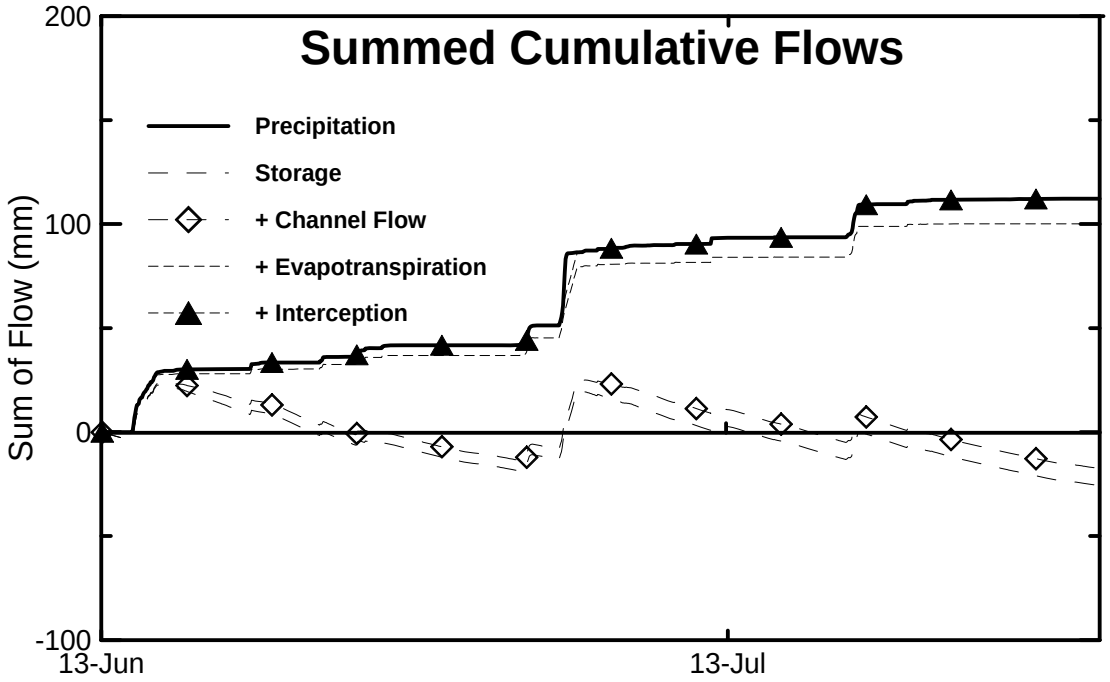

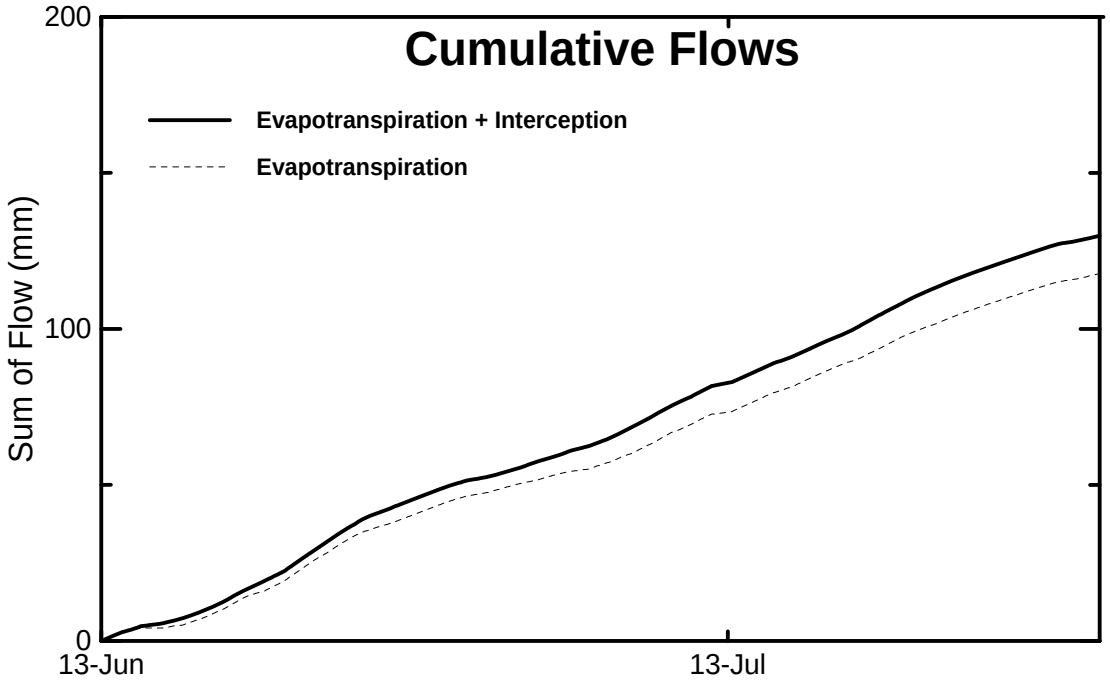

Figure E4: Simulated Water Balance

Fen Class - NSA 1994